THE MOTION OF DROPS AND SWIMMING MICROORGANISMS: MYSTERIOUS INFLUENCES OF SURFACTANTS, HYDRODYNAMIC INTERACTIONS, AND BACKGROUND STRATIFICATION

A Dissertation

Submitted to the Faculty

of

Purdue University

by

Vaseem Akram Shaik

In Partial Fulfillment of the

Requirements for the Degree

of

Doctor of Philosophy

August 2020

Purdue University

West Lafayette, Indiana

THE PURDUE UNIVERSITY GRADUATE SCHOOL
STATEMENT OF DISSERTATION APPROVAL

Dr. Arezoo M. Ardekani, Chair

School of Mechanical Engineering

Dr. Steven T. Wereley

School of Mechanical Engineering

Dr. Guang Lin

Department of Mathematics & School of Mechanical Engineering

Dr. Sangtae Kim

Davidson School of Chemical Engineering

Approved by:

Dr. Nicole Key

School of Mechanical Engineering

ACKNOWLEDGMENTS

I would like to thank my advisor Dr. Ardekani for her guidance, patience, and generosity. Her passion towards research and her hard-working attribute always inspired me. I appreciate the freedom she has given me in choosing research problems.

I want to thank Dr. Kim for always giving me time to clear my doubts despite his extremely busy schedule. I am extremely grateful for his help. I would also like to thank the fluid mechanics faculty of Chemical Engineering, especially Dr. Basaran, Dr. Kim and Dr. Ramki, for their courses on Transport phenomena and Linear operator theory. These courses have been very useful in my thesis.

I would like to thank my committee members, Dr. Wereley, Dr. Lin and Dr. Kim for devoting some time to my presentations, for reading my thesis, and for their invaluable comments.

I want to thank Dr. Uddipta Ghosh, Dr. Aditya Bandopadhyay, Dr. Ranabir Dey and Dr. Suman Chakraborty for creating a great research environment during my undergraduate years which motivated me to pursue higher studies.

My thanks are also to our group members, Nikhil, Shiyan, Rajat, Vishwa, Rishabh, and Manish. I enjoyed the philosophical as well as the intellectual discussions that I had with Nikhil. As my senior, Shiyan always provided me with the words of encouragement to boost up my confidence levels. I am going to miss the amazing collaboration with Rajat and Vishwa.

I finally want to thank my friends, Breaha, Sabiha, Rose, and Molly for their support and my parents for their love throughout these years.

TABLE OF CONTENTS

Page

Page

LIST OF FIGURES

Figure Page

Figure Page

Figure Page

Figure Page

ABSTRACT

Shaik, Vaseem A. Ph.D., Purdue University, August 2020. The Motion of Drops and Swimming Microorganisms: Mysterious Influences of Surfactants, Hydrodynamic Interactions, and Background Stratification. Major Professor: Arezoo M. Ardekani, School of Mechanical Engineering.

Microorganisms and drops are ubiquitous in nature: while drops can be found in sneezes, sprays, ink-jet printers, oceans etc, microorganisms are present in our stomach, intestine, soil, oceans etc. In most situations they are present in complex conditions: drop spreading on a rigid or soft substrate, drop covered with impurities that act as surfactants, marine microbe approaching a surfactant laden drop in density stratified oceanic waters in the event of an oil spill etc. In this thesis, we extract the physics underlying the influence of two such complicated effects (surfactant redistribution and density-stratification) on the motion of drops and swimming microorganisms when they are in isolation or in the vicinity of each other. This thesis is relevant in understanding the bioremediation of oil spill by marine microbes.

We divide this thesis into two themes. In the first theme, we analyze the motion of motile microorganisms near a surfactant-laden interface in homogeneous fluids. We begin by calculating the translational and angular velocities of a swimming microorganism outside a surfactant-laden drop by assuming the surfactant is insoluble, incompressible, and non-diffusing, as such system is relevant in the context of bioremediation of oil spill. We then study the motion of swimming microorganism lying inside a surfactant-laden drop by assuming the surfactant is insoluble, compressible, and has large surface diffusivity. This system is ideal for exploring the nonlinearities associated with the surfactant trasport phenomena and is relevant in the context of targeted drug delivery systems wherein one uses synthetic swimmers to transport the drops containing drug. We then analyze the motion of a swimming organism

in a liquid film covered with surfactant without making any assumptions about the surfactant and this system is relevant in the case of free-standing films containing swimming organisms as well as in the initial stages of the biofilm formation. In the second theme, we consider a density-stratified background fluid without any surfactants. In this theme, we examine separately a towed drop and a swimming organism, and find the drag acting on the drop, drop deformation, and the drift volume induced by the drop as well as the motility of the swimming organism.

1. INTRODUCTION

The transport of drops and swimming organisms through density-stratified fluids is important not only from the fundamental fluid mechanics perspective which improves upon our understanding based on classical microhydrodynamics [1–3] but also from the applied standpoint. For example, consider the situation of oil spill during which the spilled oil rose in the form of droplets through the stratified oceanic waters. These drops were usually covered with surfactant which was added (after the spill) with the purpose of breaking down the heavier oil components into lighter ones. It was found that the effect of oil spill on the marine life is not as devastating as expected [4]. This is because most of the spilled oil was consumed by the marine microbes as the oil served as nutrient sources for these microbes. Hence, a proper accounting of the surfactant effects on the oil-microbe interactions (see Chapter 2) as well as the stratification effects on the droplet motion (see Chapter 5) unravel the simultaneous influence of stratification and surfactant redistribution on the bioremediation of oil spill.

Stratification was found to alter the drag experienced by a towed particle or drop and the motility of swimming organisms as small as milimiter size [5,6]. For example, stratification enhances the drag acting on a towed particle or drop while it hinders the motility of organisms such as copepods, dinoflagellates, cyanobacteria, etc, leading to the formation of algal blooms at sharp density changes, which could have significant human health risks due to the toxins released by these organisms. A towed particle or drop or a freely swimming organism drags a certain volume of fluid with itself (the so called "drift volume") which is infinitely large compared to particle, drop or organism's volume at zero or finite inertia. This drift volume is directly related to the mixing caused by the sedimenting organic matter (like marine snow) and the marine organisms. As expected stratification significantly modifies the drift volume

in turn altering the biogenic contributions to the mixing. Despite the huge literature on the motion of particles, drops or swimming organisms through stratified fluids (see Refs. [5,6]), no analytical expressions for the drag acting on the drop, motility of the organisms and the drift volume induced by them were ever reported (see Chapters 5 and 6).

In microfluidic experiments, in free-standing films and during the initial stages of biofilm formation on water surface in aquatic environments, the stratification effects are negligible but not the surfactant effects. For example, synthetic swimmers can be used to transport the contents within the drop or the drop itself in a microfluidic channel and this has applications in the targeted drug delivery systems [7]. The intracicies of this transport process depends on the impurities, which act as surfactants, that are inevitably present on the droplet surface (see Chapter 3). Surfactant redistribution has been found to alter the swimming dynamics near a plane and spherical interfaces under various limits of surfactant transport phenomenon [8–10]. It is necessary to extend these theories to locomotion in films as a first step towards understanding the formation of biofilms (see Chapter 4).

Due to the small length and velocity scales, the motion of the drops and organisms inherently occur at low Reynolds number, where the Reynolds number is the ratio of the inertial forces to the viscous forces. Under the Boussinesq approximation (see Chapter 6 for details), the fluid motion is governed by the Navier-Stokes equations and the incompressibility condition while the density transport is governed by the advection-diffusion equation

$$\begin{aligned} \rho_\infty \left(\frac{\partial \mathbf{v}}{\partial t} + \mathbf{v} \cdot \nabla \mathbf{v} \right) &= -\nabla p + \mu \nabla^2 \mathbf{v} + \rho \mathbf{g}, \ \nabla \cdot \mathbf{v} = 0, \\ \frac{\partial \rho}{\partial t} + \mathbf{v} \cdot \nabla \rho &= \kappa \nabla^2 \rho, \end{aligned} \tag{1.1}$$

where ρ_∞, ρ, μ, κ, $\mathbf{v}$, and p denote respectively, reference density, density, dynamic viscosity of the fluid, diffusivity of the stratifying agent, velocity, and pressure fields. At negligible inertia and stratification, these equations become linear and independent of time. Hence, any organism that exhibits the time-reversal symmetry—the organ-

ism's gait does not change when viewed forward as well as backward in time—do not swim on an average. This statement is essentially the Purcell's scallop theorem [11]. Due to this reason, biological microswimmers adopt time irreversible stratigies to propel at low Reynolds number. These include but not limited to the propagating waves along their surface or rotating their helical flagella [12]. Along the similar lines, artifical microswimmers are designed to get away from the constraints of the scallop theorem [7].

In this thesis, we model the swimming organism in one of the three ways: (i) Taylor's swimming sheet [13], (ii) force-dipole or monopole depending on whether the organism is force-free or not [2], and (iii) spherical squirmer [14, 15]. In the first model, we represent the organism as an infinitely long 2D waving sheet of zero thickness and this model is good representation of organisms such as the tail of human spermatazoon, *Caenorhabditis elegans* etc. The second model is used to study the hydrodynamic interaction of the organism with the drop and this model represents all the organisms as we are not explicitly resolving the surface of the organism. However, this model is inaccurate when the organism is close to the drop surface. In the third model, we represent the organism as a sphere with prescribed slip on its surface and this model is a good representation of ciliated organisms such as *Paramecium*, *Opalina* as well as the colonies of green alga *Volvox*. Both the squirmer model and the far-field representation (force-dipole model) can be used to analyze the swimming dynamics of three well studied types of swimmers: pusher, puller and neutral swimmer. A puller (resp. pusher) swimmer propels by drawing fluid along its axis (resp. sides) and ejecting fluid along its sides (resp. axis). The flow field far from a neutral swimmer can be represented by a force quadrapole (instead of a dipole) placed at its center. *Escherichia coli*, *Chlamydomonas* and *Volvox* are three typical examples of pusher, puller and neutral swimmers, respectively.

We divide this thesis into two parts. In the first part, we analyze the locomotion near a surfactant-laden interface in a homogeneous fluid.

- In Chapter 2, we derive the mobility matrix for two drops of arbitrary sizes covered with an incompressible and non-diffusing surfactant. We also calculate the velocity of a swimming microorganism (modeled as a force-dipole) outside a drop covered with a similar surfactant. We use the latter results to find the swimming dynamics outside a surfactant-laden drop in an effort to ascertain the surfactant effects on the bioremediation of an oil spill (see Ref. [16, 17]).

- In Chapter 3, we investigate the dynamics of a spherical squirmer inside a spherical surfactant laden drop by assuming the surface diffusion of the surfactant is large. We find that the advection of the surfactant on the drop surface leads to a time-averaged propulsion of the drop and the time-reversible swimmer that it engulfs, thereby causing them to escape from the constraints of the scallop theorem.

- In Chapter 4, we analyze the motion of a swimming sheet located symmetrically in a film covered with surfactant. We find that the surfactant-gradient induced alterations in the swimming speed are intricately related to the corresponding alterations in the interface slip.

The second part is focused on the motion of a clean drop or swimming organism through a linearly density-stratified fluid.

- In Chapter 5, we consider a towed drop in a stratified fluid and calculate the drag acting on the drop, the flow fields inside and outside the drop, the drop deformation, and the drift volume induced by the drop. We find that the stratification enhances the drag, does not deform the drop and reduces the drift volume making it finite.

- In Chapter 6, we study the motion of a spherical squirmer in a density-stratified fluid. We find that stratification can enhance or reduce the swimming speed of the organism depending on its gait and its location relative to the neutrally buoyant position.

2. POINT FORCE SINGULARITIES OUTSIDE A DROP COVERED WITH AN INCOMPRESSIBLE SURFACTANT: IMAGE SYSTEMS AND THEIR APPLICATIONS

2.1 Introduction

Point force singularity solutions are commonly used to represent the disturbance flow field due to particles, drops and microorganisms in a low Reynolds number regime [2,18,19], where the inertial forces are negligible. For instance, the disturbance flow field due to particles of simple shape (e.g., sphere, spheroid or ellipsoid) in simple ambient flows (e.g., uniform flow, linear flow) or that due to particles of slender geometry can be represented by an internal distribution of point force singularities (and the higher order singularities) [2, 20]. More importantly, the far-field behavior of the disturbance flow field can be captured by a Stokeslet (flow field due to a point force) or a rotlet (flow field due to a point torque) or a stresslet (flow field due to a symmetric part of a force dipole), if the force, torque and the stresslet experienced by the particle are known [2]. This far-field behavior can be used to understand the interaction of particles, drops or microorganisms with interfaces [8, 21–24].

In this work, we derive the image flow field due to the point force singularities placed outside a drop covered with an insoluble, non-diffusing and an incompressible surfactant, with allowance for the interfacial viscosity of the drop. This solution can be used to understand the pair hydrodynamic interaction of bubbles and drops in the presence of surfactants in bubbly flows and emulsion flows, respectively. It can also be used to investigate bacterial dynamics in the vicinity of oil drops; an analysis that is essential in order to understand the mechanism of bioremediation of insoluble

This chapter has been reprinted with permission from the article "Point force singularities outside a drop covered with an incompressible surfactant: Image systems and their applications", by V. A. Shaik and A. M. Ardekani, Physical Review Fluids, 2(11):113606, 2017 (DOI: 10.1103/PhysRevFluids.2.113606).

hydrocarbons released in an oil spill. In the event of an oil spill, surfactants are often used to break down the 'heavier' oil components into tiny drops ($O\left(100-1000\right)\mu$m), which act as a carbon source for marine bacteria [4]. Therefore, it is important to understand the hydrodynamic interactions between bacteria and surfactant-laden drops, as a first step towards answering vital questions related to the process of bioremediation in oil spills. Also, the distribution of bacteria near bubbles is important in marine environments or in food cleaning procedures when cavitation bubbles are used to clean infectious bacteria from surface of food products [25].

Non-uniform distribution of surfactant (which leads to the non-uniform interfacial tension), caused by fluid flow near an insoluble surfactant laden interface, significantly alters the physics, e.g., the velocity of a force-free drop or the drag experienced by a drop. This fluid flow can be due to (i) externally applied force (e.g., gravity), (ii) externally imposed flow field, or (iii) hydrodynamic interactions with other particles. Among these, the buoyancy (gravity) driven motion of drops covered with surfactants in an unbounded quiescent fluid is well understood [18, 26]. There is a recent attraction to the motion of force-free, surfactant-laden-drops in an unbounded externally imposed flow field. One interesting observation is the cross-stream migration of a non-deforming surfactant laden spherical drop (towards the centerline of the flow) in an unbounded plane/cylindrical Poisuelle flow. Hanna and Vlahovska's work [27] was the first to observe this and they focused on the limits of large Marangoni number, Ma (ratio of Marangoni forces to the viscous forces) or large viscosity ratio of the drops, neglecting any surface diffusivity of the surfactant. Schwalbe *et al.* [28] studied the influence of the interfacial viscosity of the drops, where the interface is assumed to be Newtonian and the Boussinesq-Scriven constitutive law is used for the interfacial stress tensor. Pak *et al.* [29] studied the effect of surface diffusivity of the surfactant in the limit of large diffusivity (surface Péclet number, $Pe_S \ll 1$, where Pe_S is the ratio of surface advection of the surfactant to its surface diffusion).

A lot of work has been done on the interaction of particles/drops with surfactant-laden-interfaces. Depending on the shape of the interface, one can classify these works

into two categories. The first category deals with the motion of particles near a plane interface covered with a surfactant. For instance, Blawzdziewicz *et al.* [30] developed a method to find the image of an arbitrary flow field from a plane interface covered with an incompressible, insoluble and non-diffusing surfactant. They used this method to find the image of a Stokeslet, which was further utilized in deriving the mobility of a rigid sphere near a surfactant-laden interface. Recently, Lopez and Lauga [8] studied the dynamics of swimming microorganisms near a plane interface covered with an incompressible surfactant. Modeling the microorganisms with a force dipole or a rotlet dipole, they explained the attraction/repulsion of microorganisms and their swimming in circles near such complex interfaces. These two studies included the effects of interfacial viscosity. The second category deals with the interaction of two or more spherical surfactant-laden-drops. For instance, Blawzdziewicz *et al.* [31] derived the general solution of creeping flow equations surrounding a spherical drop covered with an insoluble and incompressible surfactant ($Ma \to \infty$). This solution was then used to derive the pairwise mobility functions which were further utilized to determine the collision efficiencies of two equal-sized bubbles covered with a surfactant in linear flows. In the same limit of Ma, Ramirez *et al.* [32] studied the effect of buoyancy on the interaction of neutrally buoyant rigid spheres (located outside the drop) with surfactant-covered bubbles, in the context of microflotation. Following the procedure of Ramirez *et al.* [32], Rother and Davis [33] studied the buoyancy induced coalescence of two drops (of arbitrary size) covered with an incompressible surfactant. These three works considered the additional influence of Brownian motions and van der Walls attraction on the hydrodynamic interactions. Furthermore, Blawzdziewicz *et al.* [34] studied the rheology of a dilute suspension of spherical drops covered with surfactants, subjected to linear flows. They focused on the limit where the redistribution of surfactant on the drop is significant $Ma \sim O(1)$. They observed that the presence of surfactant can give rise to shear-thinning behavior with non-zero values of first and second normal stress differences. Extension of this work to time-dependent flows was carried out by Vlahovska *et al.* [35]. In the same limit of Ma, Cristini *et al.* [36]

studied the near contact motion of surfactant covered spherical drops using lubrication theory. Also, Zinchenko *et al.* [37] studied the gravity induced collision efficiencies of two spherical drops covered with compressible surfactants (valid for arbitrary Ma and Pe_S). An intriguing result of this work is that the surfactant enhances the coalescence of drops of equal size. These works consider a linear relationship between interfacial tension and surfactant concentration and they neglect the influence of interfacial viscosity.

Mechanisms other than fluid flows can cause the non-uniform distribution of surfactants which thereby lead to the self-propulsion of particles in quiescent fluids. For instance, either during initial stages of micelle adsorption on the surface of a clean drop or by using a non-uniform mixture of two surfactants, one can observe the gradients in the surfactant concentration and consequently the interfacial tension on the surface of the drop and this propels the drop [38]. A second example is the Marangoni propulsion [39] of interface bound particles due to the release of an insoluble surface active agent. For a simple shape of these particles residing on a flat interface, such as a thin disc, Lauga and Davis derived analytical expressions for the translational velocity due to the release of surfactants [40]. Later, Masoud and Stone derived such expressions for oblate and prolate spheroidal particles using the Lorentz reciprocal theorem [41].

A traditional approach to derive the mobility of particles near a plane interface is (i) to derive the image systems of point force singularities near a *plane* interface [42–44] and then (ii) to apply the Faxén's law to a suitable combination of the images of these point force singularities. This approach is general since, once we know the images of point force singularities, we can readily derive the mobility of a rigid sphere, drop or even a swimming microorganism near a plane interface [8, 24]. Kim and Karilla [2] used this approach to derive the mobility functions for two rigid *spheres* of arbitrary sizes while Fuentes *et al.* [45, 46] derived the mobility functions for two *spherical* drops with clean interfaces. Following this analogy, we derive the image systems for point force singularities and higher order singularities placed outside a

drop covered with an incompressible surfactant, including the effects of interfacial viscosity, in Sections II and III, respectively. We thereafter, illustrate the use of the images of point force singularities by providing two examples in Sections IV and V. The first example concerns the mobility functions for two spherical drops (of arbitrary sizes) covered with an incompressible surfactant. For this purpose, we require the Faxén's laws for a spherical drop covered with an incompressible surfactant, which are derived in Appendix 2.8. In the second example, we derive the velocity of a swimming microorganism outside a stationary drop covered with an incompressible surfactant. A brief discussion on the incompressible surfactant film is provided in Appendix 2.7.

2.2 Point force outside a drop covered with an incompressible surfactant

In this section, we derive the image flow field due to a point force outside a stationary spherical drop covered with an insoluble, non-diffusing and incompressible surfactant. Assuming the interface to be Newtonian, we use the Boussinesq-Scriven constitutive law [47, 48] for modeling the interfacial viscous stresses. For deriving the image flow field, we use the multipole representation of the Lamb's general solution [49]. Kim and Karrila [2] used this method to derive the image of point force singularities near a rigid sphere while Fuentes *et al.* [45, 46] used it to derive the images outside a drop with a clean interface, without any interfacial viscosity. Recently, Daddi-Moussa-Ider and Gekle [50] used this method to derive the images of a point force outside a spherical elastic membrane for axisymmetric configurations.

Consider a point force $\mathbf{F}$ located at $\mathbf{x}_2$ outside a drop, whose center is at $\mathbf{x}_1$ (see figure 2.1). Scaling the distances by the radius of the drop, the flow fields inside and outside the drop are governed by Stokes equations and incompressibility conditions

$$-\nabla p^{(e)} + \mu_e \nabla^2 \mathbf{v}^{(e)} = -\mathbf{F}\delta\left(\mathbf{x}-\mathbf{x}_2\right), \ \nabla\cdot\mathbf{v}^{(e)} = 0, \ \text{ for } r_1 = \ |\mathbf{x}-\mathbf{x}_1| > 1, \tag{2.1}$$

$$\mu_i \nabla^2 \mathbf{v}^{(i)} = \nabla p^{(i)}, \ \nabla\cdot\mathbf{v}^{(i)} = 0, \ \text{ for } \ |\mathbf{x}-\mathbf{x}_1| < 1, \tag{2.2}$$

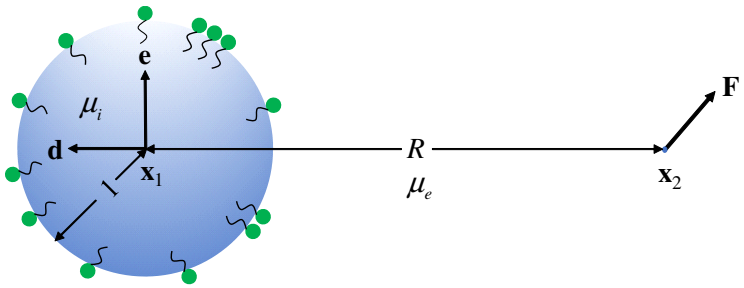

Figure 2.1. : Point force outside a surfactant covered drop and the associated coordinate system

where δ is the dirac-delta function. Here $\mathbf{v}^{(k)}$ and $p^{(k)}$ denote the velocity and pressure fields, while μ_k denote the dynamic viscosity of the fluid. Also, $k = i, e$ correspond to the interior and exterior of the drop, respectively. The solution of these equations should satisfy the boundary conditions on the surface of the drop given by

$$v_r^{(e)} = v_r^{(i)} = 0, \tag{2.3}$$

$$\mathbf{v}_S = \boldsymbol{\Delta} \cdot \mathbf{v}^{(e)} = \boldsymbol{\Delta} \cdot \mathbf{v}^{(i)}, \tag{2.4}$$

$$\nabla_S \cdot \mathbf{v}_S = 0, \tag{2.5}$$

$$\mathbf{e}_r \cdot \left(\mathbf{T}^{(i)} - \mathbf{T}^{(e)}\right) \cdot \boldsymbol{\Delta} = \nabla_S \sigma + \mu_S \left(\frac{2\mathbf{v}_S}{r_1^2} + \mathbf{e}_\theta \frac{1}{r_1 \sin(\theta)} \frac{\partial \varpi}{\partial \phi} - \mathbf{e}_\phi \frac{1}{r_1} \frac{\partial \varpi}{\partial \theta} \right), \tag{2.6}$$

where $\boldsymbol{\Delta} = \mathbf{I} - \mathbf{e}_r \mathbf{e}_r$, $\mathbf{I}$ is the identity tensor, $(\mathbf{e}_r, \mathbf{e}_\theta, \mathbf{e}_\phi)$ and (v_r, v_θ, v_ϕ) are the unit vectors and the components of the velocity vector in the radial, polar and azimuthal directions with the origin at the center of the drop. $\mathbf{T}^{(i)}$ and $\mathbf{T}^{(e)}$ represent the stress tensors in the inner and outer fluids, σ denotes the interfacial tension, and μ_S denotes the interfacial shear viscosity. ∇_S is the surface gradient operator given by $\nabla_S = \boldsymbol{\Delta} \cdot \nabla$ and $\varpi = \frac{1}{r_1 \sin(\theta)} \left(\frac{\partial v_\theta}{\partial \phi} - \frac{\partial}{\partial \theta} \left(\sin(\theta) v_\phi \right) \right)$. As the drop is not deforming, equation (2.3) states that the radial velocity is zero at the drop surface. Also, equation (2.4)

states that the tangential velocity ($\mathbf{v}_S$) is continous across the interface of the drop. The surface transport equation [51] of an insoluble, non-diffusing, incompressible surfactant reduces to equation (2.5) [8, 30] (see Appendix 2.7 for details). Using the Boussenisq-Scriven constitutive law along with equation (2.5) for the surface viscous stresses $\boldsymbol{\tau}_S$, the surface divergence of surface viscous stress $\nabla_S \cdot \boldsymbol{\tau}_S$ for a spherical interface reduces to that given on the right hand side of equation (2.6).

Since equations (2.1)-(2.6) are linear, we just need to solve for two orientations of the point force to derive the flow field for all possible orientations of the point force. One such orientation of the point force corresponds to an axisymmetric configuration, i.e. point force is oriented along the line joining $\mathbf{x}_1$ and $\mathbf{x}_2$ or $\mathbf{F} \parallel \mathbf{d}$, where $\mathbf{d} = (\mathbf{x}_1 - \mathbf{x}_2) / |\mathbf{x}_1 - \mathbf{x}_2|$. The other configuration corresponds to a transverse or asymmetric configuration, where $\mathbf{F} \perp \mathbf{d}$. For axisymmetric configuration, equation (2.5) implies $\mathbf{v}_S = \mathbf{0}$. Hence the image flow field due to an axisymmetric Stokeslet outside a drop covered with an incompressible surfactant is the same as that due to an axisymmetric Stokeslet outside a rigid sphere. Such a similarity between the images of an axisymmetric Stokeslet near a plane interface covered with an incompressible surfactant and that near a rigid wall was already noted by Blawzdziewicz *et al.* [30]. Kim and Karrila have derived the images due to a Stokeslet outside a rigid sphere [2]. Hence, we do not repeat this calculation but simply use their results in the next few sections of this work. In this section, we therefore focus on deriving the image due to a transverse Stokeslet. Utilizing the linearity of the problem, we write the flow field outside the drop as a sum of the Stokeslet and its image ($\mathbf{v}^*$)

$$\mathbf{v}^{(e)} = \mathbf{F}^{\perp} \cdot \left[\mathcal{G}\left(\mathbf{x} - \mathbf{x}_2\right) / 8\pi\mu_e\right] + \mathbf{v}^*, \tag{2.7}$$

where $\mathcal{G}$ is the free space Green's function of the Stokes equations, the point force in the transverse problem is denoted by $\mathbf{F}^{\perp}$, $\mathbf{F}^{\perp} = F^{\perp}\mathbf{e}$ and $\mathbf{e}$ is perpendicular to $\mathbf{d}$.

We hereby derive the solution of this problem, following these four steps [45, 46]:

1. We write the Stokeslet in terms of harmonics based at $\mathbf{x}_2$, which are then transformed to the harmonics based at $\mathbf{x}_1$ using a Taylor series expansion about

$\mathbf{x}_1$ (or more generally using an addition theorem). Using the properties of spherical harmonics, one can arrive at the following expression for the Stokeslet

$$\begin{aligned}\mathbf{F}^{\perp}\cdot\mathcal{G}\left(\mathbf{x}-\mathbf{x}_2\right)=&\sum_{n=0}^{\infty}\left[\left(1-n\right)R^{-(n+1)}r_1^{2n+1}+\frac{\left(2n+1\right)\left(n+1\right)}{\left(2n+3\right)R^{n+3}}r_1^{2n+3}\right]\mathbf{F}^{\perp}\frac{\left(\mathbf{d}\cdot\nabla\right)^n}{n!}\frac{1}{r_1}\\&+\sum_{n=0}^{\infty}\left[\frac{R^{-(n+3)}}{\left(2n+3\right)}r_1^{2n+5}-\frac{R^{-(n+5)}}{\left(2n+7\right)}r_1^{2n+7}\right]\nabla\left(\mathbf{F}^{\perp}\cdot\nabla\right)\frac{\left(\mathbf{d}\cdot\nabla\right)^n}{n!}\frac{1}{r_1}\\&-\sum_{n=0}^{\infty}\left[R^{-(n+2)}r_1^{2n+3}-\frac{\left(2n+3\right)}{\left(2n+5\right)}R^{-(n+4)}r_1^{2n+5}\right]\left(\mathbf{t}\times\nabla\right)\frac{\left(\mathbf{d}\cdot\nabla\right)^n}{n!}\frac{1}{r_1},\end{aligned}\tag{2.8}$$

where $R=|\mathbf{x}_1-\mathbf{x}_2|$ and $\mathbf{t}=\mathbf{F}^{\perp}\times\mathbf{d}$.

2. We then write the image flow field in terms of the multipole expansion about $\mathbf{x}_1$ as given in equation (2.9) which is eventually written in terms of harmonics based at $\mathbf{x}_1$ as given in equation (2.10)

$$\begin{aligned}\mathbf{v}^{*}=&\mathbf{F}^{\perp}\cdot\sum_{n=0}^{\infty}\left(A_n^{\perp}\frac{\left(\mathbf{d}\cdot\nabla\right)^n}{n!}\frac{\mathcal{G}\left(\mathbf{x}-\mathbf{x}_1\right)}{8\pi\mu_e}+B_n^{\perp}\frac{\left(\mathbf{d}\cdot\nabla\right)^n}{n!}\nabla^2\frac{\mathcal{G}\left(\mathbf{x}-\mathbf{x}_1\right)}{8\pi\mu_e}\right)\\&+\sum_{n=0}^{n=\infty}\left(C_n^{\perp}\frac{\left(\mathbf{d}\cdot\nabla\right)^n}{n!}\frac{\left(\mathbf{t}\times\nabla\right)}{8\pi\mu_e}\frac{1}{r_1}\right)-\left(C_0^{\perp}-A_1^{\perp}\right)\frac{\left(\mathbf{t}\times\nabla\right)}{8\pi\mu_e}\frac{1}{r_1}.\end{aligned}\tag{2.9}$$

$$\begin{aligned}\mathbf{v}^{*}=&\sum_{n=0}^{\infty}A_n^{\perp}\left[1-n+\frac{\left(2n+1\right)\left(n+1\right)}{\left(2n+3\right)}\right]\mathbf{F}^{\perp}\frac{\left(\mathbf{d}\cdot\nabla\right)^n}{n!}\frac{1}{8\pi\mu_e r_1}\\&+\sum_{n=0}^{\infty}\left[\frac{A_n^{\perp}r_1^2}{2n+3}-\frac{A_{n+2}^{\perp}}{2n+7}-2B_n^{\perp}\right]\nabla\left(\mathbf{F}^{\perp}\cdot\nabla\right)\frac{\left(\mathbf{d}\cdot\nabla\right)^n}{n!}\frac{1}{8\pi\mu_e r_1}\\&+\sum_{n=1}^{\infty}\left(C_n^{\perp}-A_{n+1}^{\perp}\right)\left(\mathbf{t}\times\nabla\right)\frac{\left(\mathbf{d}\cdot\nabla\right)^n}{n!}\frac{1}{8\pi\mu_e r_1}\\&+\sum_{n=0}^{\infty}\frac{\left(2n+3\right)}{\left(2n+5\right)}A_{n+1}^{\perp}\left(\mathbf{t}\times\nabla\right)\frac{\left(\mathbf{d}\cdot\nabla\right)^n}{n!}\frac{1}{8\pi\mu_e r_1},\end{aligned}\tag{2.10}$$

where $A_n^{\perp}$, $B_n^{\perp}$, $C_n^{\perp}$ are the unknown constants determining the image flow field.

3. We thereafter write the flow field interior to the drop using Lamb's general solution. The connection between the Lamb's general solution and the multipole

expansion is then used to write this flow field in terms of harmonics based at $\mathbf{x}_1$ as

$$\mathbf{v}^{(i)} = \sum_{n=1}^{\infty} \left\{ \begin{array}{l} c_n^{\perp} \left(r_1^{2n-1} \left(\mathbf{t} \times \nabla \right) \frac{(\mathbf{d}\cdot\nabla)^{n-1}}{(n-1)!} \frac{1}{r_1} + (2n-1)\, r_1^{2n-3} \left(\mathbf{t} \times (\mathbf{x} - \mathbf{x}_1) \right) \frac{(\mathbf{d}\cdot\nabla)^{n-1}}{(n-1)!} \frac{1}{r_1} \right) \\ + b_n^{\perp} \left(r_1^{2n+1} \nabla \left(\mathbf{F} \cdot \nabla \right) \frac{(\mathbf{d}\cdot\nabla)^{n-1}}{n!} \frac{1}{r_1} + (2n+1)\, r_1^{2n-1} \left(\mathbf{x} - \mathbf{x}_1 \right) \left(\mathbf{F} \cdot \nabla \right) \frac{(\mathbf{d}\cdot\nabla)^{n-1}}{n!} \frac{1}{r_1} \right) \\ + a_n^{\perp} \left(\begin{array}{l} \frac{(n+3)}{2} r_1^{2n+3} \nabla \left(\mathbf{F} \cdot \nabla \right) \frac{(\mathbf{d}\cdot\nabla)^{n-1}}{n!} \frac{1}{r_1} \\ + \frac{(n+1)(2n+3)}{2} r_1^{2n+1} \left(\mathbf{x} - \mathbf{x}_1 \right) \left(\mathbf{F} \cdot \nabla \right) \times \frac{(\mathbf{d}\cdot\nabla)^{n-1}}{n!} \frac{1}{r_1} \end{array} \right) \end{array} \right\}, \tag{2.11}$$

where $a_n^{\perp}$, $b_n^{\perp}$, $c_n^{\perp}$ are the unknown constants determining the flow field inside the drop.

4. As a final step in this method, we apply the boundary conditions to determine the unknown coefficients $A_n^{\perp}, B_n^{\perp}, C_n^{\perp}, a_n^{\perp}, b_n^{\perp}$ and $c_n^{\perp}$. Using equation (2.3) of the vanishing radial velocity on the surface of the drop, we obtain the following two equations

$$\frac{(n+1)}{2} a_n^{\perp} + b_n^{\perp} - c_{n+1}^{\perp} = 0, \tag{2.12}$$

$$\frac{(n+3)}{(2n+3)} A_{n+1}^{\perp} - \frac{(n+1)}{(2n-1)} A_{n-1}^{\perp} + 2\,(n+1)\, B_{n-1}^{\perp} - C_n^{\perp} = \frac{n}{(2n+3)} \frac{1}{R^{n+2}} - \frac{(n-2)}{(2n-1)} \frac{1}{R^n}. \tag{2.13}$$

After applying equation (2.4) to satisfy the continuity of tangential velocity across the interface, we obtain the following two conditions

$$\begin{aligned} -\frac{(n+3)}{2n} a_n^{\perp} - \frac{1}{n} b_n^{\perp} + \frac{1}{n} c_{n+1}^{\perp} - \frac{c_{n+3}^{\perp}}{(n+2)} - \frac{n A_{n+1}^{\perp}}{(2n+3)\,(n+2)} \\ + \frac{(n-2)}{(2n-1)\, n} A_{n-1}^{\perp} - 2 B_{n-1}^{\perp} = -\frac{(n-2)}{(2n-1)\, n} \frac{1}{R^n} + \frac{n}{(2n+3)\,(n+2)} \frac{1}{R^{n+2}}, \end{aligned} \tag{2.14}$$

$$\frac{(n+1)}{(n+2)} c_{n+3}^{\perp} - \frac{2}{(n+2)} A_{n+1}^{\perp} + C_n^{\perp} = \frac{2}{(n+2)} \frac{1}{R^{n+2}}. \tag{2.15}$$

The surface divergence of the surface flow field is zero, thus equation (2.5) applied to the flow field interior to the drop gives the following condition

$$\left(\frac{n+3}{2} \right) a_n^{\perp} + b_n^{\perp} - c_{n+1}^{\perp} = 0. \tag{2.16}$$

Lastly, in order to satisfy the tangential stress boundary condition (equation (2.6)), one should expand the interfacial tension in terms of surface spherical harmonics and derive two equations from equation (2.6). Noting that $\mathbf{e}_r \cdot \nabla \times \nabla_S \sigma = 0$, we operate $\mathbf{e}_r \cdot \nabla \times$ on equation (2.6) and derive the following equation

$$\begin{aligned} \left(c_{n+3}^{\perp}\lambda - C_n^{\perp}\right) n^2 + \left(c_{n+3}^{\perp}\lambda - 2R^{-n-2} - 5C_n^{\perp} + 2A_{n+1}^{\perp}\right) n \\ -6C_n^{\perp} + 6A_{n+1}^{\perp} = -\beta n c_{n+3}^{\perp} (n+3)(n+1), \end{aligned} \tag{2.17}$$

where $\beta = \mu_S / (\mu_e a)$ and $\lambda = \mu_i / \mu_e$. Now, we can solve equations (2.12)-(2.17) to directly determine the image flow field and the flow inside the drop. By using these flow fields, one can determine the interfacial tension satisfying equation (2.6). Note that we use the general approach of expanding the interfacial tension in terms of surface spherical harmonics in Appendix 2.8 to derive Faxén's laws for a drop covered with an incompressible surfactant.

Solving equations (2.12)-(2.17), we derive the explicit expressions for the unknown coefficients $A_n^{\perp}$, $B_n^{\perp}$, $C_n^{\perp}$, $a_n^{\perp}$, $b_n^{\perp}$, and $c_n^{\perp}$ as follows

$$a_n^{\perp} = 0, \tag{2.18}$$

$$b_n^{\perp} = c_{n+1}^{\perp}, \tag{2.19}$$

$$c_n^{\perp} = \frac{(4n-6)}{(n-2)\left[\beta n^2 + (-3\beta + \lambda + 1)n - 3\lambda\right]} \frac{1}{R^{n-1}}, \tag{2.20}$$

$$A_n^{\perp} = \frac{\left(-2n^2 - 3n - 1\right) R^{-n-3} + \left(2n^2 + n - 3\right) R^{-n-1}}{2n+4}, \tag{2.21}$$

$$B_n^{\perp} = \frac{\left[\begin{array}{l} (n+3)(n+2)(n+1)(\beta n^2+(5\beta+\lambda+1)n+4\beta+\lambda+4)R^{-n-5} \\ -2\left(\begin{array}{l}\beta n^4+(10\beta+\lambda+1)n^3+(32\beta+6\lambda+9)n^2\\ +(29\beta+8\lambda+27)n-12\beta-3\lambda+28\end{array}\right)(n+1)R^{-n-3} \\ +(n+4)(n-1)(n+3)(\beta n^2+(5\beta+\lambda+1)n+4\beta+\lambda+4)R^{-n-1}\end{array}\right]}{4(n+4)(n+3)(n+2)(\beta n^2+(5\beta+\lambda+1)n+4\beta+\lambda+4)}, \tag{2.22}$$

$$C_n^{\perp} = -\frac{\left(\begin{array}{l}(\beta n^2+3+(3\beta+\lambda+1)n)(n+2)R^{-n-4}\\ -(\beta n^2+(5\beta+\lambda+1)n+6\beta+2\lambda+3)nR^{-n-2}\end{array}\right)(2n+3)}{(n+3)(\beta n^2+3+(3\beta+\lambda+1)n)(n+2)}. \tag{2.23}$$

From the multipole representation of the image flow field, equation (2.9), we know that the hydrodynamic force and the stresslet experienced by the drop are given by $-A_0^{\perp}\mathbf{F}^{\perp}$ and $A_1^{\perp}\left(\mathbf{F}^{\perp}\mathbf{d}+\mathbf{d}\,\mathbf{F}^{\perp}\right)/2$, respectively. But from equation (2.21) and [2], we can show that

$$A_n^{\perp}\big|_{\substack{\text{point force outside a drop covered}\\ \text{with an incompressible surfactant}}} = A_n^{\perp}\big|_{\substack{\text{point force outside}\\ \text{a rigidsphere}}}. \tag{2.24}$$

Hence, we conclude that a point force outside a drop covered with an incompressible surfactant exerts a force and stresslet on the drop which are the same as those exerted on a rigid sphere in a similar configuration. This conclusion holds for all separations between the point force and the drop. This conclusion is more general since it is valid for situations such as a translating surfactant-laden-drop in an *arbitrary* flow field as shown in Appendix 2.8, where we also provide the physical reasons behind such behavior of a surfactant-laden-drop. Since the slowest decaying terms (and hence dominant in the far-field) in the multipole expansion of the image flow field are those due to the force and stresslet experienced by the drop, we expect that the flow field far away from the surfactant-laden-drop to be same as that outside a rigid sphere in the similar configuration. This observation is merely a consequence of the earlier observation - a surfactant-laden-drop experiencing the same force and stresslet as

that of a rigid sphere due to a point force outside it. For the flow field close to a surfactant-laden-drop, the higher order terms in the multipole expansion of the image flow field (which depend on the viscosity ratio and the interfacial viscosity) become important due to which, this flow field is different from that near a rigid sphere in a similar configuration. Note that for the limiting values, λ or $\beta \to \infty$, all of these expressions for $A_n^{\perp}$, $B_n^{\perp}$, $C_n^{\perp}$, $a_n^{\perp}$, $b_n^{\perp}$ and $c_n^{\perp}$ approach the corresponding expressions for a rigid sphere as expected.

2.3 Higher Order singularities outside a drop covered with an incompressible surfactant

In this section, we summarize the approach used for deriving the images of higher order singularities such as a Stokes dipole and a degenerate quadrupole from a drop covered with an incompressible surfactant.

2.3.1 Image of a Stokes dipole

We derive the images of a Stokes dipole by operating ∇_2 on the images of Stokeslet outside a drop covered with an incompressible surfactant, where ∇_2 denotes the gradient with respect to the location of the singularity. We hereby summarize the necessary operations required for obtaining the images of few Stokes dipoles in equations (2.25). As these Stokes dipoles are the only singularities required for deriving either the mobility of two drops covered with a surfactant or the velocity of a swimming microorganism near a drop covered with a surfactant, we do not report the images of other Stokes dipoles. Note that, here $\mathrm{Im}\left\{\mathbf{d}\cdot\mathcal{G}\left(\mathbf{x}-\mathbf{x}_2\right)\right\}$ denotes the image of an axisymmetric Stokeslet while $\mathrm{Im}\left\{\mathbf{e}\cdot\mathcal{G}\left(\mathbf{x}-\mathbf{x}_2\right)\right\}$ denotes the image of a transverse Stokeslet.

$$\mathrm{Im}\left\{\left(\mathbf{d}\cdot\nabla\right)\mathbf{d}\cdot\mathcal{G}\left(\mathbf{x}-\mathbf{x}_2\right)\right\} = -\left(\mathbf{d}\cdot\nabla_2\right)\mathrm{Im}\left\{\mathbf{d}\cdot\mathcal{G}\left(\mathbf{x}-\mathbf{x}_2\right)\right\} \tag{2.25a}$$

$$\mathrm{Im}\left\{(\mathbf{e}\cdot\nabla)\,\mathbf{d}\cdot\mathcal{G}\left(\mathbf{x}-\mathbf{x}_2\right)\right\} = -\left(\mathbf{e}\cdot\nabla_2\right)\mathrm{Im}\left\{\mathbf{d}\cdot\mathcal{G}\left(\mathbf{x}-\mathbf{x}_2\right)\right\} - \frac{1}{R}\mathrm{Im}\left\{\mathbf{e}\cdot\mathcal{G}\left(\mathbf{x}-\mathbf{x}_2\right)\right\} \tag{2.25b}$$

$$\mathrm{Im}\left\{(\mathbf{d}\cdot\nabla)\,\mathbf{e}\cdot\mathcal{G}\left(\mathbf{x}-\mathbf{x}_2\right)\right\} = -\left(\mathbf{d}\cdot\nabla_2\right)\mathrm{Im}\left\{\mathbf{e}\cdot\mathcal{G}\left(\mathbf{x}-\mathbf{x}_2\right)\right\} \tag{2.25c}$$

$$\mathrm{Im}\left\{(\mathbf{e}\cdot\nabla)\,\mathbf{e}\cdot\mathcal{G}\left(\mathbf{x}-\mathbf{x}_2\right)\right\} = -\left(\mathbf{e}\cdot\nabla_2\right)\mathrm{Im}\left\{\mathbf{e}\cdot\mathcal{G}\left(\mathbf{x}-\mathbf{x}_2\right)\right\} + \frac{1}{R}\mathrm{Im}\left\{\mathbf{d}\cdot\mathcal{G}\left(\mathbf{x}-\mathbf{x}_2\right)\right\} \tag{2.25d}$$

2.3.2 Image of a degenerate quadrupole

Starting with the representation of the flow field as a sum of degenerate quadrupole and its image described in equation (2.26), we use the solution methodology analogous to Section II to derive the unknown coefficients in the image flow and the flow field interior to the drop. We denote the coefficients which appear in the image flow field of an axisymmetric and transverse degenerate quadrupole as $\left(A_n^{\|Q}, B_n^{\|Q}, C_n^{\|Q}\right)$ and $\left(A_n^{\perp Q}, B_n^{\perp Q}, C_n^{\perp Q}\right)$, respectively. As these coefficients are the same as those of a rigid sphere, we note that the flow fields both inside and outside of a drop covered with an incompressible surfactant due to a degenerate quadrupole located outside the drop are same as those of flow fields due to a degenerate quadrupole outside a rigid sphere.

$$\mathbf{v} = \mathbf{F}\cdot\left[\nabla^2\mathcal{G}\left(\mathbf{x}-\mathbf{x}_2\right)/8\pi\mu_e\right] + \mathbf{v}^* \tag{2.26}$$

The image flow field from a surfactant-laden-drop can be written as a combination of surface irrotational flow (which is the same as that due to a rigid sphere) and a surface solenoidal flow (see Appendix 2.8). The image of a degenerate quadrupole from a surfactant-laden-drop is surface irrotational (i.e., the surface solenoidal part of the image flow field is zero), and the entire image flow field from the surfactant-laden-drop is the same as that from a rigid sphere.

2.4 Mobility functions for two drops covered with an incompressible surfactant

2.4.1 A small drop near a large drop

As a first application of the image flow fields of point force singularities outside a drop covered with an incompressible surfactant, we derive the mobility matrix for hydrodynamic interactions between a large drop (radius a) and a small drop (radius b) accurate to $O(\delta^5)$, where $\delta = b/a \ll 1$. As this matrix for axisymmetric configurations is the same as that for two rigid spheres [2], we only focus on the transverse configuration (the velocity of the drops is perpendicular to the line joining their centers). For this purpose, we use a procedure similar to the method of reflections, where we consider the entire multipole expansion when the images are taken with respect to the large drop. However, we truncate this multipole expansion to a prescribed order in b/R when taking images with respect to a small drop. We require Faxén's laws for a drop covered with a surfactant along with singularity representation of the flow field due to a translating drop covered with a surfactant to be able to use the method of reflections. From the derivation of Faxén's laws presented in Appendix 2.8, we conclude that the Faxén's laws for the force and stresslet experienced by a drop covered with an incompressible surfactant are the same as those of a rigid sphere. On the other hand, the Faxén's laws for the torque experienced by a drop covered with a surfactant is the same as that of a drop with a clean interface and without any interfacial viscosity, namely the drop experiences zero hydrodynamic torque. Also, since the flow field due to a translating drop covered with a surfactant is axisymmetric, it behaves as a rigid sphere (namely fluid inside the drop with respect to itself is stationary) and hence the singularity representation of the flow field due to a translating drop covered with a surfactant is the same as that of a translating rigid sphere. The

mobility functions, which relate the velocities of the drops with the forces acting on them, are written as [2]

$$\begin{pmatrix} \mathbf{U}_1 \\ \mathbf{U}_2 \end{pmatrix} = \frac{1}{\mu_e} \begin{pmatrix} y^a_{11} & y^a_{12} \\ y^a_{21} & y^a_{22} \end{pmatrix} \begin{pmatrix} \mathbf{F}^e_1 \\ \mathbf{F}^e_2 \end{pmatrix}. \tag{2.27}$$

Mobility functions y^a_{12} and y^a_{22}

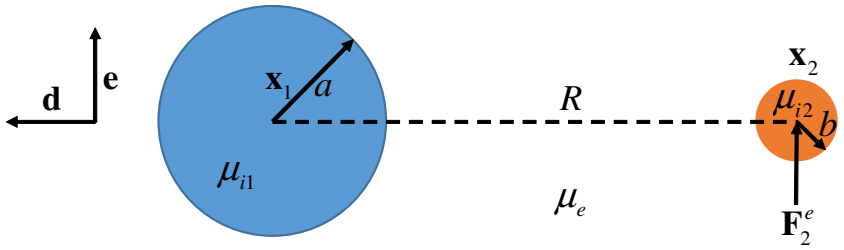

Figure 2.2. : Schematic used for deriving the mobility functions (y^a_{12}, y^a_{22}) for the transverse motion of the drops. Here, an external force, $\mathbf{F}^e_2$ is acting on the small drop while no external force is applied on the large drop.

For deriving the mobility functions y^a_{12} and y^a_{22}, we apply a force $\mathbf{F}^e_2$ on drop 2 and zero force on drop 1 (see figure 2.2). At zeroth reflection, the velocity of drop 2 and the flow field due to its translation are given by

$$6\pi\mu_e b\mathbf{U}^{(0)}_2 = \mathbf{F}^e_2, \tag{2.28}$$

$$\mathbf{v}_2 = \mathbf{F}^e_2 \cdot \left(1 + \frac{b^2\nabla^2}{6}\right) \frac{\mathcal{G}\left(\mathbf{x} - \mathbf{x}_2\right)}{8\pi\mu_e}. \tag{2.29}$$

At the first reflection, the velocity of the drop 1 is obtained by applying the Faxén's law for force (same as that of a rigid sphere) given by equation (2.30) which reduces to equation (2.31)

$$\mathbf{U}^{(1)}_1 = \left(1 + \frac{a^2\nabla^2}{6}\right) \mathbf{v}_2|_{\mathbf{x}=\mathbf{x}_1}, \tag{2.30}$$

$$6\pi\mu_e b\mathbf{U}^{(1)}_1 = \mathbf{F}^e_2 \left[\frac{3}{4}\left(\frac{b}{R}\right) + \frac{1}{4}\left(\frac{b}{R}\right)\left(\frac{a}{R}\right)^2 + \frac{1}{4}\left(\frac{b}{R}\right)^2\right]. \tag{2.31}$$

Up to this reflection, the velocities of drops covered with surfactants are the same as those of rigid spheres. For finding the flow field reflected from drop 1, $\mathbf{v}_{21}$, we need the images of a Stokeslet of strength $\mathbf{F}_2^e$ and a degenerate quadrupole of strength $\frac{b^2}{6}\mathbf{F}_2^e$ located at $\mathbf{x}_2$ (center of drop 2) from a force-free drop located at $\mathbf{x}_1$. The images from a force-free drop can be obtained by first deriving the force exerted by the flow fields of a Stokeslet and degenerate quadrupole on a stationary drop ($-\mathbf{F}_2^e A_0$) and then adding the flow field due to a translating drop, acted upon by an external force ($-\mathbf{F}_2^e A_0$), to the images of the aforementioned point force singularities with respect to a stationary drop (derived in Sections II and III). Hence the flow field reflected from a force-free drop 1 is given by

$$\begin{aligned}\mathbf{v}_{21} = \mathbf{F}_2^e \cdot \sum_{n=0}^{\infty} \left(A_n \tfrac{(\mathbf{d}\cdot\nabla)^n}{n!} \tfrac{\mathcal{G}(\mathbf{x}-\mathbf{x}_\in)}{8\pi\mu_e} + B_n \tfrac{(\mathbf{d}\cdot\nabla)^n}{n!} \nabla^2 \tfrac{\mathcal{G}(\mathbf{x}-\mathbf{x}_\in)}{8\pi\mu_e} \right) \\ + \sum_{n=0}^{\infty} C_n \left(\mathbf{t}\times\nabla\right) \tfrac{(\mathbf{d}\cdot\nabla)^n}{n!} \tfrac{1}{8\pi\mu_e r_1} - \left(C_0 - A_1\right)\left(\mathbf{t}\times\nabla\right)\tfrac{1}{8\pi\mu_e r_1} \\ \underbrace{-\mathbf{F}_2^e A_0 \cdot \left(1 + \frac{a^2\nabla^2}{6}\right) \frac{\mathcal{G}\left(\mathbf{x}-\mathbf{x}_\in\right)}{8\pi\mu_e}}_{\text{Flow added to satisfy the force-free condition for the drop}} \quad ,\end{aligned} \tag{2.32}$$

where $A_n = A_n^{\perp} + \frac{b^2}{6}A_n^{\perp Q}$, $B_n = B_n^{\perp} + \frac{b^2}{6}B_n^{\perp Q}$ and $C_n = C_n^{\perp} + \frac{b^2}{6}C_n^{\perp Q}$. At the second reflection, drop 2 is force free. Hence its velocity is obtained by applying the Faxén's law for the force

$$\mathbf{U}_2^{(2)} = \left(1 + \frac{b^2}{6}\nabla^2\right)\mathbf{v}_{21}\big|_{\mathbf{x}=\mathbf{x}_2}. \tag{2.33}$$

Using the properties of spherical harmonics, we obtain

$$6\pi\mu_e b\mathbf{U}_2^{(2)} = \mathbf{F}_2^e \begin{bmatrix} \left(\frac{b}{R}\right)\left(\frac{x^5}{16} - \frac{9}{8}\sum_{n=1}^{\infty} \frac{1+\beta_1 n^2 + \left(3\beta_1+\lambda_1-\frac{1}{3}\right)n}{3+\beta_1 n^2+(3\beta_1+\lambda_1+1)n} x^{2n+3}\right) \\ +\frac{1}{8}\left(\frac{b}{R}\right)^3 \sum_{n=1}^{\infty}\left(4n^2+6n-1\right)x^{2n+3} \\ -\frac{1}{48}\left(\frac{b}{R}\right)^5 \sum_{n=1}^{\infty}\left(2n+1\right)\left(2n+3\right)\left(n+1\right)^2 x^{2n+1} \end{bmatrix}, \tag{2.34}$$

where $x = a/R$. At this reflection, one can also derive the stresslet experienced by the drop covered with a surfactant using the Faxén's laws for a stresslet (same as that of a rigid sphere)

$$\mathbf{S}_2^{(2)} = \frac{20}{3}\pi\mu_e b^3 \mathbf{E}_{21}\big|_{\mathbf{x}=\mathbf{x}_2} + O\left[(b/a)^5\right] = \mathcal{S}_2^{(2)}\left(\mathbf{F}_2^e\mathbf{d} + \mathbf{d}\mathbf{F}_2^e\right). \tag{2.35}$$

Here, we only include the Stokeslet component of $\mathbf{v}_{21}$ in evaluating the rate of strain field $\mathbf{E}_{21}$. The flow field reflected from drop 2 is given by the flow field due to a stresslet

$$\mathbf{v}_{212} = \left(\mathbf{S}_2^{(2)} \cdot \nabla\right) \cdot \frac{\mathcal{G}\left(\mathbf{x} - \mathbf{x}_2\right)}{8\pi\mu_e}, \tag{2.36}$$

where this solution is accurate to $(b/R)^4$. At the third reflection, drop 1 is also force free. Hence, we determine its velocity by applying the Faxén's law for the force given by equation (2.37) which simplifies to equation (2.38)

$$\mathbf{U}_1^{(3)} = \left(1 + \frac{a^2}{6}\nabla^2\right) \mathbf{v}_{212}|_{\mathbf{x}=\mathbf{x}_1}, \tag{2.37}$$

$$6\pi\mu_e b\mathbf{U}_1^{(3)} = \frac{15}{16}\left(\frac{b}{R}\right)^4 \mathbf{F}_2^e \left(-\frac{x^7}{3} + \sum_{n=1}^{\infty}(2n+3)\,\frac{1+\beta_1 n^2 + \left(3\beta_1+\lambda_1+\frac{1}{3}\right)n}{3+\beta_1 n^2+(3\beta_1+\lambda_1+1)\,n}x^{2n+5}\right). \tag{2.38}$$

Using the images of a Stokes dipole from a drop covered with a surfactant which was described in Section III, we find the flow field reflected from drop 1, $\mathbf{v}_{2121}$. Applying the Faxén's law for the force to drop 2, $\mathbf{U}_2^{(4)} = \mathbf{v}_{2121}|_{\mathbf{x}=\mathbf{x}_2}$, we find

$$6\pi\mu_e b\mathbf{U}_2^{(4)} = -\frac{45}{64}\left(\frac{b}{R}\right)^4 \mathbf{F}_2^e \left(\frac{x^5}{3} - \sum_{n=1}^{\infty}(2n+3)\,\frac{1+\beta_1 n^2 + \left(3\beta_1+\lambda_1+\frac{1}{3}\right)n}{3+\beta_1 n^2+(3\beta_1+\lambda_1+1)\,n}x^{2n+3}\right)^2. \tag{2.39}$$

Equations for the droplet velocities at various reflections, equations (2.28), (2.31), (2.34), (2.38), and (2.39) can be used to find the mobility functions accurate to $O\left[(b/a)^5\right]$ as given below

$$\begin{aligned} 6\pi b y_{12}^a =& \delta\left(\frac{3}{4}x + \frac{1}{4}x^3\right) + \delta^3\left(\frac{1}{4}x^3\right) \\ &+ \delta^4\left[\frac{15}{16}\left(-\frac{x^{11}}{3} + \sum_{n=1}^{\infty}(2n+3)\,\frac{1+\beta_1 n^2 + \left(3\beta_1+\lambda_1+\frac{1}{3}\right)n}{3+\beta_1 n^2+(3\beta_1+\lambda_1+1)\,n}x^{2n+9}\right)\right] + O\left(\delta^6\right), \end{aligned} \tag{2.40}$$

$$
\begin{aligned}
6\pi b y_{22}^{a} =& 1+\delta\left(\frac{x^{6}}{16}-\frac{9}{8}\sum_{n=1}^{\infty}\frac{1+\beta_{1}n^{2}+\left(3\beta_{1}+\lambda_{1}-\frac{1}{3}\right)n}{3+\beta_{1}n^{2}+\left(3\beta_{1}+\lambda_{1}+1\right)n}x^{2n+4}\right)+\delta^{3}\left(\frac{1}{8}\frac{x^{8}\left(x^{4}-9\right)}{\left(x-1\right)^{3}\left(x+1\right)^{3}}\right)\\
&-\delta^{4}\left[\frac{45}{64}\left(\frac{x^{7}}{3}-\sum_{n=1}^{\infty}\left(2n+3\right)\frac{1+\beta_{1}n^{2}+\left(3\beta_{1}+\lambda_{1}+\frac{1}{3}\right)n}{3+\beta_{1}n^{2}+\left(3\beta_{1}+\lambda_{1}+1\right)n}x^{2n+5}\right)^{2}\right]\\
&+\delta^{5}\left[\frac{1}{16}\frac{x^{8}\left(x^{8}-5x^{6}+11x^{4}+5x^{2}+20\right)}{\left(x-1\right)^{5}\left(x+1\right)^{5}}\right]+O\left(\delta^{6}\right).
\end{aligned}
\tag{2.41}
$$

Mobility functions y_{21}^{a} and y_{11}^{a}

For deriving the mobility functions y_{21}^{a} and y_{11}^{a}, we apply an external force $\mathbf{F}_{1}^{e}$ on drop 1 and carry out the procedure outlined in the previous subsection. Doing so, we notice that $y_{21}^{a}=y_{12}^{a}$ which means the mobility matrix is symmetric for drops covered with an incompressible surfactant. Also, to an order of approximation of $O\left(\delta^{5}\right)$, only $\mathbf{U}_{1}^{(0)}$ and $\mathbf{U}_{1}^{(2)}$ contribute to y_{11}^{a}. Here, $\mathbf{U}_{1}^{(2)}$ can be easily derived by swapping $(1,2)$ and (a,b) in the equation for $\mathbf{U}_{2}^{(2)}$, equation (2.34) and truncating the resulting expression to $(b/R)^{5}$. Hence, the mobility function y_{11}^{a} is given by

$$
6\pi a y_{11}^{a}=1-\delta^{3}\left(\frac{5}{4}x^{8}\right)+\delta^{5}\left[\frac{3}{8}\left(\frac{1}{6}-\frac{2+12\beta_{2}+3\lambda_{2}}{4+4\beta_{2}+\lambda_{2}}\right)x^{6}+\frac{9}{8}x^{8}-\frac{105}{16}x^{10}\right]+O\left(\delta^{6}\right).
\tag{2.42}
$$

All of these mobility functions approach the corresponding mobility functions for rigid spheres when either $(\beta_{1},\beta_{2})\to\infty$ or $(\lambda_{1},\lambda_{2})\to\infty$.

From equations (2.40), (2.41), and (2.42), we see that the mobility functions, $y_{12}^{a}\,(=y_{21}^{a})$ and y_{11}^{a} of two surfactant-laden-drops are identical to the corresponding mobility functions of two rigid spheres, upto an approximation of δ^{3}. However, the mobility function, y_{22}^{a} of two surfactant-laden-drops is different from that of two rigid spheres. Also, we note that y_{22}^{a} does not depend on the viscosity ratio (λ_{2}) and the interfacial viscosity (β_{2}) of the small drop. So, as long as the interface of the small drop is incompressible, y_{22}^{a} does not depend on the identity of the small drop. To study the dependence of y_{22}^{a} on the viscosity ratio (λ_{1}) and the interfacial viscosity

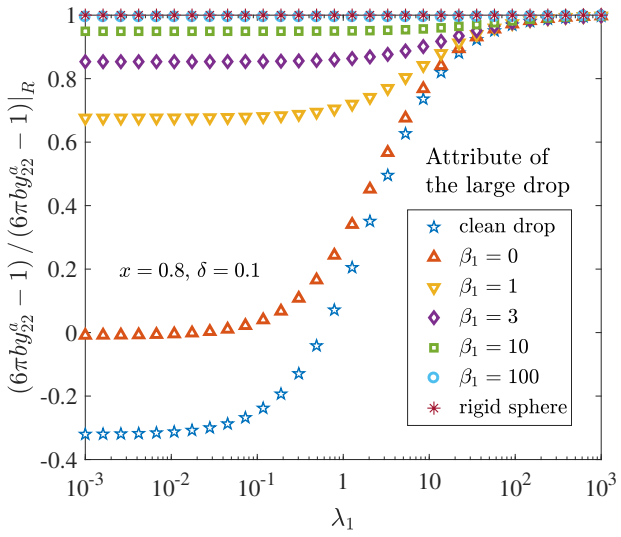

Figure 2.3. : Variation of $(6\pi by^a_{22}-1)\,/\,(6\pi by^a_{22}-1)|_R$ with the viscosity ratio (λ_1) and the interfacial viscosity (β_1) of the large drop. Here $\star$ $(*)$ denotes the situation of a small rigid sphere outside a large clean drop without any interfacial viscosity (rigid sphere). The other symbols denote the situation of two surfactant-laden-drops of disparate sizes. Also, $x = a/R = 0.8$, $\delta = b/a = 0.1$ and $\Lambda_2 = \lambda_2/\,(1+\lambda_2)$

(β_1) of the large drop, we plot in figure 2.3, the correction in y^a_{22} due to the presence of a large surfactant-laden-drop $(6\pi by^a_{22}-1)$, normalized with the correction due to the presence of a large rigid sphere $(6\pi by^a_{22}-1)|_R$ for various values of λ_1 and β_1. As y^a_{22} denotes the velocity of a small drop, we see from figure 2.3 that the velocity of a small drop near a large drop (with or without surfactants) is always less than that near a rigid sphere. Also, the velocity of small drop near a large clean drop is minimum and its velocity near a large surfactant-laden-drop increases with the interfacial viscosity. A similar trend is observed for the variation of the mobility of a particle near a plane interface covered with an incompressible surfactant [30].

2.4.2 Drops of similar sizes

In this section, we comment on the mobility functions of two drops covered with an incompressible surfactant, if the drops sizes are of the same order of magnitude. Noting that (i) the flow field due to an isolated translating drop covered with an incompressible surfactant (axisymmetric problem) is the same as that of an isolated translating rigid sphere and (ii) the Faxén laws for a drop covered with an incompressible surfactant are the same as those of a torque-free rigid sphere, we conclude that the far-field mobility functions of two similar sized drops covered with an incompressible surfactant are the same as those of two similar sized torque-free rigid spheres. Since the mobility functions for two torque-free rigid spheres were already derived in [2] (see chapter 8), we do not pursue this calculation further. As the flow field close to a translating surfactant-laden-drop, in an arbitrary ambient flow, is different from that near a translating torque-free rigid sphere, we expect the near-field mobility functions of two similar sized surfactant-laden-drops to be completely different from those of two similar sized torque-free rigid spheres.

Blawzdziewicz *et al.* [31] derived the mobility functions of two equal sized bubbles covered with an incompressible, insoluble and diffusing surfactant without accounting for the interfacial viscosity. For zero surfactant diffusivity, they report that their far-field mobility functions are the same as those of two torque-free rigid spheres. Our analysis, on the far-field mobility functions, not only agrees with that of Blawzdziewicz *et al.* [31] for zero viscosity ratio, interfacial viscosity and surfactant diffusivity but also generalizes the result − the far-field mobility functions of two *similar* sized surfactant-laden-drops is the same as those of two similar sized torque-free rigid spheres − to arbitrary values of viscosity ratio and interfacial viscosity.

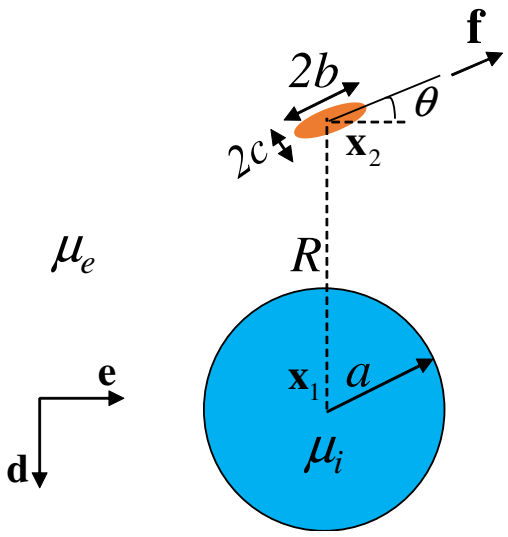

Figure 2.4. : Schematic of a spheroidal swimmer of aspect ratio $\gamma = b/c$ outside a stationary spherical drop of radius a. The drop has a viscosity of μ_i while the viscosity of the surrounding fluid is μ_e. The swimmer is oriented along $\mathbf{f}$. The distance between the center of the drop and the swimmer is denoted by R. The position vectors of the center of the drop and the swimmer are denoted by $\mathbf{x}_1$ and $\mathbf{x}_2$, respectively. The origin of the coordinate system is located at the center of the drop.

2.5 Swimming microorganism outside a stationary drop covered with an incompressible surfactant

As a second application of image flow fields, we derive the velocity of a spheroidal microorganism swimming outside the drop covered with an incompressible surfactant (see figure 2.4). We also provide the expression for the velocity of the same microorganism swimming outside a drop with a clean interface, without any interfacial viscosity using the image flow fields provided in [45,46]. Flow field far away from the microorganism in an unbounded medium is represented by a parallel Stokes dipole (force and force gradient are parallel/anti-parallel to each other). Therefore, when $R - a \gg b$, the leading order velocity of the swimmer near the drop is obtained by

applying Faxén's laws to the image of a Stokes dipole. So, the flow field outside a drop is written as sum of a Stokes dipole and its image

$$\mathbf{v} = -P\left(\mathbf{f}\cdot\nabla\right)\mathbf{f}\cdot\frac{\mathcal{G}\left(\mathbf{x}-\mathbf{x}_2\right)}{8\pi\mu_e} + \mathbf{v}^*, \tag{2.43}$$

where P is the dipole strength of the swimmer [23], $\mathbf{f}$ is the orientation of the swimmer and $\mathbf{v}^*$ is the image flow field. Here $P > 0$ means the swimmer is a pusher while $P < 0$ means the swimmer is a puller. We use the images of a Stokes dipole given in Section III to derive the image flow field $\mathbf{v}^*$. The translational velocity of the swimmer given by $\mathbf{U} = \mathbf{v}^*|_{\mathbf{x}=\mathbf{x}_2} + O\left[(b/R)^2\right]$ can be simplified to

$$\mathbf{U} = \sin^2(\theta)\,\mathbf{U}_1 - \sin(\theta)\cos(\theta)\,\mathbf{U}_2 + \cos^2(\theta)\,\mathbf{U}_3, \tag{2.44}$$

where $\mathbf{U}_1$, $\mathbf{U}_2$ and $\mathbf{U}_3$ for a drop covered with an incompressible surfactant are given by

$$\mathbf{U}_1 = -\frac{P}{8\pi\mu_e R^2}\frac{3x}{(-1+x)^2(x+1)^2}\mathbf{d}, \tag{2.45a}$$

$$\mathbf{U}_2 = -\frac{P}{8\pi\mu_e R^2}\sum_{n=0}^{\infty}\frac{3\,(2n+3)\left[1+\beta n^2+\left(3\beta+\lambda+\frac{1}{3}\right)n\right]x^{2n+3}}{6+2\beta n^2+(6\beta+2\lambda+2)\,n}\mathbf{e}, \tag{2.45b}$$

$$\mathbf{U}_3 = \frac{3P}{16\pi\mu_e R^2}\frac{x}{(-1+x)^2(x+1)^2}\mathbf{d}. \tag{2.45c}$$

The expressions for $\mathbf{U}_1$, $\mathbf{U}_2$ and $\mathbf{U}_3$ for a drop with a clean interface, without any interfacial viscosity are given by

$$\mathbf{U}_1 = -\frac{P}{8\pi\mu_e R^2}\frac{(\Lambda+2)\,x}{(-1+x)^2(x+1)^2}\mathbf{d}, \tag{2.46a}$$

$$\mathbf{U}_2 = -\frac{P}{8\pi\mu_e R^2}\sum_{n=0}^{\infty}\frac{3\Lambda\,(n-\Lambda+1)\,(2n+3)}{2n+6-6\Lambda}x^{2n+3}\mathbf{e}, \tag{2.46b}$$

$$\mathbf{U}_3 = \frac{P}{16\pi\mu_e R^2}\frac{(\Lambda+2)\,x}{(-1+x)^2(1+x)^2}\mathbf{d}, \tag{2.46c}$$

where $\Lambda = \lambda/(1+\lambda)$. Also, the angular velocity of the swimmer is given by

$$\boldsymbol{\omega} = \frac{1}{2}\nabla\times\mathbf{v}^*\Big|_{\mathbf{x}=\mathbf{x}_2} + \Gamma\,\mathbf{f}\times\mathbf{E}^*|_{\mathbf{x}=\mathbf{x}_2}\cdot\mathbf{f} + O\left[(b/R)^3\right], \tag{2.47}$$

where $\Gamma = (1-\gamma^2)/(1+\gamma^2)$, γ is the aspect ratio of the swimmer which is 1 for a spherical swimmer and tends to infinity for a rod shaped swimmer and $\mathbf{E}^* = \frac{1}{2}\left[\nabla\mathbf{v}^* + (\nabla\mathbf{v}^*)^T\right]$ is the rate of strain tensor of the image flow field. This expression for the angular velocity, $\boldsymbol{\omega} = \omega(\mathbf{e}\times\mathbf{d})$ can be simplified to

$$\omega = \omega^{(1)} + \Gamma\omega^{(2)}, \tag{2.48}$$

where $\omega^{(1)}$, $\omega^{(2)}$ for a drop covered with an incompressible surfactant are given by

$$\omega^{(1)} = \frac{3P\sin(2\theta)}{32\pi\mu_e R^3}\sum_{n=0}^{\infty}\frac{n(n+2)\left[\beta n^2 + \left(\beta+\lambda+\frac{5}{3}\right)n - 2\beta - \lambda + \frac{7}{3}\right]}{\beta n^2 + (\beta+\lambda+1)n - 2\beta - \lambda + 2}x^{2n+1}, \tag{2.49a}$$

$$\omega^{(2)} = -\frac{P\sin(2\theta)}{16\pi\mu_e R^3}\left(\tilde{\omega}\cos^2(\theta) + \hat{\omega}\right), \tag{2.49b}$$

where

$$\begin{aligned}\tilde{\omega} =& \frac{9}{8}\frac{(6\beta+3\lambda-2)}{(2\beta+\lambda-2)}x \\ &+ \frac{3}{4}\sum_{n=0}^{\infty}\frac{n^3\beta + \left(\frac{5}{2}\beta+\lambda+3\right)n^2 + \left(-\frac{1}{2}\beta+\frac{1}{2}\lambda+\frac{17}{2}\right)n - 3\beta - \frac{3}{2}\lambda + 5}{\beta n^2 + (\beta+\lambda+1)n - 2\beta - \lambda + 2}(n+3)x^{2n+1}, \\ \hat{\omega} =& -\frac{1}{2}\frac{(6\beta+3\lambda-2)}{(2\beta+\lambda-2)}x \\ &- \frac{3}{2}\sum_{n=0}^{\infty}\frac{n^3\beta + \left(2\beta+\lambda+\frac{5}{3}\right)n^2 + \left(-\beta+\frac{14}{3}\right)n - 2\beta - \lambda + \frac{8}{3}}{\beta n^2 + (\beta+\lambda+1)n - 2\beta - \lambda + 2}(n+2)x^{2n+1}.\end{aligned}$$

The expressions for $\omega^{(1)}$ and $\omega^{(2)}$ for a drop with a clean interface, without any interfacial viscosity are given by

$$\omega^{(1)} = \frac{3}{4}\frac{P\sin(2\theta)}{8\pi\mu_e R^3}\sum_{n=0}^{\infty}\frac{n(n+2)(-2\Lambda^2+n+1)}{n+2-3\Lambda}x^{2n+1}, \tag{2.50a}$$

$$\omega^{(2)} = -\frac{P\sin(2\theta)}{16\pi\mu_e R^3}\left(\tilde{\omega}\cos^2(\theta) + \hat{\omega}\right), \tag{2.50b}$$

where

$$\begin{aligned}\tilde{\omega} =& \frac{27}{8}\frac{\Lambda^2 x}{(-2+3\Lambda)} \\ &- \frac{3}{4}\sum_{n=0}^{\infty}\frac{(\Lambda-2)n^2 + \left(3\Lambda^2+\frac{5}{2}\Lambda-6\right)n + \frac{3}{2}\Lambda^2 + 4\Lambda - 4}{(n+2-3\Lambda)}(n+3)x^{2n+1}, \\ \hat{\omega} =& -\frac{3}{2}\frac{\Lambda^2 x}{(-2+3\Lambda)} - \frac{3}{2}\sum_{n=0}^{\infty}\frac{n^2 + (-2\Lambda^2-\Lambda+3)n - \Lambda^2 - 2\Lambda + 2}{(n+2-3\Lambda)}(n+2)x^{2n+1}.\end{aligned}$$

In the limit $\lambda \to \infty$ ($\Lambda \to 1$) or $\beta \to \infty$, these expressions for the swimmer velocity

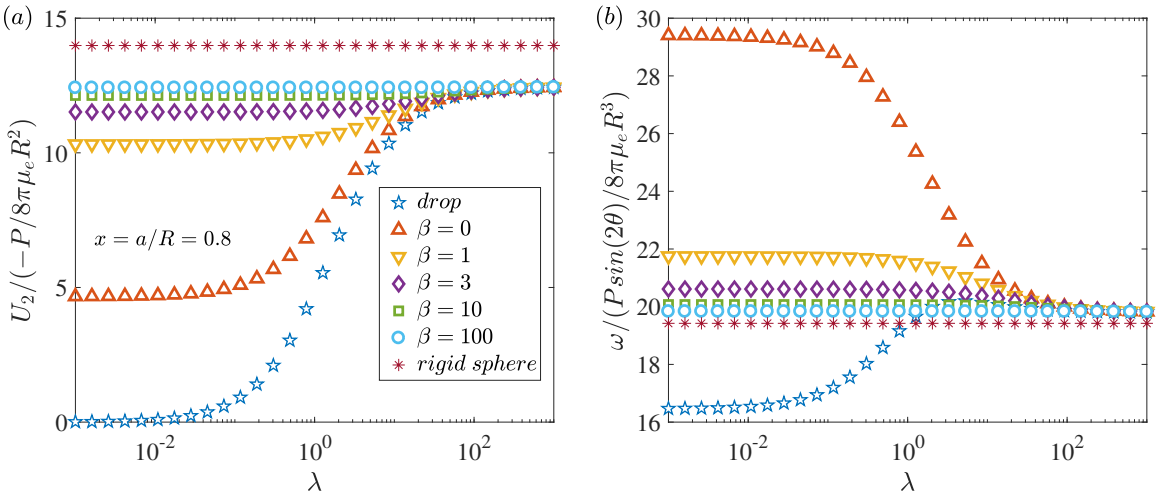

Figure 2.5. : Variation of (a) the dimensionless velocity of the swimmer that is normal to the line of centers and (b) dimensionless angular velocity of the spherical swimmer with the viscosity ratio (λ) and dimensionless interfacial viscosity (β). Here $\star$ ($*$) denotes the situation of the swimmer lying outside a clean drop without any interfacial viscosity (rigid sphere). The other symbols denote the situation of swimmer moving outside the surfactant-laden-drop.

outside a drop reduce to those outside a rigid sphere [52]. From equations (2.44), (2.45a), and (2.45c), we see that the component of the swimmer's velocity along the line of centers ($\mathbf{U} \cdot \mathbf{d}$), outside a surfactant-laden-drop, is the same as the corresponding velocity outside a rigid sphere. The viscosity ratio of the drop and its interfacial viscosity only affect the component of the velocity that is normal to the line of centers (U_2). To understand this, we plot in figure 2.5a, the dimensionless counter part of U_2 for various values of λ and β. This figure shows that, in the limit λ or $\beta \to \infty$, the velocity of the swimmer outside a drop approach its velocity outside a rigid sphere. From equation (2.46b) and also from figure 2.5a, we see that a swimmer outside a bubble ($\lambda = 0$ or $\Lambda = 0$) cannot move normal ot the line of centers. So, irrespective of its orientation and the angular velocity, a puller (pusher) outside a bubble always

moves towards (away from) the bubble along the line of centers. We can also see from figure 2.5a that the presence of an interface reduces the velocity normal to the line of centers when compared to this velocity outside a rigid sphere. The velocity of the swimmer (normal to the line of centers) outside a clean drop is minimum while that outside a surfactant-laden-drop increases with the interfacial viscosity. Similar to figure 2.5a, we plot in figure 2.5b, the variation of the angular velocity of the swimmer with the viscosity ratio and the interfacial viscosity. From figure 2.5b, we see that the angular velocity of the swimmer outside a surfactant-laden-drop decreases with the interfacial viscosity and it is always larger than that outside a rigid sphere. Also, the angular velocity of the swimmer outside a clean drop can be larger or smaller than that outside a rigid sphere, depending on the viscosity ratio of the drop.

2.6 Conclusions

Using the multipole representation of the Lamb's general solution, we derived the image systems for point force singularities located outside a stationary drop covered with an insoluble, non-diffusing and incompressible surfactant. Our derivation includes the role of the interfacial viscosity of the drop by assuming the interface to be Newtonian and using the Boussenisq-Scriven constitutive law for the interfacial stress tensor. We demonstrate the significance of these image systems by providing two examples. In the first example, we derive the mobility functions of two surfactant-laden drops of disparate sizes, using the method of reflections. We unveil the role of the viscosity ratio and the interfacial viscosity of the large surfactant-laden-drop on the mobility of the small surfactant-laden-drop. In the second example, we derive the velocity of the swimming microorganism (modeled as a Stokes dipole) outside (i) a surfactant-laden-drop and (ii) a clean drop without any interfacial viscosity.

Here, we summarize the range of separations between the drops or drop and singularity where the solutions presented in the manuscript are accurate. The image system of a point force or higher order singularity outside a drop is accurate for all

separations between the drop and the singularity except for the singularity touching the drop. The mobility functions of two drops of disparate sizes, derived in Section IV A, is accurate for all the separations between the drops whereas the mobility functions of two drops of similar sizes, discussed in Section IV B, is accurate only for the large separations between the drops. Hence, one can use twin multipole expansions along with the addition theorem to derive the mobility functions of two similar sized drops for arbitrary separations between them. Since the flow field far away from a microorganism (swimmer) can be represented by the flow due to a force dipole placed at the center of the swimmer, the velocity of such a swimmer outside a drop, derived in Section V where the swimmer is replaced by a force dipole, is accurate for large separations between the swimmer and the drop.

We emphasize that our derivations can be used to study the trapping characteristics [52] of bacteria near oil drops and air bubbles, in applications like bioremediation and food cleansing, respectively. One can proceed to determine the following quantities (a) critical trapping radius of the drop/bubble: minimum drop radius beyond which a bacteria near a drop/bubble gets trapped, (b) basin of attraction: space around the drop/bubble, with radius larger than the critical trapping radius, within which if a bacteria is present, gets trapped and (c) probability density function of mean trapping time: time during which a bacterium orbits around the surface of the drop/bubble before escaping. This analysis can then be used to understand the hydrodynamics induced trapping of bacteria near drops/bubbles and also the (possible) usefulness of surfactant in this trapping process.

2.7 Appendix A: Incompressible surfactant film

In this section, we derive the incompressible surfactant film condition, equation (2.5), which holds in one of the two limits − (a) large values of the Marangoni number (Ma, the ratio of tangential stresses generated at the surface by surface tension gradients to tangential stresses applied to the surface by bulk viscous forces) [30,31,53]

or (b) large values of the interfacial dilatational viscosity [28, 54]. Our derivation is focused on large Ma limit and it is similar to the derivation presented in [30, 31]. In addition to the incompressibility of the surfactant, we assume it to be insoluble, both inside and outside the drops and non-diffusing (the interfacial diffusivity of the surfactant is zero or the surface Péclet number is infinity). Since the interfacial tension is a function of the surfactant concentration, we can expand the former as follows

$$\delta\sigma = (\sigma - \sigma_0) = \left(\frac{d\sigma}{d\Gamma}\right)_{\Gamma=\Gamma_0} (\Gamma - \Gamma_0) = \left(\frac{d\sigma}{d\Gamma}\right)_{\Gamma=\Gamma_0} \delta\Gamma, \tag{2.51}$$

where Γ_0 and $\sigma_0 = \sigma(\Gamma_0)$ are the reference surfactant concentration and the interfacial tension, respectively. The above equation can be rewritten as

$$\frac{\delta\Gamma}{\Gamma_0} = -Ma^{-1}\frac{\delta\sigma}{\tau a}, \tag{2.52}$$

where the Marangoni number (Ma) is the ratio of the surfactant elasticity (E) and the capillary number (Ca)

$$Ma = \frac{E}{Ca};\ E = -\frac{\Gamma_0}{\sigma_0}\left(\frac{d\sigma}{d\Gamma}\right)_{\Gamma=\Gamma_0};\ Ca = \frac{\tau a}{\sigma_0}. \tag{2.53}$$

Here, τ denotes the characteristic bulk viscous stresses while a is the characteristic length scale of the problem. From the tangential stress boundary condition, equation (2.6), we deduce that

$$\frac{\delta\sigma}{\tau a} \sim O(1). \tag{2.54}$$

From this equation and equation (2.52), we conclude that

$$\frac{\delta\Gamma}{\Gamma_0} \sim O\left(Ma^{-1}\right). \tag{2.55}$$

In the limit of very large Ma, finite changes in the interfacial tension are caused by the infinitesimal changes in the surfactant concentration, and this is how the Marangoni stresses develop at the interface [30,31]. Hence, it is reasonable to assume that the surfactant is uniformly distributed over the interface, i.e., $\Gamma = \Gamma_0$. Using this condition, the transport equation for an insoluble, non-diffusing and incompressible surfactant over the surface of a stationary and non-deforming drop reduces to

equation (2.5). Since the typical value of the surfactant elasticity is $E \sim O(1)$, from equation (2.53), we conclude that the small values of Capillary number ($Ca \ll 1$) correspond to the large values of Marangoni number ($Ma \gg 1$) or the incompressible surfactant limit. This limit for the small molecular weight surfactants results from their large Marangoni numbers since the dilatational viscosity of these surfactants is not large. But, this limit for the large molecular weight surfactants is due to their large dilatational viscosity.

2.8 Appendix B: Faxén's Laws for a drop covered with an incompressible surfactant

In this section, we derive the Faxén's laws for a drop covered with an incompressible surfactant. For this purpose, one can use the Lorentz reciprocal theorem for Stokes flows with a suitable choice of the auxiliary problem [29, 55–58]. However, in this work, we use the Lamb's general solution to derive Faxén's laws for a spherical surfactant-laden-drop. This approach is used earlier to derive the Faxén's laws for drops with a clean interface [59] and for drops covered with a surfactant, without any interfacial viscosity [60]. Accordingly, we consider a drop covered with an incompressible surfactant, translating with velocity $\mathbf{U}$ in an arbitrary ambient flow field $\mathbf{V}_\infty$. In a frame of reference fixed at the center of the drop, the flow fields inside and outside of the drop should satisfy the Stokes equations along with an incompressibility condition

$$\mu_e \nabla^2 \mathbf{v}^{(e)} = \nabla p^{(e)}, \ \nabla \cdot \mathbf{v}^{(e)} = 0, \tag{2.56}$$

$$\mu_i \nabla^2 \mathbf{v}^{(i)} = \nabla p^{(i)}, \ \nabla \cdot \mathbf{v}^{(i)} = 0. \tag{2.57}$$

The flow field far away from the drop should approach the ambient flow field

$$\mathbf{v}^{(e)} = \mathbf{v}_\infty = \mathbf{V}_\infty - \mathbf{U}, \ \text{as} \ r \to \infty. \tag{2.58}$$

These flow fields should satisfy the boundary conditions at the interface given by [59, 60]

$$\mathbf{v}^{(e)*} = \mathbf{v}^{(i)*}, \tag{2.59a}$$

$$v_r^{(e)*} = v_r^{(i)*} = 0, \tag{2.59b}$$

$$\nabla_S \cdot \mathbf{v}_S^* = 0, \tag{2.59c}$$

$$\mathbf{T}_{(r)}^{(i)*} - \mathbf{T}_{(r)}^{(e)*} = \left[\nabla_S \sigma\right]^* + \mu_S \mathbf{w}_S^* + f\left(\sigma, \mathbf{v}\right) \mathbf{e}_r, \tag{2.59d}$$

where $\mathbf{T}_{(r)}^{(k)} = \mathbf{e}_r \cdot \mathbf{T}^{(k)}$, $\mathbf{w}_S = \frac{2\mathbf{v}_S}{r^2} + \mathbf{e}_\theta \frac{1}{r\sin(\theta)} \frac{\partial \varpi}{\partial \phi} - \mathbf{e}_\phi \frac{1}{r} \frac{\partial \varpi}{\partial \theta}$ and $\varpi = \frac{1}{r\sin(\theta)} \left(\frac{\partial v_\theta}{\partial \phi} - \frac{\partial}{\partial \theta} \left(\sin\left(\theta\right) v_\phi \right) \right)$. Also, $\left(\right)^*$ denotes that the variables are evaluated at the interface and $f\left(\sigma, \mathbf{v}\right)$ denotes the terms which contribute to the normal stress balance at the interface. Since, we assume the drop to be spherical, our solution does not satisfy the normal stress boundary condition, instead this condition can be used to determine the leading order interface deformation. As the governing equations and boundary conditions are linear, we initially write the exterior flow field as $\mathbf{v}^{(e)} = \mathbf{v}_\infty + \mathbf{V}$ (similarly $p^{(e)} = p + p_\infty$). Assuming that the ambient flow field satisfies the Stokes equations, we see that the disturbance flow field also satisfies the Stokes equations. Using the Lamb's general solution, we write the disturbance flow field as

$$\mathbf{V} = \sum_{n=1}^{\infty} \left[\nabla \times \left(\mathbf{r} \chi_{-n-1} \right) + \nabla \Phi_{-n-1} - \frac{\left(n-2\right)}{2n\left(2n-1\right)\mu_e} r^2 \nabla p_{-n-1} + \frac{n+1}{n\left(2n-1\right)\mu_e} \mathbf{r} p_{-n-1} \right], \tag{2.60a}$$

and

$$p = \sum_{n=0}^{\infty} p_n. \tag{2.60b}$$

As the flow field interior to the drop also satisfies the Stokes equations, we have

$$\mathbf{v}^{(i)} = \sum_{n=0}^{\infty} \left[\nabla \times \left(\mathbf{r} \chi_n \right) + \nabla \Phi_n + \frac{n+3}{2\left(n+1\right)\left(2n+3\right)\mu_i} r^2 \nabla p_n - \frac{n}{\left(n+1\right)\left(2n+3\right)\mu_i} \mathbf{r} p_n \right], \tag{2.61a}$$

and

$$p^{(i)} = \sum_{n=0}^{\infty} p_n. \tag{2.61b}$$

Similarly, we can write the ambient flow field as

$$\mathbf{v}_\infty = \sum_{n=-\infty}^{n=\infty} \left[\nabla \times (\mathbf{r}\chi_n^\infty) + \nabla\Phi_n^\infty + \frac{n+3}{2\,(n+1)\,(2n+3)\,\mu_e} r^2 \nabla p_n^\infty - \frac{n}{(n+1)\,(2n+3)\,\mu_e} \mathbf{r} p_n^\infty \right], \tag{2.62a}$$

and

$$p_\infty = \sum_{n=-\infty}^{n=\infty} p_n^\infty, \tag{2.62b}$$

where $(\chi_{-n-1}, \Phi_{-n-1}, p_{-n-1})$ and $(\chi_n, \Phi_n, p_n, \chi_n^\infty, \Phi_n^\infty, p_n^\infty)$ are the solid spherical harmonics of degree $-n-1$ and n, respectively. We hereby rewrite the boundary conditions at the interface, equation (2.59) as

$$\mathbf{v}^{(i)*} \cdot \mathbf{e}_r = 0, \tag{2.63a}$$

$$\mathbf{V}^* \cdot \mathbf{e}_r + \mathbf{v}_\infty^* \cdot \mathbf{e}_r = 0, \tag{2.63b}$$

$$\left[r \frac{\partial v_r^{(i)}}{\partial r} \right]^* = 0, \tag{2.63c}$$

$$-\left[r \frac{\partial V_r}{\partial r} \right]^* = \left[r \frac{\partial v_{\infty r}}{\partial r} \right]^*, \tag{2.63d}$$

$$\left[\mathbf{r} \cdot \nabla \times \mathbf{v}^{(i)} \right]^* - [\mathbf{r} \cdot \nabla \times \mathbf{V}]^* = [\mathbf{r} \cdot \nabla \times \mathbf{v}_\infty]^*, \tag{2.63e}$$

$$\left[\mathbf{r} \cdot \nabla \times \mathbf{T}_{(r)}^{(i)} \right]^* - \left[\mathbf{r} \cdot \nabla \times \boldsymbol{\pi}_{(r)} \right]^* = \mu_S [\mathbf{r} \cdot \nabla \times \mathbf{w}_S]^* + \left[\mathbf{r} \cdot \nabla \times \boldsymbol{\pi}_{\infty(r)} \right]^*, \tag{2.63f}$$

$$\begin{aligned} &\left[\mathbf{r} \cdot \nabla \times \left(\mathbf{r} \times \mathbf{T}_{(r)}^{(i)} \right) \right]^* - \left[\mathbf{r} \cdot \nabla \times \left(\mathbf{r} \times \boldsymbol{\pi}_{(r)} \right) \right]^* \\ &= [\mathbf{r} \cdot \nabla \times (\mathbf{r} \times \nabla_S \sigma)]^* + \mu_S [\mathbf{r} \cdot \nabla \times (\mathbf{r} \times \mathbf{w}_S)]^* + \left[\mathbf{r} \cdot \nabla \times \left(\mathbf{r} \times \boldsymbol{\pi}_{\infty(r)} \right) \right]^*. \end{aligned} \tag{2.63g}$$

Substituting equations (2.60)-(2.62) into equations (2.63), we obtain a set of seven equations. From equation (2.63a), we obtain

$$\sum_{n=1}^{\infty}\left\{\frac{na}{2\left(2n+3\right)\mu_i}p_n^*+\frac{n}{a}\Phi_n^*\right\}=0. \tag{2.64a}$$

From equation (2.63b), we obtain

$$\sum_{n=1}^{\infty}\left\{\frac{\left(n+1\right)a}{2\left(2n-1\right)\mu_e}p_{-n-1}^*-\frac{\left(n+1\right)}{a}\Phi_{-n-1}^*\right\}=-\sum_{n=\infty}^{\infty}\left\{\frac{na}{2\left(2n+3\right)\mu_e}p_n^{\infty *}+\frac{n}{a}\Phi_n^{\infty *}\right\}. \tag{2.64b}$$

From equation (2.63c), we obtain

$$\sum_{n=1}^{\infty}\left[\frac{n\left(n+1\right)a}{2\left(2n+3\right)\mu_i}p_n^*+\frac{n\left(n-1\right)}{a}\Phi_n^*\right]=0. \tag{2.64c}$$

From equation (2.63d), we obtain

$$\sum_{n=1}^{\infty}\left[\frac{n\left(n+1\right)a}{2\left(2n-1\right)\mu_e}p_{-n-1}^*-\frac{\left(n+1\right)\left(n+2\right)}{a}\Phi_{-n-1}^*\right]=\sum_{n=-\infty}^{\infty}\left[\frac{n\left(n+1\right)a}{2\left(2n+3\right)\mu_e}p_n^{\infty *}+\frac{n\left(n-1\right)}{a}\Phi_n^{\infty *}\right]. \tag{2.64d}$$

From equation (2.63e), we obtain

$$\sum_{n=1}^{\infty}\left\{n\left(n+1\right)\left[\chi_n^*-\chi_{-n-1}^*\right]\right\}=\sum_{n=-\infty}^{n=\infty}n\left(n+1\right)\chi_n^{\infty *}. \tag{2.64e}$$

From equation (2.63f), we obtain

$$\begin{aligned}&\sum_{n=1}^{\infty}\left\{n\left(n+1\right)\left[\lambda\left(n-1\right)\chi_n^*+\left(n+2\right)\chi_{-n-1}^*\right]\right\}+\sum_{n=1}^{\infty}\beta n\left(n+2\right)\left(n^2-1\right)\chi_n^*\\&=\sum_{n=-\infty}^{\infty}\left(n-1\right)n\left(n+1\right)\chi_n^{\infty *}.\end{aligned} \tag{2.64f}$$

From equation (2.63g), we obtain

$$\begin{aligned}&\sum_{n=1}^{\infty}\left\{\frac{2n\left(n+1\right)\left(n+2\right)}{a}\Phi_{-n-1}^*-\frac{\left(n+1\right)^2\left(n-1\right)a}{\left(2n-1\right)\mu_e}p_{-n-1}^*\right\}\\&+\sum_{n=1}^{\infty}\left\{\frac{2\lambda}{a}\left(n-1\right)n\left(n+1\right)\Phi_n^*+\frac{n^2\left(n+2\right)a\lambda}{\left(2n+3\right)\mu_i}p_n^*\right\}\\&+\sum_{n=1}^{\infty}\left\{-\beta\frac{\left(n+3\right)na}{\left(2n+3\right)\mu_i}p_n^*-\frac{2n\left(n+1\right)\beta}{a}\Phi_n^*\right\}+\frac{\left[\mathbf{r}\cdot\nabla\times\left(\mathbf{r}\times\nabla_S\sigma\right)\right]^*}{\mu_e}\\&=\sum_{n=-\infty}^{n=\infty}\left\{\frac{2}{a}\left(n-1\right)n\left(n+1\right)\Phi_n^{\infty *}+\frac{n^2\left(n+2\right)a}{\left(2n+3\right)\mu_e}p_n^{\infty *}\right\}.\end{aligned} \tag{2.64g}$$

The solid spherical harmonics are defined as [59, 60]

$$p_n = A_n \mu_i a^{-n-1} r^n S_n(\theta, \phi), \tag{2.65a}$$

$$p_{-n-1} = A_{-n-1} \mu_e a^n r^{-n-1} S_n(\theta, \phi), \tag{2.65b}$$

$$\Phi_n = B_n a^{-n+1} r^n S_n(\theta, \phi), \tag{2.65c}$$

$$\Phi_{-n-1} = B_{-n-1} a^{n+2} r^{-n-1} S_n(\theta, \phi), \tag{2.65d}$$

$$\chi_n = C_n a^{-n} r^n S_n(\theta, \phi), \tag{2.65e}$$

$$\chi_{-n-1} = C_{-n-1} a^{n+1} r^{-n-1} S_n(\theta, \phi), \tag{2.65f}$$

$$p_n^\infty = \frac{2(2n+3)}{n} \alpha_n \mu_e a^{-n-1} r^n S_n(\theta, \phi), \tag{2.65g}$$

$$\Phi_n^\infty = \frac{1}{n} \beta_n a^{-n+1} r^n S_n(\theta, \phi), \tag{2.65h}$$

$$\chi_n^\infty = \frac{1}{n(n+1)} \gamma_n a^{-n} r^n S_n(\theta, \phi). \tag{2.65i}$$

Furthermore, we expand the interfacial tension in terms of surface spherical harmonics as

$$\sigma = \sum_{n=0}^{\infty} \sigma_n S_n(\theta, \phi). \tag{2.66}$$

Note that, we used a shorthand notation for terms of the form $A_n S_n(\theta, \phi)$ to represent a sum of $2n+1$ terms as given below

$$A_n S_n(\theta, \phi) = \sum_{m=0}^{n} \left(A_n^m \cos(m\phi) + \hat{A}_n^m \sin(m\phi) \right) P_n^m(\cos(\theta)), \tag{2.67}$$

where $P_n^m(\cos(\theta))$ is the associated Legendre polynomial of order m and degree n. We substitute equations (2.65) and (2.66) into equation (2.64) and solve for the unknown constants A_n^m, B_n^m, C_n^m, A_{-n-1}^m, B_{-n-1}^m, C_{-n-1}^m and σ_n^m (and the corresponding variables with carat over them) in terms of the constants α_n^m, β_n^m and γ_n^m. The result of this procedure is the following equations

$$A_n^m = 0, \tag{2.68a}$$

$$B_n^m = 0, \tag{2.68b}$$

$$C_n^m = \frac{2n\gamma_n^m + \gamma_n^m}{n(n+1)\left[\beta n^2 + (\beta+\lambda+1)n - 2\beta - \lambda + 2\right]}, \tag{2.68c}$$

$$A_{-n-1}^m = -\frac{2(2n-1)\left[n(\alpha_n^m + \beta_n^m) + \frac{1}{2}\beta_n^m + \frac{3}{2}\alpha_n^m + \alpha_{-n-1}^m\right]}{n+1}, \tag{2.68d}$$

$$B_{-n-1}^m = \frac{(-2\beta_n^m - 2\alpha_n^m)n + \beta_n^m - \alpha_n^m + 2\beta_{-n-1}^m}{2n+2}, \tag{2.68e}$$

$$C_{-n-1}^m = \frac{\left\{\begin{array}{l} -\beta\left(\gamma_{-n-1}^m + \gamma_n^m\right)n^2 + \left[\left(-\gamma_{-n-1}^m - \gamma_n^m\right)\beta + (-\lambda-1)\gamma_{-n-1}^m - \gamma_n^m(\lambda-1)\right]n \\ + \left(2\gamma_n^m + 2\gamma_{-n-1}^m\right)\beta + (\lambda-2)\gamma_{-n-1}^m + (\lambda-1)\gamma_n^m \end{array}\right\}}{n(n+1)\left[\beta n^2 + (\beta+\lambda+1)n - 2\beta - \lambda + 2\right]}, \tag{2.68f}$$

$$\sigma_n^m = -\frac{2(2n+1)\left[(\alpha_n^m + \beta_n^m)n - \frac{1}{2}\beta_n^m + \frac{3}{2}\alpha_n^m\right]\mu_e}{n(n+1)}. \tag{2.68g}$$

From equation (2.68), we can make few deductions. Noting that $\gamma_{-2}^m = 0$, we find that $C_{-2}^m = -\frac{1}{2}\gamma_{-2}^m = 0$. As the torque experienced by the drop is given by $\mathbf{T} = -8\pi\mu_e\nabla(r^3\chi_{-2}) = 0$, we find that the drop covered with an incompressible surfactant does not experience any hydrodynamic torque. Furthermore, we note the following equation holds

$$A_{-n-1}^m\Big|_{\substack{\text{drop covered with an} \\ \text{incompressible surfactant}}} = A_{-n-1}^m\Big|_{\text{rigid sphere}} \tag{2.69}$$

Using the equations for force and stresslet experienced by a drop, $\mathbf{F} = -4\pi\nabla\left(r^3 p_{-2}\right)$, $\mathbf{S} = -\frac{2\pi}{3}\nabla\nabla\left(r^5 p_{-3}\right)$ and equation (2.65b), we conclude that the force and stresslet experienced by a translating drop covered with an incompressible surfactant are the same as those experienced by a translating rigid sphere. In summary, we hereby provide the Faxén's laws for a drop of radius a covered with an insoluble, non-diffusing and incompressible surfactant as

$$\mathbf{F} = 6\pi\mu_e a\left(1 + \frac{a^2\nabla^2}{6}\right)\mathbf{V}_\infty|_O - 6\pi\mu_e a\mathbf{U}, \tag{2.70a}$$

$$\mathbf{T} = \mathbf{0}, \tag{2.70b}$$

$$\mathbf{S} = \frac{20}{3}\pi\mu_e a^3\left(1 + \frac{a^2\nabla^2}{10}\right)\mathbf{E}_\infty|_O, \tag{2.70c}$$

where the subscript O denotes that the quantities are evaluated at the center of the drop and $\mathbf{E}_\infty$ denotes the rate of strain field of the ambient flow field.

For zero surface viscosity, we would like to compare this flow field due to an isolated translating drop covered with an incompressible, insoluble, and non-diffusing surfactant in an arbitrary ambient flow field with that reported in the literature [31]. For this purpose, we note that

$$\begin{aligned}
&\left\{A_n^m, B_n^m, A_{-n-1}^m, B_{-n-1}^m\right\}\Big|_{\substack{\text{drop covered with an}\\ \text{incompressible surfactant}}} = \left\{A_n^m, B_n^m, A_{-n-1}^m, B_{-n-1}^m\right\}\Big|_{\text{rigid sphere}},\\
&\left\{C_n^m, C_{-n-1}^m\right\}\Big|_{\substack{\text{drop covered with an incompressible}\\ \text{surfactant and } \beta=0}} = \left\{C_n^m, C_{-n-1}^m\right\}\Big|_{\text{clean drop}}.
\end{aligned} \tag{2.71}$$

Also, note that the flow field using Lamb's general solution, equations (2.60a), (2.61a), and (2.62a) can be written as a sum of the surface solenoidal and the surface irrotational flow fields on the family of concentric spherical surfaces

$$\mathbf{v} = \mathbf{v}^{Sol} + \mathbf{v}^{Irr}, \tag{2.72}$$

where

$$\mathbf{v}^{Sol} = \sum_{n=-\infty}^{\infty} \nabla \times (\mathbf{r}\,\chi_n),$$
$$\mathbf{v}^{Irr} = \sum_{n=-\infty}^{\infty} \left[\nabla\Phi_n + \frac{n+3}{2\,(n+1)\,(2n+3)\,\mu} r^2 \nabla p_n - \frac{n}{(n+1)\,(2n+3)\,\mu}\mathbf{r}\,p_n\right].$$

Here $\mathbf{v}^{Sol}$ and $\mathbf{v}^{Irr}$ satisfy the conditions

$$\begin{aligned} &\mathbf{i}_r \cdot \left(\nabla_S \times \mathbf{v}^{Irr}\right) = 0, \\ &\nabla_S \cdot \mathbf{v}^{Sol} = 0;\ \mathbf{i}_r \cdot \mathbf{v}^{Sol} = 0. \end{aligned} \tag{2.73}$$

In lieu of equations (2.65), (2.71), and (2.72), we conclude that the surface solenoidal flow field due to a surfactant-laden-drop with zero surface viscosity is the same as that due to a clean drop. Similarly, the surface irrotational flow field due to a surfactant-laden-drop is the same as that due to a rigid sphere. These results agree with the general solution due to a drop covered with incompressible, insoluble and non-diffusing surfactant with zero surface viscosity, as derived by Blawzdziewicz *et al* [31].

One can understand the peculiar behavior of the translating surfactant-laden-drops, in an arbitrary ambient flow, experiencing the same force and stresslet as that of rigid spheres in a similar configuration as follows. As shown earlier, any flow past a particle, irrespective of the boundary conditions on the particle (i.e., the particle can be a rigid particle, a drop or a surfactant-laden-drop), can be decomposed into a surface solenoidal flow field and a surface irrotational flow field on the family of concentric spherical surfaces. The surface irrotational flow field is torque-free and it exerts a force and a stresslet on the particle whereas the surface solenoidal flow field is force-free and stresslet-free and it exerts a torque on the particle. For a drop (both clean and surfactant laden), the surface solenoidal flow field is torque-free too. For a drop covered with an incompressible surfactant with zero surfactant diffusivity, the surface irrotational flow field due to a surfactant-laden-drop is the same as that due to a rigid sphere. Due to this reason, the force and the stresslet experienced by a surfactant-laden-drop are independent of the viscosity ratio and the interfacial

viscosity; also this force and stresslet are the same as those experienced by a rigid sphere.

3. LOCOMOTION INSIDE A SURFACTANT LADEN DROP AT LOW SURFACE PÉCLET NUMBERS

3.1 Introduction

Locomotion of motile microorganisms near a wall/interface is ubiquitous in nature, due to which there has been a large body of literature to explain the available experimental observations (see sections on swimming near surfaces in [19, 61]). The presence of a non-deforming wall/interface can influence the dynamics of a swimming microorganism near it in a few ways. First, it can modify the speed of a microorganism. For instance, a Taylor's swimming sheet, with a fixed waveform, is found to swim faster near a wall than that in bulk [62,63]. Second, it can modify the trajectory of a microorganism. For instance, microorganisms such as *Escherichia coli* (*E. coli*), which swim in straight lines in the bulk, are found to swim in circles near a plane interface [64, 65]. The direction of rotation (clockwise or anticlockwise) depends on any slip on the plane wall, viscosity ratio of the plane interface and the advection of the impurities (if any) on the plane interface [8]. Third, the wall/interface causes the reorientation and attraction of microorganisms towards it. For instance, pusher swimmers (e.g., *E. coli*) reorient parallel to a plane wall and move towards the wall. On the other hand, puller swimmers (e.g., *Chlamydomonas*) reorient normal to a plane wall and collide with it. One can explain the reorientation and attraction to the wall using either (a) the hydrodynamic interactions between the swimmer and the wall [8,23,24] or (b) the self-propulsion and Brownian motion of the swimmer [66,67].

Among the works on the motion of a motile microorganism near an interface, some have focused on the influence of (a) interface deformation [9, 68–70], (b) non-

This chapter has been reproduced with permission from the article "Locomotion inside a surfactant laden drop at low surface Péclet numbers", by V. A. Shaik, V. Vasani and A. M. Ardekani, Journal of Fluid Mechanics, 851:187-230, 2018 (DOI: 10.1017/jfm.2018.491).

Newtonian fluid behavior [71, 72] and (c) the surfactant advection [8, 16, 73] on the dynamics of the swimmer. It was found that the attraction and reorientation behavior of a pusher swimmer near a plane surfactant laden interface is similar to that near a plane wall, but the surfactant redistribution can cause the microorganism to circle the interface in an opposite direction as compared to its circling near a clean interface [8]. Later, it was observed that the swimming microorganism gets trapped onto a spherical surfactant laden drop similar to its trapping onto a rigid sphere, but the trapping due to a surfactant laden drop is stronger than that due to a rigid sphere [16, 73]. These works on the locomotion of swimming microorganisms near a plane/spherical surfactant laden interface modeled the surfactant as incompressible [74–77] with zero surface diffusivity (surface Péclet number, Pe_s, ratio of the surface advection to the surface diffusion of the surfactant, tends to infinity) accounting for the interfacial viscosity. We analyze the locomotion of swimming microorganism near a surfactant covered interface in the other limit of surface Péclet number i.e., low surface Péclet number at which the surface diffusion of the surfactant dominates its surface advection.

An artificial/biological micro-swimmer must break the time-reversal symmetry (getting around the constraints of the scallop theorem) in order to swim at low Reynolds number [11]. It can escape from the constraints of the scallop theorem through one of the following ways [12] (a) by passing waves along its flagella or the whole body, (b) by rotating the flexible flagella, (c) through the finite inertia of the fluid or the swimmer, (d) through the hydrodynamic interactions with a flexible membrane/interface, (e) due to the non-Newtonian behavior of the suspending fluid. In other words, the scallop theorem is not valid if there are any time-derivative terms or nonlinear terms in the governing equations and the boundary conditions.

Particles and drops, on the other hand, exhibit several interesting phenomena due to such nonlinearities [78]. For instance, either due to inertia, non-Newtonian suspending fluid or the deformation of the particle/drop, (a) a spherical particle placed in a unidirectional shear/Poiseuille flow field migrates in a transverse direction to a fixed

position that is independent of its initial position, (b) a sedimenting axisymmetric particle in an unbounded quiescent fluid achieves an orientation that is independent of its initial orientation and (c) a freely rotating axisymmetric particle placed in a simple shear flow achieves a final orbit that is independent of its initial orientation. Recent works [27–29]showed that the transverse migration of the drop, in an unbounded Poiseuille flow, to a fixed position is also possible due to the nonlinearities in the advection of the surfactant on the surface of the drop.

In summary, nonlinearities in the flow can enable a particle to achieve a fixed position/orientation independent of its initial configuration while they can also make a swimming microorganism to display a net motion. Since such breakdown of kinematic reversibility is recently shown in the context of surfactant laden drop achieving a fixed position (nonlinearities due to the surfactant redistribution), we would like to know if a time-reversible swimmer near a surfactant laden interface can have a net motion.

In this work, we study the locomotion of a spherical microswimmer inside a surfactant laden drop for axisymmetric configurations by taking a perturbation in Pe_s. A similar work, but on the locomotion inside a clean drop, was carried out by Reigh *et al.* [79]. One of the applications of our work is to understand the physics underlying the recent experiments on using the artificial bacterial flagella (ABF) to transport a surfactant-laden-drop [7]. According to Ding *et al.* [7], ABFs placed inside a stationary drop (since the size of the drop is larger than the microfluidic channel in which it resides, the drop is stationary) can transport the contents within the drop through the application of magnetic field. As mentioned by Reigh *et al.* [79], if the radius of the drop is smaller than the characteristic size of the microfluidic channel and the drops affinity to the wall is negligible, an ABF placed inside a drop can propel the drop, similar to the system studied in this paper.

The governing equations (Stokes) and boundary conditions concerning the locomotion of a spherical swimmer inside a surfactant covered drop are provided in Sec. 3.2. For the concentric configuration, the procedure for solving the Stokes equations using the Lamb's general solution is given in Sec. 3.3.1. For the eccentric configura-

tions, the methodology for solving the dynamic equation for the stream function in the bipolar coordinates is given in Sec. 3.3.2. We present the results of the concentric and the eccentric configurations in Sec. 3.4.1 and Sec. 3.4.2, providing reasons for the results in Sec. 3.4.2 using the drag and thrust analogy in Sec. 3.4.3. We then discuss how a time-reversible swimmer inside a surfactant laden drop escapes from the constraints of the scallop theorem in Sec. 3.4.4 and provide the main conclusions in Sec. 6.6. The technical details of several derivations, expressions for the flow field, conversion between different coordinate systems and the validation of bipolar coordinate system results are given in the Appendices.

3.2 Mathematical Model

Consider the motion of a swimming microorganism inside a surfactant laden drop, with the orientation of the swimmer along the line joining the centers of the swimmer and the drop. Assuming the Capillary number (ratio of the bulk viscous stress to the capillary stresses), $Ca \ll 1$, we neglect the deformation of the drop and regard the shape of the drop and the swimmer as sphere. The swimmer propels and through the hydrodynamic interactions, it causes the drop to move. We hereby formulate this problem in the frame of reference of the drop. The flow fields inside (phase 1) and outside the drop (phase 2) are governed by the creeping motion equations and an incompressibility condition since the inertia of the fluid can be neglected. Using the characteristic scales for the length, velocity and the stresses as the radius of the drop 'a', characteristic velocity of the swimmer in an unbounded fluid U_{sq} and $\mu^{(k)}U_{sq}/a$, where $\mu^{(k)}$ is the dynamic viscosity of the k-th phase, the dimensionless governing equations are given by

$$\nabla p^{(k)} = \nabla^2 \mathbf{v}^{(k)};\ \nabla \cdot \mathbf{v}^{(k)} = 0,\ \text{where } k = 1, 2. \tag{3.1}$$

Here, $p^{(k)}$ and $\mathbf{v}^{(k)}$ denote the pressure and the velocity of the k-th phase. The fluid inside the drop should satisfy the no-slip and no-penetration boundary conditions on the surface of the swimmer

$$\text{On the swimmer} : \mathbf{v}^{(1)} = \mathbf{U}_S - \mathbf{U}_D + \mathbf{u}^s, \tag{3.2}$$

where $\mathbf{U}_S = U_S\,\mathbf{i}_z$ and $\mathbf{U}_D = U_D\,\mathbf{i}_z$ are the velocities of the swimmer and the drop, respectively, $\mathbf{u}^s$ denotes the slip velocity on the surface of the swimmer and $\mathbf{i}_z$ is the unit vector along the z-axis. The swimmer and the drop are assumed to be neutrally buoyant. Since the external force acting on the drop and the swimmer is zero, the hydrodynamic force acting on each of them ($\mathbf{F}_S$: hydrodynamic force on the swimmer, and $\mathbf{F}_D$: hydrodynamic force on the drop) should be zero

$$\mathbf{F}_S = \int_S \mathbf{n} \cdot T^{(1)} dS = \mathbf{0}, \tag{3.3}$$

$$\mathbf{F}_D = \int_D \mathbf{n} \cdot T^{(2)} dS = \mathbf{0}, \tag{3.4}$$

where $\mathbf{n}$ is the normal vector on the surface of the swimmer (drop) pointing into the suspending fluid, $T^{(k)}$ is the stress tensor for the k-th phase, dS is an infinitesimal surface area on the surface of the swimmer (drop) and the integration is performed on the surface of the swimmer (drop). Using the Newtonian constitutive equation, the stress tensor for the k-th phase can be expressed as $T^{(k)} = -p^{(k)}I + \left[\nabla\mathbf{v}^{(k)} + \left(\nabla\mathbf{v}^{(k)}\right)^T\right]$ where I is the identity tensor and the superscript T stands for the transpose. In the frame of reference of the drop, the flow field far away from the drop should approach the negative of the drop velocity

$$\text{Far away from the drop} : \mathbf{v}^{(2)} = -\mathbf{U}_D. \tag{3.5}$$

At the surface of the drop, the flow field in both the phases should satisfy the kinematic, dynamic and the stress balance conditions. Since the drop is non-deforming and stationary, the kinematic and dynamic conditions are given as

$$\text{On the drop} : \mathbf{v}^{(1)} \cdot \mathbf{n} = \mathbf{v}^{(2)} \cdot \mathbf{n} = 0, \tag{3.6}$$

$$\text{On the drop} : \mathbf{v}^{(1)} \cdot \mathbf{\Delta} = \mathbf{v}^{(2)} \cdot \mathbf{\Delta}, \text{ where } \mathbf{\Delta} = I - \mathbf{nn}. \tag{3.7}$$

Similarly, the dimensional tangential stress balance condition is given as

$$\text{On the drop} : \mathbf{n} \cdot \left(T^{(2)} - T^{(1)}\right) \cdot \mathbf{\Delta} = -\nabla_s \gamma,$$

where γ is the interfacial tension and the surface gradient operator is $\nabla_s = \mathbf{\Delta} \cdot \nabla$. In general, the interfacial tension depends on the surfactant concentration (Γ). Assuming the local surfactant cocentration (Γ) is much smaller than the maximum possible surfactant concentration on the interface (Γ_∞), i.e., $\Gamma/\Gamma_\infty \ll 1$, we use a linear constitutive relationship between the interfacial tension and the surfactant concentration, which, in its dimensional form is given as $\gamma = \gamma_s - \Gamma RT$. Here γ_s is the interfacial tension of the clean interface, R is the ideal gas constant and T is the absolute temperature. Enforcing this relation in the stress balance equation and non-dimensionalizing it using $\Gamma_{ref} = \Gamma_{eq}$ (equilibrium concentration of surfactant), we derive the dimensionless tangential stress balance condition as

$$\text{On the drop} : \mathbf{n} \cdot \left(T^{(2)} - \lambda T^{(1)}\right) \cdot \mathbf{\Delta} = Ma\, \nabla_s \Gamma. \tag{3.8}$$

Here, $\lambda = \mu^{(1)}/\mu^{(2)}$ is the viscosity ratio and $Ma = RT\Gamma_{eq}/\left(\mu^{(2)} U_{sq}\right)$ is the Marangoni number which is the ratio of the Marangoni forces to the viscous forces.

Finally, the surfactant transport equation [18, 51] governs the distribution of surfactant on the drop surface. We simplify the surfactant transport equation in the limits of insoluble surfactant and quasi-steady state conditions [27,29,80]. In the insoluble limit, bulk surfactant does not influence the surfactant distribution on the interface. This limit is valid when $c_\infty a/\left(\Gamma_{eq} Pe^{(1)}\right) \ll O(1)$ and $c_\infty a/\left(\Gamma_{eq} Pe^{(2)}\right) \ll O(1)$ or $Bi = \alpha^{(2)} a/U_{sq} \ll O(1)$. Here c_∞ is a reference bulk concentration of the surfactant, $Pe^{(k)}$ is the Péclet number defined as the ratio of the bulk advection of the surfactant to its bulk diffusion in the k-th fluid, Bi is the Biot number characterizing the strength of kinetic desorption relative to the interfacial convection and $\alpha^{(2)}$ is

the desoprtion rate constant. In these limits, the dimensionless surfactant transport equation is given as

$$Pe_s \nabla_s \cdot (\Gamma \, \mathbf{v}_s) = \nabla_s^2 \Gamma. \tag{3.9}$$

Here, $Pe_s = U_{sq} a / D_s$ is the surface or interface Péclet number, D_s is the surface or interface diffusivity and $\mathbf{v}_s$ is the tangential velocity of the fluid on the surface of the drop, i.e., $\mathbf{v}_s = \boldsymbol{\Delta} \cdot \mathbf{v}^{(1)}\big|_{Drop} = \boldsymbol{\Delta} \cdot \mathbf{v}^{(2)}\big|_{Drop}$.

The problem governed by equations (3.1)-(3.9) is essentially nonlinear, so we need to make an assumption to analytically solve these equations. We assume $Pe_s \ll 1$ and expand all the variables as a regular perturbation in Pe_s.

$$\left\{\mathbf{v}^{(k)}, p^{(k)}, T^{(k)}, \Gamma, \mathbf{U}_S, \mathbf{U}_D\right\} = \sum_{j=0}^{\infty} Pe_s^j \left\{\mathbf{v}_j^{(k)}, p_j^{(k)}, T_j^{(k)}, \Gamma_j, \mathbf{U}_{j,S}, \mathbf{U}_{j,D}\right\}. \tag{3.10}$$

Substituting this expansion in equations (3.1)-(3.9) and collecting terms at various orders of Pe_s, we derive the governing equations and boundary conditions at several orders of Pe_s which are summarized in the following subsection.

3.2.1 Governing equations and boundary conditions at various orders of Pe_s

The flow field at each order of Pe_s satisfies the creeping flow equations and an incompressibility condition

$$\nabla p_j^{(k)} = \nabla^2 \mathbf{v}_j^{(k)}; \;\; \nabla \cdot \mathbf{v}_j^{(k)} = 0, \;\; \text{where } k = 1, 2. \tag{3.11}$$

Assuming the slip velocity $\mathbf{u}^s$ is $O(1)$, the flow field should satisfy the following boundary condition on the swimmer

$$\text{On the swimmer}: \;\; \mathbf{v}_j^{(1)} = \mathbf{U}_{j,S} - \mathbf{U}_{j,D} + \delta_{j,0} \mathbf{u}^s, \tag{3.12}$$

where $\delta_{j,0}$ is the Kronecker delta. The force-free conditions on the swimmer and the drop are given as

$$\mathbf{F}_{j,S} = \int_S \mathbf{n} \cdot T_j^{(1)} dS = \mathbf{0}, \tag{3.13}$$

$$\mathbf{F}_{j,D} = \int_D \mathbf{n} \cdot T_j^{(2)} dS = \mathbf{0}. \tag{3.14}$$

Far away from the drop, the flow field should approach the negative of the drop velocity at various orders of Pe_s

$$\text{Far away from the drop}: \ \mathbf{v}_j^{(2)} = -\mathbf{U}_{j,D}. \tag{3.15}$$

On the surface of the drop, the kinematic, dynamic and the shear-stress balance conditions are given as

$$\text{On the drop}: \ \mathbf{v}_j^{(1)} \cdot \mathbf{n} = \mathbf{v}_j^{(2)} \cdot \mathbf{n} = 0, \tag{3.16}$$

$$\text{On the drop}: \ \mathbf{v}_j^{(1)} \cdot \mathbf{\Delta} = \mathbf{v}_j^{(2)} \cdot \mathbf{\Delta}, \tag{3.17}$$

$$\text{On the drop}: \ \mathbf{n} \cdot \left(T_j^{(2)} - \lambda T_j^{(1)} \right) \cdot \mathbf{\Delta} = Ma \, \nabla_s \Gamma_j. \tag{3.18}$$

The perturbed surfactant transport equations at different orders of Pe_s are given as

$$\text{At } O(1): \ \nabla_s^2 \Gamma_0 = 0 \Rightarrow \Gamma_0 = 1, \tag{3.19}$$

$$\text{At } O(Pe_s): \ \nabla_s \cdot (\Gamma_0 \mathbf{v}_{0,s}) = \nabla_s^2 \Gamma_1, \tag{3.20}$$

$$\text{At } O\left(Pe_s^2\right): \ \nabla_s \cdot (\Gamma_0 \mathbf{v}_{1,s} + \Gamma_1 \mathbf{v}_{0,s}) = \nabla_s^2 \Gamma_2, \tag{3.21}$$

where $\mathbf{v}_{j,s}$ is the tangential velocity of the fluid at $O(Pe_s^j)$ evaluated on the surface of the drop, i.e., $\mathbf{v}_{j,s} = \mathbf{\Delta} \cdot \mathbf{v}_j^{(1)}\Big|_{Drop} = \mathbf{\Delta} \cdot \mathbf{v}_j^{(2)}\Big|_{Drop}$.

3.3 Solution Methodology

In this section, we describe the techniques used to solve the above mentioned perturbed equations for axisymmetric configurations. For all non-zero values of eccentricities, we use the bipolar coordinates approach to solve for the stream function.

For the concentric configuration, since the bipolar coordinate solution is singular, we use the Lamb's general solution to solve for the flow field. Solving for the concentric configuration is especially important, as the expressions for the flow field are simple and hence they can be used to describe the underlying physics.

When the perturbation is taken in Pe_s [29], the key idea is to first find the surfactant concentration at $O\left(Pe_s^j\right)$ $\left(\Gamma_j\right)$ by solving the surfactant transport equation at the same order in Pe_s. This equation can be solved to determine Γ_j because it contains only the flow field and surfactant concentrations at lower orders of Pe_s, which are known quantities (see equations (3.19)-(3.21) for instance). Once Γ_j is found, one can use it to solve the Stokes equations at $O\left(Pe_s^j\right)$ so as to find the swimmer and drop velocities at $O\left(Pe_s^j\right)$. Instead, one can avoid the process of solving for $O\left(Pe_s^j\right)$ flow field and use an integral theorem to directly find the $O\left(Pe_s^j\right)$ swimmer and drop velocities from the knowledge of $O\left(Pe_s^j\right)$ surfactant concentration and the solution of two auxiliary problems. We direct the reader to Appendix 3.8 for a detailed derivation of this integral theorem, equations (3.90)-(3.91) and a demonstration of the use of this integral theorem in calculating the swimmer and drop velocities. We, however, do not use this integral theorem and use the former approach of solving the Stokes equations at any order of Pe_s to find the swimmer and drop velocities at that order in Pe_s.

We further note that the surfactant concentration at $O\left(1\right)$ is uniform $\left(\Gamma_0 = 1\right)$ and hence the Marangoni term, proportional to the gradient of the surfactant concentration, is zero. Therefore, the flow field and the dynamics of the swimmer and the drop at $O\left(1\right)$ are the same as those for the motion of a swimmer inside a clean drop. Reigh *et al.* [79] studied the motion of a swimmer inside a clean drop for concentric and eccentric configurations using the Lamb's general solution and the boundary element method, respectively. Analytical results given in the present study recovers their results in the limit of zero Pe_s or Ma, corresponding to a clean drop.

3.3.1 Concentric configuration

In this section, we provide the methodology to derive the surfactant concentration, flow field, swimmer and drop velocities at $O\left(Pe_s^j\right)$ when the swimmer is located at the center of the drop. We hereby place the origin at the center of the drop and choose a spherical coordinate system (see figure 3.1 for the schematic), the most suitable coordinate system for the concentric configuration. In this coordinate system, the surface of the drop is located at $r = 1$, while the surface of the swimmer is at $r = \chi$.

The most general form for the surfactant transport equation at $O\left(Pe_s^j\right)$, where $j \geq 1$, is given as

$$\nabla_s^2 \Gamma_j = f\left(\Gamma_0, \Gamma_1, ...\Gamma_{j-1}, \mathbf{v}_{0,s}, \mathbf{v}_{1,s}, ...\mathbf{v}_{j-1,s}\right). \tag{3.22}$$

We expand the surfactant concentration Γ_j in terms of the Legendre polynomials [29, 60, 80]

$$\Gamma_j = \sum_{n=1}^{\infty} \Gamma_{j,n} P_n\left(\cos\theta\right),$$

where $\Gamma_{j,n}$ is a constant and θ is the polar angle. We then substitute this expansion in the left hand side of the surfactant transport equation (equation (3.22)) and use the orthogonality of the Legendre polynomials to determine $\Gamma_{j,n}$.

Using the Lamb's general solution [1] for the axisymmetric configuration, we write the flow field in the k-th phase as

$$\mathbf{v}_j^{(k)} = \sum_{n=-\infty}^{\infty} \left[\nabla \phi_{j,n}^{(k)} + \frac{n+3}{2\left(n+1\right)\left(2n+3\right)} r^2 \nabla p_{j,n}^{(k)} - \frac{n}{\left(n+1\right)\left(2n+3\right)} \mathbf{r} p_{j,n}^{(k)}\right], \tag{3.23}$$

where $\phi_{j,n}^{(k)}$ and $p_{j,n}^{(k)}$ are the solid spherical harmonics, $\mathbf{r} = r\,\mathbf{i}_r$ and $\mathbf{i}_r$ is the unit vector in the radial direction. For axisymmetric flows, we can write these harmonics in terms of the Legendre polynomials as

$$p_{j,n}^{(k)} = \tilde{p}_{j,n}^{(k)} r^n P_n\left(\cos\theta\right), \;\; \phi_{j,n}^{(k)} = \tilde{\phi}_{j,n}^{(k)} r^n P_n\left(\cos\theta\right),$$

where $\tilde{p}_{j,n}^{(k)}$ and $\tilde{\phi}_{j,n}^{(k)}$ are arbitrary constants. Following Reigh *et al.* [79], we modify these constants as follows

$$\bar{p}_{j,n}^{(k)} = \frac{n}{2\left(2n+3\right)} \tilde{p}_{j,n}^{(k)}; \;\; \bar{\phi}_{j,n}^{(k)} = n\tilde{\phi}_{j,n}^{(k)},$$

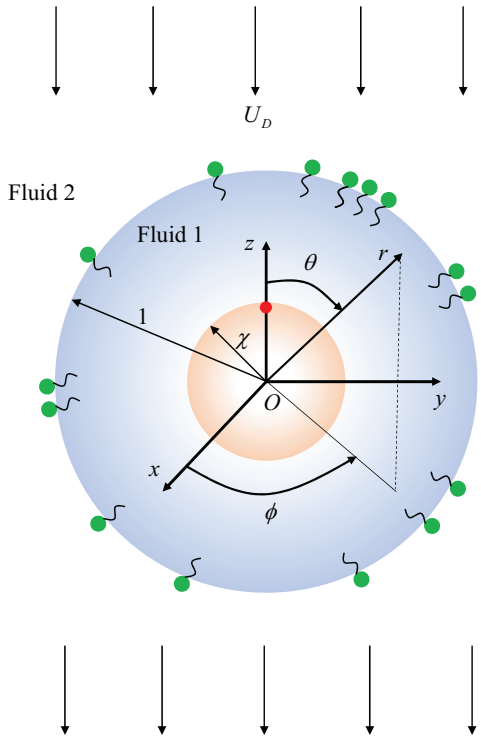

Figure 3.1. : A schematic showing the geometric configuration of a swimmer located at the center of the drop. A vector from the swimmer's center to the red circle gives the orientation of the swimmer. The origin O is coincident with the center of the swimmer and the drop. (x, y, z) and (r, θ, ϕ) denote the cartesian and spherical coordinate variables, respectively. $r = 1$ and $r = \chi$ denote the surface of the drop and the swimmer, respectively. We denote the fluid inside and outside the drop as phase 1 and phase 2, respectively. In the drop frame of reference, the drop is stationary and it is placed in a uniform streaming flow, $-U_D\,\mathbf{i}_z$.

where $\bar{p}_{j,n}^{(k)}$ and $\bar{\phi}_{j,n}^{(k)}$ are again arbitrary constants. Hence, the radial and tangential components of flow field at $O\left(Pe_s^j\right)$ and in the k-th phase are given as

$$v_{j,r}^{(k)} = \sum_{n=0}^{\infty} \left[\bar{p}_{j,n}^{(k)} r^{n+1} + \bar{\phi}_{j,n}^{(k)} r^{n-1} + \bar{p}_{j,-n-1}^{(k)} r^{-n} + \bar{\phi}_{j,-n-1}^{(k)} r^{-n-2} \right] P_n\left(\cos\theta\right), \tag{3.24}$$

$$v_{j,\theta}^{(k)} = \sum_{n=1}^{\infty} \left[\begin{array}{l} -\dfrac{(n+3)}{2} \bar{p}_{j,n}^{(k)} r^{n+1} - \dfrac{(n+1)}{2} \bar{\phi}_{j,n}^{(k)} r^{n-1} \\ +\dfrac{(n-2)}{2} \bar{p}_{j,-n-1}^{(k)} r^{-n} + \dfrac{n}{2} \bar{\phi}_{j,-n-1}^{(k)} r^{-n-2} \end{array} \right] V_n\left(\cos\theta\right), \tag{3.25}$$

where $\frac{dP_n(\cos\theta)}{d\theta} = -\frac{n(n+1)}{2} V_n\left(\cos\theta\right) = -P_n^1\left(\cos\theta\right)$ and P_n^1 is the associated Legendre polynomial of the first order. Substituting these expressions for the velocity components into the expression for the stress tensor on the surface of a sphere, given in Happel & Brenner [1], we derive an expression for the tangential stress, $T_{j,r\theta}^{(k)}$ as

$$T_{j,r\theta}^{(k)} = \sum_{n=1}^{\infty} -\frac{1}{r} \left[\begin{array}{l} \left(n^2-1\right) r^{n-1} \bar{\phi}_{j,n}^{(k)} + n\left(n+2\right) r^{n+1} \bar{p}_{j,n}^{(k)} \\ +n\left(n+2\right) r^{-n-2} \bar{\phi}_{j,-n-1}^{(k)} + \left(n^2-1\right) r^{-n} \bar{p}_{j,-n-1}^{(k)} \end{array} \right] V_n\left(\cos\theta\right). \tag{3.26}$$

We substitute the expressions for the flow field, shear stress and the surfactant concentration in the boundary conditions (equations (3.12)-(3.18)) and use the orthogonality of the Legendre polynomials to derive a system of linear equations in the unknowns – $\bar{p}_{j,n}^{(1)}$, $\bar{p}_{j,-n-1}^{(1)}$, $\bar{p}_{j,n}^{(2)}$, $\bar{p}_{j,-n-1}^{(2)}$, $\bar{\phi}_{j,n}^{(1)}$, $\bar{\phi}_{j,-n-1}^{(1)}$, $\bar{\phi}_{j,n}^{(2)}$, $\bar{\phi}_{j,-n-1}^{(2)}$, $U_{j,S}$ and $U_{j,D}$. We then solve this system of linear algebraic equations to determine the flow field, swimmer and drop velocities at this order in Pe_s. We summarize the algebraic equations obtained in satisfying the boundary conditions (equations (3.12)-(3.18)) in Appendix 3.6. For a squirmer with both radial and tangential modes located at the center of the drop, we provide the expressions for the surfactant concentration, flow field, swimmer and drop velocities at $O\left(1\right)$, $O\left(Pe_s\right)$ and $O\left(Pe_s^2\right)$ in Appendix 3.7.

3.3.2 Eccentric configurations

In this section, we provide a method to evaluate the swimmer and drop velocities for an eccentrically located swimmer inside a drop. To simplify the calculation, we

derive these velocities accurate to $O(Pe_s)$. For this purpose, we solve the dynamic equation for stream function in the bipolar coordinates. A useful relation between the cylindrical coordinate variables (ρ, z, ϕ) and the bipolar coordinate variables (ξ, η, ϕ) is given as

$$z = \frac{c \sinh \xi}{\cosh \xi - \cos \eta}, \ \rho = \frac{c \sin \eta}{\cosh \xi - \cos \eta}, \tag{3.27}$$

where c is a constant that depends on the specific geometric configuration (the radii of the swimmer and the drop and the separation between them). In the bipolar coordinates, the surfaces generated by ξ = constant are eccentric non-intersecting spheres. We therefore denote the surface of the swimmer as $\xi = \xi_S$ and that of drop as $\xi = \xi_D$. There are two possibilities for eccentric configurations namely swimmer lying above or below the drop. For swimmer above (below) the drop, we place the origin of the coordinate system above (below) the drop, corresponding to ξ_S and $\xi_D < 0$ (ξ_S and $\xi_\mathrm{D} > 0$) (see figure 3.2 for the schematic of the problem). Explicit expressions for ξ_S, ξ_D and c are given as

$$\xi_S = \mp \cosh^{-1}\left(\frac{1-\chi^2-d^2}{2d\chi}\right); \ \xi_D = \mp \cosh^{-1}\left(\frac{1-\chi^2+d^2}{2d}\right); \ c = |\sinh \xi_D| \tag{3.28}$$

where $d = |e|$ and $e = z_S - z_D$. Here z_S and z_D denote the z-coordinate of the center of the swimmer and the drop, respectively. Also the minus (plus) sign should be used for a swimmer located above (below) the drop.

In the bipolar coordinates, the velocity components are related to the stream function via

$$v_{j,\xi}^{(k)} = \frac{h}{\rho}\frac{\partial \psi_j^{(k)}}{\partial \eta}; \ v_{j,\eta}^{(k)} = -\frac{h}{\rho}\frac{\partial \psi_j^{(k)}}{\partial \xi}, \tag{3.29}$$

where $h = (\cosh \xi - \cos \eta)/c$ is one of the metrical coefficient of the bipolar coordinates . We enforce these relations in the creeping flow equations to derive the dynamic equation for the stream function, given as $E^4 \psi_j^{(k)} = 0$, where

$$E^2 = \rho h^2 \left[\frac{\partial}{\partial \xi}\left(\frac{1}{\rho}\frac{\partial}{\partial \xi}\right) + \frac{\partial}{\partial \eta}\left(\frac{1}{\rho}\frac{\partial}{\partial \eta}\right)\right] \tag{3.30}$$

Similarly, one can express the boundary conditions given by equations (3.12) and (3.16)-(3.18) in terms of velocity components in bipolar coordinates which can be eventually written in terms of stream function using equation (3.29).

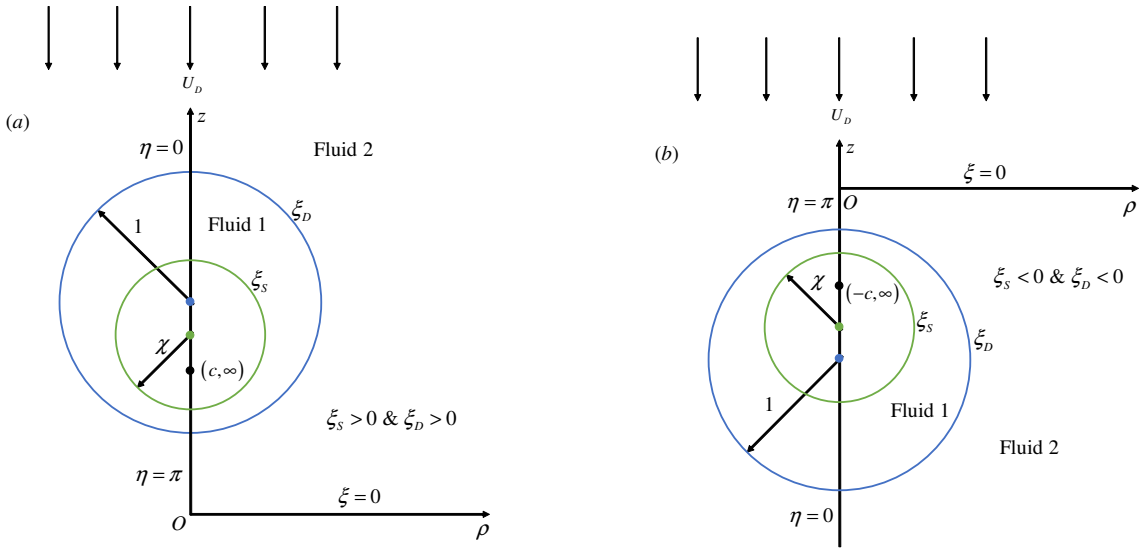

Figure 3.2. : A schematic showing the geometric configuration and its associated coordinate system for (a) swimmer located below the drop and (b) swimmer located above the drop. Here (z, ρ) and (ξ, η) denote the coordinate variables of the cylindrical and the bipolar coordinate systems, respectively. O is the origin of the coordinate systems and it is located below (above) the drop for a swimmer located below (above) the drop. $\xi = \xi_S$ and ξ_D denote the surface of the swimmer and the drop. $\xi = 0$ denote the plane $z = 0$. $\eta = 0$ and $\eta = \pi$ denote the lines $|z| \geq c$ and $|z| \leq c$, respectively. In the frame of reference of the drop, it is stationary and is placed in a uniform streaming flow, $-U_D\, \mathbf{i}_z$.

On the swimmer:

$$\begin{aligned} v_{j,\xi}^{(1)} &= \left(U_{j,S} - U_{j,D}\right)\, \mathbf{i}_z \cdot \mathbf{i}_\xi + \, \delta_{j,0}\, u_\xi^s \\ v_{j,\eta}^{(1)} &= \left(U_{j,S} - U_{j,D}\right)\, \mathbf{i}_z \cdot \mathbf{i}_\eta \, + \, \delta_{j,0} u_\eta^s \end{aligned} \tag{3.31}$$

On the drop:

$$\begin{aligned} v_{j,\xi}^{(1)} &= v_{j,\xi}^{(2)} = 0 \\ v_{j,\eta}^{(1)} &= v_{j,\eta}^{(2)} \\ -\mathrm{sgn}\left(\xi_D\right)\left(T_{j,\xi\eta}^{(2)} - \lambda T_{j,\xi\eta}^{(1)}\right) &= Ma\, h\, \frac{d\Gamma_j}{d\eta} \end{aligned} \tag{3.32}$$

where

$$T_{j,\xi\eta}^{(k)} = h\left(\frac{\partial v_{j,\xi}^{(k)}}{\partial \eta} + \frac{\partial v_{j,\eta}^{(k)}}{\partial \xi}\right) - h^2\left(v_{j,\xi}^{(k)} \frac{\partial}{\partial \eta}\left(\frac{1}{h}\right) + v_{j,\eta}^{(k)} \frac{\partial}{\partial \xi}\left(\frac{1}{h}\right)\right) \tag{3.33}$$

Here, $\mathbf{i}_\xi$ and $\mathbf{i}_\eta$ are the unit vectors in the increasing direction of ξ and η, respectively. Also u_ξ^s and u_η^s are the components of the swimmer's surface velocity in the bipolar coordinates while $\delta_{j,0}$ is the Kronecker delta. We outline the steps used for converting the swimmer's surface velocity from the spherical coordinate system to the bipolar coordinate system in Appendix 3.9. The far-field condition (equation (3.15)) gives the following condition for the stream function [1]

$$\text{As } \xi, \eta \to 0, \quad \psi_j^{(2)} \to \frac{1}{2}\rho^2 U_{j,D} \tag{3.34}$$

Stimson & Jeffery [81] derived a general solution of $E^4\psi_j^{(k)} = 0$, when E^2 is expressed in bipolar coordinates and it is given as

$$\psi_j^{(k)} = \left(\cosh\xi - \cos\eta\right)^{-3/2} \sum_{n=0}^{\infty} W_{j,n}^{(k)}\left(\xi\right)\, C_{n+1}^{-1/2}\left(\cos\eta\right) \tag{3.35}$$

where

$$W_{j,n}^{(k)} = A_{j,n}^{(k)} \cosh\left(n - \tfrac{1}{2}\right)\xi + B_{j,n}^{(k)} \sinh\left(n - \tfrac{1}{2}\right)\xi + C_{j,n}^{(k)} \cosh\left(n + \tfrac{3}{2}\right)\xi + D_{j,n}^{(k)} \sinh\left(n + \tfrac{3}{2}\right)\xi$$

Here $C_{n+1}^{-1/2}\left(\cos\eta\right)$ is a Gegenbauer polynomial [82] of order $n+1$ and degree $-1/2$ while $A_{j,n}^{(k)}$, $B_{j,n}^{(k)}$, $C_{j,n}^{(k)}$ and $D_{j,n}^{(k)}$ are the unknown constants. We substitute equation

(3.35) in the boundary conditions and the far-field condition, written in terms of the stream function, to derive 8 linear algebraic equations in the unknowns – $A^{(1)}_{j,n}$, $B^{(1)}_{j,n}$, $C^{(1)}_{j,n}$, $D^{(1)}_{j,n}$, $A^{(2)}_{j,n}$, $B^{(2)}_{j,n}$, $C^{(2)}_{j,n}$ and $D^{(2)}_{j,n}$ – at each order in Pe_s and for each n. These equations are summarized in Appendix 3.10. We then solve these equations to derive the explicit expressions for the unknowns.

As outlined in the solution methodology for concentric configuration, we first need to solve for the surfactant concentration before solving for the flow field at any order in Pe_s. The surfactant concentration at $O(1)$ is uniform and hence it is a known quantity. Since, we are solving the flow field up to $O(Pe_s)$, we need to find the surfactant concentration at $O(Pe_s)$ by solving the corresponding surfactant transport equation, equation (3.20). Using the definition of surface gradient operator in bipolar coordinates, $\nabla_s = \mathbf{i}_\eta\, h\, \frac{\partial}{\partial \eta} + \mathbf{i}_\phi \frac{1}{\rho} \frac{\partial}{\partial \phi}$, we simplify the surfactant transport equation at $O(Pe_s)$ as follows

$$\frac{d}{d\eta}\left(h \frac{d\Gamma_1}{d\eta}\right) = \frac{d\, v^{(1)}_{0,\eta}(\xi = \xi_D)}{d\eta} = \frac{d\, v^{(2)}_{0,\eta}(\xi = \xi_D)}{d\eta} \tag{3.36}$$

This equation can be easily integrated with respect to η to obtain $h\frac{d\Gamma_1}{d\eta} = v^{(1)}_{0,\eta}(\xi = \xi_D) = v^{(2)}_{0,\eta}(\xi = \xi_D)$. Since, only the gradient of the surfactant concentration affects the flow field, through the shear-stress boundary condition, equation (3.18), we use the above equation to rewrite the shear-stress boundary condition at $O(Pe_s)$ as follows.

$$-\mathrm{sgn}(\xi_D)\left(T^{(2)}_{1,\xi\eta} - \lambda T^{(1)}_{1,\xi\eta}\right) = Ma\, v^{(1)}_{0,\eta}(\xi = \xi_D) = Ma\, v^{(2)}_{0,\eta}(\xi = \xi_D) \tag{3.37}$$

Therefore, once the flow field at $O(1)$ is known, we can directly evaluate the flow field at $O(Pe_s)$ without finding the surfactant concentration at $O(Pe_s)$. Mandal *et al.* [80] provided a similar procedure for finding the flow field due to weakly deforming, surfactant laden compound drops. We used this method to derive the linear algebraic equations in the unknown coefficients provided in Appendix 3.10.

The solution of the linear algebraic equations provided in the Appendix 3.10 furnishes the explicit expressions for the unknown coefficients in $W^{(k)}_{j,n}$. These coefficients

are linear in the swimmer and drop velocities at any order in Pe_s. For instance, the coefficient $A_{j,n}^{(k)}$ is given as

$$A_{j,n}^{(k)} = Q_{j,n}^{(k)}\left(\lambda, \chi, Ma\right)\, U_{j,S} + R_{j,n}^{(k)}\left(\lambda, \chi, Ma\right)\, U_{j,D} \,+\, S_{j,n}^{(k)}\left(\lambda, \chi, Ma\right) \tag{3.38}$$

where $Q_{j,n}^{(k)}$, $R_{j,n}^{(k)}$ and $S_{j,n}^{(k)}$ are the functions of χ, λ and Ma. We then impose the force-free conditions for the swimmer and the drop given as [1, 81, 83, 84]

$$\sum_{n=1}^{\infty}\left[A_{j,n}^{(1)} + C_{j,n}^{(1)} + \mathrm{sgn}\left(\xi_S\right)\left(B_{j,n}^{(1)} + D_{j,n}^{(1)}\right)\right] = 0 \tag{3.39}$$

$$\sum_{n=1}^{\infty}\left[A_{j,n}^{(2)} + C_{j,n}^{(2)} + \mathrm{sgn}\left(\xi_D\right)\left(B_{j,n}^{(2)} + D_{j,n}^{(2)}\right)\right] = 0 \tag{3.40}$$

We solve these two equations to find the swimmer and drop velocities at any order in Pe_s. Since, these two equations contain an infinite number of coefficients, we truncate this sum to a finite number N such that the error in the evaluation of the swimmer and drop velocities is less than 10^{-6}.

3.4 Results and Discussion

We note that the formulation provided in the previous two sections is entirely general as long as the swimmer's surface velocity $\mathbf{u}^s$ is axisymmetric. To perform further analysis, we need to choose a specific functional form for $\mathbf{u}^s$. For this purpose, we model the swimmer as 'squirmer' having both radial and tangential modes. Such model is used to describe the ciliated microorganisms which propel through the metachronal beating of flexible cilia on their surface. According to this model [14,15], one does not worry about the individual cilia but instead apply a boundary condition for the velocity on a spherical surface that encompasses the cilia. Hence, the slip velocity on the squirmer's surface, $\mathbf{u}^s$ is given as

$$\mathbf{u}^s = \sum_{n=0}^{\infty} A_n\, P_n\left(\cos\theta\right)\, \mathbf{i}_r + \sum_{n=1}^{\infty} B_n\, V_n\left(\cos\theta\right) \mathbf{i}_\theta \tag{3.41}$$

where $\mathbf{i}_r$ and $\mathbf{i}_\theta$ are the unit vectors in the radial and the polar directions with the origin located at the center of the squirmer while A_n and B_n are known constants, the

so called modes of a squirmer. We, however, do not consider the A_0 mode since there is no solution of the governing equations satisfying all the boundary conditions when such a swimmer (squirmer having only A_0 mode) is located inside a drop. A squirmer, possessing only the tangential squirming modes, moves with a speed of $U_{sq} = 2\,B_1/3$ in an unbounded quiescent fluid and we can represent the flow field far away from it by placing a force dipole at its center, the strength of which depends on B_2 mode. Since the swimming velocity and the far-field hydrodynamics are dictated by only B_1 and B_2 modes, we can discard all other modes and study the hydrodynamics of this two-mode squirmer whose flow field is characterized by a single parameter, $\beta = B_2/B_1$. The swimmers possessing $\beta < 0$ are called the pushers and they swim by repelling fluid along their axis while drawing the fluid along the sides. The swimmers having $\beta > 0$ are called the pullers and they swim by repelling fluid along their sides while drawing the fluid along their axis. The swimmers having $\beta = 0$ are called neutral swimmers and their flow field is represented by a degenerate quadrupole placed at the center of the squirmer. Due to its mathematical simplicity, the two-mode squirmer model was used vastly in the literature to study several physical processes involving microswimmers [9, 85–87]. Due to this reason, we present most of our results for this two-mode squirmer. The analyses in Secs. 3.4.1, 3.4.2, 3.4.3 and 3.4.4 are carried out for a two-mode squirmer while the analysis in subsection (Coswimming) is valid for a three-mode squirmer possessing A_1, B_1, and B_2 modes. For a swimmer at the center of the drop, since the velocity of the swimmer and the drop depend only on A_1 and B_1 modes, we note that the results and discussion provided in Sec. 3.4.1 (Sec. 3.4.1) are valid for a swimmer with more general boundary conditions - a swimmer with 'n' tangential squirming modes (a swimmer with both tangential and radial squirming modes as long as A_1 mode is chosen according to equation (3.55)).

Recall the perturbation scheme, $\mathbf{v} = \mathbf{v}_0 + Pe_s\mathbf{v}_1 + O\,(Pe_s^2)$. Since $\mathbf{v}_1 \propto Ma$, we can write $\mathbf{v}_1 = Ma\,\widehat{\mathbf{v}}_1$, hence $\mathbf{v} = \mathbf{v}_0 + Pe_s\,Ma\,\widehat{\mathbf{v}}_1$. In our case, $\widehat{\mathbf{v}}_1$ is at most $O\,(0.1)$ (for instance, see figure 3.5b for the $O\,(Pe_s)$ flow field due to a pusher swimmer at

the center of drop at $Ma = 1$). So, for small Pe_s analysis to be valid, Ma can be at most $O(10)$.

We give a justification for the range of parameter values used in this paper. We assume that water droplets are immersed in oil and take the viscosity of oil to lie in the range $0.1\mu_{\text{water}}$ to $10\mu_{\text{water}}$, where μ_{water} is the dynamic viscosity of the water. So, λ lies in between 0.1 to 10. This assumption of water in oil drops is in accordance with the experiments of Ding *et al.* [7], where $\mu_{\text{oil}} = 4.6\mu_{\text{water}}$ (for FC-40) also lies in the range of oil viscosities used in this manuscript. We take the size ratio, χ, to lie in the range 0 to 1, where $\chi \ll 1$ means the size of the swimmer is much smaller than the drop size (this is similar to the experiments [7]). On the other hand, $\chi \to 1$ means that the swimmer and the drop are approximately of the same size. We note that the speed of an *E. coli* or an ABF in an unbounded fluid is $U_{sq} \approx 10\,\mu$m/s [7, 19]. Since the size of an *E. coli* or an ABF is [7, 19] $1 - 10\,\mu$m, we take the size of the drop to lie in the range, $a \approx 1 - 100\,\mu$m. Also, we choose the equilibrium surfactant concentration and the surface diffusivity of the surfactant to lie in the range [88], $\Gamma_{eq} \approx 10^{-13} - 10^{-10}\,\text{mol/cm}^2$ and $D_s \approx 10^{-6} - 10^{-5}\,\text{cm}^2/s$. Using these parameter values, we determine the surface Péclet number and the Marangoni number to lie in the range, $Pe_s \approx O\left(10^{-2} - 10\right)$ and $Ma \approx O\left(10 - 10^6\right)$. Noting that $\Gamma_{eq} = 0$ or $Ma = 0$ for a clean drop, we extend the range of Marangoni number to $Ma \approx 0 - O\left(10^6\right)$ so as to include the scenarios of a clean drop or very small surfactant concentrations. As a small surface Péclet calculation is done in this paper, we choose $Pe_s \approx O\left(10^{-2} - 10^{-1}\right)$ and $Ma \approx 0 - O(10)$.

3.4.1 Concentric configuration

Swimmer and drop velocities

The swimmer and drop velocities accurate to $O(Pe_s)$ are given as (noting that $\mathbf{U}_S = U_S\mathbf{i}_z; \mathbf{U}_{j,S} = U_{j,S}\mathbf{i}_z;\ \mathbf{U}_D = U_D\,\mathbf{i}_z;\ \mathbf{U}_{j,D} = U_{j,D}\,\mathbf{i}_z$)

$$U_S = U_{0,S} + Pe_s\,U_{1,S};\ U_D = U_{0,D} + Pe_s\,U_{1,D}. \tag{3.42}$$

When the drop and the swimmer are in a concentric configuration, the expressions for $U_{0,S}$, $U_{1,S}$, $U_{0,D}$, and $U_{1,D}$ for a general n-mode squirmer inside a drop are given as (see equations (3.68)-(3.71))

$$U_{0,S} = \frac{-12\left(\lambda-1\right)\left(A_1+B_1/2\right)\chi^5 + 10\chi^3\left(A_1+B_1\right)\left(\lambda-1\right) - 3\left(A_1-2B_1\right)\left(\lambda+2/3\right)}{\left(6\lambda-6\right)\chi^5+9\lambda+6}, \tag{3.43}$$

$$U_{0,D} = 10\frac{\chi^3\lambda\left(A_1+B_1\right)}{\left(6\lambda-6\right)\chi^5+9\lambda+6}, \tag{3.44}$$

$$U_{1,S} = -\frac{25Ma\chi^3\lambda\left(1-\chi\right)\left(\chi+1\right)\left(A_1+B_1\right)}{12\left(\left(\lambda-1\right)\chi^5+3/2\lambda+1\right)^2}, \tag{3.45}$$

$$U_{1,D} = -\frac{5}{6}\frac{Ma\lambda\left(A_1+B_1\right)\chi^3\left(1-\chi^5\right)}{\left(\left(\lambda-1\right)\chi^5+3/2\lambda+1\right)^2}. \tag{3.46}$$

Our expressions for $U_{0,S}$ and $U_{0,D}$ match with the corresponding expressions derived for the motion of a swimmer inside a clean drop [79]. We note that the swimmer and drop velocities at $O\left(1\right)$ and at $O\left(Pe_s\right)$ depend only on A_1 and B_1 modes. Also since $0 < \chi < 1$, it can be clearly seen that for positive values of A_1 and B_1, $U_{1,S} \leq 0$ and $U_{1,D} \leq 0$. We plot in figure 3.3, the swimmer and drop velocities accurate to $O\left(Pe_s\right)$ for various values of size ratio χ, viscosity ratio λ and Marangoni number Ma. Even though the expressions for the swimmer and drop velocities accurate to $O\left(Pe_s\right)$ are valid for n-mode squirmer, we plot these velocities for a two mode squirmer inside a drop in figure 3.3. In this case, the swimmer and drop velocities are always positive if the drop is clean. Since $U_{1,S}$, $U_{1,D} \leq 0$ while $U_{0,S}$, $U_{0,D} \geq 0$ for a two mode squirmer inside a drop, the leading order effect of the surfactant is to reduce the swimmer and drop velocities. This can be seen from figure 3.3 where the swimmer and drop velocities for a surfactant-laden-drop (symbols) are less than the corresponding velocities for a clean drop (lines).

We hereby compare the swimmer and drop velocities for a surfactant covered drop with those of a clean drop. But first, we make the following observations that hold irrespective of the presence of the surfactant on the drop surface. The swimmer and

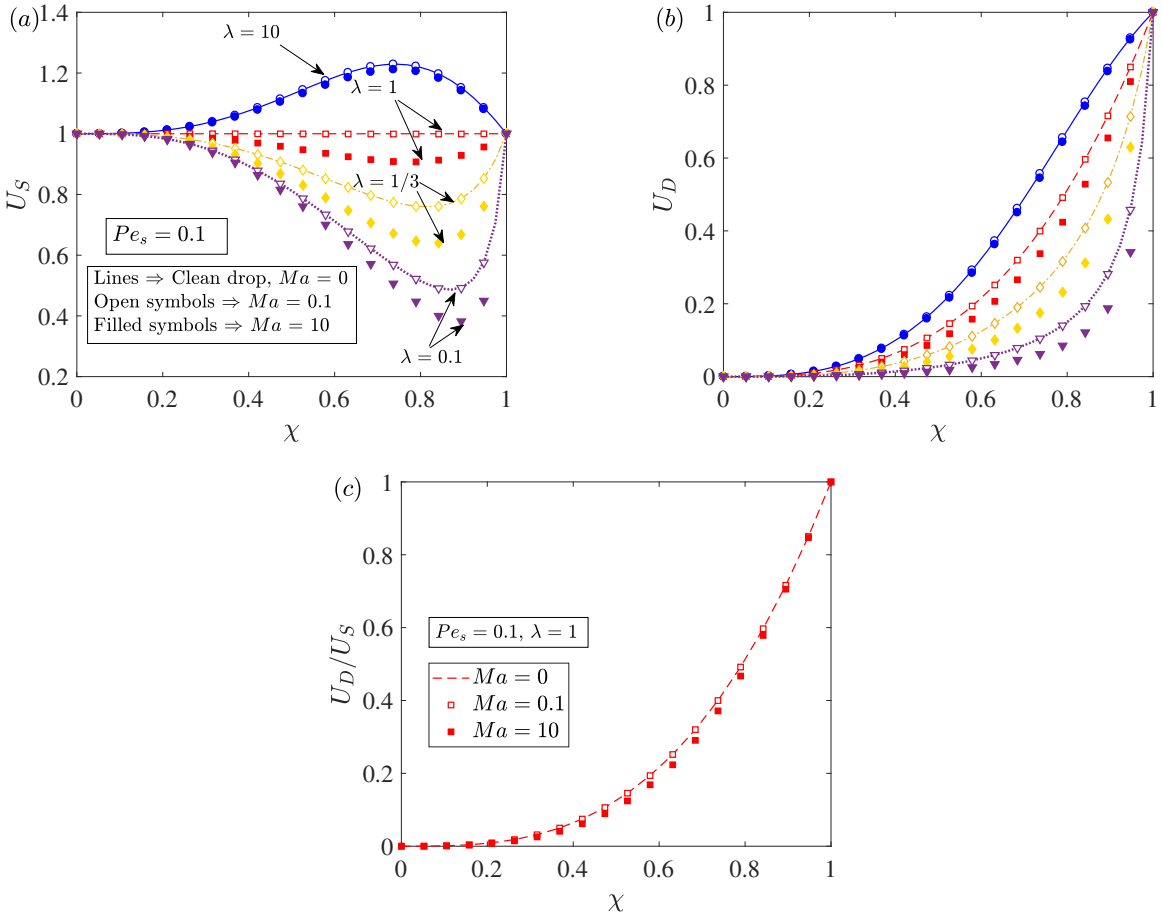

Figure 3.3. : Velocity of (a) a two mode squirmer, U_S and (b) drop, U_D as a function of the size ratio χ for various values of viscosity ratio λ and Ma. The variation of U_D/U_S with size ratio, χ and Marangoni number is plotted in figure (c) for $\lambda = 1$. Lines denote these velocities evaluated for a clean drop while the open and filled symbols denote the velocities evaluated for a surfactant laden drop with $Ma = 0.1$ and 10, respectively. The surface Péclet number, Pe_s is chosen as 0.1 in all these calculations. All the velocities are non-dimensionalized using $U_{sq} = 2B_1/3$.

drop velocities decrease with the decreasing viscosity ratio, λ. Also, the drop velocity decreases with the decreasing size ratio, χ. When the size of the swimmer is much less than the size of the drop ($\chi \ll 1$) or if it is approximately the same as the drop size ($\chi \approx 1$), the swimmer velocity is equal to its velocity in an unbounded medium. Similarly, the drop velocity is zero when $\chi \ll 1$ and it is equal to the velocity of the swimmer in unbounded medium when $\chi \approx 1$. The surfactant does not affect the swimmer and drop velocities in the limits of $\chi \ll 1$ or $\chi \approx 1$ because $U_{1,S} = U_{1,D} = 0$ in these limits. The swimmer velocity exhibits a maximum (minimum) for those viscosity ratios at which it moves faster (slower) than that in an unbounded fluid.

One feature that distinguishes the swimmer velocity in a clean drop with that inside a surfactant laden drop is the viscosity ratio at which the swimmer velocity equals to its velocity in an unbounded medium for all size ratios. For instance, consider the swimmer inside a clean drop. It moves with its velocity in an unbounded medium when $\lambda = 1$(viscosity of the drop is the same as that of the suspended fluid), whereas it propels with a speed smaller (larger) than its unbounded swimming speed, when $\lambda < 1$ ($\lambda > 1$). Notably, $\lambda = 1$ demarcates the $U_S > 1$ region (faster swimming region) from the $U_S < 1$ region (slower swimming region). Now consider the swimmer inside a surfactant laden drop. Here $\lambda = \lambda_{app} > 1$ demarcates the faster swimming region from the slower swimming region. This is because even for $\lambda = 1$, the swimmer moves with a velocity smaller than its velocity in an unbounded medium, so there exists a viscosity of the drop, $\lambda = \lambda_{app} > 1$ at which the swimmer moves with a velocity equal to its unbounded swimming velocity. Also, for the viscosities of the drop larger than this apparent viscosity (for instance $\lambda = 10$), the swimmer moves with a velocity larger than its unbounded swimming velocity.

In figure 3.3c, we plot the variation of the ratio U_D/U_S with the size ratio and the Marangoni number. We see that the reduction in the drop velocity is more than the reduction in the swimmer velocity due to the surfactant redistribution. Also, this ratio is always less than 1 irrespective of the presence of the surfactant. This means

that a two-mode squirmer located at the center of a drop is faster than the drop and hence the concentric configuration is not a steady state configuration.

To understand the variation of the swimmer and drop velocities accurate to $O(Pe_s)$ with λ, χ and Ma, we need to understand the dependence of swimmer and drop velocities at various orders of Pe_s on the aforementioned parameters. For instance, we would like to understand − why does the swimmer and drop velocities for a surfactant laden drop show large deviations as compared to those of clean interface velocities when $\chi \approx 0.8 - 0.9$.We already plotted in figure 3.3 the swimmer and the drop velocities for a clean drop which are the same as the $O(1)$ velocities for a surfactant laden drop. Hence, we plot in figure 3.4, the variation of swimmer velocity at $O(Pe_s)$ with χ, λ and Ma. From equation (3.45), we see that $U_{1,S}$ depends linearly on the Marangoni number, Ma. A similar trend can also be observed from figure 3.4a where we plotted $U_{1,S}$ for various χ and Ma. It can be seen from equation (3.45) that $U_{1,S}$ vanishes for either $\chi \approx 1$ or $\chi \to 0$, for all values of λ and Ma. But since $U_{1,S}$ is non-zero for intermediate values of χ and it cannot be positive, it should exhibit a local minimum at some intermediate value of χ. This trend is readily observed from figure 3.4b. Similarly, we see that $U_{1,S}$ becomes zero when $\lambda \to 0$ or $\lambda \to \infty$ for all values of χ and Ma. Since $U_{1,S}$ is non-zero for any finite value of λ and it cannot be positive, it should display a local minimum at some intermediate value of λ. We again see such trend in figure 3.4b or in its inset. Such non-monotonic variation of $U_{1,S}$ with λ and χ explains the non-monotonic variation of the deviation between the swimmer velocity accurate to $O(Pe_s)$ and the swimmer velocity at $O(1)$ as seen in figure 3.3. The dependence of the drop velocity at $O(Pe_s)$, $U_{1,D}$, on the aforementioned parameters is qualitatively the same as the dependence of the swimmer velocity at $O(Pe_s)$, $U_{1,S}$, so we do not report the variation of $U_{1,D}$.

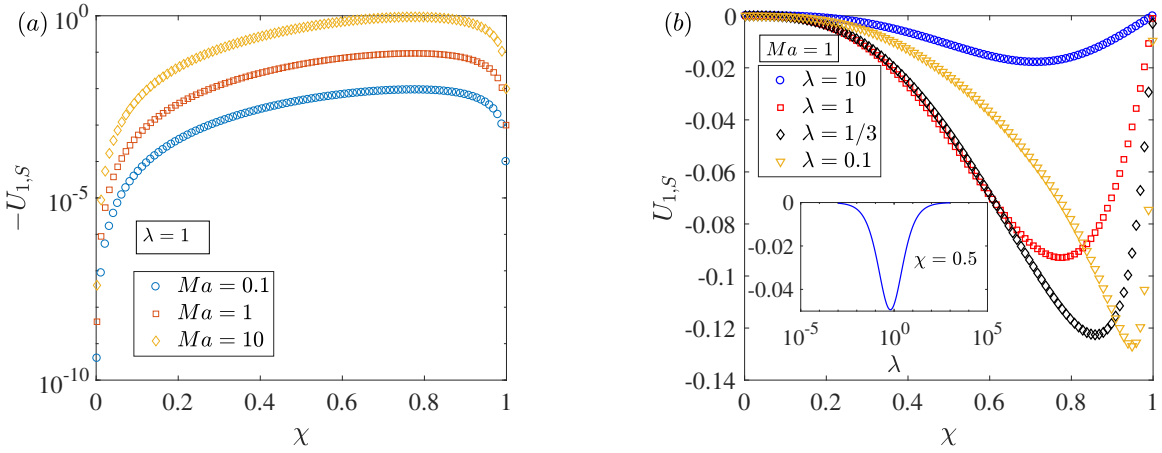

Figure 3.4. : The variation of a two-mode squirmer velocity at $O\left(Pe_s\right)$, $U_{1,S}$, with the size ratio χ for several values of (a) Ma with $\lambda = 1$ and (b) λ with $Ma = 1$. Inset in the subfigure (b) shows the non-monotonic variation of $U_{1,S}$ with the viscosity ratio λ for $\chi = 0.5$. All the velocities are non-dimensionalized using $U_{sq} = 2B_1/3$.

Far-field representation

In this section, we analyze how the advection of the surfactant modifies the far-field representation of the flow field due to drop enclosing a swimmer at its center. Far-field representation is useful in understanding the interaction of a particle (or a drop or a swimming microorganism) with an interface or other particles. Even though the concentric configuration is unstable, simple expressions of flow field associated with this configuration enable us to evaluate several quantities of interest.

In the lab frame, the radial component of the velocity far away from a two-mode swimmer in an unbounded fluid is given as [15]

$$\bar{u}_r|_{\text{leading}} = -B_2 P_2 (\cos\theta)\ \frac{\chi^2}{r^2}, \tag{3.47}$$

where variables with overbar indicate that they are written in the lab frame of reference. The radius of the drop is still used for non-dimensionalizing the length in the problem of swimmer in an unbounded fluid and this justifies the appearance of χ in equation (3.47). Similarly, the radial component of velocity outside a drop enclosing a swimmer and far away from the drop is given as

$$\bar{v}_r^{(2)}\Big|_{\text{leading}} = \bar{v}_{0,r}^{(2)}\Big|_{\text{leading}} + Pe_s\, \bar{v}_{1,r}^{(2)}\Big|_{\text{leading}} + O\left(Pe_s^2\right), \tag{3.48}$$

where

$$\bar{v}_{j,r}^{(2)}\Big|_{\text{leading}} = \left[\bar{\phi}_{j,-1}^{(2)} + \bar{p}_{j,-3}^{(2)} P_2(\cos\theta)\right] \frac{1}{r^2}.$$

Using the expressions provided in the Appendix 3.7, we derive the following two ratios

$$\frac{\bar{v}_{0,r}^{(2)}\Big|_{\text{leading}}}{\bar{u}_r|_{\text{leading}}} = -\frac{6\Lambda\left(\chi^4 + 3\chi^3 + 11/3\chi^2 + 3\chi + 1\right)}{\left(\begin{array}{c} 4 + (8\Lambda - 4)\chi^7 + (24\Lambda - 12)\chi^6 + (48\Lambda - 24)\chi^5 \\ + (45\Lambda - 15)\chi^4 + (15\Lambda + 15)\chi^3 + 24\chi^2 + 12\chi \end{array}\right)} < 0, \tag{3.49}$$

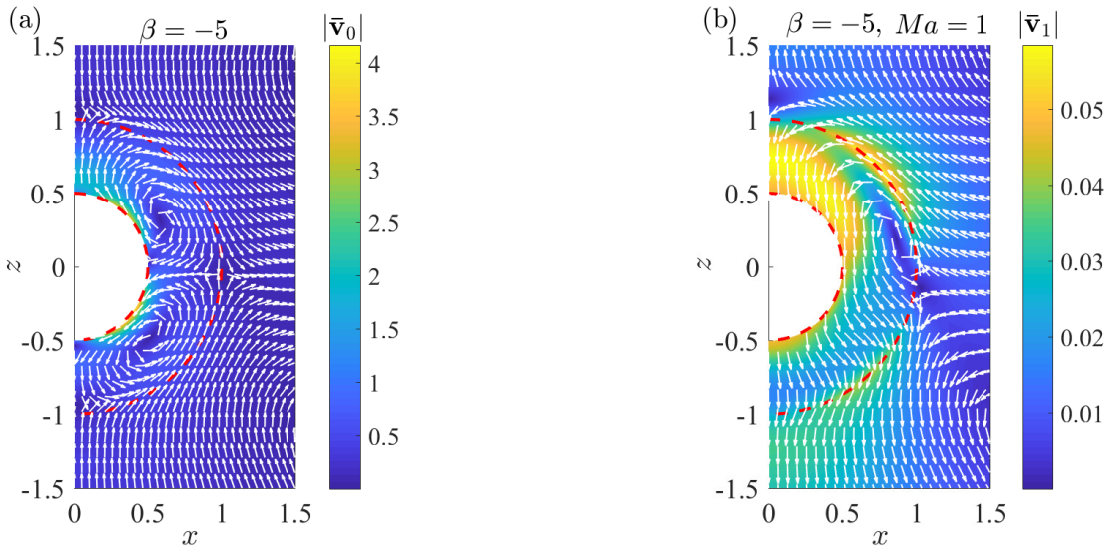

Figure 3.5. : The (a) $O(1)$ and (b) $O(Pe_s)$ flow fields outside a surfactant laden drop containing a pusher swimmer at its center in the lab frame of reference. The background color and the unit vectors denote the magnitude and the direction of the velocity. The red dashed lines denote the surfaces of the swimmer and the drop. Here, $\beta = B_2/B_1 = -5$, $Ma = 1$, $\chi = 0.5$ and $\lambda = 1$. All the velocities are non-dimensionalized using $U_{sq} = 2B_1/3$.

$$\frac{\bar{v}_{1,r}^{(2)}\Big|_{\text{leading}}}{\bar{u}_r|_{\text{leading}}} = \frac{\left(\begin{array}{l} (24-24\chi)(1-\Lambda)\Lambda Ma\,(\chi^4+3\chi^3+11/3\chi^2+3\chi+1)\times \\ (\chi^6+4\chi^5+10\chi^4+55/4\chi^3+10\chi^2+4\chi+1) \end{array} \right)}{5\left(\begin{array}{l} 8\Lambda\chi^7+24\Lambda\chi^6-4\chi^7+48\Lambda\chi^5-12\chi^6+45\Lambda\chi^4 \\ -24\chi^5+15\Lambda\chi^3-15\chi^4+15\chi^3+24\chi^2+12\chi+4 \end{array} \right)^2} > 0, \tag{3.50}$$

where $\Lambda = \lambda/(\lambda+1)$. From equation (3.49), we deduce that the far-field representation of an $O(1)$ flow field due to a pusher (puller) inside a drop is that of a puller (pusher) for all values of viscosity ratio and size ratio. Reigh *et al.* [79] derived a similar far-field representation of the flow field due to a clean drop encompassing a swimmer. On the other hand, the far-field representation of the $O(Pe_s)$ flow field due to a pusher (puller) inside a drop is that of a pusher (puller), see equation (3.50). This far-field behavior of a surfactant covered drop containing a swimmer at its center can be understood by plotting the $O(1)$ and $O(Pe_s)$ flow fields in the lab frame of reference. We plot these flow fields for a pusher swimmer at the center of the surfactant laden drop for the viscosity ratio and the size ratio of 1 and 0.5, respectively, in figure 3.5. A pusher swimmer in an unbounded fluid sucks fluid normal to its axis and ejects the fluid along its axis while a puller swimmer draws fluid along its axis and ejects the fluid normal to its axis. As per the $O(1)$ flow field outside a drop, we see that a drop containing a pusher sucks fluid along its axis while ejecting normal to its axis; this flow field being the characteristic of a puller swimmer. Hence, the far-field representation of a clean drop containing a pusher swimmer at its center is that of a puller swimmer. Similarly based on the $O(Pe_s)$ flow field outside a drop, we see that a drop containing a pusher draws fluid normal to its axis while ejecting along its axis. As this flow is the characteristic of a pusher swimmer, it can be said that the far-field representation of $O(Pe_s)$ flow field due to a surfactant laden drop containing a pusher swimmer at its center is that of a pusher swimmer.Any deviation in the flow field outside the drop from this far-field behavior is due to the contribution of the near-field flow. Since the $O(Pe_s)$ flow field is an order of magnitude

smaller than the $O(1)$ flow field and it is opposite to the $O(1)$ flow in the far-field, we conclude that the surfactant covered drop containing a pusher swimmer at its center behaves as a puller, the strength of the far-field flow is reduced due to the surfactant redistribution.

Surfactant concentration

In this section, we will provide physical reasons for the decrease in the drop and swimmer velocities due to the surfactant redistribution when the swimmer is at the center of the drop. For this purpose, we will utilize the justification provided to explain a similar decrease in the rise velocity of a drop (without any swimmer inside) due to the surfactant advection on its surface [18]. The key idea is to analyze the surfactant concentration and the surface velocity of a drop containing a two-mode squirmer at its center. Analytical expression for the surfactant concentration accurate to $O(Pe_s)$ is given as

$$\Gamma = \Gamma_0 + Pe_s\,\Gamma_1 + O\left(Pe_s^2\right), \tag{3.51}$$

where $\Gamma_0 = 1$ and $\Gamma_1 = \Gamma_{1,1}\,P_1(\cos\theta) + \Gamma_{1,2}\,P_2(\cos\theta)$. Here, $\Gamma_{1,1}$ and $\Gamma_{1,2}$ are given as

$$\begin{aligned}
\Gamma_{1,1} &= -\frac{3}{2}\frac{5\chi^3\lambda}{(2\lambda-2)\,\chi^5+3\lambda+2},\\
\Gamma_{1,2} &= \frac{3}{2}\frac{6\left(\chi^4+3\chi^3+11/3\chi^2+3\chi+1\right)\beta\,\chi^2\lambda}{\left(\begin{array}{l}(12\lambda-12)\,\chi^7+(36\lambda-36)\,\chi^6+(72\lambda-72)\,\chi^5+(90\lambda-45)\,\chi^4\\+(90\lambda+45)\,\chi^3+(72\lambda+72)\,\chi^2+(36\lambda+36)\,\chi+12\lambda+12\end{array}\right)}.
\end{aligned} \tag{3.52}$$

Similarly, the expression for the surface velocity of the drop accurate to $O(Pe_s)$ is given as

$$v_\theta|_{r=1} = v_{0,\theta}|_{r=1} + Pe_s\,v_{1,\theta}|_{r=1} + O\left(Pe_s^2\right), \tag{3.53}$$

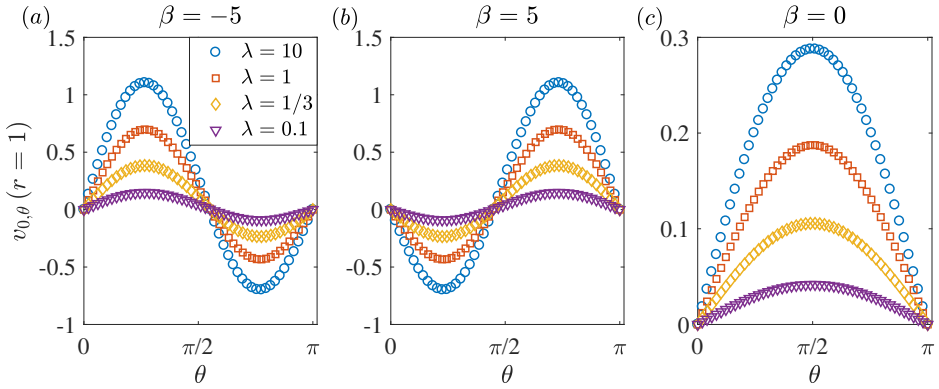

Figure 3.6. : The surface velocity of a clean drop containing (a) pusher ($\beta = -5$), (b) puller ($\beta = 5$) and (c) a neutral swimmer ($\beta = 0$) at its center, plotted as a function of the polar angle for various viscosity ratios. Here, the size ratio χ is taken as 0.5. All the velocities are non-dimensionalized using $U_{sq} = 2B_1/3$.

where

$$
\begin{aligned}
v_{0,\theta}|_{r=1} &= \frac{5\chi^3 B_1 \lambda \sin(\theta)}{2\chi^5\lambda - 2\chi^5 + 3\lambda + 2} \\
&\quad - \frac{6\cos(\theta)\, B_2 \lambda \sin(\theta)\, \chi^2 \left(\chi^4 + 3\chi^3 + 11/3\chi^2 + 3\chi + 1\right)}{\left(\begin{array}{l}(4\lambda-4)\,\chi^7 + (12\lambda-12)\,\chi^6 + (24\lambda-24)\,\chi^5 + (30\lambda-15)\,\chi^4 \\ +(30\lambda+15)\,\chi^3 + (24\lambda+24)\,\chi^2 + (12\lambda+12)\,\chi + 4\lambda + 4\end{array}\right)}, \\
v_{1,\theta}|_{r=1} &= \frac{5Ma\,\chi^3\lambda B_1\,(\chi^5-1)\sin(\theta)}{\left(2\chi^5\lambda - 2\chi^5 + 3\lambda + 2\right)^2} \\
&\quad - \frac{3}{10}\frac{\left(\begin{array}{l}(\chi-1)\cos(\theta)\,\chi^2\lambda\left(\chi^4 + 3\chi^3 + 11/3\chi^2 + 3\chi + 1\right)\sin(\theta) \\ \times Ma\, B_2\left(\chi^6 + 4\chi^5 + 10\chi^4 + \frac{55\chi^3}{4} + 10\chi^2 + 4\chi + 1\right)\end{array}\right)}{\left(\begin{array}{l}(\lambda-1)\,\chi^7 + (3\lambda-3)\,\chi^6 + (6\lambda-6)\,\chi^5 + \left(15/2\lambda - \frac{15}{4}\right)\chi^4 \\ +\left(15/2\lambda + \frac{15}{4}\right)\chi^3 + (6\lambda+6)\,\chi^2 + (3\lambda+3)\,\chi + \lambda + 1\end{array}\right)}.
\end{aligned}
\tag{3.54}
$$

For a clean interface, the swimmer velocity, the drop velocity and the drop surface velocity decrease as the viscosity ratio λ decreases (see figures 3.3a, 3.3b and 3.6). A similar decrease in the velocity of a swimming microorganism, modeled as a Stokes dipole, near a plane clean interface was already reported [8]; the reason is the decrease

in the strength of the image flow field with a decrease in λ. Now, for a swimmer inside a clean drop, we attribute the decrease in the swimmer velocity, drop velocity and the drop surface velocity to a corresponding decrease in the strength of the image flow field with a decrease in λ

We plot in figure 3.7, variation of the surface velocity of the drop and the surfactant concentration with the polar angle (θ) for various values of Marangoni number, Ma and β. We note that v_θ should be zero at the front and at the back of the drop due to the axisymmetric condition. Analyzing the results for a neutral swimmer ($\beta = 0$), we see that the surface velocity at $O(1)$ is always positive which leads to a monotonically increasing surfactant concentration as shown in figure 3.7d. This give rise to a maximum (minimum) interfacial tension at the front (back) of the drop. This inhomogeneous interfacial tension generates a tensile stress imbalance which pulls the drop surface elements from the back to the front, thereby reducing the drop surface velocity. The fluid in the vicinity of the drop also gets pulled from the back to the front of the drop and since this direction of pull is opposite to the free-stream velocity, the drop velocity reduces due to the surfactant redistribution. Similarly, for a pusher inside a drop, since the drop surface velocity (at $O(1)$) is positive near the front and negative near the back, it brings the surfactant from both the front and back to the center of the drop as shown in figure 3.7d. This gives rise to a minimum (maximum) interfacial tension at the center (the front and the back) of the drop. Again, such inhomogeneous interfacial tension pulls the drop surface elements from the center towards the front (the back) in the upper (lower) half of the drop thereby reducing the drop surface velocity. This Marangoni induced drop surface flow pulls the fluid nearby in the same direction. Since this induced flow near the upper (lower) half of the drop is opposite to (along) the free-stream flow and the flow near the upper half is dominant due to $\gamma|_{\text{top}} - \gamma|_{\text{center}} > \gamma|_{\text{bottom}} - \gamma|_{\text{center}}$, we expect the drop velocity to be reduced due to the surfactant redistribution. One can use a similar reasoning to understand the Marangoni induced decrease in the drop velocity and the drop surface velocity for a puller swimmer at the center of a drop. In conclusion,

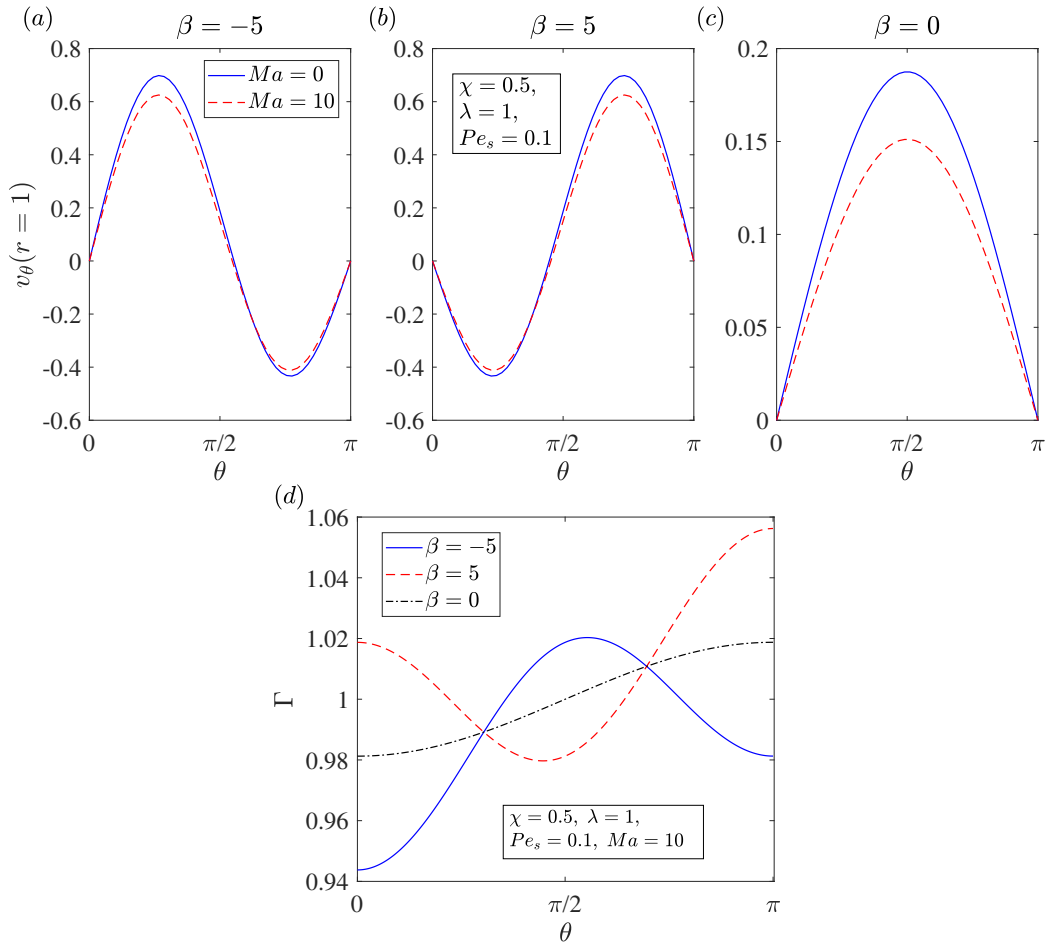

Figure 3.7. : The variation of the surface velocity of the drop with the polar angle for (a) a pusher ($\beta = -5$), (b) a puller ($\beta = 5$) and (c) a neutral swimmer ($\beta = 0$) at the center of a drop. Solid lines indicate the results obtained for a clean drop while the dashed lines denote the results of a surfactant laden drop with $Ma = 10$ and $Pe_s = 0.1$. (d) Variation of the surfactant concentration with the polar angle. Here the solid, dashed and dash-dotted lines denote the results obtained for a pusher, a puller and a neutral swimmer inside the drop, respectively. The size ratio, χ, and the viscosity ratio, λ, are taken as 0.5 and 1, respectively. All the velocities are non-dimensionalized using $U_{sq} = 2B_1/3$.

for any two-mode swimmer at the center of the drop, the surfactant redistribution on the drop surface reduces the drop velocity and the drop surface velocity. We recall that the drop surface velocity also decreases due to a decrease in λ for a clean drop containing a swimmer at its center. So, for a swimmer at the center of the drop, one can understand the influence of surfactant redistribution on the swimmer or the drop velocity by assuming that the surfactant advection solely decreases the apparent viscosity ratio (apparent because the actual viscosity ratio is not affected by the surfactant redistribution). Since the swimmer and the drop velocities reduce due to a decrease in λ for a clean drop containing a swimmer at its center, we expect a similar decrease in the swimmer and the drop velocities due to the advection of the surfactant on the drop surface.

Co-swimming

As mentioned earlier, a two-mode swimmer located at the center of the drop always has a velocity larger than that of the drop, thereby making the concentric configuration unsteady. Due to the recent advancement in the artificial micro-swimmers, one can make a swimmer such that it transports the drop by lying at the center of the drop for all times. Since the swimmer and drop velocities accurate to $O\left(Pe_s\right)$ depend only on A_1 and B_1 modes, we can choose A_1 mode such that $U_S = U_D$. Using the equations (3.43)-(3.46), we derive the dimensionless A_1 mode as

$$\alpha_{co} = \frac{A_1}{B_1} = \frac{\begin{pmatrix} -12\left(\chi-1\right)\left(\left(\lambda-1\right)\chi^4+\left(\lambda-1\right)\chi^3+\left(\lambda+\frac{2}{3}\right)\chi^2+\left(\lambda+\frac{2}{3}\right)\chi+\lambda+\frac{2}{3}\right) \\ \times\left(\left(\lambda-1\right)\chi^5+\frac{3}{2}\lambda+1\right)-5Ma\,Pe_s\chi^3\lambda\left(2\chi^5-5\chi^2+3\right) \end{pmatrix}}{\begin{pmatrix} \left(2\chi^5\lambda-2\chi^5+3\lambda+2\right)\left(12\chi^5\lambda-12\chi^5+10\chi^3+3\lambda+2\right) \\ +5Ma\,Pe_s\,\chi^3\lambda\left(2\chi^5-5\chi^2+3\right) \end{pmatrix}} \tag{3.55}$$

We plot the variation of the co-swimming speed, U_{SD}, with the viscosity ratio, size ratio and Ma in figure 3.8. We note that the results of this section are valid for any general squirmer inside a drop except that A_1 is chosen according to equation (3.55).

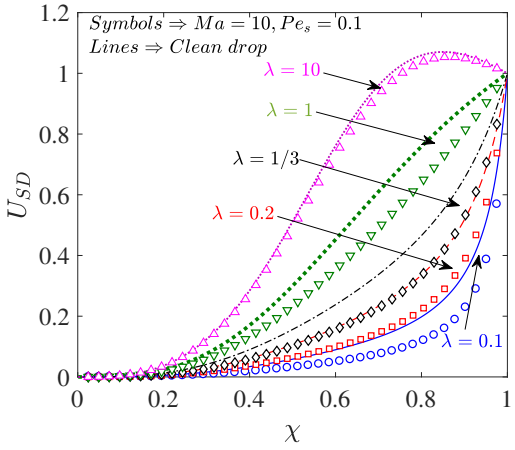

Figure 3.8. : The variation of the co-swimming speed, U_{SD}, with the size ratio for various values of the viscosity ratio and the Marangoni number. The lines indicate the results obtained for a clean drop while the symbols denote the results obtained for a surfactant laden drop with $Ma = 10$ and $Pe_s = 0.1$. Here $U_{sq} = 2B_1/3$ is used to non-dimensionalize the co-swimming speed.

Analysis of the two-mode squirmer at the center of the drop revealed that the swimmer and drop velocities approach unity when the size of the swimmer approaches the size of the drop, i.e., $\chi \to 1$. Due to this reason, as $\chi \to 1$, α_{co} should approach zero while the co-swimming speed should approach unity for all values of viscosity ratio and Ma as shown in figure 3.8. Furthermore, for large values of the drop viscosities (for instance, for $\lambda = 10$), the co-swimming microswimmer and drop have speeds larger than the speed of the swimmer in an unbounded fluid. Similar to the results of two-mode swimmer inside a drop, we see that the advection of surfactant also reduces the co-swimming speed as shown in figure 3.8.

3.4.2 Eccentric configurations

In this section, we study the variation of the swimmer and drop velocities with the eccentricity. Using this analysis, we answer the following questions: Does a two-mode squirmer inside a clean drop achieve a configuration where it will swim with the drop ($U_S = U_D$)? If such a configuration exists and it is stable, what is the effect of the advection of the surfactant on this configuration? How does the surfactant redistribution affect the swimmer and drop velocities for eccentric configurations? Prior to the analysis, we validate the velocities of the swimmer and drop for small eccentricities (obtained using bipolar coordinate method) with the velocities for a concentric configuration (obtained using Lamb's general solution) and these results are plotted in figures 14 and 15 in appendix 3.11.

In the top row of figure 3.9, we plot the swimmer and drop velocities at $O(1)$ (this corresponds to the swimmer inside a clean drop) as a function of the eccentricity. Since the dependence of these velocities on the eccentricity is qualitatively the same for various values of the size ratio (χ) and the viscosity ratio (λ), we report these plots for a single representative value of χ and λ, namely $\chi = 0.5$ and $\lambda = 1$. In the bottom row of figure 3.9, we plot the time evolution of the position of the swimmer for various initial positions of the swimmer inside a drop. Here the first, second and

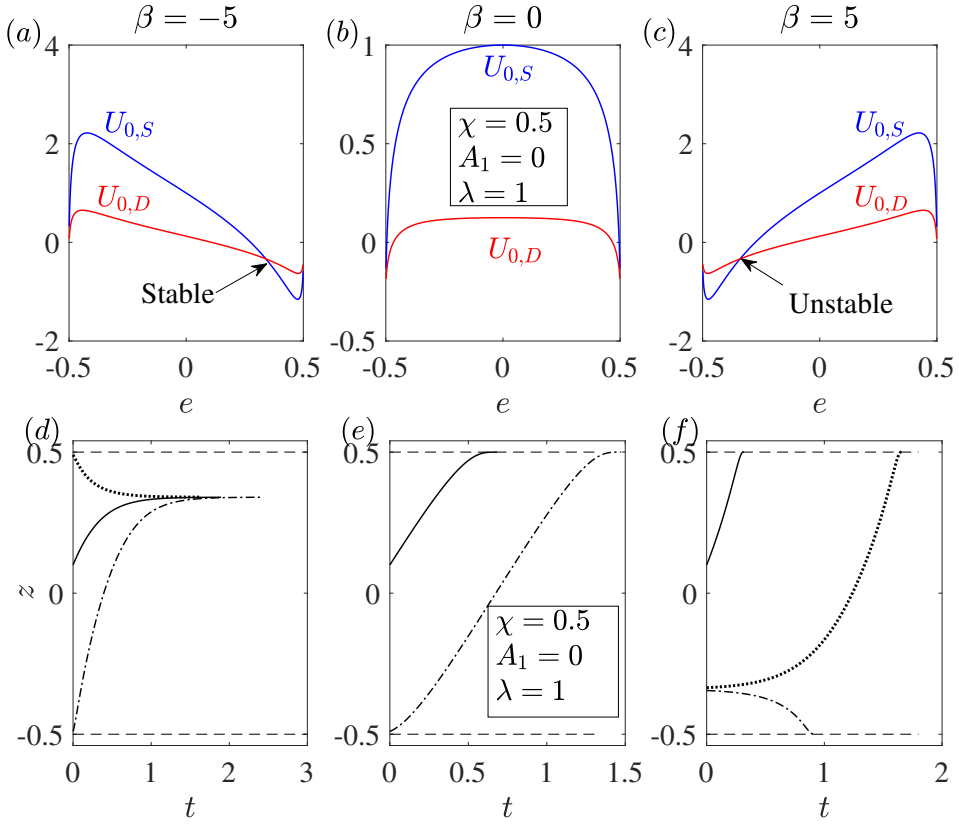

Figure 3.9. : For a two-mode swimmer inside a clean drop, velocity of the swimmer ($U_{0,S}$) (blue lines) and the drop ($U_{0,D}$) (red lines) are plotted as a function of the eccentricity (e) in (a), (b) and (c). Time evolution of the center of the swimmer when released from different positions inside a clean drop are plotted in (d), (e) and (f). Subfigures (a), (d) denote the results of a pusher ($\beta = -5$) while (b), (e) denote those of a neutral swimmer ($\beta = 0$) and (c), (f) denote those of a puller ($\beta = 5$). Here $e > 0$ ($e < 0$) indicates that the center of the swimmer is above (below) the center of the drop. The size ratio, χ and the viscosity ratio λ were taken as 0.5 and 1, respectively. All the velocities are non-dimensionalized using $U_{sq} = 2B_1/3$. The dashed lines indicate the positions at which the swimmer touches the drop.

third columns present the results for a pusher ($\beta = -5$), a neutral swimmer ($\beta = 0$) and a puller ($\beta = 5$) inside a drop, respectively. From figure 3.9b, we observe that a neutral swimmer inside a drop has a velocity larger than that of a drop for all values of eccentricities. Hence a neutral swimmer inside a clean drop moves towards the front of the drop as shown by the time evolution of its position in figure 3.9e. From figure 3.9c, we see that a puller inside a clean drop has a fixed point (at which $e < 0$), in the sense that the swimmer and drop velocities are the same at this fixed point. But this fixed point is globally unstable. This is because a swimmer located above (below) the fixed point has a positive (negative) velocity with respect to the drop because of which it moves away from the fixed point, towards the top (bottom) surface of the drop as shown by the time evolution of its position in figure 3.9f. Finally, from figure 3.9a, we notice that a pusher inside a clean drop has a globally stable fixed point (at which $e > 0$). This is because a swimmer located above (below) the fixed point has a negative (positive) velocity with respect to the drop, due to which it moves towards the fixed point as shown by the time evolution of its position in figure 3.9d. To generalize these observations, we note that for a two-mode swimmer inside a clean drop, there exists a value of $\beta = \beta_c$, where $\beta_c < 0$ is a function of viscosity ratio and the size ratio, such that a swimmer with $|\beta| < -\beta_c$ behaves as a neutral swimmer. Such a swimmer does not have any fixed points inside the drop and since it is faster than the drop, it moves to the top surface of the drop. On the other hand, a two-mode swimmer with $\beta < \beta_c$ has a stable fixed point because of which it achieves an eccentrically stable configuration irrespective of its initial position. Furthermore, a two-mode swimmer with $\beta > -\beta_c$ has an unstable fixed point because of which it moves either to the top or the bottom of the drop depending on its initial position being above or below the fixed point. We note that Reigh *et al.* [79] carried out a similar analysis for a three mode (A_1, B_1 and B_2) co-swimming squirmer inside a clean drop using the boundary element method.

Earlier, we showed that the redistribution of the surfactant decreases the velocity of a swimmer and a drop when the swimmer is located at the center of the drop. To

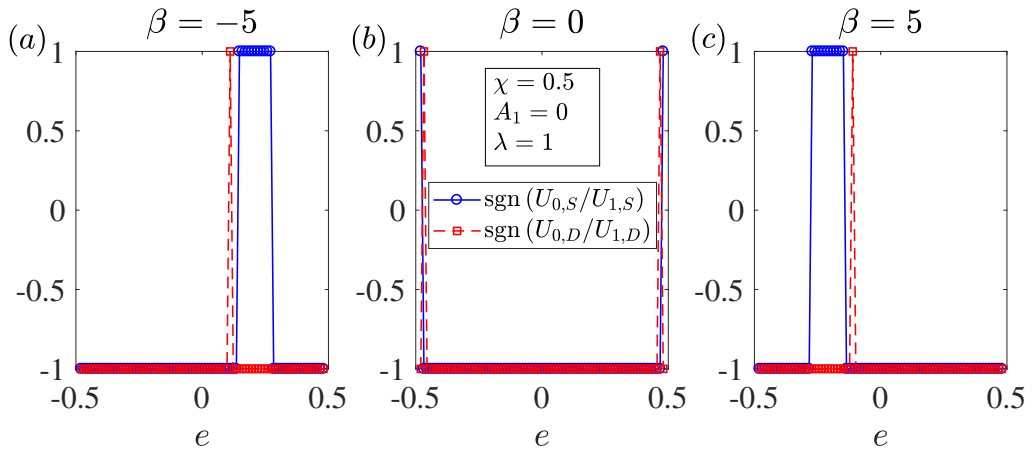

Figure 3.10. : The signs of the ratios $U_{0,S}/U_{1,S}$ and $U_{0,D}/U_{1,D}$ plotted as a function of eccentricity e for (a) a pusher ($\beta = -5$), (b) a neutral swimmer ($\beta = 0$) and (c) a puller ($\beta = 5$) inside a surfactant laden drop. The size ratio, χ and the viscosity ratio λ were taken as 0.5 and 1, respectively.

understand the influence of the surfactant redistribution on the swimmer and drop velocities for an eccentrically located swimmer inside a drop, we plot in figure 3.10 the ratios $\mathrm{sgn}\,(U_{0,S}/U_{1,S})$ and $\mathrm{sgn}\,(U_{0,D}/U_{1,D})$ as a function of the eccentricity. Here sgn( ) denotes the sign function. Since $U_{1,S}$ and $U_{1,D}$ are proportional to Ma and $Ma > 0$, these plots are valid for all finite values of Ma at which the perturbation in Pe_s is valid. A positive (negative) value of the ratio $U_{0,S}/U_{1,S}$ means that the surfactant redistribution increases (decreases) the magnitude of swimmer velocity. One can similarly deduce the relation between the sign of the ratio $U_{0,D}/U_{1,D}$ and the effect of the surfactant redistribution on the magnitude of drop velocity. From figure 3.10, we see that the advection of the surfactant reduces the magnitude of swimmer and drop velocities for a swimmer located at the center of the drop, consistent with the concentric calculations. Even though this trend of surfactant redistribution decreasing the magnitude of swimmer and the drop velocities holds for most of the values of eccentricities, we see that there exist some values of eccentricities at which the surfactant redistribution increases the magnitude of swimmer or drop velocity. Also, at an eccentrically stable position corresponding to a clean drop, the surfactant redistribution decreases the magnitude of swimmer and drop velocities. We note that for eccentric configurations, the drop surface velocity decreases due to the surfactant redistribution and also the drop surface velocity, swimmer and drop velocities decrease with a decrease in λ for a clean drop containing a swimmer. Due to this reason, the observations in figure 3.10 cannot be explained by studying the influence of the surfactant advection on the drop surface velocity, as was done for the concentric configuration. Motivated by the physical reasoning provided to explain the change in the velocity of a swimmer in a shear-thinning fluid [89, 90] (as compared to that in a Newtonian fluid), we analyze the drag and thrust problems separately in the next section to explain the effect of surfactant redistribution on the swimmer and drop velocities, as shown in figure 3.10.

At an eccentrically stable position corresponding to a clean drop, since the surfactant redistribution reduces the magnitude of swimmer and drop velocities by unequal

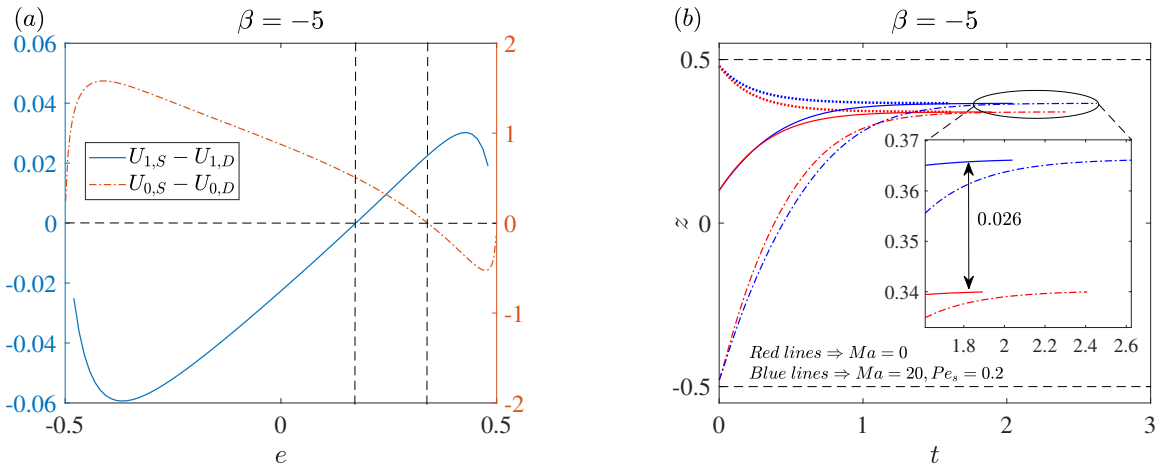

Figure 3.11. : (a) The velocity of a pusher swimmer with respect to drop at $O(1)$ (red dash-dotted line) and that at $O(Pe_s)$ (blue solid line) as a function of eccentricity. The axis for the $O(Pe_s)$ relative velocity is on the left while that for an $O(1)$ relative velocity is on the right. Here $Ma = 1$. The dashed lines are just for reference. (b) Time evolution of the center of a pusher swimmer when released from different positions. Here red lines denote the results for clean drop while blue lines denote the results for a surfactant laden drop with $Ma = 20$ and $Pe_s = 0.2$, respectively. The inset shows the shift in the location of an eccentrically stable position induced by the advection of the surfactant. The size ratio, χ and the viscosity ratio λ are taken as 0.5 and 1, respectively. All the velocities are non-dimensionalized using $U_{sq} = 2B_1/3$. The dashed lines indicate the positions at which the swimmer touches the drop.

amounts, this stable position shifts due to the surfactant advection. To understand this shift, we plot in figure 3.11a, the relative velocity of a pusher swimmer at $O(1)$ $(U_{0,S} - U_{0,D})$ and that at $O(Pe_s)$ $(U_{1,S} - U_{1,D})$ for various eccentricities. The axis for the $O(Pe_s)$ relative velocity is on the left while that for an $O(1)$ relative velocity is on the right. As seen from this figure, at an eccentrically stable position corresponding to a clean drop, the $O(1)$ relative velocity is zero while the $O(Pe_s)$ relative velocity is positive. So, the eccentrically stable position shifts towards the top surface of the drop due to the surfactant redistribution, as shown in figure 3.11b. This figure shows the time evolution of the center of a pusher swimmer when released from different positions inside a drop. As seen from the inset of this figure, the time taken by the swimmer to reach an eccentrically stable position depends on its initial position and the presence of the surfactant on the drop. This time scales as $t \sim d_0/|U_S - U_D|$, where d_0 is the distance between the initial swimmers position and its eccentrically stable position. Hence, the swimmer takes a long (short) time to reach the stable position if it is initially far away from (close enough to) this position; compare solid and dash-dotted lines of same color in the inset of figure 3.11b. Also, for most of the swimmer positions inside the drop, the surfactant redistribution decreases the magnitude of relative velocity of the swimmer $|U_S - U_D|$ (see figure 3.11a). Hence, for a given initial position, a swimmer inside a surfactant-laden-drop takes a longer time than that inside a clean drop to reach its eccentrically stable position; compare the blue and red colored lines which are of the same style.

3.4.3 Drag and Thrust

In this section, we analyze the thrust and drag forces on the swimmer and the drop separately to explain the observations in figure 3.10. As the influence of the surfactant redistribution on the swimmer and the drop velocities for a pusher inside a drop at some eccentricity $e = e_1 > 0$ is the same as that for a puller inside a drop

at the eccentricity $e = -e_1$, we would only analyze the results for a neutral swimmer and a puller i.e., figures 3.10b and 3.10c.

We define the thrust and drag problems for the swimmer as follows: the thrust problem consists of a fixed swimmer, with a slip velocity on its surface, inside a force-free surfactant-laden-drop whereas the drag problem consists of a translating rigid sphere with a velocity $\mathbf{U}_{0,S}$ inside a force-free surfactant-laden-drop. We call the hydrodynamic force experienced by the swimmer in the thrust (drag) problem as the thrust force (drag force) and denote this force at $O\left(Pe_s^j\right)$ by $F_{j,TS}\,\mathbf{i}_z$ ($F_{j,DS}\,\mathbf{i}_z$). Similarly, we define the thrust and the drag problems for the drop as follows: the thrust problem consists of a stationary surfactant covered drop encapsulating a swimmer whereas the drag problem consists of surfactant-laden-drop engulfing a force-free rigid sphere, the drop itself is translating with a velocity $\mathbf{U}_{0,D}$. Again, we denote the thrust force and the drag force acting on the drop at $O\left(Pe_s^j\right)$ by $F_{j,TD}\,\mathbf{i}_z$ and $F_{j,DD}\,\mathbf{i}_z$, respectively. If the drag problem for the swimmer were to consist of a rigid sphere translating with a velocity $\mathbf{U}_{0,S} + Pe_s\,\mathbf{U}_{1,S}$ inside a force-free surfactant-laden-drop, then the sum of the thrust and drag problems for the swimmer give the original problem of swimmer inside a force-free surfactant-laden-drop accurate to $O\left(Pe_s\right)$. One can think along the similar lines regarding the thrust and drag problems for the drop. Since we would like to estimate the sign of $U_{1,S}$ ($U_{1,D}$), we did not include it in the drag problem of the swimmer (drop). As the sum of $O\left(1\right)$ thrust and drag problems for either the swimmer or the drop give the $O\left(1\right)$ original problem (swimmer inside a clean drop where both swimmer and drop are force-free), we expect $F_{0,TS} + F_{0,DS} = 0$ and $F_{0,TD} + F_{0,DD} = 0$. So, only one of the $O\left(1\right)$ thrust and drag forces is an independent quantity.

To understand how the surfactant redistribution affects the swimmer velocity for eccentric configuration, we plot the $O\left(1\right)$ thrust, $O\left(Pe_s\right)$ thrust and (negative of the) $O\left(Pe_s\right)$ drag on the swimmer as a function of eccentricity in figure 3.12. Figure 3.12a is for a neutral swimmer while figure 3.12b is for a puller inside a surfactant-laden-drop. The axis for the $O\left(Pe_s\right)$ ($O\left(1\right)$) forces is on the left (right).

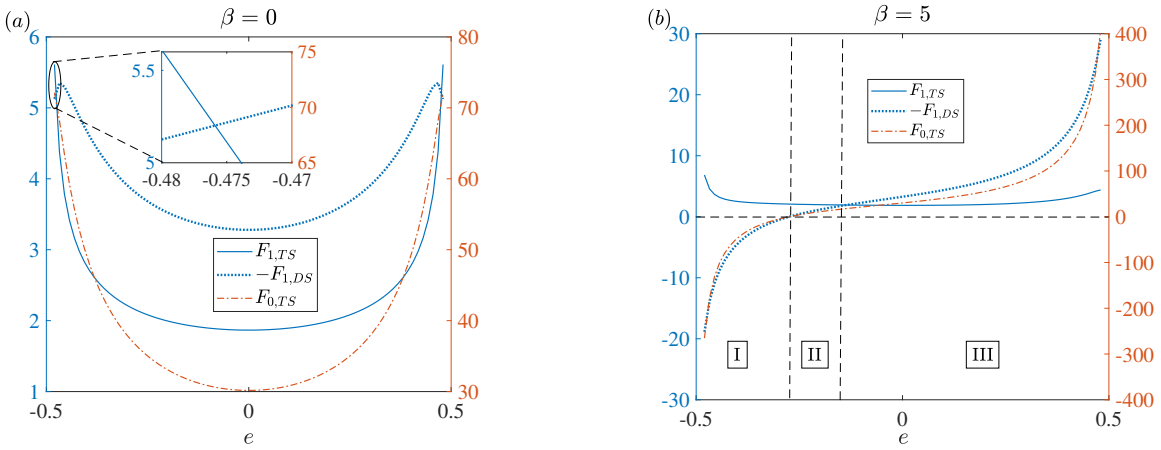

Figure 3.12. : The variation of the thrust and drag forces acting on the swimmer at various order of Pe_s with the eccentricity for (a) neutral swimmer ($\beta = 0$) and (b) puller ($\beta = 5$) inside a surfactant covered drop. The blue solid line, blue dotted line and red dash-dotted line denote the $O(Pe_s)$ thrust, $O(Pe_s)$ (negative) drag and $O(1)$ thrust forces, respectively. The axis for the $O(Pe_s)$ forces is on the left while that for an $O(1)$ force is on the right.

On analyzing the thrust and drag for a neutral swimmer inside a drop, we see from figure 3.12a that the $O(1)$ thrust, $O(Pe_s)$ thrust and (negative of the) $O(Pe_s)$ drag are all positive i.e., $F_{0,TS} > 0$, $F_{1,TS} > 0$, and $-F_{1,DS} > 0$. Noting that the (negative of the) $O(1)$ drag is positive i.e., $-F_{0,DS} = F_{0,TS} > 0$, we conclude that the surfactant redistribution increases the magnitude of both the thrust and the drag for a neutral swimmer inside a drop. But since the increase in the magnitude of the drag is more than the increase in the thrust i.e., $-F_{1,DS} > F_{1,TS}$ for most of the eccentricities, the magnitude of the swimmer velocity should decrease due to the surfactant redistribution for most of the eccentricities i.e., $\text{sgn}(U_{0,S}/U_{1,S}) = -1$. However, at $e = \pm 0.48$, as the increase in the thrust is more than the increase in the magnitude of the drag i.e., $F_{1,TS} > -F_{1,DS}$ as shown in the inset of figure 3.12a, the magnitude of the swimmer velocity should increase due to the surfactant redistribution i.e., $\text{sgn}(U_{0,S}/U_{1,S}) = +1$. This behavior predicted for the $\text{sgn}(U_{0,S}/U_{1,S})$ from the drag and thrust analysis matches exactly with that reported in figure 3.10b.

On analyzing the thrust and drag for a puller inside a drop, we see from figure 3.12b that for eccentricities in regions II and III, the $O(1)$ thrust force, the $O(Pe_s)$ thrust and (negative of the) $O(Pe_s)$ drag are positive i.e., $F_{0,TS} > 0$, $F_{1,TS} > 0$, and $-F_{1,DS} > 0$. Since $-F_{0,DS} = F_{0,TS} > 0$, (negative of the) $O(1)$ drag is positive for the aforementioned eccentricities. So, for these values of eccentricities, the surfactant redistribution increases the magnitude of both the thrust and drag. For eccentricities in region III (II), since $-F_{1,DS} > F_{1,TS}$ ($-F_{1,DS} < F_{1,TS}$), the increase in the magnitude of drag is more (less) than the increase in the thrust, hence the magnitude of the swimmer velocity should decrease (increase) due to the surfactant redistribution i.e., $\text{sgn}(U_{0,S}/U_{1,S}) = -1$ ($\text{sgn}(U_{0,S}/U_{1,S}) = +1$). For eccentricities in region I, the $O(1)$ thrust is negative, so (negative of the) $O(1)$ drag is negative whereas the $O(Pe_s)$ thrust is positive and (negative of the) $O(Pe_s)$ drag is negative i.e., $F_{0,TS} < 0$, $-F_{0,DS} < 0$, $F_{1,TS} > 0$, and $-F_{1,DS} < 0$. Hence, for these eccentricities, the surfactant redistribution increases the magnitude of drag but decreases the magnitude of thrust. This means that for eccentricities in region I, the magnitude of the swimmer velocity

should decrease due to the surfactant redistribution i.e., $\mathrm{sgn}\,(U_{0,S}/U_{1,S}) = -1$. Again, the behavior predicted for the variation of $\mathrm{sgn}\,(U_{0,S}/U_{1,S})$ with the eccentricity from the drag and thrust analysis matches exactly with that reported in figure 3.10c.

A similar analysis can be carried out to understand the influence of surfactant redistribution on the drop velocity (instead of swimmer velocity) for eccentric configurations. For this purpose, we plot in figure 3.13, the $O\,(1)$ thrust, the $O\,(Pe_s)$ thrust, and (negative of the) $O\,(Pe_s)$ drag on the drop for various eccentricities. Again, figure 3.13a is for a neutral swimmer and figure 3.13b is for a puller inside a surfactant-laden-drop.

We analyze the thrust and drag forces acting on a drop containing a neutral swimmer, as plotted in figure 3.13a. For $|e| < 0.466$, we see from this figure that the $O\,(1)$ thrust is positive, so (negative of the) $O\,(1)$ drag is also positive i.e., $-F_{0,DD} = F_{0,TD} > 0$. Also, for these eccentricities, the $O\,(Pe_s)$ thrust is negative and (negative of the) $O\,(Pe_s)$ drag is positive i.e., $F_{1,TD} < 0$, $-F_{1,DD} > 0$. Hence, for $|e| < 0.466$, the surfactant redistribution decreases the thrust but increases the magnitude of drag, so the drop velocity should decrease i.e., $\mathrm{sgn}\,(U_{0,D}/U_{1,D}) = -1$ (compare with figure 3.10b). For $|e| \in (0.466, 0.47)$, there exist some eccentricities (see inset of figure 3.13a) at which the $O\,(1)$ thrust, (negative of the) $O\,(1)$ drag, $O\,(Pe_s)$ thrust, and (negative of the) $O\,(Pe_s)$ drag are all negative i.e., $-F_{0,DD} = F_{0,TD} < 0$, $F_{1,TD} < 0$, $-F_{1,DD} < 0$. So, the surfactant redistribution increases the magnitude of both thrust and drag. But since the increase in the magnitude of thrust is more than the increase in the magnitude of drag for some $|e| \in (0.466, 0.47)$ i.e., $|F_{1,TD}| > |F_{1,DD}|$, the drop velocity should increase i.e., $\mathrm{sgn}\,(U_{0,D}/U_{1,D}) = +1$. This behavior predicted for the $\mathrm{sgn}\,(U_{0,D}/U_{1,D})$ from the drag and thrust analysis matches with that reported in figure 3.10b.

We finally analyze the thrust and drag forces acting on a drop containing a puller swimmer, as plotted in figure 3.13b. For $e > -0.1$, the $O\,(1)$ thrust, (negative of the) $O\,(1)$ drag, and negative of the $O\,(Pe_s)$ drag are positive while $O\,(Pe_s)$ thrust is negative i.e., $-F_{0,DD} = F_{0,TD} > 0$, $-F_{1,DD} > 0$, $F_{1,TD} < 0$. Also, for $e < -0.12$,

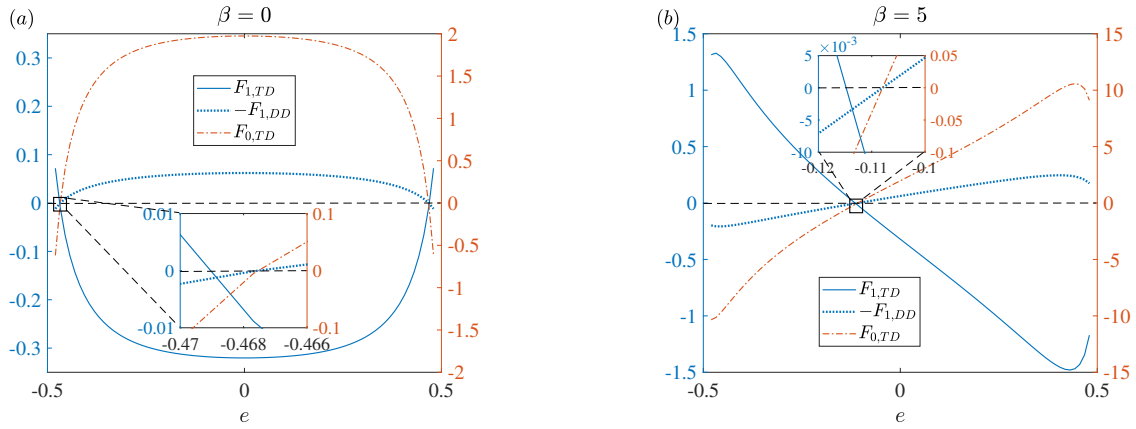

Figure 3.13. : Variation of the thrust and drag forces acting on the drop at various order of Pe_s with the eccentricity for (a) neutral swimmer ($\beta = 0$) and (b) puller ($\beta = 5$) inside a surfactant covered drop. The blue solid line, blue dotted line and red dash-dotted line denote the $O(Pe_s)$ thrust, $O(Pe_s)$ (negative) drag and $O(1)$ thrust forces, respectively. The axis for the $O(Pe_s)$ forces is on the left while that for an $O(1)$ force is on the right.

the $O(1)$ thrust, (negative of the) $O(1)$ drag, and (negative of the) $O(Pe_s)$ drag are negative while the $O(Pe_s)$ thrust is positive i.e., $-F_{0,DD} = F_{0,TD} < 0$, $-F_{1,DD} < 0$, $F_{1,TD} > 0$. Hence, for $e < -0.12$ or $e > -0.1$, the surfactant redistribution decreases the magnitude of the thrust but increases the magnitude of drag, so the drop velocity should decrease i.e., $\text{sgn}(U_{0,D}/U_{1,D}) = -1$ (compare with figure 3.10c). For $e \in (-0.12, -0.1)$, there exist some eccentricities at which the $O(1)$ thrust, (negative of the) $O(1)$ drag, $O(Pe_s)$ thrust, and (negative of the) $O(Pe_s)$ drag are all negative. So, the surfactant redistribution increases the magnitude of both thrust and drag. Also, for some $e \in (-0.12, -0.1)$, as the increase in the magnitude of thrust is more than the increase in the magnitude of drag i.e., $|F_{1,TD}| > |F_{1,DD}|$, the drop velocity increases due to surfactant redistribution i.e., $\text{sgn}(U_{0,D}/U_{1,D}) = +1$. Again, the behavior predicted for the variation of $\text{sgn}(U_{0,D}/U_{1,D})$ with the eccentricity from the drag and thrust analysis matches with that reported in figure 3.10c.

3.4.4 Can a time-reversible swimmer inside a surfactant-laden-drop have a net motion?

We see that the only non-linearity in the governing equations and the boundary conditions occurs in the surfactant transport equation (3.9). But this non-linearity does not appear in the perturbed surfactant transport equations until the equation at $O(Pe_s^2)$, equation (3.21). Hence, the governing equations and the boundary conditions at $O(1)$ and $O(Pe_s)$ are linear in the squirming modes, but not those at $O(Pe_s^2)$. Due to this reason, the swimmer and drop velocities at $O(1)$ and $O(Pe_s)$ should be linear in the swimming modes B_1, B_2... but these velocities at $O(Pe_s^2)$ should be non-linear. So, if these swimming modes are time-periodic with zero time-average (such a swimmer is called time-reversible swimmer), the leading order contribution to the time-averaged swimmer and drop velocities should come from the $O(Pe_s^2)$ problem. Therefore, it seems that the swimmer and drop might propel with non-zero time-averaged velocities even if the swimmer is time-reversible due to the advection

of the surfactant on the surface of the drop. This is a remarkable result since it provides a method to escape from the constraints of the scallop theorem which can have potential applications in the motion of synthetic swimmers near interfaces as the interfaces are inevitably covered with some impurities.

We illustrate the physical reasoning provided earlier by deriving the time-averaged swimmer and drop velocities of a two-mode time-reversible swimmer, initially located at the center of the surfactant-laden-drop. Since $U_S > U_D$ for the concentric configuration, the swimmer never stays at the center of the drop. However, if the time period of the swimming modes is much smaller than the time taken by the swimmer or the drop to traverse a drop radius i.e., $T = 2\pi/\omega \ll a/U_{sq}$ (T and ω are the time period and the angular frequency of the swimming modes), then eccentricity changes negligibly during one time period. In this case, we can calculate the time-averaged swimmer and drop velocities by fixing the eccentricity at its initial value. Hence, the time-averaged swimmer and drop velocities

$$\langle U_S \rangle = \frac{1}{T}\int_0^T U_S\left(e\left(t\right);t\right)dt; \;\; \langle U_D \rangle = \frac{1}{T}\int_0^T U_D\left(e\left(t\right);t\right)dt$$

can be simplified as

$$\langle U_S \rangle = \frac{1}{T}\int_0^T U_S\left(e\left(0\right);t\right)dt; \;\; \langle U_D \rangle = \frac{1}{T}\int_0^T U_D\left(e\left(0\right);t\right)dt$$

Since the swimmer is at the center of the drop at $t = 0$ i.e., $e\left(0\right) = 0$, we have

$$\langle U_S \rangle = \frac{1}{T}\int_0^T U_S\left(0;t\right)dt; \;\; \langle U_D \rangle = \frac{1}{T}\int_0^T U_D\left(0;t\right)dt$$

Here, we denoted the swimmer and drop velocities by $U_S\left(e\left(t\right);t\right)$ and $U_D\left(e\left(t\right);t\right)$, respectively. This is because as the time progresses, the eccentricity changes which in turn modifies the swimmer and drop velocities. Also, for a fixed eccentricity U_S and

U_D can change with time since the swimming modes are time-dependent. Denoting $\frac{1}{T}\int_0^T U(0;t)\,dt$ by $\langle U|_{e=0}\rangle$, we have

$$\begin{aligned}\langle U_S\rangle &= \langle U_S|_{e=0}\rangle = \langle U_{0,S}|_{e=0}\rangle + Pe_s\langle U_{1,S}|_{e=0}\rangle + Pe_s^2\langle U_{2,S}|_{e=0}\rangle + O\left(Pe_s^3\right)\\ \langle U_D\rangle &= \langle U_D|_{e=0}\rangle = \langle U_{0,D}|_{e=0}\rangle + Pe_s\langle U_{1,D}|_{e=0}\rangle + Pe_s^2\langle U_{2,D}|_{e=0}\rangle + O\left(Pe_s^3\right)\end{aligned} \tag{3.56}$$

Here $(\,)|_{e=0}$ denotes the quantity when the swimmer is at the center of the drop and hence the expressions for $U_{0,S}|_{e=0}$, $U_{0,D}|_{e=0}$, $U_{1,S}|_{e=0}$, $U_{1,D}|_{e=0}$, $U_{2,S}|_{e=0}$, and $U_{2,D}|_{e=0}$ are given by equations (3.43)-(3.46), (3.72)-(3.73). From the equations (3.43)-(3.46), we see that $U_{0,S}|_{e=0}$, $U_{0,D}|_{e=0}$, $U_{1,S}|_{e=0}$, and $U_{1,D}|_{e=0}$ are linear in the swimming modes. Also since the swimming modes are time periodic with zero time-average i.e., $\langle A_n\rangle = \langle B_n\rangle = 0$, we deduce that

$$\langle U_{0,S}|_{e=0}\rangle = \langle U_{0,D}|_{e=0}\rangle = \langle U_{1,S}|_{e=0}\rangle = \langle U_{1,D}|_{e=0}\rangle = 0 \tag{3.57}$$

Hence the equations for the time-averaged swimmer and drop velocities simplify to

$$\begin{aligned}\langle U_S\rangle &= Pe_s^2\langle U_{2,S}|_{e=0}\rangle + O\left(Pe_s^3\right)\\ \langle U_D\rangle &= Pe_s^2\langle U_{2,D}|_{e=0}\rangle + O\left(Pe_s^3\right)\end{aligned} \tag{3.58}$$

Using the equations (3.72)-(3.73) along with the time-reversibility of the swimming modes, we derive

$$\begin{aligned}\langle U_S\rangle &= Pe_s^2\, J_1\langle B_1B_2\rangle + O\left(Pe_s^3\right)\\ \langle U_D\rangle &= Pe_s^2\, K_1\langle B_1B_2\rangle + O\left(Pe_s^3\right)\end{aligned} \tag{3.59}$$

where

$$K_1 = \frac{2}{5}\frac{(\chi^4+\chi^3+\chi^2+\chi+1)}{(\chi+1)}J_1$$

$$J_1 = \frac{(15\chi^4+45\chi^3+55\chi^2+45\chi+15)\,\chi^5\lambda^2 Ma\,(\chi^2-1)}{36((\lambda-1)\,\chi^5+3/2\lambda+1)^2\left(\begin{array}{l}(\lambda-1)\,\chi^7+(3\lambda-3)\,\chi^6+(6\lambda-6)\,\chi^5+\left(\frac{15}{2}\lambda-\frac{15}{4}\right)\chi^4\\ +\left(\frac{15}{2}\lambda+\frac{15}{4}\right)\chi^3+(6\lambda+6)\,\chi^2+(3\lambda+3)\,\chi+\lambda+1\end{array}\right)}$$

As $\langle B_1B_2\rangle$ is non-zero for non-orthogonal time periodic functions with zero time-average $B_1(t)$ and $B_2(t)$, we see from equations (3.59) that the time-averaged swimmer and drop velocities of a time-reversible swimmer inside a drop are non-zero at

$O\left(Pe_s^2\right)$. Therefore, the surfactant advection on the drop surface enables a drop containing a time-reversible swimmer to evade the scallop theorem, thereby leading to a time-averaged proplusion of the swimmer and the drop.

3.5 Conclusions

We studied the motion of a spherical swimmer inside a surfactant laden drop for axisymmetric configurations by expanding the variables in terms of surface Péclet number (Pe_s), under the assumption of zero Reynolds number. This small surface Péclet analysis is valid when small drops (of size $1-100\,\mu$m), covered with small sized surfactants [91, 92], contain small microswimmers (of size $1-10\,\mu$m) whose speed in an unbounded fluid is small ($\approx 1-100\,\mu$m/s). Thermal noise in experiments may change the orientation of the swimmer from the axisymmetric configuration. Numerical studies, not in the scope of this manuscript, are needed to investigate the stability of this configuration.

For a two-mode squirmer inside a drop, the surfactant redistribution can either increase or decrease the magnitude of swimmer and drop velocities, depending on the value of eccentricity. This was explained using the drag and thrust decomposition for the swimmer and the drop separately. Due to the surfactant redistribution, the magnitude of the drag on the swimmer or the drop increases at all eccentricities, but the magnitude of thrust increases for some eccentricities while decreasing at other eccentricities. When the increase in the magnitude of thrust is more than the increase in the magnitude of drag, the magnitude of swimmer or drop velocity increases due to the surfactant redistribution. If the increase in the magnitude of thrust is less than the increase in the magnitude of drag or if the magnitude of thrust decreases due to the surfactant redistribution, the magnitude of swimmer or drop velocity decrease.

The far-field representation of a clean drop engulfing a pusher swimmer at its center is a puller; the strength of this far-field is reduced if the drop is covered with a surfactant. Due to the advection of the surfactant on the drop surface, a

time-reversible swimmer and the drop, within which the swimmer is engulfed, propel in a time-averaged sense by escaping from the constraints of the scallop theorem. Hence, one can use simple time-reversible swimmers [93] instead of sophisticated helical swimmers such as artificial bacterial flagella [7] (which are not time-reversible) to transport either the contents of the drop or the drop itself.

Inside a clean drop, a two-mode squirmer with $\beta < \beta_c$ (β is the ratio of the squirming modes) achieves an eccentrically stable configuration (where the velocity of the swimmer is equal to the velocity of the drop), while squirmers with $\beta > \beta_c$ move to the top or bottom surface of the drop. Here, β_c is negative and depends on the viscosity ratio and the size ratio. The effect of surfactant redistribution is to shift the eccentrically stable position, achieved by swimmers with $\beta < \beta_c$, towards the top surface of the drop, albeit this shift is very small.

3.6 Appendix A: Linear equations obtained while satisfying equations (3.12)-(3.18) for the concentric configuration

Enforcing the boundary condition on the surface of the swimmer, equation (3.12), we obtain

$$\bar{p}^{(1)}_{j,n}\,\chi^{n+1}+\bar{\phi}^{(1)}_{j,n}\,\chi^{n-1}+\bar{p}^{(1)}_{j,-n-1}\,\chi^{-n}+\bar{\phi}^{(1)}_{j,-n-1}\,\chi^{-n-2}=\frac{2n+1}{2}\int_{-1}^{1} v^{(1)}_{j,r}\ (r=\chi)\,P_n\,(\mu)\ d\mu, \tag{3.60}$$

$$\begin{aligned}\left[\begin{array}{l} -\dfrac{(n+3)}{2}\bar{p}^{(1)}_{j,n}\,\chi^{n+1}-\dfrac{(n+1)}{2}\bar{\phi}^{(1)}_{j,n}\,\chi^{n-1} \\ +\dfrac{(n-2)}{2}\bar{p}^{(1)}_{j,-n-1}\,\chi^{-n}+\dfrac{n}{2}\,\bar{\phi}^{(1)}_{j,-n-1}\,\chi^{-n-2}\end{array}\right] &=\frac{2n+1}{4}\int_{-1}^{1} v^{(1)}_{j,\theta}\,(r=\chi)\,P^1_n\,(\mu)\,d\mu \\ &=\frac{n\,(n+1)\,(2n+1)}{8}\int_{-1}^{1} v^{(1)}_{j,\theta}\,(r=\chi)\,V_n\,(\mu)\,d\mu.\end{aligned} \tag{3.61}$$

For the swimmer and drop to be force-free, we derive respectively,

$$p^{(1)}_{j,-2}=0, \tag{3.62}$$

$$p^{(2)}_{j,-2} = 0. \tag{3.63}$$

For the flow field far away from the drop to approach the negative of the velocity of the drop, we obtain

$$\begin{aligned} &\bar{\phi}^{(2)}_{j,n} = 0, \text{ for } n \geq 2, \\ &\bar{p}^{(2)}_{j,n} = 0, \text{ for } n \geq -1, \\ &\bar{\phi}^{(2)}_{j,1} = -U_{j,D}. \end{aligned} \tag{3.64}$$

In order to satisfy the boundary conditions on the surface of the drop, equations (3.16)-(3.18), we obtain respectively

$$\bar{p}^{(k)}_{j,n} + \bar{\phi}^{(k)}_{j,n} + \bar{p}^{(k)}_{j,-n-1} + \bar{\phi}^{(k)}_{j,-n-1} = 0, \text{ where } k = 1, 2, \tag{3.65}$$

$$\begin{aligned} &-\frac{(n+3)}{2}\left(\bar{p}^{(1)}_{j,n} - \bar{p}^{(2)}_{j,n}\right) - \frac{(n+1)}{2}\left(\bar{\phi}^{(1)}_{j,n} - \bar{\phi}^{(2)}_{j,n}\right) \\ &+\frac{(n-2)}{2}\left(\bar{p}^{(1)}_{j,-n-1} - \bar{p}^{(2)}_{j,-n-1}\right) + \frac{n}{2}\left(\bar{\phi}^{(1)}_{j,-n-1} - \bar{\phi}^{(2)}_{j,-n-1}\right) = 0, \end{aligned} \tag{3.66}$$

$$\begin{aligned} &\left(n^2-1\right)\left(-\bar{\phi}^{(2)}_{j,n} + \lambda\bar{\phi}^{(1)}_{j,n}\right) + n\left(n+2\right)\left(-\bar{p}^{(2)}_{j,n} + \lambda\bar{p}^{(1)}_{j,n}\right) + n\left(n+2\right)\left(-\bar{\phi}^{(2)}_{j,-n-1} + \lambda\bar{\phi}^{(1)}_{j,-n-1}\right) \\ &+\left(n^2-1\right)\left(-\bar{p}^{(2)}_{j,-n-1} + \lambda\bar{p}^{(1)}_{j,-n-1}\right) = -Ma \times \frac{n\left(n+1\right)}{2}\Gamma_{j,n}. \end{aligned} \tag{3.67}$$

These equations for $n = 0$ and 1 are first solved to determine the swimmer and drop velocities along with some unknown constants in the flow fields. These equations for $n \geq 2$ are then solved to determine the remaining constants and hence the flow fields in both phases.

3.7 Appendix B: Flow field due to a 'squirmer' at the center of a drop at various orders of Pe_s

In this section, we provide the expressions for the constants encountered in the velocity components along with the swimmer and drop velocities at $O\left(1\right)$, $O\left(Pe_s\right)$

and $O\left(Pe_s^2\right)$. We note that the flow field, swimmer and the drop velocities at $O\left(1\right)$ and $O\left(Pe_s\right)$ are derived for a general n mode squirmer. At $O\left(Pe_s^2\right)$, we derived the swimmer and drop velocities for a squirmer having few modes, namely A_1, A_2, A_3, B_1, B_2 and B_3.

3.7.1 Flow field at $O\left(1\right)$

For $n = 0, 1$, we have

$$\bar{p}^{(2)}_{0,-1} = \bar{p}^{(2)}_{0,-2} = \bar{p}^{(2)}_{0,1} = \bar{p}^{(1)}_{0,-1} = \bar{p}^{(1)}_{0,-2} = \bar{\phi}^{(2)}_{0,-1} = \bar{\phi}^{(1)}_{0,-1} = 0,$$

$$\bar{\phi}^{(2)}_{0,1} = -10\frac{\chi^3\lambda\left(A_1+B_1\right)}{\left(6\lambda-6\right)\chi^5+9\lambda+6},$$

$$\bar{p}^{(1)}_{0,1} = -2\frac{\chi^3\left(A_1+B_1\right)\left(\lambda-1\right)}{\left(2\lambda-2\right)\chi^5+3\lambda+2},$$

$$\bar{\phi}^{(1)}_{0,1} = -10\frac{\chi^3\left(A_1+B_1\right)}{\left(6\lambda-6\right)\chi^5+9\lambda+6},$$

$$\bar{\phi}^{(2)}_{0,-2} = 10\frac{\chi^3\lambda\left(A_1+B_1\right)}{\left(6\lambda-6\right)\chi^5+9\lambda+6},$$

$$\bar{\phi}^{(1)}_{0,-2} = 6\frac{\left(A_1+B_1\right)\left(\lambda+2/3\right)\chi^3}{6\chi^5\lambda-6\chi^5+9\lambda+6}.$$

For $n \geq 2$, we have

$$\bar{p}^{(2)}_{0,-n-1} = 2\frac{\left(\begin{array}{l}-\left(n+3/2\right)\left(A_n n+A_n+2B_n\right)\chi^{3n-1}+\left(n-1/2\right)\left(A_n n+3A_n+2B_n\right)\chi^{3n+1}\\+\left(n-1/2\right)\left(A_n n-2B_n\right)\chi^{n-2}-\left(A_n n-2A_n-2B_n\right)\chi^n\left(n+3/2\right)\end{array}\right)\chi^3\lambda}{\left(\begin{array}{l}4\left(n+1/2\right)\left(n-\lambda+1/2\right)\chi^{4+2n}+\left(-8n^2-8n+6\right)\chi^{2+2n}\\+\left(4\lambda-4\right)\chi^{4n+3}+4\left(n+1/2\right)\left(n+\lambda+1/2\right)\chi^{2n}-4\chi\left(\lambda+1\right)\end{array}\right)},$$

$$\bar{p}^{(1)}_{0,-n-1} = -2\frac{\chi^3\left(\begin{array}{l}-\left(A_n n+3A_n+2B_n\right)\left(n-\lambda+1/2\right)\chi^{3n+1}\\+\left(n+3/2\right)\left(A_n n+A_n+2B_n\right)\chi^{3n-1}+\chi^{n-2}\left(\lambda+1\right)\left(A_n n-2B_n\right)\end{array}\right)}{\left(\begin{array}{l}4\left(n+1/2\right)\left(n-\lambda+1/2\right)\chi^{4+2n}+\left(-8n^2-8n+6\right)\chi^{2+2n}\\+\left(4\lambda-4\right)\chi^{4n+3}+4\left(n+1/2\right)\left(n+\lambda+1/2\right)\chi^{2n}-4\chi\left(\lambda+1\right)\end{array}\right)},$$

$$\bar{p}^{(1)}_{0,n} = -2\frac{\chi^3\begin{pmatrix}(\lambda-1)\left(A_n n + A_n + 2B_n\right)\chi^{3n-1} + (n-1/2)\left(A_n n - 2B_n\right)\chi^{n-2}\\ -\left(A_n n - 2A_n - 2B_n\right)\chi^n\left(n-\lambda+1/2\right)\end{pmatrix}}{\begin{pmatrix}4\left(n+1/2\right)\left(n-\lambda+1/2\right)\chi^{4+2n} + \left(-8n^2-8n+6\right)\chi^{2+2n}\\ +\left(4\lambda-4\right)\chi^{4n+3} + 4\left(n+1/2\right)\left(n+\lambda+1/2\right)\chi^{2n} - 4\chi\left(\lambda+1\right)\end{pmatrix}},$$

$$\bar{\phi}^{(1)}_{0,n} = 2\frac{\chi^3\begin{pmatrix}(\lambda-1)\left(A_n n + 3A_n + 2B_n\right)\chi^{3n+1} + (n+\lambda+1/2)\left(A_n n - 2B_n\right)\chi^{n-2}\\ -\left(A_n n - 2A_n - 2B_n\right)\chi^n\left(n+3/2\right)\end{pmatrix}}{\begin{pmatrix}4\left(n+1/2\right)\left(n-\lambda+1/2\right)\chi^{4+2n} + \left(-8n^2-8n+6\right)\chi^{2+2n}\\ +\left(4\lambda-4\right)\chi^{4n+3} + 4\left(n+1/2\right)\left(n+\lambda+1/2\right)\chi^{2n} - 4\chi\left(\lambda+1\right)\end{pmatrix}},$$

$$\bar{\phi}^{(2)}_{0,-n-1} = -\frac{2\chi^3\lambda\begin{pmatrix}-\left(n+\frac{3}{2}\right)\left(\left(n+1\right)A_n + 2B_n\right)\chi^{3n-1} + \left(n-\frac{1}{2}\right)\left(\left(n+3\right)A_n + 2B_n\right)\chi^{3n+1}\\ +\left(n-\frac{1}{2}\right)\left(A_n n - 2B_n\right)\chi^{n-2} - \left(\left(n-2\right)A_n - 2B_n\right)\chi^n\left(n+\frac{3}{2}\right)\end{pmatrix}}{\begin{pmatrix}4\left(n+\frac{1}{2}\right)\left(n-\lambda+\frac{1}{2}\right)\chi^{4+2n} + \left(-8n^2-8n+6\right)\chi^{2+2n}\\ +\left(4\lambda-4\right)\chi^{4n+3} + 4\left(n+\frac{1}{2}\right)\left(n+\lambda+\frac{1}{2}\right)\chi^{2n} - 4\chi\left(\lambda+1\right)\end{pmatrix}},$$

$$\bar{\phi}^{(1)}_{0,-n-1} = 2\frac{\chi^3\begin{pmatrix}\left(n+\lambda+1/2\right)\left(A_n n + A_n + 2B_n\right)\chi^{3n-1} - \left(n-1/2\right)\left(A_n n + 3A_n + 2B_n\right)\chi^{3n+1}\\ +\chi^n\left(\lambda+1\right)\left(A_n n - 2A_n - 2B_n\right)\end{pmatrix}}{\begin{pmatrix}4\left(n+1/2\right)\left(n-\lambda+1/2\right)\chi^{4+2n} + \left(-8n^2-8n+6\right)\chi^{2+2n} + \left(4\lambda-4\right)\chi^{4n+3}\\ +4\left(n+1/2\right)\left(n+\lambda+1/2\right)\chi^{2n} - 4\chi\left(\lambda+1\right)\end{pmatrix}}.$$

3.7.2 Swimmer and drop velocities at $O(1)$

$$U_{0,S} = \frac{-12\left(\lambda-1\right)\left(A_1 + B_1/2\right)\chi^5 + 10\chi^3\left(A_1+B_1\right)\left(\lambda-1\right) - 3\left(A_1 - 2B_1\right)\left(\lambda+2/3\right)}{\left(6\lambda-6\right)\chi^5 + 9\lambda + 6}, \tag{3.68}$$

$$U_{0,D} = 10\frac{\chi^3\lambda\left(A_1+B_1\right)}{\left(6\lambda-6\right)\chi^5 + 9\lambda + 6}. \tag{3.69}$$

3.7.3 Surfactant concentration at $O(Pe_s)$

Noting that the flow field on the surface of the drop at $O(1)$ can be written as $v_{0,\theta}|_{Drop} = \sum_{n=1}^{\infty} u_{0,n} V_n(\cos\theta)$, the surfactant concentration at $O(Pe_s)$, $\Gamma_1 = \sum_{n=1}^{\infty} \Gamma_{1,n} P_n(\cos\theta)$ is evaluated using

$$\Gamma_{1,n} = -\frac{2u_{0,n}}{n(n+1)}.$$

3.7.4 Flow field at $O(Pe_s)$

For $n = 0, 1$, we have

$$\bar{p}^{(2)}_{1,-1} = \bar{p}^{(2)}_{1,-2} = \bar{p}^{(2)}_{1,1} = \bar{p}^{(1)}_{1,-1} = \bar{p}^{(1)}_{1,-2} = \bar{\phi}^{(2)}_{1,-1} = \bar{\phi}^{(1)}_{1,-1} = 0,$$

$$\bar{\phi}^{(2)}_{1,1} = -\frac{10}{3}\frac{Ma\lambda(A_1+B_1)\chi^3(\chi^5-1)}{4\chi^{10}\lambda^2 - 8\chi^{10}\lambda + 4\chi^{10} + 12\chi^5\lambda^2 - 4\chi^5\lambda - 8\chi^5 + 9\lambda^2 + 12\lambda + 4},$$

$$\bar{p}^{(1)}_{1,1} = \frac{5Ma\lambda(A_1+B_1)\chi^3}{(2\chi^5\lambda - 2\chi^5 + 3\lambda + 2)^2},$$

$$\bar{\phi}^{(1)}_{1,1} = -\frac{5}{6}\frac{(A_1+B_1)Ma(\chi^5+3/2)\lambda\chi^3}{((\lambda-1)\chi^5 + 3/2\lambda + 1)^2},$$

$$\bar{\phi}^{(2)}_{1,-2} = \frac{5}{6}\frac{Ma\lambda(A_1+B_1)\chi^3(\chi^5-1)}{((\lambda-1)\chi^5 + 3/2\lambda + 1)^2},$$

$$\bar{\phi}^{(1)}_{1,-2} = \frac{5}{6}\frac{Ma\lambda(A_1+B_1)\chi^8}{((\lambda-1)\chi^5 + 3/2\lambda + 1)^2}.$$

For $n \geq 2$, we have

$$\bar{p}^{(2)}_{1,-n-1} = \frac{Ma}{2}\frac{\begin{pmatrix} -1/2(n+1/2)^2\chi^{2n-1} + \left(n^2+n-3/4\right)\chi^{2n+1} \\ -1/2(n+1/2)^2\chi^{2n+3} + 1/2\chi^{4n+2} + 1/2 \end{pmatrix} n(n+1)\Gamma_{1,n}\chi}{(n+1/2)\begin{pmatrix} (n+1/2)(n-\lambda+1/2)\chi^{4+2n} + \left(-2n^2-2n+3/2\right)\chi^{2+2n} \\ +(\lambda-1)\chi^{4n+3} + (n+1/2)(n+\lambda+1/2)\chi^{2n} - \chi(\lambda+1) \end{pmatrix}},$$

$$\bar{p}^{(1)}_{1,-n-1} = \frac{Ma}{8}\frac{n(n+1)\Gamma_{1,n}\chi^3(2\chi^{2n-3}n - 2\chi^{2n-1}n + 2\chi^{4n} + \chi^{2n-3} - 3\chi^{2n-1})}{(n+1/2)\begin{pmatrix} (n+1/2)(n-\lambda+1/2)\chi^{4+2n} + \left(-2n^2-2n+3/2\right)\chi^{2+2n} \\ +(\lambda-1)\chi^{4n+3} + (n+1/2)(n+\lambda+1/2)\chi^{2n} - \chi(\lambda+1) \end{pmatrix}},$$

$$\bar{p}^{(1)}_{1,n} = \frac{Ma}{8}\frac{n\left(n+1\right)\Gamma_{1,n}\chi\left(2\chi^{2n+1}n-2\chi^{2n-1}n-\chi^{2n+1}-\chi^{2n-1}+2\right)}{\left(n+1/2\right)\left(\begin{array}{l}\left(n+1/2\right)\left(n-\lambda+1/2\right)\chi^{4+2n}+\left(-2n^2-2n+3/2\right)\chi^{2+2n}\\+\left(\lambda-1\right)\chi^{4n+3}+\left(n+1/2\right)\left(n+\lambda+1/2\right)\chi^{2n}-\chi\left(\lambda+1\right)\end{array}\right)},$$

$$\bar{\phi}^{(1)}_{1,n} = -\frac{Ma}{8}\frac{n\left(n+1\right)\Gamma_{1,n}\chi\left(2\chi^{2n+3}n-2\chi^{2n+1}n+\chi^{2n+3}+2-3\chi^{2n+1}\right)}{\left(n+1/2\right)\left(\begin{array}{l}\left(n+1/2\right)\left(n-\lambda+1/2\right)\chi^{4+2n}+\left(-2n^2-2n+3/2\right)\chi^{2+2n}\\+\left(\lambda-1\right)\chi^{4n+3}+\left(n+1/2\right)\left(n+\lambda+1/2\right)\chi^{2n}-\chi\left(\lambda+1\right)\end{array}\right)},$$

$$\bar{\phi}^{(2)}_{1,-n-1} = -\frac{Ma}{2}\frac{\left(\begin{array}{l}-1/2(n+1/2)^2\chi^{2n-1}+\left(n^2+n-3/4\right)\chi^{2n+1}\\-1/2(n+1/2)^2\chi^{2n+3}+1/2\chi^{4n+2}+1/2\end{array}\right)n\left(n+1\right)\Gamma_{1,n}\chi}{\left(n+1/2\right)\left(\begin{array}{l}\left(n+1/2\right)\left(n-\lambda+1/2\right)\chi^{4+2n}+\left(-2n^2-2n+3/2\right)\chi^{2+2n}\\+\left(\lambda-1\right)\chi^{4n+3}+\left(n+1/2\right)\left(n+\lambda+1/2\right)\chi^{2n}-\chi\left(\lambda+1\right)\end{array}\right)},$$

$$\bar{\phi}^{(1)}_{1,-n-1} = -\frac{Ma}{4}\frac{\left(\left(n-1/2\right)\chi^{2n-1}+\left(-n-1/2\right)\chi^{2n+1}+\chi^{4n}\right)n\left(n+1\right)\Gamma_{1,n}\chi^3}{\left(n+1/2\right)\left(\begin{array}{l}\left(n+1/2\right)\left(n-\lambda+1/2\right)\chi^{4+2n}+\left(-2n^2-2n+3/2\right)\chi^{2+2n}\\+\left(\lambda-1\right)\chi^{4n+3}+\left(n+1/2\right)\left(n+\lambda+1/2\right)\chi^{2n}-\chi\left(\lambda+1\right)\end{array}\right)}.$$

3.7.5 Swimmer and drop velocities at $O\left(Pe_s\right)$

$$U_{1,S} = -\frac{25Ma\chi^3\lambda\left(1-\chi\right)\left(\chi+1\right)\left(A_1+B_1\right)}{12\left(\left(\lambda-1\right)\chi^5+3/2\lambda+1\right)^2}, \tag{3.70}$$

$$U_{1,D} = -\frac{5}{6}\frac{Ma\lambda\left(A_1+B_1\right)\chi^3\left(1-\chi^5\right)}{\left(\left(\lambda-1\right)\chi^5+3/2\lambda+1\right)^2}. \tag{3.71}$$

3.7.6 Surfactant concentration at $O\left(Pe_s^2\right)$

Since the $O\left(Pe_s^2\right)$ problem is nonlinear in the squirming modes, for simplicity, we only consider few modes, namely A_1, A_2, A_3, B_1, B_2 and B_3. Noting that the flow field on the surface of the drop at $O\left(Pe_s\right)$ can be written as $v_{1,\theta}|_{Drop} = \sum_{n=1}^{\infty} u_{1,n}\, V_n\left(\cos\theta\right)$, the component of surfactant concentration at $O\left(Pe_s^2\right)$ useful for evaluating the swimmer and drop velocities at $O\left(Pe_s^2\right)$ is given as

$$\Gamma_{2,1} = \frac{2}{15}u_{0,1}u_{0,2} + \frac{1}{70}u_{0,2}u_{0,3} - u_{1,1}.$$

3.7.7 Swimmer and drop velocities at $O\left(Pe_s^2\right)$

$$U_{2,S} = \frac{5\left(1-\chi^2\right) Ma\, \Gamma_{2,1}}{(6\lambda-6)\,\chi^5 + 9\lambda + 6}, \tag{3.72}$$

$$U_{2,D} = \frac{2\left(1-\chi^5\right) Ma\, \Gamma_{2,1}}{(6\lambda-6)\,\chi^5 + 9\lambda + 6}. \tag{3.73}$$

3.8 Appendix C: Integral theorem

In this appendix, we derive an integral theorem for the locomotion of a swimmer inside a surfactant covered drop. A version of this theorem was derived earlier in the context of the motion of compound drops [94]. Using this theorem, one can find the swimmer and drop velocities at $O\left(Pe_s^j\right)$ using only the knowledge of surfactant concentration at $O\left(Pe_s^j\right)$ and the solution of two auxiliary problems. Notably, one does not need to determine the flow field at $O\left(Pe_s^j\right)$ to find the swimmer and drop velocities at $O\left(Pe_s^j\right)$. Also since the auxiliary problems are the same at each order of Pe_s, they have to be solved only once and their solution can be used in the integral theorems at any order of Pe_s. Even though this theorem is valid for axisymmetric configurations, we illustrate its use in finding the swimmer and drop velocities for concentric configuration.

We consider a uniform flow past a stationary clean drop containing a stationary rigid sphere as the first auxiliary problem. We denote the variables of this problem with a caret over them. A translating rigid sphere embedded in a stationary clean drop, the drop itself suspended in a quiescent fluid is considered as the second auxiliary problem. We denote the variables of this problem with a tilde over them. We note that the geometric configuration of the auxiliary problems is the same as that of the original problem i.e., the position of a rigid sphere inside a clean drop, in the auxiliary problem, is the same as that of the swimmer inside a surfactant-laden-drop, in the original problem. Since the flow field of the auxiliary problem satisfies the Stokes equations along with the incompressibility condition, we proceed to specify the non-

dimensionalized boundary conditions. Here, the non-dimensionalization is carried out in the same fashion as that of the original problem. The boundary conditions on the drop surface are the same for both auxiliary problems. These conditions for the first auxiliary problem are given as

$$\begin{aligned} &\text{On the drop :} \\ &\qquad \hat{\mathbf{v}}^{(1)} \cdot \mathbf{n} = \hat{\mathbf{v}}^{(2)} \cdot \mathbf{n} = 0 \\ &\qquad \hat{\mathbf{v}}^{(1)} \cdot \boldsymbol{\Delta} = \hat{\mathbf{v}}^{(2)} \cdot \boldsymbol{\Delta} \\ &\qquad \mathbf{n} \cdot \left(\hat{T}^{(2)} - \lambda \hat{T}^{(1)} \right) \cdot \boldsymbol{\Delta} = \mathbf{0} \end{aligned} \tag{3.74}$$

These conditions for the second auxiliary problem can be derived by replacing the variables of the first auxiliary problem with those of second auxiliary problem in equation (3.74). The remaining boundary conditions for the auxiliary problems are given as

For the first auxiliary problem

$$\begin{aligned} &\text{On the sphere : } \hat{\mathbf{v}}^{(1)} = \mathbf{0} \\ &\text{Far} - \text{away from the drop : } \hat{\mathbf{v}}^{(2)} = \hat{\mathbf{U}} \end{aligned} \tag{3.75}$$

For the second auxiliary problem

$$\begin{aligned} &\text{On the sphere : } \tilde{\mathbf{v}}^{(1)} = \tilde{\mathbf{U}} \\ &\text{Far} - \text{away from the drop : } \tilde{\mathbf{v}}^{(2)} \to \mathbf{0} \end{aligned} \tag{3.76}$$

where $\hat{\mathbf{U}}$ and $\tilde{\mathbf{U}}$ represent the uniform stream far-away from the drop and the translational velocity of the rigid sphere in the first and second auxiliary problems, respectively. We also denote the hydrodynamic force experienced by the rigid sphere and the drop in the first auxiliary problem (second auxiliary problem) by $\hat{\mathbf{F}}_{Sp}$ and $\hat{\mathbf{F}}_{D}$ $\left(\tilde{\mathbf{F}}_{Sp} \text{and} \, \tilde{\mathbf{F}}_{D} \right)$, respectively.

We start with the reciprocal theorem between two flow fields $\left(\bar{\mathbf{v}}, \bar{T} \right)$ and $(\mathbf{v}, T)$ given as

$$\nabla \cdot \left(T \cdot \bar{\mathbf{v}} - \bar{T} \cdot \mathbf{v} \right) = 0 \tag{3.77}$$

We apply this relation to the flows $\left(\mathbf{v}_j^{(2)}, T_j^{(2)}\right)$ and $\left(\hat{\mathbf{v}}^{(2)}, \hat{T}^{(2)}\right)$, integrate over the domain $\mathcal{D}_2$ and use the Gauss-Divergence theorem to get

$$\int_\infty \mathbf{n} \cdot \left(T_j^{(2)} \cdot \hat{\mathbf{v}}^{(2)} - \hat{T}^{(2)} \cdot \mathbf{v}_j^{(2)}\right) dS = \int_D \mathbf{n} \cdot \left(T_j^{(2)} \cdot \hat{\mathbf{v}}^{(2)} - \hat{T}^{(2)} \cdot \mathbf{v}_j^{(2)}\right) dS \qquad (3.78)$$

Here $\mathcal{D}_2$ denotes the volume of fluid contained in the annulus bounded by the drop surface and a spherical surface far away from the drop (S_∞). The surface integral over this spherical surface (S_∞) is denoted as $\int_\infty$ and $\mathbf{n}$ points out of the spherical surfaces. We similarly apply the relation (3.77) to the flows $\left(T_j^{(1)}, \mathbf{v}_j^{(1)}\right)$ and $\left(\hat{T}^{(1)}, \hat{\mathbf{v}}^{(1)}\right)$, integrate over the domain $\mathcal{D}_1$ and use the Gauss-Divergence theorem to get

$$\int_S \mathbf{n} \cdot \left(T_j^{(1)} \cdot \hat{\mathbf{v}}^{(1)} - \hat{T}^{(1)} \cdot \mathbf{v}_j^{(1)}\right) dS = \int_D \mathbf{n} \cdot \left(T_j^{(1)} \cdot \hat{\mathbf{v}}^{(1)} - \hat{T}^{(1)} \cdot \mathbf{v}_j^{(1)}\right) dS \qquad (3.79)$$

Here $\mathcal{D}_1$ denotes the volume of fluid bounded by the drop surface and the rigid sphere. We then multiply equation (3.79) with λ, subtract it from equation (3.78) and use the boundary conditions on the drop surface to arrive at

$$\int_\infty \mathbf{n} \cdot \left(T_j^{(2)} \cdot \hat{\mathbf{v}}^{(2)} - \hat{T}^{(2)} \cdot \mathbf{v}_j^{(2)}\right) dS = \lambda \int_S \mathbf{n} \cdot \left(T_j^{(1)} \cdot \hat{\mathbf{v}}^{(1)} - \hat{T}^{(1)} \cdot \mathbf{v}_j^{(1)}\right) dS + Ma \int_D \hat{\mathbf{v}} \cdot \nabla_s \Gamma_j \, dS \qquad (3.80)$$

As equation (3.80) was derived by applying a reciprocal theorem to the original problem and the first auxiliary problem, we can derive an equation similar to equation (3.80) by applying the reciprocal theorem to the original problem and the second auxiliary problem. This equation can be written by simply replacing the variables of the first auxiliary problem in equation (3.80) with those of the second auxiliary problem. This is because of using only the boundary conditions on the drop surface in deriving equation (3.80) and these boundary conditions being the same for both auxiliary problems.

$$\int_\infty \mathbf{n} \cdot \left(T_j^{(2)} \cdot \tilde{\mathbf{v}}^{(2)} - \tilde{T}^{(2)} \cdot \mathbf{v}_j^{(2)}\right) dS = \lambda \int_S \mathbf{n} \cdot \left(T_j^{(1)} \cdot \tilde{\mathbf{v}}^{(1)} - \tilde{T}^{(1)} \cdot \mathbf{v}_j^{(1)}\right) dS + Ma \int_D \tilde{\mathbf{v}} \cdot \nabla_s \Gamma_j \, dS \qquad (3.81)$$

$\hat{\mathbf{v}}$ and $\tilde{\mathbf{v}}$ appearing in the second integral on the right hand side of equations (3.80) and (3.81), respectively, are given by $\hat{\mathbf{v}}|_{Drop} = \hat{\mathbf{v}}^{(1)}\big|_{Drop} = \hat{\mathbf{v}}^{(2)}\big|_{Drop}$ and $\tilde{\mathbf{v}}|_{Drop} = \tilde{\mathbf{v}}^{(1)}\big|_{Drop} = \tilde{\mathbf{v}}^{(2)}\big|_{Drop}$.

We are now left with simplifying the integrals appearing in equations (3.80)-(3.81) to derive the integral theorem required for finding the swimmer and drop velocities at any order in Pe_s. As the flow field far-away from the drop approaches $\hat{\mathbf{U}}$ in the first auxiliary problem and the drop is force-free in the original problem, we can show that

$$\int_{\infty} \mathbf{n} \cdot T_j^{(2)} \cdot \hat{\mathbf{v}}^{(2)} dS = \left(\int_{\infty} \mathbf{n} \cdot T_j^{(2)} dS \right) \cdot \hat{\mathbf{U}} = \left(\int_{D} \mathbf{n} \cdot T_j^{(2)} dS \right) \cdot \hat{\mathbf{U}} = 0 \tag{3.82}$$

As $r \to \infty$, we note that $\tilde{\mathbf{v}}^{(2)}$ goes to $\mathbf{0}$ at least as fast as $1/r$, $T_j^{(2)}$ goes to $\mathbf{0}$ at least as fast as $1/r^2$ and dS grows as r^2, hence the product $\mathbf{n} \cdot T_j^{(2)} \cdot \tilde{\mathbf{v}}^{(2)} dS$ decays to 0 at least as fast as $1/r$ and we arrive at the result

$$\int_{\infty} \mathbf{n} \cdot T_j^{(2)} \cdot \tilde{\mathbf{v}}^{(2)} dS = 0 \tag{3.83}$$

Since the flow field far-away from the drop approaches $-\mathbf{U}_{j,D}$ in the original problem and the drop experiences a hydrodynamic force $\hat{\mathbf{F}}_D$ $\left(\tilde{\mathbf{F}}_D\right)$ in the first (second) auxiliary problem, we derive the following results

$$\int_{\infty} \mathbf{n} \cdot \hat{T}^{(2)} \cdot \mathbf{v}_j^{(2)} dS = -\hat{\mathbf{F}}_D \cdot \mathbf{U}_{j,D} \tag{3.84}$$

$$\int_{\infty} \mathbf{n} \cdot \tilde{T}^{(2)} \cdot \mathbf{v}_j^{(2)} dS = -\tilde{\mathbf{F}}_D \cdot \mathbf{U}_{j,D} \tag{3.85}$$

Using $\hat{\mathbf{v}}^{(1)}\big|_{\text{Sphere}} = \mathbf{0}$, we arrive at

$$\int_{S} \mathbf{n} \cdot T_j^{(1)} \cdot \hat{\mathbf{v}}^{(1)} dS = 0 \tag{3.86}$$

Using $\tilde{\mathbf{v}}^{(1)}\big|_{\text{Sphere}} = \tilde{\mathbf{U}}$ and the force-free condition on the swimmer in the original problem, we arrive at

$$\int_{S} \mathbf{n} \cdot T_j^{(1)} \cdot \tilde{\mathbf{v}}^{(1)} dS = \left(\int_{S} \mathbf{n} \cdot T_j^{(1)} dS \right) \cdot \tilde{\mathbf{U}} = 0 \tag{3.87}$$

Using $\mathbf{v}_j^{(1)}\Big|_{\text{Swimmer}} = \mathbf{U}_{j,S} - \mathbf{U}_{j,D} + \delta_{j,0}\, \mathbf{u}^s$ and the condition that the rigid sphere experiences a hydrodynamic force $\hat{\mathbf{F}}_{Sp}$ $\left(\tilde{\mathbf{F}}_{Sp}\right)$ in the first (second) auxiliary problem, we derive the following results

$$\int_{S} \mathbf{n} \cdot \hat{T}^{(1)} \cdot \mathbf{v}_j^{(1)} dS = \hat{\mathbf{F}}_{Sp} \cdot (\mathbf{U}_{j,S} - \mathbf{U}_{j,D}) + \delta_{j,0} \int_{S} \mathbf{n} \cdot \hat{T}^{(1)} \cdot \mathbf{u}^s dS \tag{3.88}$$

$$\int_S \mathbf{n}\cdot\tilde{T}^{(1)}\cdot\mathbf{v}_j^{(1)}dS=\tilde{\mathbf{F}}_{Sp}\cdot(\mathbf{U}_{j,S}-\mathbf{U}_{j,D})+\delta_{j,0}\int_S \mathbf{n}\cdot\tilde{T}^{(1)}\cdot\mathbf{u}^s dS \tag{3.89}$$

Enforcing the equations (3.82)-(3.89) in the equations (3.80)-(3.81), we arrive at the integral theorem given by the following two equations

$$\hat{\mathbf{F}}_D\cdot\mathbf{U}_{j,D}+\lambda\hat{\mathbf{F}}_{Sp}\cdot(\mathbf{U}_{j,S}-\mathbf{U}_{j,D})=-\lambda\,\delta_{j,0}\int_S \mathbf{n}\cdot\hat{T}^{(1)}\cdot\mathbf{u}^s dS+Ma\int_D \hat{\mathbf{v}}\cdot\nabla_s\Gamma_j dS \tag{3.90}$$

$$\tilde{\mathbf{F}}_D\cdot\mathbf{U}_{j,D}+\lambda\tilde{\mathbf{F}}_{Sp}\cdot(\mathbf{U}_{j,S}-\mathbf{U}_{j,D})=-\lambda\,\delta_{j,0}\int_S \mathbf{n}\cdot\tilde{T}^{(1)}\cdot\mathbf{u}^s dS+Ma\int_D \tilde{\mathbf{v}}\cdot\nabla_s\Gamma_j dS \tag{3.91}$$

We note that this integral theorem is valid for axisymmetric configurations.

Now, we explain how to use this theorem to derive the swimmer and drop velocities at $O(1)$ and $O(Pe_s)$ for the concentric configuration. At $O(1)$, as $\Gamma_0=1$, the integral theorem simplifies to

$$\hat{\mathbf{F}}_D\cdot\mathbf{U}_{0,D}+\lambda\hat{\mathbf{F}}_{Sp}\cdot(\mathbf{U}_{0,S}-\mathbf{U}_{0,D})=-\lambda\int_S \mathbf{n}\cdot\hat{T}^{(1)}\cdot\mathbf{u}^s dS \tag{3.92}$$

$$\tilde{\mathbf{F}}_D\cdot\mathbf{U}_{0,D}+\lambda\tilde{\mathbf{F}}_{Sp}\cdot(\mathbf{U}_{0,S}-\mathbf{U}_{0,D})=-\lambda\int_S \mathbf{n}\cdot\tilde{T}^{(1)}\cdot\mathbf{u}^s dS \tag{3.93}$$

For the concentric scenario, we use the Lamb's general solution to solve both auxiliary problems thereby finding $\hat{\mathbf{F}}_D$, $\hat{\mathbf{F}}_{Sp}$, $\left(\mathbf{n}\cdot\hat{T}^{(1)}\right)\Big|_{\text{Sphere}}$, $\tilde{\mathbf{F}}_D$, $\tilde{\mathbf{F}}_{Sp}$, and $\left(\mathbf{n}\cdot\tilde{T}^{(1)}\right)\Big|_{\text{Sphere}}$

$$\hat{\mathbf{F}}_D=\frac{4\pi\left(6\chi^3\lambda-4\chi^3+9\chi^2\lambda-3\chi^2+9\chi\lambda+3\chi+6\lambda+4\right)}{(4\lambda-4)\chi^3+(6\lambda-3)\chi^2+(3+6\lambda)\chi+4\lambda+4}\,\hat{\mathbf{U}} \tag{3.94}$$

$$\hat{\mathbf{F}}_{Sp}=\frac{8\left(\chi^3+2\chi^2+3\chi+3/2\right)\chi\pi}{4\chi^4\lambda-4\chi^4+2\chi^3\lambda+\chi^3+6\chi^2-2\chi\lambda+\chi-4\lambda-4}\,\hat{\mathbf{U}} \tag{3.95}$$

$$\begin{aligned}\left(\mathbf{n}\cdot\hat{T}^{(1)}\right)\Big|_{\text{Sphere}}=&\frac{3\cos(\theta)\hat{U}\left(4\chi^3+8\chi^2+2\chi+1\right)}{\chi\left(4\chi^4\lambda-4\chi^4+2\chi^3\lambda+\chi^3+6\chi^2-2\chi\lambda+\chi-4\lambda-4\right)}\mathbf{i}_r\\&+\frac{3\left(\chi^2+3\chi+1\right)\sin(\theta)\hat{U}}{(4\lambda-4)\chi^4+(6\lambda-3)\chi^3+(3+6\lambda)\chi^2+(4\lambda+4)\chi}\mathbf{i}_\theta\end{aligned} \tag{3.96}$$

$$\tilde{\mathbf{F}}_D = -\frac{4\pi\left(2\chi^3+4\chi^2+6\chi+3\right)\lambda\chi}{4\chi^4\lambda-4\chi^4+2\chi^3\lambda+\chi^3+6\chi^2-2\chi\lambda+\chi-4\lambda-4}\tilde{\mathbf{U}} \tag{3.97}$$

$$\tilde{\mathbf{F}}_{Sp} = \frac{8\pi\chi\left(2\chi^5\lambda-3\chi^5+3\lambda+3\right)}{\left(4\lambda-4\right)\chi^6+\left(-6\lambda+9\right)\chi^5-10\chi^3+\left(6\lambda+9\right)\chi-4\lambda-4}\tilde{\mathbf{U}} \tag{3.98}$$

$$\begin{aligned}\left(\mathbf{n}\cdot\tilde{T}^{(1)}\right)\Big|_{\text{Sphere}} =& \frac{6\left(4\chi^5\lambda-6\chi^5+5\chi^3+\lambda+1\right)\cos\left(\theta\right)\tilde{U}}{\chi\left(4\chi^6\lambda-4\chi^6-6\chi^5\lambda+9\chi^5-10\chi^3+6\chi\lambda+9\chi-4\lambda-4\right)}\mathbf{i}_r \\ &+ \frac{6\left(\left(\lambda-3/2\right)\chi^4+\left(\lambda-3/2\right)\chi^3+\left(\lambda+1\right)\chi^2+\left(\lambda+1\right)\chi+\lambda+1\right)\sin\left(\theta\right)\tilde{U}}{\left(4\chi^3\lambda-4\chi^3+6\chi^2\lambda-3\chi^2+6\chi\lambda+3\chi+4\lambda+4\right)\chi\left(\chi-1\right)^2}\mathbf{i}_\theta\end{aligned} \tag{3.99}$$

Noting that $\left(\mathbf{n}\cdot\hat{T}^{(1)}\right)\Big|_{\text{Sphere}} = \hat{T}^{(1)}_{rr}\,\mathbf{i}_r + \hat{T}^{(1)}_{r\theta}\,\mathbf{i}_\theta$ where $\hat{T}^{(1)}_{rr}$ and $\hat{T}^{(1)}_{r\theta}$ are of the form $\hat{T}^{(1)}_{rr} = \hat{A}\hat{U}\,P_1\left(\cos\theta\right)$, $\hat{T}^{(1)}_{r\theta} = \hat{B}\hat{U}\,V_1\left(\cos\theta\right)$, we can simplify the integral $\int_S \mathbf{n}\cdot\hat{T}^{(1)}\cdot\mathbf{u}^s dS$ as follows

$$\begin{aligned}\int_S \mathbf{n}\cdot\hat{T}^{(1)}\cdot\mathbf{u}^s dS =& 2\pi\chi^2\int_0^\pi\left(\hat{T}^{(1)}_{rr}u^s_r+\hat{T}^{(1)}_{r\theta}u^s_\theta\right)\sin\theta\,d\theta \\ =& 2\pi\chi^2\left[\hat{A}\hat{U}\int_{-1}^{1}u^s_r P_1\left(\zeta\right)d\zeta+\hat{B}\hat{U}\int_{-1}^{1}u^s_\theta\,V_1\left(\zeta\right)d\zeta\right]\end{aligned} \tag{3.100}$$

where $\zeta = cos\theta$. Using the orthogonality of the Legendre polynomials $P_n\left(\zeta\right)$ and that of $V_n\left(\zeta\right)$ (see equation (3.101)), it can be seen from the above equation that only A_1 and B_1 modes contribute to the non-zero value of the integral $\int_S \mathbf{n}\cdot\hat{T}^{(1)}\cdot\mathbf{u}^s dS$ and hence to the swimmer and drop velocities at $O\left(1\right)$. Enforcing the expressions in the equations (3.92)-(3.93), we solve the linear system of equations to find the swimmer and drop velocities at $O\left(1\right)$

$$\begin{aligned}\int_{-1}^{1}P_n\left(\zeta\right)P_m\left(\zeta\right)d\zeta =& \frac{2}{2n+1}\delta_{mn} \\ \int_{-1}^{1}V_n\left(\zeta\right)V_m\left(\zeta\right)d\zeta =& \frac{8}{n\left(n+1\right)\left(2n+1\right)}\delta_{mn}\end{aligned} \tag{3.101}$$

At $O\left(Pe_s\right)$, the integral theorem simplifies to

$$\hat{\mathbf{F}}_D \cdot \mathbf{U}_{1,D} + \lambda \hat{\mathbf{F}}_{Sp} \cdot \left(\mathbf{U}_{1,S} - \mathbf{U}_{1,D}\right) = Ma \int_D \hat{\mathbf{v}} \cdot \nabla_s \Gamma_1 dS \tag{3.102}$$

$$\tilde{\mathbf{F}}_D \cdot \mathbf{U}_{1,D} + \lambda \tilde{\mathbf{F}}_{Sp} \cdot \left(\mathbf{U}_{1,S} - \mathbf{U}_{1,D}\right) = Ma \int_D \tilde{\mathbf{v}} \cdot \nabla_s \Gamma_1 dS \tag{3.103}$$

The expressions for $\hat{\mathbf{v}}$ and $\tilde{\mathbf{v}}$ on the drop surface are given as

$$\hat{\mathbf{v}}|_{\text{Drop}} = \frac{\left(\chi - 1\right)\hat{U}\left(4\chi^2 + 7\chi + 4\right)\sin\left(\theta\right)}{\left(8\lambda - 8\right)\chi^3 + \left(12\lambda - 6\right)\chi^2 + \left(12\lambda + 6\right)\chi + 8\lambda + 8}\mathbf{i}_\theta \tag{3.104}$$

$$\tilde{\mathbf{v}}|_{\text{Drop}} = -\frac{\left(2\chi^3 + 4\chi^2 + 6\chi + 3\right)\lambda\tilde{U}\chi\sin\left(\theta\right)}{4\chi^4\lambda - 4\chi^4 + 2\chi^3\lambda + \chi^3 + 6\chi^2 - 2\chi\lambda + \chi - 4\lambda - 4}\mathbf{i}_\theta \tag{3.105}$$

Once again, noting that $\hat{\mathbf{v}}$ is of the form $\hat{\mathbf{v}} = \hat{C}\hat{U}\,V_1\left(\cos\theta\right)\,\mathbf{i}_\theta$ and $\Gamma_1 = \sum_{n=1}^{\infty}\Gamma_{1,n}\,P_n\left(\cos\theta\right)$, we can simplify the right hand side of equation (3.102) as

$$\int_D \hat{\mathbf{v}} \cdot \nabla_s \Gamma_1 \, dS = -\hat{C}\hat{U}\sum_{n=1}^{\infty}\frac{n\left(n+1\right)}{2}\Gamma_{1,n}\int_{-1}^{1} V_1\left(\zeta\right)\,V_n\left(\zeta\right)\,d\zeta \tag{3.106}$$

Using the orthogonality of $V_n\left(\zeta\right)$, we see that only $\Gamma_{1,1}$ contributes to the above integral and hence to the swimmer and drop velocities at $O\left(Pe_s\right)$. Substituting the expressions (3.104)-(3.105) into the equations (3.102)-(3.103) and solving the resulting linear system of equations, we determine the swimmer and drop velocities $O\left(Pe_s\right)$. We note that the swimmer and drop velocities at $O\left(1\right)$ and at $O\left(Pe_s\right)$ derived using the reciprocal theorem are the same as those obtained by solving the full Stokes equations

3.9 Appendix D: Expressing the slip velocity on the surface of the swimmer in bipolar coordinates

In general, the slip velocity on the swimmer is specified in spherical coordinates,

$$\mathbf{u}^s = u_r^s\,\mathbf{i}_r + u_\theta^s\,\mathbf{i}_\theta. \tag{3.107}$$

For calculations in bipolar coordinates, it is easy to handle the velocity components in bipolar coordinates, expressed in terms of the corresponding coordinate variables (ξ, η). For this purpose, we first write the slip velocity in cylindrical coordinates, $\mathbf{u}^s = u^s_\rho \, \mathbf{i}_\rho + u^s_z \, \mathbf{i}_z$ where $u^s_\rho = u^s_r \, \sin\theta + u^s_\theta \, \cos\theta$ and $u^s_z = u^s_r \, \cos\theta - u^s_\theta \, \sin\theta$. We then express this velocity in bipolar coordinates $\mathbf{u}^s = u^s_\xi \, \mathbf{i}_\xi + u^s_\eta \, \mathbf{i}_\eta$, where

$$u^s_\eta = h \left(u^s_\rho \frac{\partial \rho}{\partial \eta} + u^s_z \frac{\partial z}{\partial \eta} \right); \; u^s_\xi = h \left(u^s_\rho \frac{\partial \rho}{\partial \xi} + u^s_z \frac{\partial z}{\partial \xi} \right),$$

$$\sin\theta = \mathrm{sgn}\,(\xi_S) \left(\frac{\sin\eta \sinh\xi_S}{\cosh\xi_S - \cos\eta} \right); \; \cos\theta = \mathrm{sgn}\,(\xi_S) \left(\frac{\cosh\xi_S \cos\eta - 1}{\cosh\xi_S - \cos\eta} \right).$$

For instance, for a swimmer having only three modes (A_1, B_1, B_2), the boundary condition on its surface is written as

$$\begin{aligned} v^{(1)}_{0,\xi}\Big|_{\xi=\xi_S} &= (A_1 + U_{0,S} - U_{0,D}) \cosh\xi_S - \frac{(A_1 + U_{0,S} - U_{0,D}) \sinh^2\xi_S}{\cosh\xi_S - \cos\eta}, \\ v^{(1)}_{0,\eta}\Big|_{\xi=\xi_S} &= \frac{(-B_2 \cosh\xi_S \, \mathrm{sgn}\,(\xi_S) + B_1 - U_{0,S} + U_{0,D})}{\cosh\xi_S - \cos\eta} \sin\eta \sinh\xi_S + \frac{B_2 \, \mathrm{sgn}\,(\xi_S) \sinh^3\xi_S \sin\eta}{(\cosh\xi_S - \cos\eta)^3}, \end{aligned} \tag{3.108}$$

where, we have used

$$\mathbf{i}_z = \mathbf{i}_\eta \, h \frac{\partial z}{\partial \eta} + \mathbf{i}_\xi \, h \frac{\partial z}{\partial \xi}.$$

3.10 Appendix E: Linear equations obtained while satisfying (3.31)-(3.34)

Using the boundary conditions on the surface of the drop, equation (3.32), we get

$$W^{(1)}_{j,n}(\xi_D) = 0; \; W^{(2)}_{j,n}(\xi_D) = 0, \tag{3.109}$$

$$\left. \frac{dW^{(1)}_{j,n}}{d\xi} \right|_{\xi=\xi_D} = \left. \frac{dW^{(2)}_{j,n}}{d\xi} \right|_{\xi=\xi_D}, \tag{3.110}$$

$$\operatorname{sgn}(\xi_D)\left(\frac{d^2W_{j,n}^{(2)}}{d\xi^2}-\lambda\frac{d^2W_{j,n}^{(1)}}{d\xi^2}\right)_{\xi=\xi_D}$$
$$=-\delta_{j,1}\frac{n(n+1)(2n+1)}{2}Ma\times c\sum_{m=0}^{\infty}\left.\frac{dW_{0,m}^{(2)}}{d\xi}\right|_{\xi=\xi_D}\int_{-1}^{1}\frac{C_{n+1}^{-1/2}(\mu)\,C_{m+1}^{-1/2}(\mu)}{(\cosh\xi_D-\mu)(1-\mu^2)}d\mu. \tag{3.111}$$

Using the far-field condition, equation (3.34), we obtain

$$\frac{A_{j,n}^{(2)}-\operatorname{sgn}(\xi_D)B_{j,n}^{(2)}}{2}=\frac{c^2U_{j,D}}{2\sqrt{2}}\frac{n(n+1)}{\left(n-\frac{1}{2}\right)}, \tag{3.112}$$

$$\frac{C_{j,n}^{(2)}-\operatorname{sgn}(\xi_D)D_{j,n}^{(2)}}{2}=-\frac{c^2U_{j,D}}{2\sqrt{2}}\frac{n(n+1)}{\left(n+\frac{3}{2}\right)}. \tag{3.113}$$

Using the boundary conditions on the surface of the swimmer, equation (3.31), we get

$$\sum_{n=0}^{\infty}W_{j,n}^{(1)}(\xi_S)\;C_{n+1}^{-1/2}(\cos\eta)=(\cosh\xi_S-\cos\eta)^{3/2}\int_0^{\eta}\frac{c^2\sin\eta'}{(\cosh\xi_S-\cos\eta')^2}\,v_{j,\xi}^{(1)}\Big|_{\xi=\xi_S}d\eta', \tag{3.114}$$

$$\sum_{n=0}^{\infty}\left.\frac{dW_{j,n}^{(1)}}{d\xi}\right|_{\xi=\xi_S}C_{n+1}^{-1/2}(\cos\eta)=\frac{3}{2}(\cosh\xi_S-\cos\eta)^{1/2}\sinh\xi_S\int_0^{\eta}\frac{c^2\sin\eta'}{(\cosh\xi_S-\cos\eta')^2}\,v_{j,\xi}^{(1)}\Big|_{\xi=\xi_S}d\eta'$$
$$-\frac{c^2\sin\eta}{(\cosh\xi_S-\cos\eta)^{1/2}}\,v_{j,\eta}^{(1)}\Big|_{\xi=\xi_S}. \tag{3.115}$$

We then use the following identity, the identities derived from differentiating it with respect to ξ along with the orthogonality of Gegenbauer polynomials to simplify equations (3.114) and (3.115)

$$\frac{\sin^2\eta}{(\cosh\xi-\cos\eta)^{1/2}}=\sqrt{2}\sum_{n=1}^{\infty}n(n+1)\left[\frac{e^{-\left(n-\frac{1}{2}\right)|\xi|}}{(2n-1)}-\frac{e^{-\left(n+\frac{3}{2}\right)|\xi|}}{(2n+3)}\right]C_{n+1}^{-1/2}(\cos\eta). \tag{3.116}$$

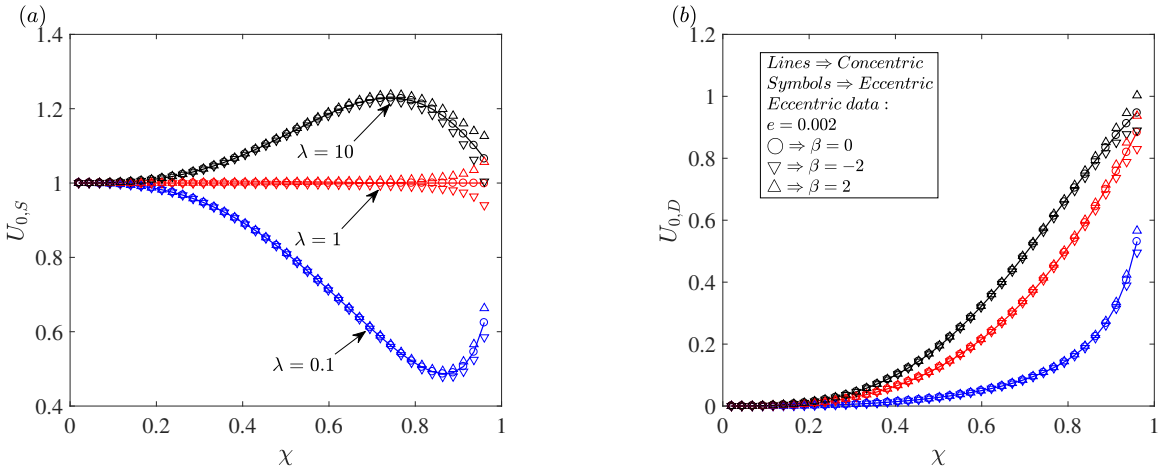

Figure 3.14. : The velocities of (a) a two-mode squirmer ($U_{0,S}$) and (b) a drop ($U_{0,D}$) at $O(1)$ plotted as a function of the size ratio for various values of viscosity ratio. The lines denote the results obtained for concentric configuration while the symbols indicate the results of an eccentric configuration with an eccentricity $e = 0.002$. The symbols ◯, ▽ and △ are used to denote the results of a neutral swimmer ($\beta = 0$), pusher ($\beta = -2$) and puller ($\beta = 2$), respectively. All the velocities are non-dimensionalized using $U_{sq} = 2B_1/3$.

3.11 Appendix F: Validation of bipolar coordinate results

In this section, we validate the solution for the eccentric configurations by comparing the swimmer and drop velocities for small eccentricity ($e = 0.002$) with the corresponding velocities for the concentric configuration.

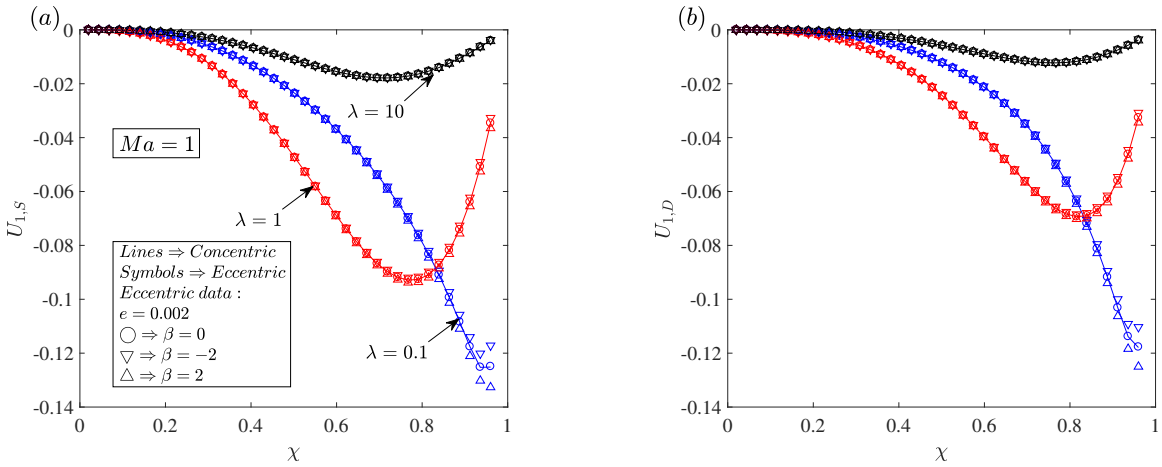

Figure 3.15. : The velocities of (a) a two-mode squirmer ($U_{1,S}$) and (b) a drop ($U_{1,D}$) at $O\left(Pe_s\right)$ plotted as a function of the size ratio for various values of viscosity ratio. Here we choose $Ma = 1$. The lines denote the results obtained for concentric configuration while the symbols indicate the results of an eccentric configuration with an eccentricity $e = 0.002$. The symbols ◯, ▽ and △ are used to denote the results of a neutral swimmer ($\beta = 0$), pusher ($\beta = -2$) and puller ($\beta = 2$), respectively. All the velocities are non-dimensionalized using $U_{sq} = 2B_1/3$.

4. SWIMMING SHEET NEAR A PLANE SURFACTANT LADEN INTERFACE

4.1 Introduction

Our world is filled with motile microorganisms—*Helicobacter pylori* in stomach, *Escherichia coli* in intestines, *Chlamydomonas* in oceans and snow, *Paramecium* in stagnant basins and ponds etc. Understanding the motion of these organisms in complex flow conditions is essential for addressing several biophysical questions [10]. One such complex bacterial motion is concerned with its locomotion near an interface which has applications in the biofilm formation and bioremediation of an oil spill. Researchers working on this topic have successfully explained (i) how the swimming speed of an organism gets altered near an interface [62, 63, 95, 96], (ii) why these organisms move in circles near a plane interface [64, 65] and (iii) why they reorient and get attracted towards an interface [8, 16, 23, 73]. Recent works have also analyzed the change in the bacterial dynamics near an interface due to the (i) interface deformation [9, 69, 70], (ii) finite inertia of the swimmer or fluid [97, 98], (iii) non-Newtonian suspending fluid [72, 99, 100], and (iv) presence of surfactants [8, 16, 73].

We briefly review the works on locomotion near a surfactant covered interface. Near a plane surfactant laden interface, the attraction and reorientation of a swimming microorganism is similar to its behavior near a plane wall but its circling direction can be opposite to the one near a clean interface [8]. Considering the trapping of marine microbes onto drops, it was reported that the trapping dynamics outside drops is similar to that outside a rigid sphere, but the surfactant laden drops have better trapping characteristics than a rigid sphere or a clean drop [16]. This is non-intuitive as a surfactant laden drop usually has characteristics that are intermediate

This chapter has been reprinted with permission from the article "Swimming sheet near a plane surfactant laden interface", by V. A. Shaik and A. M. Ardekani, Physical Review E, 99(3):033101, 2019 (DOI: 10.1103/PhysRevE.99.033101).

between a rigid sphere and a clean drop. Analogous to the interface deformations, finite inertia of the fluid or the organism and the non-Newtonian rheology of the fluid, the surfactant redistribution can enable a time-reversible swimming microorganism near an interface to achieve a net motion [101].

These works on the locomotion near a surfactant laden interface assumed the surfactant to be either incompressible (valid at large Marangoni numbers Ma, ratio of Marangoni stresses to the bulk viscous stresses) [74–76] or compressible [77] but its surface advection being negligible compared to its surface diffusion (valid at small surface Péclet numbers Pe_s, ratio of surface advection to the surface diffusion of the surfactant). The objective of this work is to analyze the locomotion near a surfactant laden interface for all values of surface Péclet and Marangoni numbers.

To model the surfactant as generally as possible without losing the analytical tractability, we use a simple model microorganism. Hence, we model the organism as a 2D infinitely long swimming sheet that propels by propagating waves along its surface. This model was first proposed by Taylor [13] who considered a sheet passing transverse waves to represent the monoflagellated organism such as spermatozoon. It was later extended by Blake [102] who allowed the passage of both longitudinal and transverse waves along the sheet to represent the almost flat ciliated organisms such as *Paramecium* or *Opalina*. Due to the mathematical simplicity associated with this model, it has been used to study the locomotion (i) in a complex fluid [103–110], (ii) in a gel [111, 112], (iii) in a liquid crystal [113], (iv) in a porous media [114], (v) under confinement [62, 63, 95, 115–121], (vi) at finite inertia of the fluid or the organism [62, 122–124] and (vii) under transient effects [125]. The research on the locomotion under confinement has been restricted to the confinements caused by a rigid or soft wall [62, 63, 115–118, 121], a plane clean interface [95], a deforming membrane [119] or a gel [120] with a Newtonian or a non-Newtonian suspending fluid.

Noting that any interface is inevitably covered with impurities that act as surfactants, it is essential to generalize the theory of locomotion near a clean interface to

accommodate the effects of surfactant redistribution. Even though the locomotion under confinement depends on the swimmer's shape, most of the earlier research on the sheet's motion under confinement is devoted to a sheet passing transverse waves along its surface (or a Taylor's swimming sheet [13]). To emphasize the influence of the swimmer's shape on locomotion and also to generalize the results associated with the sheet passing transverse waves, we analyze the motion of a sheet passing both longitudinal and transverse waves near a surfactant laden interface.

This paper is organized as follows. We provide the governing equations and boundary conditions associated with the motion of a sheet near a plane surfactant laden interface and present the perturbation technique and the solution methodology in Sec. 4.2. We provide simple expressions for the swimming velocity under various limiting conditions in Sec. 4.3. We then analyze the influence of surfactant redistribution on the swimming velocity of a sheet passing only transverse wave and that passing both longitudinal and transverse waves in Secs. 4.4.1 and 4.4.2 respectively. We finally provide several concluding remarks in Sec. 4.5 and present the expressions for the flow field, sheet's velocity, and validate our results in appendices.

4.2 Mathematical Model

Consider a 2D infinitely long sheet near a surfactant laden interface (see figure 4.1 for schematic). We formulate this problem in a frame of reference moving with the swimming velocity of the sheet. The sheet deforms in such a manner that point $(x, 0)$ on its undeformed surface is located at (x_0, y_0) at time t, where x_0 and y_0 are given by

$$\begin{aligned} x_0 =& x + a\cos k\left(x + ct\right) + d\sin k\left(x + ct\right), \\ y_0 =& b\sin k\left(x + ct\right). \end{aligned} \tag{4.1}$$

Here a, d (b) are the amplitudes of longitudinal (transverse) waves while c and k are the wave speed and wave number, respectively.

For analytical tractability, we make the following assumptions. We assume the interface is plane and non-deforming; such a non-deforming interface assumption is valid at small Capillary numbers (ratio of bulk viscous stresses to the capillary stresses). We assume the sheet is located symmetrically between two surfactant laden interfaces which can occur for locomotion in a film [126–128]. Hence, we only solve for the fluid flow above the sheet. We assume the amplitude of sheet's deformation is much smaller than the wavelength, i.e., $ak \ll 1$, $bk \ll 1$, and $dk \ll 1$. Hence, we can write $ak = \epsilon\tilde{a}$, $bk = \epsilon\tilde{b}$, and $dk = \epsilon\tilde{d}$, where $\epsilon \ll 1$ while the magnitudes of $\tilde{a}$, $\tilde{b}$, and $\tilde{d}$ can be at most $O(1)$. We denote the distance between the mid plane of the sheet and the interface by h, which is at least as large as the wavelength i.e., $hk \geq O(1)$. The surfactant is insoluble and we neglect any kind of interfacial rheology imparted by the surfactant to the interface. Insoluble surfactant limit is valid when the interfacial transport of the surfactant is much faster than the bulk transport and the adsorption-desorption between the bulk fluid and the interface. Hence in this limit, the bulk surfactant does not influence the interfacial surfactant transport. Also, assuming the local surfactant concentration on the interface (Γ) is much smaller than the maximum possible surfactant concentration on the interface (Γ_∞), we use a linear constitutive equation to relate the interfacial tension (γ) to the surfactant concentration [129] i.e., $\gamma = \gamma_s - \Gamma RT$. Here γ_s is the interfacial tension of the clean interface, R is the ideal gas constant and T is the absolute temperature.

We use the following characteristic parameters to scale all variables to dimensionless variables: a reference length $l_{ref} = 1/k$, reference velocity $u_{ref} = c$, reference time $t_{ref} = 1/(ck)$, reference pressure $\left(p^{(j)}_{ref}\right)$ and stress $\left(T^{(j)}_{ref}\right)$ in the j-th fluid $p^{(j)}_{ref} = T^{(j)}_{ref} = \mu_j ck$, where μ_j is the dynamic viscosity of the j-th fluid. As the problem is two dimensional, we use the stream function (ψ) to solve it. We non-dimensionalize the stream function and surfactant concentration via $\psi_{ref} = c/k$ and $\Gamma_{ref} = \Gamma_{eq}$ respectively, where Γ_{eq} is the equilibrium surfactant concentration. We hereby formulate the problem of sheet near a surfactant laden interface in dimensionless variables.

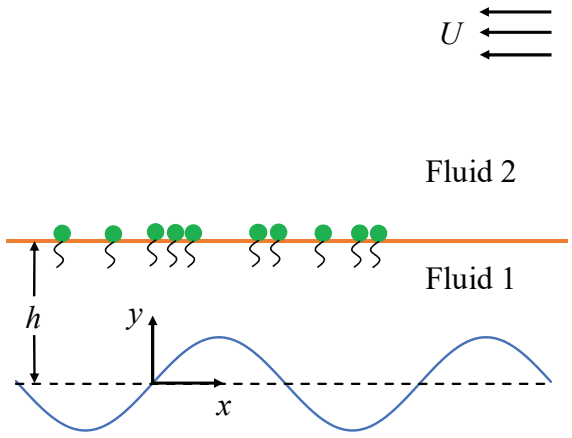

Figure 4.1. : A schematic showing a swimming sheet located near a plane surfactant laden interface. The sheet propels by passing waves along its surface. The distance between the midplane of the sheet and the interface is h. We denote the fluid in which the swimmer is suspended as 'Fluid 1' while the fluid above the interface as 'Fluid 2'. In the frame moving with the swimming velocity of the sheet, a uniform streaming flow exists in fluid 2 far away from the sheet with the velocity that is negative of the sheet's swimming velocity. The origin of the coordinate system is located at the midplane of the sheet.

As the inertia of the flow due to the swimming microorganism is typically negligible, the flow field is governed by the Stokes equations and the incompressibility condition. Using the relation between velocity components and the stream function, equation (4.2), the governing equations are simply the biharmonic equations for the stream functions, equation (4.3)

$$u^{(j)} = \frac{\partial \psi^{(j)}}{\partial y}; v^{(j)} = -\frac{\partial \psi^{(j)}}{\partial x}, \text{ where } j = 1, 2, \tag{4.2}$$

$$\nabla^4 \psi^{(j)} = 0, \tag{4.3}$$

where $u^{(j)}$ and $v^{(j)}$ indicate the x and y components of the velocity of j-th fluid while $\psi^{(j)}$ denotes the stream function concerning the j-th fluid. Point $(x, 0)$ on the undeformed sheet is located at (x_0, y_0) on the sheet's surface at time t, where (x_0, y_0) is given by

$$\begin{aligned} x_0 =& x + \epsilon \left[\tilde{a} \cos(x+t) + \tilde{d} \sin(x+t) \right], \\ y_0 =& \epsilon \tilde{b} \sin(x+t). \end{aligned} \tag{4.4}$$

As the flow field in phase 1 should satisfy the no-slip and no-penetration boundary conditions on the sheet, we have

$$\begin{aligned} \left. \frac{\partial \psi^{(1)}}{\partial y} \right|_{(x_0,y_0)} =& \frac{\partial x_0}{\partial t} = \epsilon \left[-\tilde{a} \sin(x+t) + \tilde{d} \cos(x+t) \right], \\ \left. \frac{\partial \psi^{(1)}}{\partial x} \right|_{(x_0,y_0)} =& -\frac{\partial y_0}{\partial t} = -\epsilon \tilde{b} \cos(x+t). \end{aligned} \tag{4.5}$$

Either neglecting gravity or by assuming the density of the sheet is the same as the density of the fluid in which it is suspended, we find that the external force on the sheet is zero. Consequently, due to negligible inertia of the sheet, the net hydrodynamic force on the sheet must be zero i.e., $\int_{\text{Sheet}} \mathbf{n} \cdot \mathbf{T}^{(1)}\big|_{\text{Sheet}} dS = \mathbf{0}$ which simplifies to

$$\int_0^{2\pi} \left\{ -\epsilon \tilde{b} \cos(x+t)\, \mathbf{i} + \left[1 - \epsilon \tilde{a} \sin(x+t) + \epsilon \tilde{d} \cos(x+t) \right] \mathbf{j} \right\} \cdot \mathbf{T}^{(1)}\big|_{(x_0,y_0)} dx = \mathbf{0}, \tag{4.6}$$

where $\mathbf{i}$ and $\mathbf{j}$ denote the unit vectors along x and y directions, respectively. Also, $\mathbf{n}$ is the normal to the sheet pointing into fluid 1 while $\mathbf{T}^{(j)}$ is the stress tensor for j-th fluid. Using the Newtonian fluid constitutive equation, $\mathbf{T}^{(j)}$ can be written in terms of pressure $\left(p^{(j)}\right)$ and velocity fields $\left(\mathbf{v}^{(j)}\right)$ of the j-th fluid as $\mathbf{T}^{(j)} = -p^{(j)}\mathbf{I} + \left[\nabla\mathbf{v}^{(j)} + \left(\nabla\mathbf{v}^{(j)}\right)^{\dagger}\right]$, where $\dagger$ stands for the transpose and $\mathbf{I}$ is an identity tensor. Far away from the sheet, the velocity of fluid 2 should approach the negative of sheet's swimming velocity ($\mathbf{U} = U\,\mathbf{i}$). In terms of stream function, this condition simplifies to

$$\text{as } y \to \infty,\ \psi^{(2)} \sim -Uy. \tag{4.7}$$

Since the interface is non-deforming, the fluid velocity (in both phases) at the interface but normal to the interface must be zero,

$$\text{at } y = h:\ \frac{\partial\psi^{(1)}}{\partial x} = 0; \frac{\partial\psi^{(2)}}{\partial x} = 0. \tag{4.8}$$

The fluid velocity at the interface but tangential to the interface must be continuous across the interface

$$\text{at } y = h:\ \frac{\partial\psi^{(1)}}{\partial y} = \frac{\partial\psi^{(2)}}{\partial y}. \tag{4.9}$$

Also, the jump in the tangential stresses across the interface should be balanced by the Marangoni stresses which using the relationship between interfacial tension and the surfactant concentration simplifies to

$$\text{at } y = h:\ \lambda T^{(2)}_{yx} - T^{(1)}_{yx} = Ma\frac{\partial\Gamma}{\partial x};\ Ma = \frac{RT\Gamma_{eq}}{\mu_1 c}, \tag{4.10}$$

where $T^{(j)}_{yx}$ denotes the yx component of stress tensor in the j-th fluid and the viscosity ratio $\lambda = \mu_2/\mu_1$. Finally, the transport of an insoluble surfactant on a non-deforming interface is governed by

$$Pe_s\left[\frac{\partial\Gamma}{\partial t} + \frac{\partial}{\partial x}\left(\Gamma\, u|_{y=h}\right)\right] = \frac{\partial^2\Gamma}{\partial x^2};\ Pe_s = \frac{c}{kD_s}, \tag{4.11}$$

where D_s is the surface or interface diffusivity of the surfactant and the slip of an interface is written as $u|_{y=h} = \left.\frac{\partial\psi^{(1)}}{\partial y}\right|_{y=h} = \left.\frac{\partial\psi^{(2)}}{\partial y}\right|_{y=h}$.

We compare our formulation with those of Taylor [13] and Katz [63], where Taylor considered a sheet in an unbounded fluid while Katz analyzed the motion of sheet located asymmetrically between two walls. In these two works, the inertia of the flow was negligible due to which the stream function was governed by the biharmonic equation. The shape of sheet in Katz's work is same as that considered by us but Taylor's sheet passes only transverse waves along positive x-direction $\Big[x_0 = x, y_0 = \epsilon\,\tilde{b}\sin(x-t)\Big]$. Katz worked in a frame moving with velocity $(U-1)\,\mathbf{i}$ unlike the frame moving with the velocity $U\,\mathbf{i}$ considered by us and Taylor. Due to the different sheet's shape (respectively, frame of reference) considered by Taylor (respectively, by Katz), the boundary condition on the sheet given in these two works is different from that reported here [equation (4.5)]. The force-free condition is identically satisfied for the Taylor's sheet in an unbounded fluid. As Katz considered a sheet asymmetrically located between two walls, the sum of hydrodynamic forces acting on the top and bottom surfaces of the sheet must be zero and this force-free condition of Katz reduces to equation (4.6) for a sheet symmetrically located between two walls. A far-field condition similar to equation (4.7) exists for a fluid in which the sheet is immersed in Taylor's work, but no such condition exists for a sheet bounded by walls as considered by Katz. To ensure the fluid does not penetrate the walls, Katz applied a condition similar to equation (4.8) at the walls. Instead of the continuous tangential velocity condition [equation (4.9)], shear stress balance condition [equation (4.10)], and the surfactant transport equation [equation (4.11)] at the interface, there is a no-slip boundary condition at the wall in Katz's work.

We need to solve equations (4.3)-(4.11) to determine the swimming velocity of the sheet, $U\mathbf{i}$. As the surfactant transport equation is nonlinear, it is not possible to solve these equations analytically for an arbitrary value of ϵ. However, for $\epsilon \ll 1$, we can use the following traditional technique to find the leading order approximation of the sheet's swimming velocity: (i) express the boundary condition on the sheet's surface as a series of boundary conditions applied at the mid plane of the sheet by doing a

Taylor series expansion of any function $f(x_0, y_0)$ about $(x, 0)$ and (ii) expand all the variables as a power series in ϵ

$$\begin{aligned}\left\{\mathbf{v}^{(j)}, \mathbf{T}^{(j)}, p^{(j)}, U, \psi^{(j)}, u|_{y=h}\right\} &= \sum_{n=1}^{\infty} \epsilon^n \left\{\mathbf{v}_n^{(j)}, \mathbf{T}_n^{(j)}, p_n^{(j)}, U_n, \psi_n^{(j)}, u_n|_{y=h}\right\} \\ \Gamma &= 1 + \sum_{n=1}^{\infty} \epsilon^n \Gamma_n\end{aligned} \tag{4.12}$$

The resulting perturbed equations are linear and have the following general solution for the stream function and the surfactant concentration at $O(\epsilon^n)$

$$\begin{aligned}\psi_n^{(1)} = \sum_{m=1}^{\infty} &\left\{ \begin{array}{l} \left[\left(A_{n,m}^{(1)} + E_{n,m}^{(1)} y\right) \cos m(x+t) + \left(B_{n,m}^{(1)} + F_{n,m}^{(1)} y\right) \sin m(x+t)\right] \cosh my \\ + \left[\left(C_{n,m}^{(1)} + G_{n,m}^{(1)} y\right) \cos m(x+t) + \left(D_{n,m}^{(1)} + H_{n,m}^{(1)} y\right) \sin m(x+t)\right] \sinh my \end{array} \right\} \\ &+ \alpha_n y + \beta_n y^2 + \gamma_n y^3\end{aligned} \tag{4.13}$$

$$\psi_n^{(2)} = -U_n y + \sum_{m=1}^{\infty} \left[\left(A_{n,m}^{(2)} + E_{n,m}^{(2)} y\right) \cos m(x+t) + \left(B_{n,m}^{(2)} + F_{n,m}^{(2)} y\right) \sin m(x+t)\right] e^{-my}, \tag{4.14}$$

$$\Gamma_n = \sum_{m=1}^{\infty} \left[J_{n,m} \cos m(x+t) + L_{n,m} \sin m(x+t)\right], \tag{4.15}$$

where $A_{n,m}^{(1)}$, $B_{n,m}^{(1)}$, $C_{n,m}^{(1)}$, $D_{n,m}^{(1)}$, $E_{n,m}^{(1)}$, $F_{n,m}^{(1)}$, $G_{n,m}^{(1)}$, $H_{n,m}^{(1)}$, $A_{n,m}^{(2)}$, $B_{n,m}^{(2)}$, $E_{n,m}^{(2)}$, $F_{n,m}^{(2)}$, α_n, β_n, γ_n, $J_{n,m}$, and $L_{n,m}$ are unknown constants that need to be determined while satisfying the perturbed boundary conditions. The expressions of the constants that determine the $O(\epsilon)$ and $O(\epsilon^2)$ flow fields along with the expression of the leading order swimming velocity U_2 are provided in Appendix 4.6. We also verify our calculation by comparing the leading order swimming velocity of the sheet U_2 with that reported in the literature in various limits. This validation is presented in Appendix 4.7.

4.3 Limiting cases

We note that the swimming velocity depends in a complex fashion on Ma and Pe_s as can be seen in equation (4.37) derived for a sheet passing transverse waves near

an air-water interface. So, to understand the surfactants influence on the swimming velocity U, we need to numerically evaluate U for various Ma and Pe_s. Before doing this, in this section we report some simple expressions for the swimming velocity in the limits of small or large Ma or Pe_s. Through such expressions, one can easily find out how the surfactant redistribution affects the swimming velocity. We report these limiting forms for a sheet near an air-water interface ($\lambda = 0$) by noting that the leading order swimming occurs at $O(\epsilon^2)$ i.e., $U = \epsilon^2 U_2 + O(\epsilon^4)$.

At small Ma, we get

$$\begin{aligned} U_2 &= U_{2,clean} + \frac{Pe_s Ma}{\left(Pe_s^2+1\right)\left(\sinh(2h)-2h\right)^2}\left[\begin{array}{l}\left(\begin{array}{l} h^2\cosh(2h) - 2h\sinh(2h) \\ +h^2+\cosh(2h)-1 \end{array}\right)\tilde{b}\left(\tilde{a}-Pe_s\tilde{d}\right) \\ +\left(h\sinh(2h)-\cosh(2h)+1\right)\tilde{b}^2 h \end{array}\right] \\ &+ O\left(Ma^2\right) \end{aligned} \tag{4.16}$$

Here $U_{2,clean}$ is the swimming velocity near a plane clean interface whose expression for $\tilde{a} = \tilde{d} = 0$ is given in equation (4.40). We see that the correction due to surfactant redistribution depends nonlinearly on Pe_s. As long as $\tilde{d} = 0$, we see that the surfactant redistribution increases the sheet's velocity because $(h\sinh(2h) - \cosh(2h) + 1) > 0$ and $(h^2\cosh(2h) - 2h\sinh(2h) + h^2 + \cosh(2h) - 1) > 0$ for all h. When $\tilde{a} = 0$, the surfactant redistribution can increase or even decrease the sheet's velocity depending on whether the following ratio is respectively great than or less than 1.

$$\frac{\left(h\sinh(2h)-\cosh(2h)+1\right)h}{\left(h^2\cosh(2h)-2h\sinh(2h)+h^2+\cosh(2h)-1\right)Pe_s}\frac{\tilde{b}}{\tilde{d}} \tag{4.17}$$

In the more general case when $\tilde{a} \neq 0$, $\tilde{d} \neq 0$, and $\tilde{b} \neq 0$, the surfactant redistribution can increase or decrease the swimmer's velocity depending on Pe_s, h and relative order of magnitude of the wave amplitudes.

At small Pe_s, we get

$$\begin{aligned} U_2 &= U_{2,clean} + \frac{Pe_s Ma \times \tilde{b}}{\left(\sinh(2h)-2h\right)^2}\left[\begin{array}{l}\tilde{a}\left(h^2\cosh(2h)-2h\sinh(2h)+h^2+\cosh(2h)-1\right) \\ +\tilde{b}h\left(h\sinh(2h)-\cosh(2h)+1\right)\end{array}\right] \\ &+ O\left(Pe_s^2\right) \end{aligned} \tag{4.18}$$

From this expression, we see that the swimming velocity does not depend on 'd' modes. Also as $(h^2\cosh(2h) - 2h\sinh(2h) + h^2 + \cosh(2h) - 1) > 0$ and $(h\sinh(2h) - \cosh(2h) + 1) > 0$, we see that the surfactant redistribution always increases the swimming velocity at small Pe_s. This is in contrast with the observation that the surfactant redistribution can increase or even decrease the velocity of a swimming microorganism inside a surfactant laden drop at small Pe_s [101]. These different influences of the surfactant on the swimming velocity, reported in Ref. [101] and this work, is due to different shapes of the swimmer and the interface used in these two works.

At large Ma, we get

$$\begin{aligned} U_2 &= U_{2,wall} - \frac{4\tilde{b}}{Pe_s Ma(2h^2 - \cosh(2h) + 1)^2} \left[\begin{array}{l} \left(\begin{array}{l} h^2\cosh(2h) - 2h\sinh(2h) \\ +h^2 + \cosh(2h) - 1 \end{array} \right) \left(\tilde{a} + \tilde{d} \times Pe_s\right) \\ + (h\sinh(2h) - \cosh(2h) + 1)\,\tilde{b}h \end{array} \right] \\ &+ O\left(Ma^{-2}\right) \end{aligned} \tag{4.19}$$

Here $U_{2,wall}$ is the swimming velocity near a plane wall whose expression is given in equation (4.39). Again as $(h^2\cosh(2h) - 2h\sinh(2h) + h^2 + \cosh(2h) - 1) > 0$ and $(h\sinh(2h) - \cosh(2h) + 1) > 0$, we see that the swimming velocity near a surfactant laden interface at large Ma is always less than that near a plane wall.

4.4 Results

In this section, we examine the influence of surfactant redistribution on the swimming velocity of the sheet near a surfactant laden interface.

It was reported that the swimming velocity of a sheet, propagating longitudinal waves, near a plane wall is the same as its velocity in an unbounded fluid [63] i.e., $U = -\frac{\epsilon^2}{2}\left(\tilde{a}^2 + \tilde{d}^2\right) + O(\epsilon^4)$. Our analysis suggests the presence of a surfactant laden interface instead of a wall near such a sheet, does not modify its velocity, i.e., velocity of a sheet propagating longitudinal waves near a plane surfactant laden interface is the same as its velocity in an unbounded fluid.

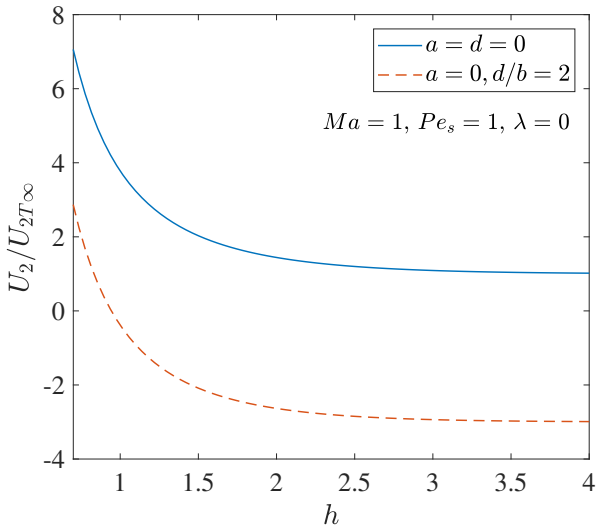

Figure 4.2. : The variation of the swimming velocity with the distance between the interface and (the mid plane of) the sheet for a sheet passing only transverse waves (blue solid line) and that passing both longitudinal and transverse waves (red dashed line). Here the swimming velocity is normalized with the swimming velocity of a sheet passing only transverse waves in an unbounded fluid ($U_{2T\infty}$). The viscosity ratio $\lambda = 0$, Marangoni number $Ma = 1$ and the surface Péclet number $Pe_s = 1$.

As we have analyzed the velocity of a sheet propagating longitudinal waves near a plane surfactant laden interface, we then proceed to examine the velocity of a sheet (near a surfactant laden interface) passing only transverse waves and that passing both longitudinal and transverse waves in the following two subsections. Even though the expressions for the leading order swimming velocity are derived for any arbitrary viscosity ratio λ, we only report the influence of surfactant redistribution on this velocity for an air-water interface ($\lambda = 0$) as experiments on locomotion in films are mainly performed for an air-water interface [126–128].

For a fixed Ma and Pe_s, we found that the swimming velocity increases as h decreases (see figure 4.2). Similar trend with decreasing h was reported for confinements caused by a rigid plane wall [63], a plane clean interface [95] or a gel [120]. Also, the variation of the swimming velocity with Ma and Pe_s is qualitatively the same for any

fixed value of h. For this reason, we report and analyze this variation with Ma and Pe_s for a typical value of $h = 1$.

We report here the typical values of Ma and Pe_s. For the tail of a spermatozoon [130], the wave speed $c \sim (200 - 1200) \times 10^{-6}$ m/s and the wave number $k \sim (1.14 - 4.18) \times 10^5$ m^{-1}. The maximum possible surfactant concentration at an air-water interface [131, 132] $\Gamma_\infty \sim 10^{-6} - 10^{-4}$ mol/m^2. Assuming that the equilibrium surfactant concentration $\Gamma_{eq} \sim \left(10^{-3} - 10^{-1}\right)\Gamma_\infty$, we get $\Gamma_{eq} \sim \left(10^{-9} - 10^{-5}\right)$ mol/m^2. The surface diffusivity of the surfactant [133] $D_s \sim (1 - 10) \times 10^{-9}$ m^2/s. Using the definitions of Ma, Pe_s along with the viscosity of water (μ_1) and the temperature of $T = 298$ K, we get $Ma \sim O(1) - O\left(10^5\right)$ and $Pe_s \sim 0.05 - O(10)$.

4.4.1 Sheet passing only transverse wave along its surface

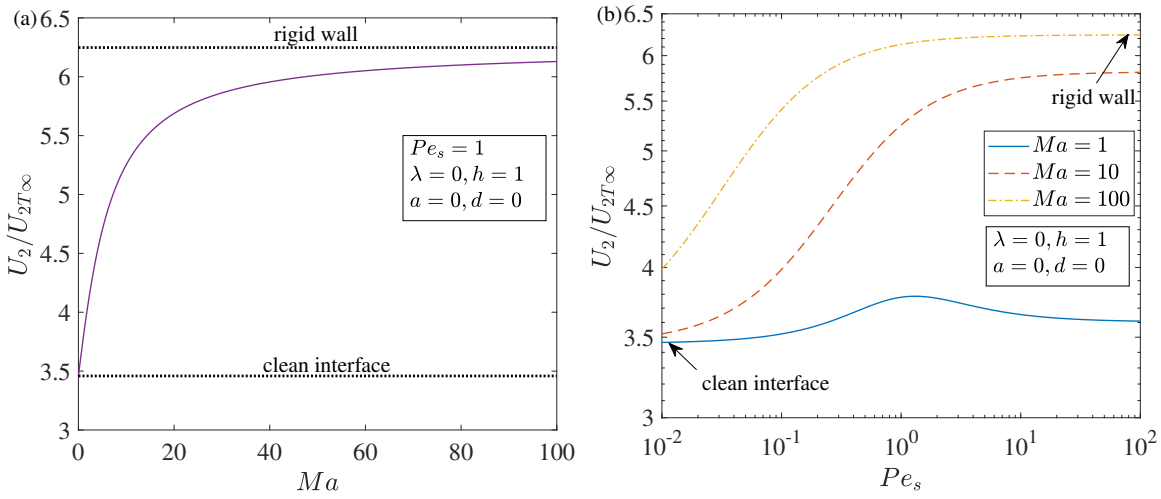

Figure 4.3. : For a sheet passing transverse waves near a plane surfactant laden interface, the variation of the leading order swimming velocity with (a) Ma for $Pe_s = 1$ and (b) Pe_s for $Ma = 1$, 10, and 100. Here the swimming velocity is normalized with the swimming velocity of the same sheet in an unbounded fluid ($U_{2T\infty}$). The distance between the midplane of the sheet and the interface is $h = 1$, the viscosity ratio $\lambda = 0$, and the amplitudes of the longitudinal waves $a = d = 0$.

When a sheet passing only transverse waves is located near a plane surfactant laden interface, the dependence of its swimming velocity on Ma (for a fixed Pe_s) and on Pe_s (for a fixed Ma) is given in figure 4.3. We observe the following from this figure. As the minimum velocity occurs at $Ma = 0$ or $Pe_s \to 0$ and since $Ma = 0$ or $Pe_s \to 0$ represents a clean interface, we conclude that the swimming velocity near a plane surfactant laden interface is always more than that near a plane clean interface. Near a plane surfactant laden interface, (a) the swimming velocity increases with an increase in Ma for any fixed Pe_s, (b) it increases with an increase in Pe_s for any fixed but large Ma i.e., $Ma \geq O(10)$, and (c) it initially increases and then decreases with an increase in Pe_s for any fixed but small Ma i.e., $Ma \leq O(1)$.

4.4.2 Sheet passing both longitudinal and transverse waves along its surface

In this section, we discuss how the effect of surfactant redistribution on the swimming velocity gets modified, in comparison to this effect presented in the earlier section, if a sheet is passing both longitudinal and transverse waves along its surface. For this purpose, we plot the variation of the swimming velocity with Ma (for a fixed Pe_s) and Pe_s (for a fixed Ma) in figure 4.4. From this figure, we observe the following. The swimming velocity for a sheet near a plane surfactant laden interface can be more or even less than that for a sheet near a plane clean interface ($Ma \to 0$ or $Pe_s \to 0$). Unlike the case of a sheet passing only transverse waves, the swimming velocity near a surfactant laden interface might not lie in between the swimming velocity near a plane clean interface and that near a plane wall. Desai *et al.* [16] reported a similar observation by noting that the critical trapping radius of a surfactant-laden drop is less than those of a clean drop and a rigid sphere where a particle or a drop would trap a nearby swimming microorganism if their radius is more than the critical trapping radius. When a sheet is in the vicinity of a surfactant laden interface, (a) the swimming velocity increases with an increase in Ma for a fixed but small Pe_s ($\leq O(1)$),

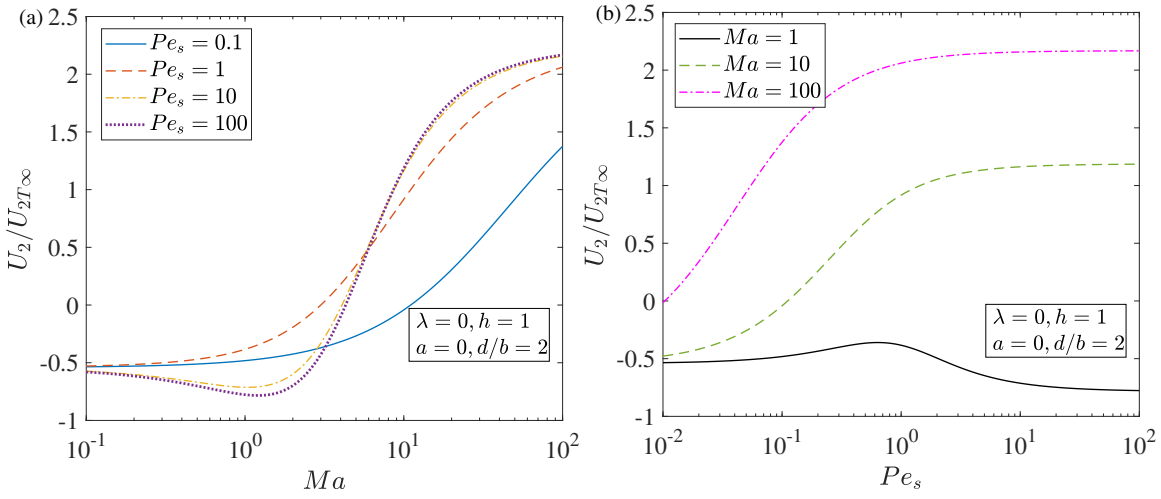

Figure 4.4. : For a sheet passing both longitudinal and transverse waves near a plane surfactant laden interface, the variation of the leading order swimming velocity with (a) Ma for $Pe_s = 0.1, 1, 10, 100$ and with (b) Pe_s for $Ma = 1, 10, 100$. Here the swimming velocity is normalized with the swimming velocity of a sheet passing transverse waves in an unbounded fluid ($U_{2T\infty}$). The distance between the midplane of the sheet and the interface is $h = 1$, the viscosity ratio $\lambda = 0$, and the amplitudes of the waves $a = 0$, and $d/b = 2$.

(b) it initially decreases and then increases with an increase in Ma for a fixed but large Pe_s ($\geq O(10)$), (c) it increases with an increase in Pe_s for a fixed yet large Ma ($\geq O(10)$), (d) it initially increases and then decreases with an increase in Pe_s for a fixed but small Ma ($\leq O(1)$).

It seems non-intuitive for the swimming velocity near a surfactant laden interface to lie outside the range corresponding to the one near a clean interface and a rigid wall. If we had a rigid particle moving near a surfactant laden interface due to some fixed force acting on it, its velocity always lies in between its velocities near a clean interface and a plane wall [30]. So, the motion of organisms is defying the intuition built on the basis of particle motion. This is not the first time that such phenomenon is reported. Considering the motion of particles or organisms in complex fluids, we

find that the particle experiencing a fixed force moves faster in a shear-thinning fluid than that in a Newtonian fluid but the velocity of a swimming microorganism in a shear-thinning fluid can be more or even less than that in a Newtonian fluid [90]. Similar observation has been made for the velocity of a swimming microorganism in a viscoelastic fluid [109].

Even though most of the observations in figures 4.3-4.4 can be qualitatively explained by analyzing the influence of surfactant redistribution on the amplitude of leading order interface slip (see Appendix 4.8), such reasoning is not useful to understand the swimming velocity near a surfactant laden interface if this velocity lies outside the range bounded by the velocities near a clean interface and a plane wall. Consequently, the amplitude of leading order interface slip is not determinative of the swimming velocity changes. Hence to get a proper understanding of the variation of the swimming velocity with all values of Ma and Pe_s, we need to correlate the surfactant induced changes in either (i) the amplitude and phase of the leading order slip (not just the amplitude) or (ii) the second order slip (instead of first order slip) with the swimming velocity which are not done in this work.

4.4.3 Apparent viscosity ratio

As the expression for the swimming velocity of a sheet near a surfactant laden interface is quite lengthy, we represent the surfactant laden interface as a clean interface with a modified or apparent viscosity ratio (λ_{app}) to convey the effects of surfactant redistribution in a succinct manner. The expression for λ_{app} is simpler than the expression for the swimming velocity. Using this expression for λ_{app} and the dependence of sheet's velocity on the viscosity ratio for a sheet near a clean interface [95], we can evaluate the sheet's velocity at this apparent viscosity ratio to find its velocity near a surfactant laden interface. To determine the apparent viscosity ratio, we simply equate the sheet's velocity near a surfactant laden interface with zero viscosity ratio to its velocity near a clean interface with a viscosity ratio that is equal to the apparent

viscosity ratio. We then solve this equation for the apparent viscosity ratio to obtain

$$\lambda_{app} = \frac{Ma\,Pe_s \begin{pmatrix} \left(\left(-Ma\,Pe_s\,\tilde{a} - 2\,\tilde{b}\right)h - 2\,\tilde{d}Pe_s + 2\,\tilde{a}\right)\left(\cosh(h)\right)^3 \\ -2\left(\left(\left(1/2\,Ma\,\tilde{b} - \tilde{d}\right)Pe_s + \tilde{a}\right)h - 1/2\,Ma\,Pe_s\,\tilde{a}\right)\sinh(h)\left(\cosh(h)\right)^2 \\ +\begin{pmatrix} Ma\,Pe_s\,\tilde{a}h^3 + \left(-2\,\tilde{d}Pe_s + 2\,\tilde{a}\right)h^2 \\ +\left(Ma\,Pe_s\,\tilde{a} + 2\,\tilde{b}\right)h + 2\,\tilde{d}Pe_s - 2\,\tilde{a} \end{pmatrix}\cosh(h) \\ -\begin{pmatrix} -Ma\,Pe_s\,\tilde{b}h^3 + \left(Ma\,Pe_s\,\tilde{a} - 2\,\tilde{b}\right)h^2 \\ +\left(\left(-Ma\,\tilde{b} - 2\,\tilde{d}\right)Pe_s + 2\,\tilde{a}\right)h + Ma\,Pe_s\,\tilde{a} \end{pmatrix}\sinh(h) \end{pmatrix}}{\begin{bmatrix} \left(\left(\left(-2\,Ma\,\tilde{d} - 4\,\tilde{b}\right)Pe_s^2 - 2\,Ma\,Pe_s\,\tilde{a} - 4\,\tilde{b}\right)h + 4\,Pe_s^2\tilde{a} + 4\,\tilde{a}\right)\left(\cosh(h)\right)^3 \\ -4\left(\left(Pe_s^2\tilde{a} + 1/2\,\tilde{b}Ma\,Pe_s + \tilde{a}\right)h - 1/2\,Ma\,Pe_s\left(\tilde{d}Pe_s + \tilde{a}\right)\right)\sinh(h)\left(\cosh(h)\right)^2 \\ +\begin{pmatrix} 2\,Ma\,Pe_s\left(\tilde{d}Pe_s + \tilde{a}\right)h^3 + \left(4\,Pe_s^2\tilde{a} + 4\,\tilde{a}\right)h^2 \\ +\left(\left(2\,Ma\,\tilde{d} + 4\,\tilde{b}\right)Pe_s^2 + 2\,Ma\,Pe_s\,\tilde{a} + 4\,\tilde{b}\right)h - 4\,Pe_s^2\tilde{a} - 4\,\tilde{a} \end{pmatrix}\cosh(h) \\ -2\begin{pmatrix} -Ma\,Pe_s\,\tilde{b}h^3 + \left(\left(Ma\,\tilde{d} - 2\,\tilde{b}\right)Pe_s^2 + Ma\,Pe_s\,\tilde{a} - 2\,\tilde{b}\right)h^2 \\ +\left(-\tilde{b}Ma\,Pe_s + 2\,Pe_s^2\tilde{a} + 2\,\tilde{a}\right)h + Ma\,Pe_s\left(\tilde{d}Pe_s + \tilde{a}\right) \end{pmatrix}\sinh(h) \end{bmatrix}} \tag{4.20}$$

which simplifies for a sheet passing only transverse waves to

$$\lim_{\tilde{a}\to 0,\tilde{d}\to 0}\lambda_{app} = \frac{2MaPe_s\left(-\sinh(2h) - 1/2MaPe_s\cosh(2h) + Ma\left(h^2 + 1/2\right)Pe_s + 2h\right)}{\left(-4Pe_s^2 - 4\right)\sinh(2h) - 2MaPe_s\cosh(2h) + 8Pe_s^2h + \left(4h^2 + 2\right)MaPe_s + 8h} \tag{4.21}$$

In the limit $Ma \to 0$ or $Pe_s \to 0$, the surfactant laden interface behaves like a clean interface due to which λ_{app} approaches the actual viscosity ratio that is zero. Hence, $\lambda_{app} \to 0$ as $Ma \to 0$ or $Pe_s \to 0$. In the limit $Ma \to \infty$, the surfactant becomes incompressible [30,73] and the surfactant laden interface behaves like a rigid wall (see Appendix 4.7 for discussion on the incompressible surfactant). Hence, $\lambda_{app} \to \infty$ as $Ma \to \infty$. As $Pe_s \to \infty$, λ_{app} approaches a constant value given by

$$\lim_{Pe_s\to\infty,\tilde{a}\to 0,\tilde{d}\to 0}\lambda_{app} = \frac{Ma^2\left(\left(\cosh(h)\right)^2 - h^2 - 1\right)}{4\sinh(h)\cosh(h) - 4h}, \tag{4.22}$$

for a sheet passing only transverse waves.

For a sheet passing transverse wave near a surfactant laden interface, typical variation of λ_{app} with Pe_s for various Ma is shown in figure 4.5. From this figure, we

observe that λ_{app} increases with an increase in Pe_s at large Ma ($\geq O(10)$) while it initially increases and then decreases with an increase in Pe_s at small Ma ($\leq O(1)$). Combining this dependence of λ_{app} on Ma, Pe_s with the dependence of U_2 on λ for a sheet near a clean interface (figure 4.6b), we expect the velocity of a sheet near a surfactant laden interface to increase monotonically (resp. vary non-monotonically) with an increase in Pe_s at large Ma (resp. at small Ma), consistent with the observations of figure 4.3b.

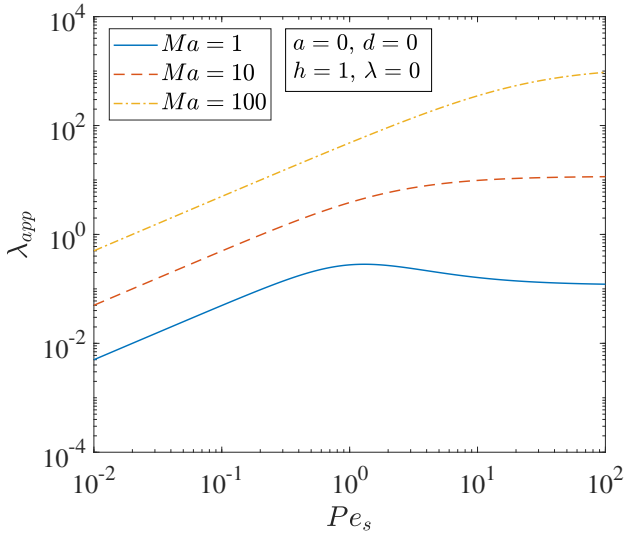

Figure 4.5. : The variation of apparent viscosity ratio with Pe_s at $Ma = 1$ (blue solid line), 10 (red dashed line) and 100 (yellow dash-dotted line). Here, the sheet is passing only transverse waves, hence $a = d = 0$. The actual viscosity ratio of the surfactant laden interface $\lambda = 0$ while $h = 1$.

4.5 Conclusions

We aimed to understand the dependence of a microorganism's swimming velocity on the Marangoni number (Ma) and the surface Péclet number (Pe_s) when it is near a surfactant covered interface. For this purpose, we derived the velocity of a 2D infinitely long swimming sheet near a surfactant laden interface under the assumptions

of zero Reynolds number, zero interface deformation and small sheet's deformation. We observed that the swimming velocity near a surfactant laden interface can be more or even less than that near a clean interface and this velocity varies non-monotonically with Ma and Pe_s, these observations being highly sensitive to the type of wave passing through the sheet. Unlike the rigid particles near a surfactant laden interface, we found that the swimming microorganisms near such an interface can have a velocity that does not lie in between their velocities near a clean interface and a rigid wall. To succinctly express the effects of surfactant redistribution, we represented the surfactant laden interface as a clean interface with a viscosity ratio equal to apparent viscosity ratio whose expression is found by equating the swimming velocities near a clean and surfactant laden interface.

4.6 Appendix A: Expressions for constants that appear in stream function and surfactant concentration

In this section, we provide expressions for the constants appearing in equations (4.13)-(4.15) that enable us to determine the stream function and the surfactant concentration at various orders of ϵ. Even though we derived these expressions for any arbitrary viscosity ratio λ and for non-zero wave amplitudes $\tilde{a} \neq 0$, $\tilde{b} \neq 0$, and $\tilde{d} \neq 0$, as these expressions are lengthy, we provide these expressions only for the special case of an air-water interface ($\lambda = 0$) and sheet passing only transverse waves $\left(\tilde{a} = 0, \tilde{d} = 0\right)$.

4.6.1 Expressions for constants appearing in $O(\epsilon)$ stream function and surfactant concentration

Here, we present the expressions for constants appearing in $\psi_1^{(1)}$, $\psi_1^{(2)}$ and Γ_1.

$$A_{1,1}^{(1)} = 0, \tag{4.23}$$

$$B_{1,1}^{(1)} = -\tilde{b}, \tag{4.24}$$

$$-C_{1,1}^{(1)} = E_{1,1}^{(1)} = \frac{2(\sinh(h))^2 Pe_s^2 Ma\tilde{b}h^2}{\mathcal{D}}, \tag{4.25}$$

$$-D_{1,1}^{(1)} = F_{1,1}^{(1)} = \frac{\left(\begin{array}{l} -4Ma(\cosh(h))^4 Pe_s - ((Ma^2+4)Pe_s^2+4)\sinh(h)(\cosh(h))^3 \\ +((-Ma^2h+4h)Pe_s^2+(2h^2+4)MaPe_s+4h)(\cosh(h))^2 \\ +Ma^2Pe_s^2\sinh(h)(h^2+1)\cosh(h)+hPe_sMa(Ma(h^2+1)Pe_s+2h) \end{array} \right)\tilde{b}}{\mathcal{D}}, \tag{4.26}$$

$$G_{1,1}^{(1)} = \frac{-2Pe_s^2 hMa\tilde{b}\sinh(h)(\cosh(h)h-\sinh(h))}{\mathcal{D}}, \tag{4.27}$$

$$H_{1,1}^{(1)} = \frac{-\sinh(h)\tilde{b}\left(\begin{array}{l} -4MaPe_s(\cosh(h))^3 - ((Ma^2+4)Pe_s^2+4)\sinh(h)(\cosh(h))^2 \\ +(4Pe_s^2h+(2h^2+4)MaPe_s+4h)\cosh(h) \\ +Pe_s\sinh(h)Ma(Ma(h^2+1)Pe_s+2h) \end{array} \right)}{\mathcal{D}}, \tag{4.28}$$

$$A_{1,1}^{(2)} = -\frac{2h^2 \mathrm{e}^h Ma\sinh(h)Pe_s^2\tilde{b}\left((\cosh(h))^2-h^2-1\right)}{\mathcal{D}}, \tag{4.29}$$

$$B_{1,1}^{(2)} = \frac{2h^2\tilde{b}\left(\begin{array}{l} -Ma(\cosh(h))^2 Pe_s + (-2Pe_s^2-2)\sinh(h)\cosh(h) \\ +2Pe_s^2h+Ma(h^2+1)Pe_s+2h \end{array} \right)\sinh(h)\mathrm{e}^h}{\mathcal{D}}, \tag{4.30}$$

$$E_{1,1}^{(2)} = \frac{2\mathrm{e}^h Ma\sinh(h)Pe_s^2\tilde{b}h\left((\cosh(h))^2-h^2-1\right)}{\mathcal{D}}, \tag{4.31}$$

$$F_{1,1}^{(2)} = \frac{-2h\tilde{b}\left(\begin{array}{l} -Ma(\cosh(h))^2 Pe_s + (-2Pe_s^2 - 2)\sinh(h)\cosh(h) \\ +2Pe_s^2 h + Ma\left(h^2+1\right)Pe_s + 2h \end{array}\right)\sinh(h)\,\mathrm{e}^h}{\mathcal{D}}, \tag{4.32}$$

$$J_{1,1} = \frac{2hPe_s\sinh(h)\,\tilde{b}\left(-Ma(\cosh(h))^2 Pe_s - 2\cosh(h)\sinh(h) + Ma\left(h^2+1\right)Pe_s + 2h\right)}{\mathcal{D}}, \tag{4.33}$$

$$L_{1,1} = \frac{4Pe_s^2\tilde{b}h\sinh(h)\left(-\cosh(h)\sinh(h) + h\right)}{\mathcal{D}}, \tag{4.34}$$

where

$$\begin{aligned} \mathcal{D} = {} & \left(\left(Ma^2+4\right)Pe_s^2 + 4\right)(\cosh(h))^4 + 4Ma(\cosh(h))^3\sinh(h)\,Pe_s \\ & + \left(-4 + \left(-4 + \left(-2h^2 - 2\right)Ma^2\right)Pe_s^2 - 4MaPe_s h\right)(\cosh(h))^2 \\ & -4\left(2Pe_s^2 h + Ma\left(h^2+1\right)Pe_s + 2h\right)\sinh(h)\cosh(h) \\ & + \left(\left(h^2+1\right)^2 Ma^2 + 4h^2\right)Pe_s^2 + 4hMa\left(h^2+1\right)Pe_s + 4h^2, \end{aligned}$$

$$U_1 = \alpha_1 = \beta_1 = \gamma_1 = 0. \tag{4.35}$$

4.6.2 Expressions for constants appearing in $O(\epsilon^2)$ stream function

Here, we present the expressions for constants appearing in $\psi_2^{(1)}$ and $\psi_2^{(2)}$.

$$\beta_2 = \gamma_2 = 0, \tag{4.36}$$

$$U_2 = -\alpha_2 = \frac{-\left(\begin{array}{l}\left(-4+\left(-Ma^2-4\right)Pe_s^2\right)\left(\cosh\left(h\right)\right)^4-4\sinh\left(h\right)\left(\cosh\left(h\right)\right)^3 Ma\,Pe_s\\+\left(4+\left(2\,Ma^2+4\right)Pe_s^2\right)\left(\cosh\left(h\right)\right)^2+4\sinh\left(h\right)\cosh\left(h\right)Ma\,Pe_s\\+\left(\left(h^4-1\right)Ma^2+4\,h^2\right)Pe_s^2+4\,Ma\,Pe_s\,h^3+4\,h^2\end{array}\right)\tilde{b}^2}{\left[\begin{array}{l}\left(\left(2\,Ma^2+8\right)Pe_s^2+8\right)\left(\cosh\left(h\right)\right)^4+8\sinh\left(h\right)\left(\cosh\left(h\right)\right)^3 Ma\,Pe_s\\+\left(-8+\left(-8+\left(-4\,h^2-4\right)Ma^2\right)Pe_s^2-8\,Ma\,Pe_s\,h\right)\left(\cosh\left(h\right)\right)^2\\-8\left(2\,Pe_s^2 h+Ma\left(h^2+1\right)Pe_s+2\,h\right)\sinh\left(h\right)\cosh\left(h\right)\\+\left(2\left(h^2+1\right)^2 Ma^2+8\,h^2\right)Pe_s^2+8\,hMa\left(h^2+1\right)Pe_s+8\,h^2\end{array}\right]}. \tag{4.37}$$

4.7 Appendix B: Validation of results

In this section, we verify the expression for the velocity of a sheet near a surfactant laden interface by comparing it with similar expressions derived in the literature for several special cases. For instance, when a sheet is far away from the interface, its velocity should be the same as the sheet's velocity in an unbounded fluid [102]

$$\lim_{h\to\infty} U_2 = \frac{1}{2}\left(-\tilde{a}^2-\tilde{d}^2+\tilde{b}^2+2\tilde{a}\tilde{b}\right) \tag{4.38}$$

As $\lambda \to \infty$ or $Ma \to \infty$, the sheet's velocity should approach the velocity of a sheet placed symmetrically between two plane walls [63].

$$\lim_{\lambda\to\infty} U_2 = \lim_{Ma\to\infty} U_2 = \frac{\left(\begin{array}{l}\left(\tilde{a}^2-\tilde{b}^2+\tilde{d}^2\right)\left(\cosh\left(h\right)\right)^2-2\cosh\left(h\right)\sinh\left(h\right)\tilde{a}\tilde{b}\\+\left(-h^2-1\right)\tilde{a}^2+2\tilde{a}\tilde{b}h+\left(-h^2+1\right)\tilde{b}^2-\tilde{d}^2\left(h^2+1\right)\end{array}\right)}{2h^2-2\left(\cosh\left(h\right)\right)^2+2} \tag{4.39}$$

It is obvious that a surfactant laden interface behaves as a rigid wall in the limit $\lambda \to \infty$ but such a behavior in the limit $Ma \to \infty$ requires some explanation. As $Ma \to \infty$, the surfactant becomes incompressible [30,73], i.e., $O\left(1\right)$ changes in interfacial tension are caused by infinitesimal changes in the surfactant concentration. So, treating Γ as constant, the surfactant transport equation simplifies to $\frac{\partial}{\partial x}\left(u|_{y=h}\right) = 0$. The only solution of this equation that enables the velocity of fluid 2 to approach the

negative of sheet's velocity, far away from the interface, is $u|_{y=h} = -U$. The sheet near an interface with such interface boundary conditions $\left(u|_{y=h} = -U,\, v|_{y=h} = 0\right)$ is essentially equivalent to a sheet near a plane wall.

In the limit $Ma \to 0$ or $Pe_s \to 0$, the sheet's velocity should approach its velocity near a plane clean interface. This velocity was derived for a sheet passing transverse waves in the positive x-direction (Taylor's sheet) [95]. As we considered the sheet passing transverse waves in the negative x-direction, its velocity near a plane surfactant laden interface in the limits $Ma \to 0$ or $Pe_s \to 0$ should approach the negative of Taylor's swimming sheet velocity near a plane clean interface.

$$\lim_{Ma,\tilde{a},\tilde{d}\to 0} U_2 = \lim_{Pe_s,\tilde{a},\tilde{d}\to 0} U_2 = \frac{\tilde{b}^2}{2} - \frac{\tilde{b}^2 h\left(h\lambda+1\right)}{h^2\lambda - \left(\cosh\left(h\right)\right)^2\lambda - \sinh\left(h\right)\cosh\left(h\right) + h + \lambda} \tag{4.40}$$

4.8 Appendix C: Effect of surfactant redistribution on the interface slip

In this section, we analyze the influence of surfactant redistribution on the leading order interface slip when a sheet passing transverse waves is located near an interface. Let us first discuss how the viscosity ratio of an interface affects the interface slip and the swimming velocity for a sheet near a plane clean interface. We plot these features for a sheet passing transverse waves near a plane clean interface in figure 4.6. We observe that the interface slip decreases while the swimming velocity increases with an increase in the viscosity ratio of a clean interface. As an increase in the viscosity ratio corresponds to an increase in the viscosity of fluid above the interface (for a fixed viscosity of fluid below the interface), such high viscosity fluid above the interface hinders the interface slip.

When a sheet is near a clean interface, the interface slip varies in a sinusoidal fashion with the x-coordinate, i.e., $u_1|_{y=h} = A\sin\left(x+t+\phi\right)$, where A, and ϕ are the amplitude and phase of the slip, respectively (see blue solid line in figure 4.7; vector field of the interface slip is shown by blue (upper) arrows in this figure). When we compare slip (such as slip of clean and surfactant laden interface or slip of a surfactant

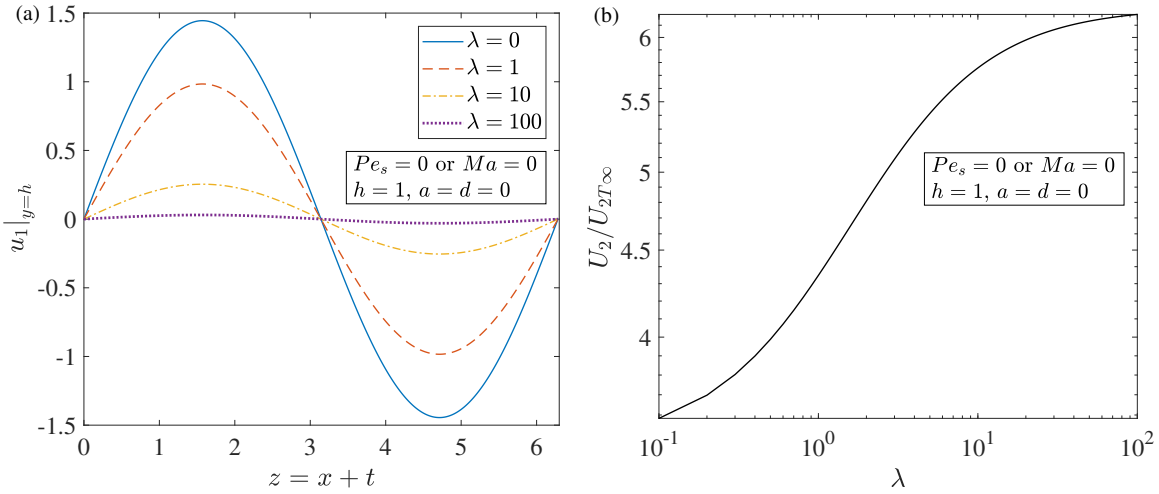

Figure 4.6. : For a sheet passing transverse waves near a plane clean interface, the variation of the (a) leading order interface slip and (b) leading order swimming velocity with the viscosity ratio λ. Here the swimming velocity is normalized with the swimming velocity of the same sheet in an unbounded fluid ($U_{2T\infty}$). The values of other parameters h, a, and d are kept the same as those of figure 4.3.

laden interface at various values of Ma or Pe_s), we are essentially comparing the amplitude of the sinusoidal functions. Now, if a sheet is near a surfactant laden interface, the surfactant concentration varies non-monotonically with the position, as shown by red dash-dotted lines in figure 4.7. As the interfacial tension decreases with an increase in the surfactant concentration, this non-homogeneous surfactant concentration gives rise to a non-homogeneous interfacial tension which in turn causes the tensile stress imbalance on the interface, pulling the fluid from the regions of maximum Γ towards the regions of minimum Γ. This Marangoni induced slip velocity is shown by red (lower) arrows in figure 4.7. The slip of a surfactant laden interface is the sum of the slip of a clean interface and the Marangoni induced slip. As this Marangoni induced slip is directed oppositely to the clean interface's slip at most of the locations, the slip of a surfactant laden interface is less than the slip of a clean interface (see blue dotted line in figure 4.7 for the slip of a surfactant laden interface).

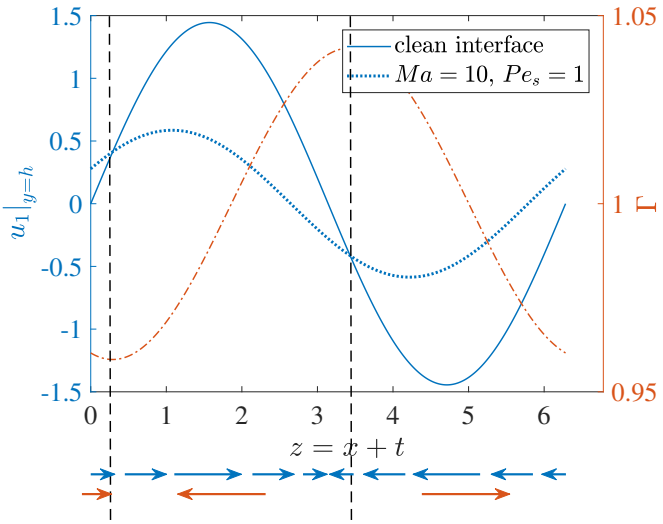

Figure 4.7. : Comparison of interface slip of a clean interface (blue solid line) with that of a surfactant laden interface (blue dotted line). Also plotted is the surfactant concentration on the surfactant laden interface (red dash-dotted line). The vertical dashed lines are just for reference. The blue (upper) and red (lower) arrows denote, respectively, the vector field of clean interface slip and the direction of Marangoni induced slip. The axis for the interface slip is on the left while that for surfactant concentration is on the right. Here, $Ma = 10$ and $Pe_s = 1$ for the surfactant laden interface. Also, $\epsilon = 0.1$ is used to calculate Γ while the values of the other parameters h, λ, a, and d are kept the same as those of figure 4.3.

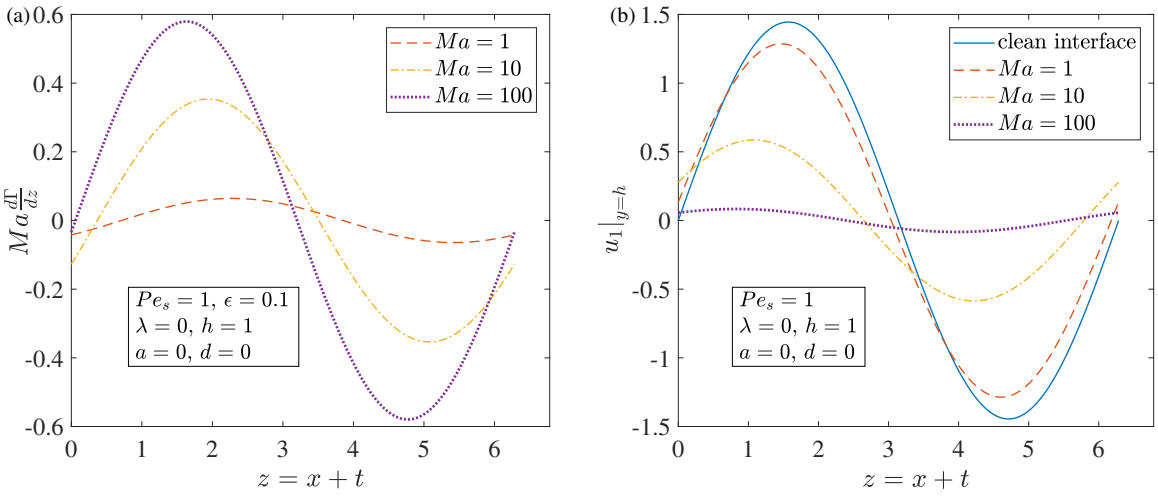

Figure 4.8. : The variation of (a) the Marangoni stress and (b) the leading order interface slip with the Marangoni number Ma for a fixed surface Péclet number $Pe_s = 1$. Here $\epsilon = 0.1$ is used to calculate the Marangoni stresses while the values of other parameters λ, h, a, and d are kept the same as those of figure 4.3.

With an increase in Ma, the Marangoni stresses increase (see figure 4.8a) which in turn reduce the slip of an interface (see figure 4.8b). At large Ma like $Ma = 100$, with an increase in Pe_s the advective transport of surfactant increases in comparison to its diffusive transport; this increases the gradients in the surfactant concentration (see figure 4.9a) or Marangoni stresses which in turn reduce the interface slip (see figure 4.9b). For these values of Ma and Pe_s at which the interface slip decreases with an increase in Ma for a fixed Pe_s (or with an increase in Pe_s for a fixed Ma), the swimming velocity increases with the corresponding variation of Ma or Pe_s (see figure 4.3).

We note that the Marangoni stresses increase with an increase in Pe_s at any fixed Ma, not just at large Ma. But at small Ma, with an increase in Pe_s, the increasing Marangoni stresses reduce the interface slip during the initial increase of Pe_s (see figure 4.10a) while they increase the interface slip during the latter increase of Pe_s (see figure 4.10b). This is expected because during the initial (respectively, latter) increase

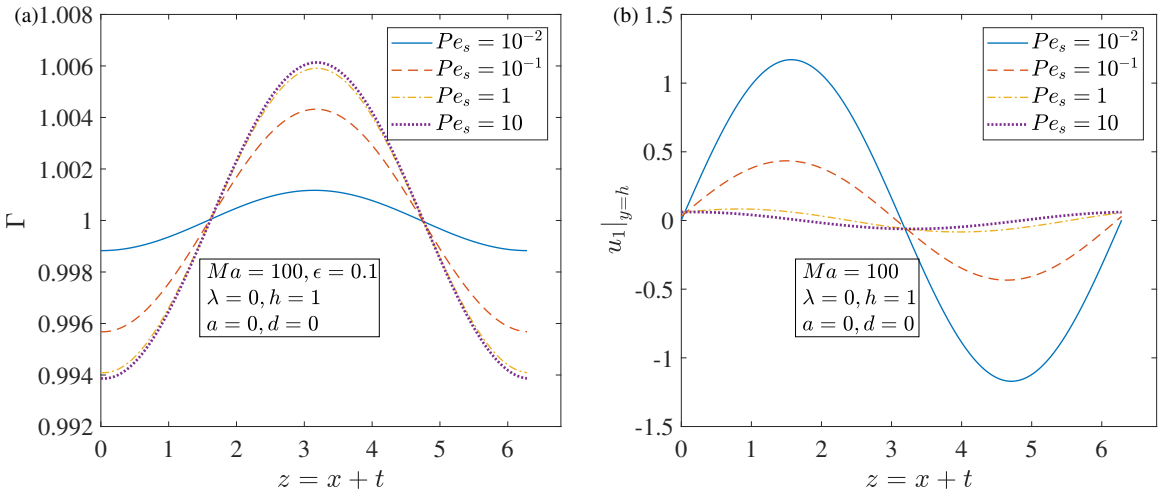

Figure 4.9. : The variation of (a) the surfactant concentration and (b) the leading order interface slip with the surface Péclet number Pe_s for a fixed Marangoni number $Ma = 100$. Here $\epsilon = 0.1$ is used to calculate surfactant concentration while the values of other parameters λ, h, a, and d are kept the same as those of figure 4.3.

in Pe_s, the Marangoni induced slip is directed opposite to (respectively, along) the slip of a relatively clean interface at most of the interface locations. Compare the red (lower) arrows with blue (upper) arrows in figure 4.10 to understand this observation. Here relatively clean interface is an interface with lower Pe_s. At this value of Ma at which the interface slip varies non-monotonically with an increase in Pe_s, the swimming velocity also varies non-monotonically with an increase in Pe_s (see figure 4.3b).

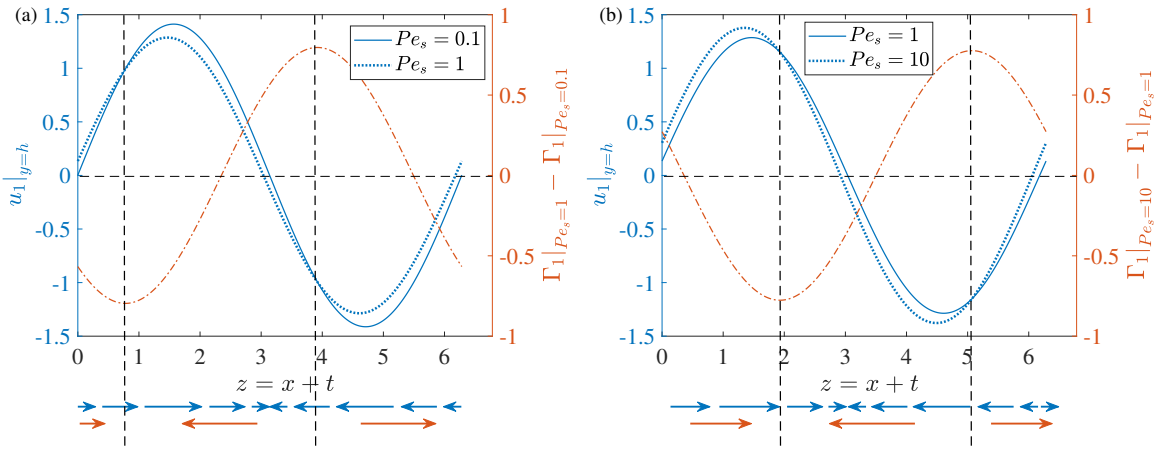

Figure 4.10. : Comparison of the interface slip of surfactant laden interfaces with different Pe_s but with a fixed $Ma = 1$. In each plot, the interface slip at low and high Pe_s are denoted, respectively, by blue solid and blue dotted lines. Also plotted is the change in the surfactant concentration at high Pe_s in comparison to that at low Pe_s (red dash-dotted line). The dashed lines are just for reference. In subfigure (a) the low and high Pe_s are 0.1 and 1 while in subfigure (b) they are 1 and 10, respectively. The blue (upper) and red (lower) arrows denote, respectively, the vector field of surfactant laden interface's slip at low Pe_s and the direction of Marangoni induced slip as Pe_s is increased from its low to high value. The axis for the interface slip is on the left while that for the change in the surfactant concentration is on the right. The values of the other parameters h, λ, a, and d are kept the same as those of figure 4.3.

5. DRAG, DEFORMATION, AND DRIFT VOLUME ASSOCIATED WITH A DROP RISING IN A DENSITY-STRATIFIED FLUID

5.1 Introduction

In lakes, ponds or oceans, the variation of temperature or salt concentration with height causes density stratification. Drops in stratified fluids are encountered when one uses bubble plumes for destratification to get rid of the harmful effects associated with the stratification [134] or during an oil spill as oil drops rise through stratified water in the ocean [135]. It is then necessary to find the forces acting on a drop rising in a stratified fluid to estimate the efficiency of destratification process or to understand the consequences of an oil spill [5, 6].

There was a tremendous effort to understand the settling motion of spheres in a stratified fluid for different values of Re, Fr, Pr where Re, Fr, Pr are the Reynolds, Froude, and Prandtl numbers, respectively [136–144]. These works used two types of stratification – linearly stratified fluid or two homogeneous miscible fluids of different densities separated by a density stratified interface of finite or zero thickness (call this step stratification). All these works reported a drag enhancement due to stratification, the physics behind this drag enhancement being dependent on the type of stratification, Re, and Fr.

For a sphere settling through a step stratification at 1.5 <Re< 15, it was found that its velocity changes nonmonotonically from its terminal velocity in upper fluid to its terminal velocity in the lower fluid displaying a minimum somewhere in the interface due to the stratification enhanced drag [136]. A similar nonmonotonic variation of the settling velocity with time was also found for a sphere crossing

This chapter has been reprinted with permission from the article "Drag, deformation, and drift volume associated with a drop rising in a density-stratified fluid", by V. A. Shaik and A. M. Ardekani, Physical Review Fluids, 5(1):013604, 2020 (DOI: 10.1103/PhysRevFluids.5.013604).

an interface separating two homogeneous fluids (with zero interface thickness) even at zero Re [138, 139]. Again considering the settling through step stratification at 20 <Re< 450, it was found that the sphere decelerates so much due to enhanced drag that it levitates (comes to rest in a fluid that is lighter than it) and reverses its direction of motion for sometime before continuing to fall down [137]. In these works, the sphere leaving the upper homogeneous fluid (by entering the stratified interface or lower homogeneous fluid), drags this low density fluid with it and the buoyancy of this low density fluid manifests as an enhanced drag on the sphere. As long as the low density fluid is attached to the sphere, it decelerates achieving a minimum velocity, at which point the entire low density fluid is detached from the sphere due to which it begins to accelerate. This leads to the nonmonotonic variation of velocity with time.

When a sphere is settling through a linearly stratified fluid at moderate Re (10 <Re< 1000), it was observed that a standing vortex which typically occurs in homogeneous fluids is suppressed by stratification in turn giving rise to strong vertical jet behind the sphere [140–142]. A mechanism for the appearance of this jet is given as follows. As the sphere settles it drags a low density fluid which initially is located near the front of the sphere in the density boundary layer. Due to the buoyancy, this low density fluid rises to the back of the sphere in an attempt to return to its original position in turn generating a vertical jet. This jet is similar to the caudal fluid dragged from upper homogeneous layer when a sphere is settling in a step stratification. The buoyancy of the low density fluid in the jet and the generated internal waves as low density fluid returns to its initial density level are responsible for the increased drag due to stratification [143].

The physics associated with a particle settling in a linearly stratified fluid at moderate Re is interesting yet quite complex to understand as in this case after the particle reaches its peak velocity, other than monotonic deceleration, the particle can levitate momentarily, reverse its direction of motion and even oscillate with a frequency proportional to the Brunt-Väisälä frequency [143]. The wake structure behind

such settling particle is also complicated and can be one of the seven types depending on Re and Fr [145]. On the other hand, settling at low Re is well understood. In this case, the buoyancy of a light fluid immediately adjacent to the sphere manifests as the enhanced drag which was shown to be proportional to $\mathrm{Ri}^{0.51}$ where Ri is the viscous Richardson number [146].

Most of the previous works attributed the stratification enhanced drag to the buoyancy of the dragged lighter fluid. In an attempt to identify the origin of this stratification enhanced drag, a recent work [147] divided the contributions of the stratification to the drag into two parts—the first one coming from the buoyancy of the lighter fluid and the second one arising from the baroclinic torque induced modifications in the vorticity field around the settling particle. For most values of Re, Fr, Pr, the force due to the change in vorticity dominates and is responsible for the observed stratification enhanced drag.

A few theoretical works were also carried out to derive the stratification enhanced drag acting on a particle settling in a linearly stratified fluid [148–150]. Due to the coupling between the equations governing the fluid flow and density transport, such calculation was only done for weak stratifications, in turn enabling one to take perturbations in terms of small stratification parameter. It was shown that such perturbation is singular similar to the perturbation in Re [151] as the matching zone where the viscous forces balance the buoyancy forces occurs far away from the particle. The exact location of the matching zone depends on whether advection of density transport dominates the diffusion or vice-versa. Neglecting inertia, Zvirin & Chadwick [148] calculated this stratification enhanced drag assuming the advection is more important while Candelier's work [149] is valid if diffusion is more important. It was recently shown in Ref. [150] that Zvirin & Chadwick's calculation holds not only in the limits of dominant advection or dominant diffusion but also uniformly between these two limits. The main focus of Ref. [150] was to estimate the inertial effects on the stratification enhanced drag for a settling rigid particle. We use a similar perturbation scheme to find the influence of inertia on the stratification enhanced

drag acting on a rising drop. We extend the scope of the work by evaluating the drop deformation and the drift volume induced by the drop as well.

There are few numerical works that analyzed the settling or rising dynamics of a drop in a stratified fluid. In this case, either the stratification or the presence of surfactants can cause the spatial inhomogeneties in the interfacial tension that complicates the rising dynamics [152, 153]. Analyzing the settling motion of a drop in a step stratification, it was found that the slip boundary condition on the drop causes it to entrain less amount of low density fluid than that of a rigid sphere which manifests as a smaller stratification enhanced drag [152]. Similar to a settling particle, a drop rising in a linearly stratified fluid at moderate Re can levitate, reverse its direction of motion and even oscillate about certain fluid density level [154]. In a linearly stratified fluid, two drops rising in tandem or in side by side configuration were found to retain their configuration during interaction [155]. This observation for drops in tandem motion in a stratified fluid holds for stronger stratifications and is in contrast to their motion in a homogeneous fluid. After the drops approach their neutrally buoyant density level, they oscillate, and eventually the trailing drop rotates around the leading one, forming a side-by-side configuration. For a swarm of drops rising in a linearly stratified fluid, it was reported that the stratification hinders the vertical rise velocity of the swarm but increases the probability of cluster formation [156].

A drop rising in a homogeneous or stratified fluid drags a certain volume of fluid with it, the so called drift volume. An estimate of drift volume induced by a rising drop would answer if the drop mixes its surrounding environment. It was Darwin [157] who introduced the drift volume and he found that the drift volume induced by a translating sphere in an inviscid fluid is equal to the added mass divided by the fluid density. In a viscous fluid, at $\mathrm{Re} = 0$, Eames et al calculated the drift volume induced by a rising drop and found that a slow $1/r$ velocity decay causes the drift volume to become infinite [158]. They also evaluated the drift volume induced by a drop translating normal to a wall and found that a faster $1/r^3$ velocity decay makes the drift volume finite but much large compared to drop's volume. Here r is the

distance measured from the center of the drop. At finite Re, the ever increasing extent of wake behind a towed particle and a slow $1/r$ decay of velocity in the wake produces an infinite drift volume [159]. Such infinite drift volume induced by towing particles at zero or finite Re prompted the drift based explanations in support of biogenic mixing contributions to oceanic circulation [160, 161]. But effects such as density stratification [143, 162], background turbulence [163] and force-free nature of swimming organisms [164, 165] reduce the drift volume and make it finite.

Despite several studies on the subject, a theoretical investigation of drop transport in a stratified fluid and the induced drift volume is missing, which is the focus of the present work. This paper is organized as follows. We present the dimensionless governing equations and boundary conditions in Sec. 5.2. We then derive the drag, first order flow fields, drop deformation, and the induced drift volume in Secs. 5.3, 5.4, 5.5, and 5.6 respectively. We finally provide some concluding remarks in Sec. 5.7.

5.2 Problem Formulation

In this section, we present the dimensionless governing equations and boundary conditions for the fluid flow and density disturbance when a drop is rising in a stratified fluid (see figure 6.1 for schematic). We work in a frame moving with the drop. In this frame the drop is stationary and the fluid velocity $\mathbf{w}$ far away from the drop approaches the negative of the drop velocity $\mathbf{u}$, i.e., $\mathbf{w} \sim -\mathbf{u}$ as $r = |\mathbf{r}| \to \infty$. In this far-field region, the fluid density ρ is equal to the ambient density ρ_0 that varies linearly with the vertical position x_3, i.e., $\rho \sim \rho_0 = \rho_\infty - \gamma x_3$ as $r \to \infty$. Here $\mathbf{r}$, $\mathbf{x}$ are the position vectors with respect to the drop center and a fixed point in the lab frame, so $\mathbf{x} = \mathbf{r} + \mathbf{x}_d$, where $\mathbf{x}_d$ gives drop's position in the lab frame. Also ρ_∞ is the reference density while $\gamma > 0$ is the density gradient. The pressure p in the far-field is equal to p_0 that is governed by $-\nabla p_0 + \rho_0 \mathbf{g} = \mathbf{0}$, where $\mathbf{g} = -g\,\mathbf{e}_3$ is a gravity vector whose magnitude is equal to the acceleration due to gravity g and $\mathbf{e}_3$ is a unit vector pointing vertically upwards.

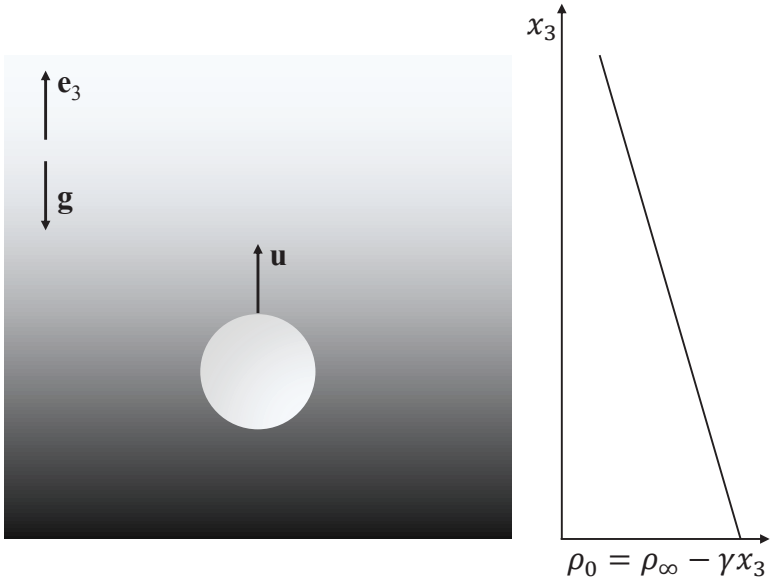

Figure 5.1. : A schematic showing a drop of constant density and uniform interfacial tension rising through a stratified fluid whose ambient density $\rho_0 = \rho_\infty - \gamma x_3$ decreases with the height. Also shown is a unit vector $\mathbf{e}_3$ pointing vertically upwards and a gravity vector $\mathbf{g} = -g\mathbf{e}_3$.

We define the disturbance velocity, pressure and density fields outside the drop as $\mathbf{w}' = \mathbf{w} + \mathbf{u}$, $p' = p - p_0$, $\rho' = \rho - \rho_0$. Here we use the Boussinesq approximation. The disturbance pressure, velocity and density outside the drop are governed by the continuity, Navier-Stokes and the advection-diffusion equations

$$\nabla \cdot \mathbf{w}' = 0, \tag{5.1}$$

$$\rho_\infty \left[\frac{\partial \mathbf{w}'}{\partial t} + (\mathbf{w}' \cdot \nabla)\, \mathbf{w}' - (\mathbf{u} \cdot \nabla)\, \mathbf{w}' \right] = -\nabla p' + \rho_\infty\, \nu\, \nabla^2 \mathbf{w}' + \rho' \mathbf{g}, \tag{5.2}$$

$$\frac{\partial \rho'}{\partial t} + \mathbf{w}' \cdot \nabla \rho' - \mathbf{u} \cdot \nabla \rho' - \gamma\, (\mathbf{w}' \cdot \mathbf{e}_3) = \kappa\, \nabla^2 \rho'. \tag{5.3}$$

Here ν is the kinematic viscosity of the fluid outside the drop and κ is the diffusivity. In general, the variations in density are caused by the variations in temperature or salt concentration. For small changes in temperature or salt concentrations, these changes are linearly proportional to the changes in density and in this case we can directly write an advection-diffusion equation for density with κ being the diffusion coefficient of the associated transport phenomenon (thermal or salt transport).

We assume the density of the fluid inside the drop ρ_d to be constant. Writing the pressure inside the drop p_d as $p_d = p_d' - \rho_d g x_3$, we find that the fluid flow $\mathbf{w}_d$ and the pressure field inside the drop are governed by

$$\nabla \cdot \mathbf{w}_d = 0, \tag{5.4}$$

$$\rho_d \left[\frac{\partial \mathbf{w}_d}{\partial t} + (\mathbf{w}_d \cdot \nabla)\, \mathbf{w}_d \right] = -\nabla p_d' + \rho_d \nu_d \nabla^2 \mathbf{w}_d - \rho_d \frac{d\mathbf{u}}{dt}, \tag{5.5}$$

where ν_d is the kinematic viscosity of the fluid inside the drop.

We use the undeformed drop radius a, time scale t_c and the drop speed in a homogeneous fluid of reference density u_c to non-dimensionalize the length, time and velocity. We non-dimensionalize the density by γa while the pressure or stress field outside (resp. inside) the drop is non-dimensionalized by $\rho_\infty \nu u_c/a$ (resp. $\rho_d \nu_d u_c/a$).

We find that the dimensionless governing equations and the boundary conditions are characterised by six dimensionless parameters - the Reynolds number Re which is the ratio of inertia forces to the viscous forces, the Péclet number Pe that is the ratio of the advective transport rate of density to its diffusive transport rate, the viscous Richardson number Ri which is the ratio of buoyancy forces to the viscous forces, the Strouhal number Sl that is the ratio of advective time scale to the characteristic time scale t_c, the dynamic viscosity ratio λ and the kinematic viscosity ratio χ. Their expressions are given as

$$\mathrm{Re} = \frac{au_c}{\nu}, \mathrm{Pe} = \frac{au_c}{\kappa}, \mathrm{Ri} = \frac{\gamma a^3 g}{\rho_\infty \nu u_c}, \mathrm{Sl} = \frac{a}{u_c t_c}, \lambda = \frac{\rho_d \nu_d}{\rho_\infty \nu}, \chi = \frac{\nu_d}{\nu}. \tag{5.6}$$

We carry out a quasi-steady analysis in which we neglect the unsteady terms proportional to ReSl or PeSl or ReSl/χ. This analysis is valid for $\mathrm{Re} \ll 1, \mathrm{Ri} \ll 1$ and $\chi \geq 1$ as in this case we can estimate the time scale of velocity variations t_c and show that $\mathrm{Sl} \sim \mathrm{Ri}$ [150] which makes the unsteady terms smaller than the rest of the terms in any governing equation. We rewrite Re, Pe, Ri in terms of $\epsilon = a/l_s$, l_s/l_o and Pr [149]. Here $l_s = (\nu\kappa/N^2)^{1/4}$ is the stratification length scale [166], the distance from the drop at which the buoyancy forces become as important as the viscous forces when $\mathrm{Pe} \ll 1$, where $N = \sqrt{g\gamma/\rho_\infty}$ is the Brunt-Väisälä frequency, the typical frequency at which a displaced fluid parcel in a stratified fluid oscillates. Also $l_o = a/\mathrm{Re}$ is the Oseen length scale, the distance from the drop at which the inertia forces balance the viscous forces and $\mathrm{Pr} = \nu/\kappa$ is the Prandtl number. Hence, the dimensionless governing equations for the disturbance flow and the disturbance density outside the drop after rescaling the density as $\tilde{\rho} = \frac{\rho'}{\mathrm{Pe}} = \frac{\rho'}{\epsilon \frac{l_s}{l_o} \mathrm{Pr}}$ are

$$\nabla \cdot \mathbf{w}' = 0, \tag{5.7}$$

$$\epsilon \frac{l_s}{l_o} \left[(\mathbf{w}' \cdot \nabla) \mathbf{w}' - (\mathbf{u} \cdot \nabla) \mathbf{w}' \right] = -\nabla p' + \nabla^2 \mathbf{w}' - \epsilon^4 \tilde{\rho}\, \mathbf{e}_3, \tag{5.8}$$

$$-\mathbf{w}' \cdot \mathbf{e}_3 + \epsilon \frac{l_s}{l_o} \mathrm{Pr} \left[\mathbf{w}' \cdot \nabla \tilde{\rho} - \mathbf{u} \cdot \nabla \tilde{\rho} \right] = \nabla^2 \tilde{\rho}. \tag{5.9}$$

Similarly, the flow field inside the drop is governed by

$$\nabla \cdot \mathbf{w}_d = 0, \tag{5.10}$$

$$\frac{\epsilon}{\chi}\frac{l_s}{l_o}\left(\mathbf{w}_d \cdot \nabla\right)\mathbf{w}_d = -\nabla p_d' + \nabla^2 \mathbf{w}_d. \tag{5.11}$$

Far away from the drop, the disturbance velocity and the disturbance density decay to zero

$$\mathbf{w}' = \mathbf{0} \text{ and } \tilde{\rho} = 0 \text{ as } r \to \infty. \tag{5.12}$$

At the drop surface, the flow field normal to the drop must be zero

$$\mathbf{n} \cdot \mathbf{w}_d = \mathbf{n} \cdot (\mathbf{w}' - \mathbf{u}) = 0 \text{ on the drop.} \tag{5.13}$$

The flow field tangential to the drop must be continuous across the drop surface

$$(\mathbf{I} - \mathbf{nn}) \cdot \mathbf{w}_d = (\mathbf{I} - \mathbf{nn}) \cdot (\mathbf{w}' - \mathbf{u}) \text{ on the drop.} \tag{5.14}$$

The shear stress must be continuous across the drop surface

$$\mathbf{n} \cdot (\mathbf{T}' - \lambda \mathbf{T}_d) \cdot (\mathbf{I} - \mathbf{nn}) = \mathbf{0} \text{ on the drop.} \tag{5.15}$$

Here $\mathbf{n}$ is the vector normal to the drop pointing into the suspending fluid, $\mathbf{I}$ is the identity tensor, $\mathbf{T}'$ (resp. $\mathbf{T}_d$) is the stress tensor associated with the disturbance flow outside the drop $\mathbf{w}'$ (resp. the flow inside the drop $\mathbf{w}_d$), which using the Newtonian constitutive relation can be written as $\mathbf{T}' = -p'\mathbf{I} + \left[\nabla \mathbf{w}' + (\nabla \mathbf{w}')^{\dagger}\right]$, $\dagger$ represents the transpose. We impose the no flux condition on the drop surface for the density field which is equivalent to ensuring that the drop surface is adiabatic (resp. impermeable) for the stratification caused by thermal transport (resp. salt transport)

$$\frac{\partial \tilde{\rho}}{\partial r} = \frac{\cos\theta}{\mathrm{Pe}} = \frac{\cos\theta}{\epsilon \frac{l_s}{l_o}\mathrm{Pr}} \text{ on the drop,} \tag{5.16}$$

where $\cos\theta = \frac{\mathbf{r}\cdot\mathbf{e}_3}{r} = \frac{r_3}{r}$.

We solve equations (5.7)-(5.16) to find the drag and deformation of a drop along with the flow field in the limit

$$\epsilon \ll 1, \ \frac{l_s}{l_o} \ll \epsilon^{-1}, \ \chi \geq 1, \ \mathrm{Pr}, \ \lambda \text{ arbitrary but fixed.} \tag{5.17}$$

5.3 Drag

We expand the field variables inside the drop and in the inner zone close to the drop as follows

$$\{\mathbf{w}', p', \tilde{\rho}, \mathbf{w}_d, {p'}_d\} = \left\{{\mathbf{w}'}_0, {p'}_0, \tilde{\rho}_0, \mathbf{w}_{0,d}, {p'}_{0,d}\right\} + \epsilon \left\{{\mathbf{w}'}_1, {p'}_1, \tilde{\rho}_1, \mathbf{w}_{1,d}, {p'}_{1,d}\right\} + o(\epsilon). \tag{5.18}$$

We find that the leading order flow variables $\left({\mathbf{w}'}_0, {p'}_0, \mathbf{w}_{0,d}, {p'}_{0,d}\right)$ satisfy the Stokes equations for a homogeneous fluid whose solution is well known [3]. The leading order drag experienced by the drop is $\mathbf{F}_0 = -2\pi\mathcal{R}\mathbf{u}$ where $\mathcal{R} = (2+3\lambda)/(1+\lambda)$ and it varies from 2 (for a bubble) to 3 (for a rigid sphere). It was already reported that the drop does not deform due to this leading order flow (see Sec. 5.5 for more details) [18, 167]. So we can consider a spherical drop for solving the first order problem.

We now use the leading order inner flow ${\mathbf{w}'}_0$ to estimate the order of magnitude of various terms in the Navier-Stokes and density transport equations in the matching zone that occurs at $r \gg 1$. As ${\mathbf{w}'}_0 \sim 1/r$ for $r \gg 1$, we see that $\mathbf{w}' \cdot \nabla \mathbf{w}' \sim 1/r^3$ while $\mathbf{u} \cdot \nabla \mathbf{w}' \sim 1/r^2$ for $r \gg 1$. Hence we neglect $\mathbf{w}' \cdot \nabla \mathbf{w}'$ as compared to $\mathbf{u} \cdot \nabla \mathbf{w}'$ for $r \gg 1$. Similarly we notice that $\mathbf{w}' \cdot \nabla \tilde{\rho} \sim \tilde{\rho}/r^2$ and $\mathbf{u} \cdot \nabla \tilde{\rho} \sim \tilde{\rho}/r$ for $r \gg 1$ due to which we neglect $\mathbf{w}' \cdot \nabla \tilde{\rho}$ in comparison to $\mathbf{u} \cdot \nabla \tilde{\rho}$ in the matching zone. So the equations governing the leading order flow disturbance and density disturbance in the matching or outer zone at $r \gg 1$ are

$$\nabla \cdot \mathbf{w}' = 0, \tag{5.19}$$

$$-\epsilon \frac{l_s}{l_o} (\mathbf{u} \cdot \nabla \mathbf{w}') = -\nabla p' + \nabla^2 \mathbf{w}' - \epsilon^4 \tilde{\rho}\, \mathbf{e}_3 + 2\pi\mathcal{R}\mathbf{u}\delta(\mathbf{r}), \tag{5.20}$$

$$-\mathbf{w}' \cdot \mathbf{e}_3 - \epsilon \frac{l_s}{l_o} \mathrm{Pr} (\mathbf{u} \cdot \nabla) \tilde{\rho} = \nabla^2 \tilde{\rho}. \tag{5.21}$$

In the far-field, we represent the drop by a point force equal to the negative of drag acting on the drop [168, 169] which justifies the source term $-\mathbf{F}_0 \delta(\mathbf{r}) = 2\pi\mathcal{R}\mathbf{u}\,\delta(\mathbf{r})$

appearing in equation (5.20). The no-flux boundary condition for density on the drop surface precludes such source terms in the density transport equation.

As equations (5.19)-(5.21) are linear, we solve them by taking the Fourier transform where the Fourier and inverse Fourier transforms are defined as

$$\hat{\mathbf{w}}'(\mathbf{k}) = \int d\mathbf{r}\, \mathbf{w}'(\mathbf{r})\, \mathrm{e}^{-i\mathbf{k}\cdot\mathbf{r}} \text{ and } \mathbf{w}'(\mathbf{r}) = \frac{1}{8\pi^3}\int d\mathbf{k}\, \hat{\mathbf{w}}'(\mathbf{k})\, \mathrm{e}^{i\mathbf{k}\cdot\mathbf{r}}, \tag{5.22}$$

where $i = \sqrt{-1}$. In the Fourier space, the disturbance flow in the outer zone is given by

$$\hat{\mathbf{w}}' = 2\pi\mathcal{R}\left[A - \epsilon^4 B + \epsilon^4 D\right]^{-1} E\mathbf{u}, \text{ where} \tag{5.23}$$

$$A = \left[k^2 - i\epsilon\frac{l_s}{l_o}(\mathbf{u}\cdot\mathbf{k})\right]\mathbf{I},\ B = \frac{k_3}{k^2\left[k^2 - i\epsilon\frac{l_s}{l_o}\Pr(\mathbf{u}\cdot\mathbf{k})\right]}\mathbf{k}\mathbf{e}_3,$$

$$D = \frac{\mathbf{e}_3\mathbf{e}_3}{\left[k^2 - i\epsilon\frac{l_s}{l_o}\Pr(\mathbf{u}\cdot\mathbf{k})\right]},\ \text{and } E = \left(\mathbf{I} - \frac{\mathbf{k}\mathbf{k}}{k^2}\right).$$

We represented the second order tensors as matrices while the vectors as column vectors in equation (5.23). We interpret $\hat{\mathbf{w}}'$ as a generalized function and for $\epsilon \ll 1$, we perform a Taylor series expansion of it about $\epsilon = 0$ to get

$$\hat{\mathbf{w}}' = \hat{T}'_0 + \epsilon\hat{T}'_1 + ... + \epsilon^n\hat{T}'_n, \text{ where } \hat{T}'_n = \lim_{\epsilon\to 0}\frac{1}{n!}\frac{d^n\hat{\mathbf{w}}'}{d\epsilon^n}. \tag{5.24}$$

We find that $\hat{T}'_0$ is the Fourier transform of the Stokeslet flow field $\mathbf{w}_S$ that is governed by

$$\nabla\cdot\mathbf{w}_S = 0,\ \ -\nabla p_S + \nabla^2\mathbf{w}_S + 2\pi\mathcal{R}\mathbf{u}\,\delta(\mathbf{r}) = \mathbf{0}. \tag{5.25}$$

It can be shown that in the matching zone, the inverse Fourier transform of $\hat{T}'_0$ matches with the Stokeslet part of the leading order inner flow $\mathbf{w'}_0$.

We write $\hat{T}'_1$ as

$$\begin{aligned}\hat{T}'_1 &= \lim_{\epsilon\to 0}\frac{1}{\epsilon}\left[\hat{\mathbf{w}}'(\mathbf{k}) - \hat{T}'_0(\mathbf{k})\right] = \lim_{\epsilon\to 0}\frac{1}{\epsilon}\left[\hat{\mathbf{w}}'(\mathbf{k}) - \hat{\mathbf{w}}_S(\mathbf{k})\right]\\ &= \lim_{\epsilon\to 0}\frac{1}{\epsilon^3}\left[\hat{\mathbf{w}}'\left(\frac{\mathbf{k}}{\epsilon}\right) - \hat{\mathbf{w}}_S\left(\frac{\mathbf{k}}{\epsilon}\right)\right] = \delta(\mathbf{k})\int d\mathbf{k}'\left[\hat{\mathbf{w}}'\left(\frac{\mathbf{k}'}{\epsilon}\right) - \hat{\mathbf{w}}_S\left(\frac{\mathbf{k}'}{\epsilon}\right)\right]_{\epsilon=1}\\ &= \delta(\mathbf{k})\int d\mathbf{k}'\left[\hat{\mathbf{w}}'|_{\epsilon=1}(\mathbf{k}') - \hat{\mathbf{w}}_S(\mathbf{k}')\right],\end{aligned} \tag{5.26}$$

where $\hat{\mathbf{w}}_S$ is the Fourier transform of $\mathbf{w}_S$, $\delta(\mathbf{k})$ is the delta function and we used the properties of generalized functions to evaluate the limit [170, 171]. We find that the inverse Fourier transform of $\hat{T}_1'$ is given by

$$T_1' = \frac{1}{8\pi^3}\int d\mathbf{k}' \left[\hat{\mathbf{w}}'|_{\epsilon=1}(\mathbf{k}') - \hat{\mathbf{w}}_S(\mathbf{k}')\right]. \tag{5.27}$$

This is a uniform flow and it should match with the uniform flow part of $\mathbf{w}'_1$ in the matching zone.

We only need the knowledge of the flow field in the outer zone to determine the first order force acting on the drop. This force is given by [172]

$$\mathbf{F}_1 = 2\pi\mathcal{R}T_1'. \tag{5.28}$$

Using $\mathbf{u} = u_3\mathbf{e}_3$ we find that $T_1' = -M_{33,drop}u_3\mathbf{e}_3$ and the drag acting on the drop is $\mathbf{F} = F_3\mathbf{e}_3$ where

$$F_3 = -2\pi\mathcal{R}u_3\left(1+\epsilon\, M_{33,drop}\right), \quad M_{33,drop} = \frac{\mathcal{R}}{3}M_{33,rgsp}, \text{ and} \tag{5.29}$$

$$M_{33,rgsp} = -\frac{3}{2\pi}\int_0^\infty dk \int_0^\pi d\theta \frac{\sin^3\theta\left\{1-\left[\mathrm{Pr}\left(\frac{l_s}{l_o}\right)^2 u_3^2k^2+1\right]\cos^2\theta - i\cos\theta\frac{l_s}{l_o}u_3k^3\right\}}{\left[\mathrm{Pr}\left(\frac{l_s}{l_o}\right)^2 u_3^2k^2+1\right]\cos^2\theta + i\frac{l_s}{l_o}u_3k^3\left(\mathrm{Pr}+1\right)\cos\theta - k^4 - 1}. \tag{5.30}$$

The expression for $M_{33,rgsp}|_{u_3=1}$ is the same as that reported by Mehaddi et al. (see equation 5.3b in Ref. [150]) for falling rigid sphere in a stratified fluid except there is a missing negative sign in their expression which might be a typo. From equation (5.29), we see that the stratification enhanced drag acting on a drop is equal to $(\mathcal{R}/3)^2$ times the enhanced drag on a rigid sphere. As the governing equations and the boundary conditions associated with the leading order and the first order flows in the inner zone and inside the drop derived in our work are the same as those reported for a drop moving in a shear flow of a homogeneous fluid (in the limit of zero shear rate), we can use the physical arguments reported in the latter case [167] to find the scaling of stratification enhanced drag with $\mathcal{R}$. This way, we can deduce the form

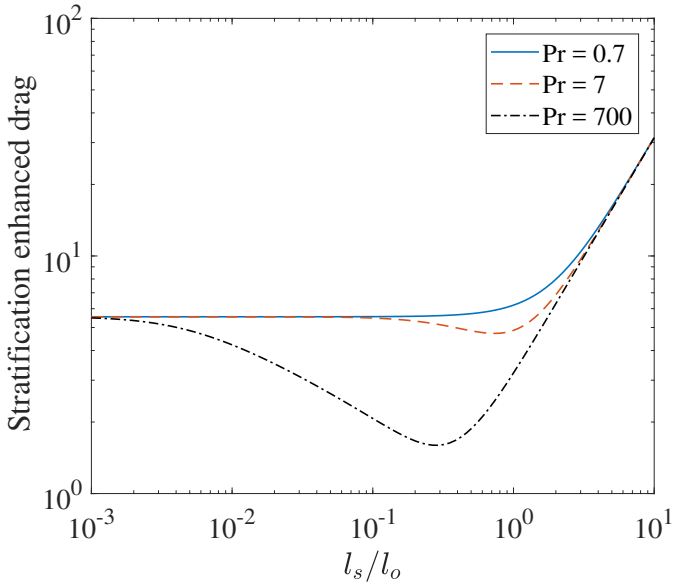

Figure 5.2. : The variation of the stratification enhanced drag acting on a bubble, $8\pi M_{33,rgsp}/3$, with l_s/l_o and Pr. The blue solid, red dashed and black dash-dotted lines denote the data for Pr = 0.7, 7 (temperature stratified water) and 700 (salt stratified water), respectively. This variation of drag acting on a bubble with l_s/l_o and Pr is similar to that reported for a rigid sphere [150].

of drag force, equation (5.29) without finding any of the flow fields. According to these arguments, one relates the drag force with the strength of vorticity on the drop surface. It is evident from equation (5.20) that the disturbance flow in the outer zone is proportional to $\mathcal{R}$ and hence the uniform flow $T_1' \propto \mathcal{R}$. To satisfy this uniform flow boundary condition at infinity, a vorticity of strength proportional to $\mathcal{R}T_1'$ is induced on the drop surface which justifies why $\mathbf{F}_1 \propto \mathcal{R}^2$. We plot the stratification enhanced drag acting on a bubble for various l_s/l_o and Pr in figure 5.2.

We can simplify the expression for drag in some limiting cases. For $l_s/l_o \ll \mathrm{Pr}^{-1}$, the buoyancy forces balance the viscous forces in the matching zone and the density transport is governed by diffusion. When $\mathrm{Pr}^{-1} \ll l_s/l_o \ll \mathrm{Pr}^{-1/4}$, again the buoyancy forces balance the viscous forces in the matching zone but the density transport is governed by advection. And for $l_s/l_o \gg \mathrm{Pr}^{-1/4}$, the inertia forces balance the viscous

forces in the matching zone. In these three regimes, for $u_3 = 1$, the drag simplifies to

$$F_3 = -2\pi\mathcal{R}\begin{cases} 1 + 0.2207\mathcal{R}\,\epsilon & \text{for } l_s/l_o \ll \mathrm{Pr}^{-1} \\ 1 + 0.3533\mathcal{R}\,\mathrm{Ri}^{1/3} & \text{for } \mathrm{Pr}^{-1} \ll l_s/l_o \ll \mathrm{Pr}^{-1/4} \\ 1 + (\mathcal{R}/8)\,\mathrm{Re} & \text{for } l_s/l_o \gg \mathrm{Pr}^{-1/4} \end{cases} \tag{5.31}$$

This relationship recovers the result reported for a rigid sphere [150] when $\lambda \to \infty$ (equivalently $\mathcal{R} = 3$). We can rewrite the correction to drag in terms of Re, Fr, Pr using $\mathrm{Ri} = \frac{\mathrm{Re}}{\mathrm{Fr}^2}$. We multiply the resulting expression with Re^{-1} to find the drag correction non-dimensionalized by $\rho_\infty u_c^2 a^2$. We find that drag correction scales as $(\mathrm{ReFr})^{-1/2}\mathrm{Pr}^{1/4}$ in the diffusive regime and as $(\mathrm{ReFr})^{-2/3}$ in the advective regime. Numerical results of Ref. [147] have also captured these force scales. For $\mathrm{Fr} > \mathrm{Re}^{-1}$, it was noted in Ref. [147] the existence of another scaling regime in which the drag correction scales as $(\mathrm{ReFr})^{-1}$. For these Fr and for any Pr of interest (i.e., $\mathrm{Pr} \leq 700$), our calculation holds but we do not see such a scaling regime perhaps due to some inaccuracy in their numerical results. Our results also provide the flow field around a settling rigid sphere in a stratified fluid when $\lambda \to \infty$. This solution was not provided in Refs. [149, 150].

5.4 Flow field

In this section, we derive the first order flow fields inside the drop and in the inner zone outside the drop which will be used in the next section to determine the drop deformation. These flows can be combined with the leading order flows in both zones to determine a uniform approximation to the flow field. Generally, we need the entire leading order flow in the outer zone to determine the required first order flows. But in this problem, we see that only the uniform part of the leading order flow in the outer zone T_1' is sufficient to determine the required flows.

After substituting the expansion (5.18) in equations (5.7),(5.8),(5.10),(5.11), collecting the terms of order ϵ and expressing the velocity fields in terms of stream functions (equation (5.32)), we find that at first order, the stream function inside the

drop $\psi_{1,d}$ and that in the inner zone outside the drop ψ_1' are governed by equations (5.33)-(5.34).

$$w_{1,r}' = -\frac{1}{r^2}\frac{\partial \psi_1'}{\partial \eta},\ w_{1,\theta}'\sqrt{1-\eta^2} = -\frac{1}{r}\frac{\partial \psi_1'}{\partial r},\ \text{where } \eta = \cos\theta, \tag{5.32}$$

$$E^4 \psi_{1,d} = 0, \tag{5.33}$$

$$E^4 \psi_1' = 3\mathcal{R}u_3^2 \frac{l_s}{l_o}\left\{\frac{1}{r^2} - \frac{1}{2r^3}\left(\frac{3\lambda+2}{\lambda+1}\right) + \frac{1}{2r^5}\frac{\lambda}{\lambda+1}\right\} Q_2(\eta). \tag{5.34}$$

Here $E^2 = \frac{\partial^2}{\partial r^2} + \frac{\left(1-\eta^2\right)}{r^2}\frac{\partial^2}{\partial \eta^2}$, $Q_n(\eta) = \int_{-1}^{\eta} P_n(\xi)\, d\xi$ and P_n is the Legendre polynomial of degree n. The conditions of zero normal velocity on the drop surface, continuity of tangential velocity and shear stress across the drop surface and the axisymmetricity of velocity fields can be expressed in terms of stream functions as follows

$$\psi_1'|_{r=1} = \psi_{1,d}|_{r=1} = 0, \tag{5.35}$$

$$\left.\frac{\partial \psi_1'}{\partial r}\right|_{r=1} = \left.\frac{\partial \psi_{1,d}}{\partial r}\right|_{r=1}, \tag{5.36}$$

$$\left.\frac{\partial}{\partial r}\left(\frac{1}{r^2}\frac{\partial \psi_1'}{\partial r}\right)\right|_{r=1} = \lambda \left.\frac{\partial}{\partial r}\left(\frac{1}{r^2}\frac{\partial \psi_{1,d}}{\partial r}\right)\right|_{r=1}, \tag{5.37}$$

$$\begin{aligned} \psi_1' &= 0 \text{ along } \eta = \pm 1 \text{ and } r \geq 1, \\ \psi_{1,d} &= 0 \text{ along } \eta = \pm 1 \text{ and } r \leq 1. \end{aligned} \tag{5.38}$$

The general solution of equation (5.34) that satisfies the zero stream function on the drop surface and along the axis of symmetry is

$$\begin{aligned} \psi_1' =& u_3^2 \frac{l_s}{l_o}\frac{\mathcal{R}}{8}\left\{r^2 - \frac{r}{2}\left(\frac{3\lambda+2}{\lambda+1}\right) + \frac{\lambda}{\lambda+1} - \frac{1}{2r}\left(\frac{\lambda}{\lambda+1}\right)\right\} Q_2(\eta) \\ &+ \sum_{n=1}^{\infty}\left\{A_n\left(r^{n+3} - r^{-n}\right) + B_n\left(r^{n+1} - r^{-n}\right) + C_n\left(r^{2-n} - r^{-n}\right)\right\} Q_n(\eta). \end{aligned} \tag{5.39}$$

Using a relation similar to equation (5.32) between the leading order stream function in the inner zone ψ_0' and the flow field $\mathbf{w'}_0$, we find that ψ_0' is given by

$$\psi_0' = -\frac{u_3}{2}\left[\mathcal{R}r - \left(\frac{\lambda}{\lambda+1}\right)\frac{1}{r}\right] Q_1(\eta). \tag{5.40}$$

In the matching zone $r \gg 1$, we have

$$\begin{aligned}\psi_0' + \epsilon\psi_1' = &-\frac{\mathcal{R}}{2}u_3 r Q_1(\eta) + \epsilon\frac{l_s}{l_o}u_3^2\frac{\mathcal{R}}{8}r^2 Q_2(\eta) \\ &+\epsilon\sum_{n=1}^{\infty}\left\{A_n r^{n+3} + B_n r^{n+1}\right\} Q_n(\eta) + O(\epsilon r)\end{aligned} \tag{5.41}$$

Again using a relation similar to equation (5.32), we connect the flow fields in the outer zone T_0', T_1' to the stream functions Ψ_0', Ψ_1', in turn deriving the following expressions for the stream functions

$$\Psi_0' = -\frac{\mathcal{R}}{2}u_3 r Q_1(\eta), \Psi_1' = \frac{\mathcal{R}}{3}M_{33,rgsp}u_3 r^2 Q_1(\eta), \tag{5.42}$$

$$\Rightarrow \Psi_0' + \epsilon\,\Psi_1' = \left(-\frac{\mathcal{R}}{2}u_3 r + \epsilon\frac{\mathcal{R}}{3}M_{33,rgsp}u_3 r^2\right) Q_1(\eta). \tag{5.43}$$

We now match equation (5.41) with equation (5.43) in the matching zone $r \gg 1$. For this purpose, we require that ψ_1' does not grow faster than r^2 and that the coefficient of $r^2 Q_1(\eta)$ is the same in these two equations. These conditions are satisfied provided

$$A_n = 0 \text{ for } n \geq 1,\ B_n = 0 \text{ for } n \geq 2, \text{ and } B_1 = \frac{\mathcal{R}}{3}M_{33,rgsp}u_3. \tag{5.44}$$

We cannot match the term $\epsilon\frac{l_s}{l_o}u_3^2\frac{\mathcal{R}}{8}r^2 Q_2(\eta)$ in $\psi_0' + \epsilon\psi_1'$ with any of the terms in $\Psi_0' + \epsilon\,\Psi_1'$. This is expected as the term $\frac{l_s}{l_o}u_3^2\frac{\mathcal{R}}{8}r^2 Q_2(\eta)$ in ψ_1' represents a non-uniform flow which cannot be matched with the (only found) uniform flow part of the leading order flow (minus the Stokeslet) in the outer zone.

The solution of equation (5.33) that ensures the stream function to be zero on the drop surface and along the axis of symmetry and which gives finite velocities at the drop center is

$$\psi_{1,d} = \sum_{n=1}^{\infty} A_{n,d}\left(r^{n+3} - r^{n+1}\right) Q_n(\eta). \tag{5.45}$$

We now enforce the conditions (5.36), (5.37) on ψ_1', $\psi_{1,d}$ to determine the remaining unknown constants C_n, $A_{n,d}$ whose expressions are given as

$$\begin{gathered} C_1 = -\frac{\mathcal{R}^2 u_3}{6} M_{33,rgsp},\ C_2 = -\frac{l_s}{l_o}\frac{u_3^2}{80}\frac{\mathcal{R}\lambda\left(5\lambda+6\right)}{\left(\lambda+1\right)^2}, \\ A_{1,d} = \frac{\mathcal{R}u_3}{6}\frac{M_{33,rgsp}}{\left(\lambda+1\right)},\ A_{2,d} = \frac{l_s}{l_o}\frac{u_3^2}{80}\frac{\mathcal{R}\left(4\lambda+5\right)}{\left(\lambda+1\right)^2}, \\ C_n = A_{n,d} = 0 \ \text{ for } \ n \geq 3. \end{gathered} \tag{5.46}$$

As the first order drag acting on the drop is given by [18] $4\pi C_1\,\mathbf{e}_3 = -\frac{2\pi}{3}\mathcal{R}^2 u_3 M_{33,rgsp}\,\mathbf{e}_3$, this validates the drag determined in the previous section without calculating the flow field. Using equations (5.44), (5.46), the expressions for the first order stream functions inside the drop and in the inner zone outside the drop are given as

$$\psi_{1,d} = -\frac{\mathcal{R}}{2\left(\lambda+1\right)}\left\{\frac{M_{33,rgsp}u_3}{3}\left(r^2-r^4\right)Q_1\left(\eta\right) + \frac{l_s}{l_o}\frac{\left(4\lambda+5\right)}{40\left(\lambda+1\right)}u_3^2\left(r^3-r^5\right)Q_2\left(\eta\right)\right\}, \tag{5.47}$$

$$\begin{aligned} \psi_1' = {} & \frac{\mathcal{R}}{3}M_{33,rgsp}u_3\left\{r^2 - \frac{\mathcal{R}}{2}r + \frac{1}{2r}\left(\frac{\lambda}{\lambda+1}\right)\right\}Q_1\left(\eta\right) \\ & + \frac{\mathcal{R}}{8}\frac{l_s}{l_o}u_3^2\left\{r^2 - \frac{\mathcal{R}}{2}r + \frac{1}{10}\frac{\lambda\left(5\lambda+4\right)}{\left(\lambda+1\right)^2} - \frac{1}{2r}\left(\frac{\lambda}{\lambda+1}\right) + \frac{1}{10}\frac{\lambda\left(5\lambda+6\right)}{\left(\lambda+1\right)^2}\frac{1}{r^2}\right\}Q_2\left(\eta\right). \end{aligned} \tag{5.48}$$

From these calculations, we notice that the stratification modifies the flow field close to the drop at $O\left(\epsilon\right)$, so the flow field close to the drop in a stratified fluid should be approximately same as that in a homogeneous fluid. We also infer that the stratification should alter the flow field far away from the drop in a significant manner because unlike the inner zone the influence of stratification is felt at leading order in the outer zone. By looking at the equations governing flow field in the outer zone equations (5.19)-(5.21), we see that this flow is essentially the flow due to a point force singularity placed in a stratified fluid which was already analyzed by Ardekani & Stocker [166] in the limit $\mathrm{Pe} \ll \epsilon$ or $l_s/l_o \ll \mathrm{Pr}^{-1}$. Hence, the flow field far away from the drop in a stratified fluid should be a Stratlet. Most of these deductions are consistent with figure 5.3 where we plotted the streamlines associated

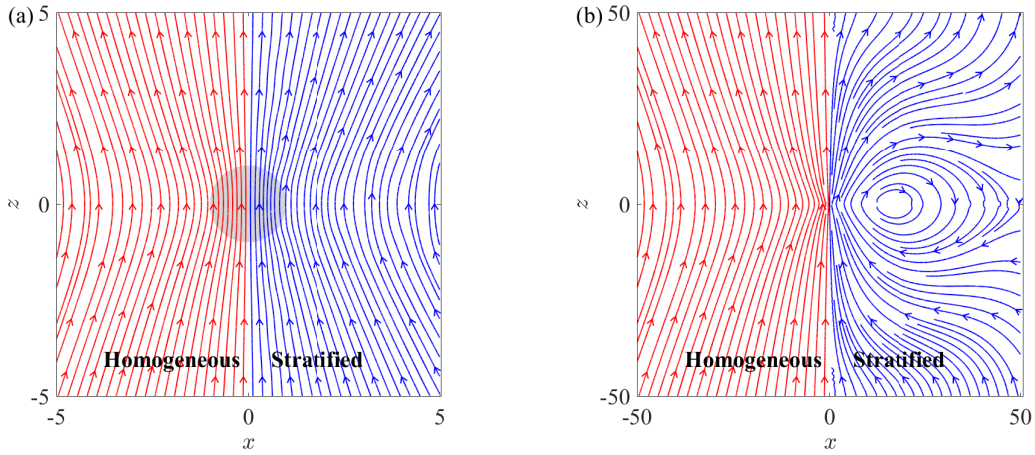

Figure 5.3. : In the lab frame of reference, we compare the streamlines in a homogeneous fluid (red lines) with those in a stratified fluid (blue lines) both near the drop (a) and far away from it (b). The streamlines in a stratified fluid are determined from the composite expansion of flow field accurate to $O(\epsilon)$ at $\mathrm{Pe} \ll \epsilon$, $\lambda = 1$ and $\epsilon = 0.1$. For finding this composite expansion, we combined the flow fields in the inner zone and the outer zone in the usual manner [173] where the flow in the outer zone is determined by doing an inverse Fourier transform of equation (5.23) using the FFT package of MATLAB [174].

with the composite expansion of flow field accurate to $O(\epsilon)$ for $\mathrm{Pe} \ll \epsilon$, $\lambda = 1$ and $\epsilon = 0.1$. From figure 5.3b, we see that the flow field far away from the drop in a stratified fluid is not Stratlet. This is because, at these distances from the drop, the Stokeslet contribution of the first order inner flow field is significant enough to alter the expected Stratlet flow field. We expect to recover the Stratlet flow at even farther distances from the drop.

5.5 Drop Deformation

In this section, we determine the leading order deformation of a drop rising in a stratified fluid. For this purpose, we consider the normal stress balance condition

on the drop surface and solve for the deformation knowing the flow field inside and outside but close to the drop. The dimensionless normal stress boundary condition is given by

$$\left\{\begin{array}{c}\left[\lambda {p'}_d - p' + 2\dfrac{\partial {w'}_r}{\partial r} - 2\lambda\dfrac{\partial w_{d,r}}{\partial r}\right]_{r=1} \\ +\dfrac{ga^2\eta}{\nu u_c}\left(1 - \dfrac{\gamma a}{\rho_\infty}x_{d,3} - \alpha\right) - \dfrac{\epsilon^3}{2\frac{l_s}{l_o}\,\mathrm{Pr}}\eta^2\end{array}\right\} = \frac{1}{\mathrm{Ca}}\left(\nabla\cdot\mathbf{n}\right) = \frac{1}{\mathrm{Ca}}\left\{2 - 2\zeta - \frac{d}{d\eta}\left[\left(1-\eta^2\right)\frac{d\zeta}{d\eta}\right]\right\}. \tag{5.49}$$

As the term $\frac{\epsilon^3}{2\frac{l_s}{l_o}\,\mathrm{Pr}}\eta^2$ is much smaller than the remaining terms on the left-hand side of equation (5.49) and also since we are only interested in finding the leading order drop deformation, we neglect this term. Here $x_{d,3} = \mathbf{x}_d\cdot\mathbf{e}_3$, $\mathrm{Ca} = \rho_\infty\nu u_c/\sigma$ is the Capillary number which is the ratio of bulk viscous forces to the capillary forces, $\alpha = \frac{\rho_d}{\rho_\infty} = \frac{\lambda}{\chi}$ is the density ratio and we assumed the drop's shape to be $r = 1+\zeta\left(\eta\right)$, $\max|\zeta| \ll 1$ in evaluating the curvature term.

We first evaluate the normal stress boundary condition accurate to $O\left(1\right)$ to find the drop deformation accurate to $O\left(\mathrm{Ca}\right)$. For this purpose, we simply substitute the leading order pressure fields inside the drop and in the inner zone outside the drop (see equation (5.50)), the corresponding radial derivative of flow fields (see equation (5.51)) into equation (5.49) and simplify it to obtain equation (5.52)

$${p'}_{0,d}\big|_{r=1} = -\frac{5}{(\lambda+1)}u_3\eta + c_{0,d},\;\; {p'}_0|_{r=1} = \frac{1}{2}\left(\frac{3\lambda+2}{\lambda+1}\right)u_3\eta + c_0, \tag{5.50}$$

$$\left.\frac{\partial w_{0,d,r}}{\partial r}\right|_{r=1} = \left.\frac{\partial {w'}_{0,r}}{\partial r}\right|_{r=1} = -\frac{u_3\eta}{(\lambda+1)}, \tag{5.51}$$

$$\eta\left[\frac{ga^2}{\nu u_c}\left(1 - \frac{\gamma a}{\rho_\infty}x_{d,3} - \alpha\right) - \frac{3\mathcal{R}u_3}{2}\right] + \Pi_0 = \frac{1}{\mathrm{Ca}}\left\{2 - 2\zeta - \frac{d}{d\eta}\left[\left(1-\eta^2\right)\frac{d\zeta}{d\eta}\right]\right\}. \tag{5.52}$$

Here c_0, $c_{0,d}$, and $\Pi_0 = \lambda c_{0,d} - c_0$ are constants.

As the drop is undergoing quasi-steady motion, the net force acting on it should be zero. The drop experiences three kinds of forces – buoyancy, drag and its own

weight. The buoyancy can be found by integrating the hydrostatic pressure acting on the drop i.e., $-\int_{r=1} p_0 \mathbf{n} dS = \left(1 - \frac{\gamma a}{\rho_\infty} x_{d,3}\right) \frac{ga^2}{\nu u_c} \int_{r=1} r_3 \mathbf{n} dS - \frac{\epsilon^3}{2\frac{l_s}{l_o}\,\mathrm{Pr}} \int_{r=1} r_3^2 \mathbf{n} dS = \frac{4\pi}{3}\left(1 - \frac{\gamma a}{\rho_\infty} x_{d,3}\right) \frac{ga^2}{\nu u_c} \mathbf{e}_3$, where the last simplification is done using $\int_{r=1} r_3 \mathbf{n} dS = \frac{4\pi}{3}\mathbf{e}_3$ and $\int_{r=1} r_3^2 \mathbf{n} dS = \mathbf{0}$. Using this expression for buoyancy, equation (5.29) for drag and usual expression for drop's weight, the force balance condition simplifies to

$$\frac{ga^2}{\nu u_c}\left(1 - \frac{\gamma a}{\rho_\infty} x_{d,3} - \alpha\right) - \frac{3\mathcal{R} u_3}{2} = \frac{\epsilon \mathcal{R}^2}{2} M_{33,rgsp} u_3. \tag{5.53}$$

This condition is accurate to $O(\epsilon)$ and we can simply set the right-hand side to zero to find the force balance condition at $O(1)$.

We now simplify the leading order normal stress boundary condition, equation (5.52) using the force balance condition at $O(1)$ to obtain

$$\Pi_0 = \frac{1}{\mathrm{Ca}} \left\{ 2 - 2\zeta - \frac{d}{d\eta}\left[\left(1 - \eta^2\right) \frac{d\zeta}{d\eta}\right] \right\}. \tag{5.54}$$

Enforcing the constraints that the drop's volume does not change $\int_{-1}^{1} \zeta(\eta)\, d\eta = 0$ and its center of mass remains fixed $\int_{-1}^{1} \eta\zeta(\eta)\, d\eta = 0$ during the process of deformation, we find that the deformation is zero i.e., $\zeta = 0$ while $\Pi_0 = 2/\mathrm{Ca}$. This is not surprising because at $O(1)$, the stratification and inertia do not affect the flow and we have a drop rising in a homogeneous fluid at zero Re which was shown to not deform [18,167].

To determine the effect of inertia and stratification on drop deformation, we evaluate the normal stress boundary condition accurate to $O(\epsilon)$. To do so, we substitute equations (5.50), (5.51), (5.55)-(5.57) in equation (5.49) and simplify it to obtain equation (5.58)

$$\begin{aligned} {p'}_{1,d}\big|_{r=1} = {} & \frac{l_s}{l_o} \frac{\alpha {u_3}^2}{24(\lambda+1)^2\lambda} + c_{1,d} - \frac{5(3\lambda+2)\, M_{33,rgsp}\, u_3}{3(\lambda+1)^2} P_1(\eta) \\ & + \frac{l_s}{l_o} \frac{{u_3}^2 \left(-252\lambda^3 + 20\lambda\alpha - 483\lambda^2 + 20\alpha - 210\lambda\right)}{240\,\lambda(\lambda+1)^3} P_2(\eta), \end{aligned} \tag{5.55}$$

$$\begin{aligned} {p'}_1\big|_{r=1} = {} & -\frac{l_s}{l_o} \frac{\left(\lambda^2 + 2\lambda + \frac{4}{3}\right) {u_3}^2}{16(\lambda+1)^2} + c_1 + \frac{(3\lambda+2)^2 M_{33,rgsp} u_3}{6(\lambda+1)^2} P_1(\eta) \\ & + \frac{l_s}{l_o} \frac{{u_3}^2 \left(135\lambda^3 + 333\lambda^2 + 272\lambda + 80\right)}{240(\lambda+1)^3} P_2(\eta), \end{aligned} \tag{5.56}$$

$$\left.\frac{\partial w_{1,d,r}}{\partial r}\right|_{r=1} = \left.\frac{\partial w'_{1,r}}{\partial r}\right|_{r=1} = -\frac{(3\lambda+2)\,M_{33,rgsp}\,u_3}{3(\lambda+1)^2}P_1(\eta) - \frac{l_s}{l_o}\frac{(3\lambda+2)\,(4\lambda+5)\,{u_3}^2}{40(\lambda+1)^3}P_2(\eta)\,, \tag{5.57}$$

$$\left\{\begin{array}{l} \eta\left[\dfrac{ga^2}{\nu u_c}\left(1-\dfrac{\gamma a}{\rho_\infty}x_{d,3}-\alpha\right)-\dfrac{3\mathcal{R}u_3}{2}-\dfrac{\epsilon\mathcal{R}^2}{2}M_{33,rgsp}u_3\right] \\ +\Pi_0+\epsilon\left[\Pi_1+\dfrac{l_s}{l_o}\dfrac{u_3^2}{48}\dfrac{(3\lambda^2+2\alpha+6\lambda+4)}{(\lambda+1)^2}\right] \\ +\epsilon\dfrac{l_s}{l_o}\dfrac{u_3^2}{240}\dfrac{\left(\begin{array}{l}-243\lambda^3+20\alpha\lambda-684\lambda^2\\ +20\alpha-638\lambda-200\end{array}\right)}{(\lambda+1)^3}P_2(\eta) \end{array}\right\} = \frac{1}{\mathrm{Ca}}\left\{2-2\zeta-\frac{d}{d\eta}\left[\left(1-\eta^2\right)\frac{d\zeta}{d\eta}\right]\right\}. \tag{5.58}$$

Here c_1, $c_{1,d}$, and $\Pi_1 = \lambda c_{1,d} - c_1$ are constants. We note that only the first term on the left-hand side of equation (5.58) that is proportional to η contains the information of stratification through this term's dependence on $M_{33,rgsp}$. But this term is identically zero due to the force balance condition accurate to $O(\epsilon)$, equation (5.53), making the drop deformation independent of stratification. Using $\Pi_0 = 2/\mathrm{Ca}$ and the force balance condition accurate to $O(\epsilon)$, equation (5.58) simplifies to

$$\left\{\begin{array}{l} \epsilon\left[\Pi_1+\dfrac{l_s}{l_o}\dfrac{u_3^2}{48}\dfrac{(3\lambda^2+2\alpha+6\lambda+4)}{(\lambda+1)^2}\right] \\ +\epsilon\dfrac{l_s}{l_o}\dfrac{u_3^2}{240}\dfrac{\left(\begin{array}{l}-243\lambda^3+20\alpha\lambda-684\lambda^2\\ +20\alpha-638\lambda-200\end{array}\right)}{(\lambda+1)^3}P_2(\eta) \end{array}\right\} = -\frac{1}{\mathrm{Ca}}\left\{2\zeta+\frac{d}{d\eta}\left[\left(1-\eta^2\right)\frac{d\zeta}{d\eta}\right]\right\}. \tag{5.59}$$

We solve this equation for the drop deformation by making sure the drop's volume and its center of mass remain fixed during the process of deformation to obtain

$$\zeta(\eta) = \frac{\mathrm{We}\,u_3^2}{960}\frac{(-243\lambda^3+20\alpha\lambda-684\lambda^2+20\alpha-638\lambda-200)}{(\lambda+1)^3}P_2(\eta)\,, \tag{5.60}$$

where the Weber number $\mathrm{We} = \mathrm{Re}\,\mathrm{Ca}$. We note that this is exactly the deformation of a drop rising in a homogeneous fluid at small Re [18, 167], in which case, the drop

deforms into an oblate spheroid. Hence, the stratification does not affect the drop's deformation to this order of approximation. To understand this observation, let us see how inertia or stratification modifies the flow field in the inner zone. Let us first consider the case of zero inertia. The effect of stratification is to induce a uniform flow far away from drop, due to which at $O(\epsilon)$, we have a stationary drop placed in a homogeneous fluid that is undergoing uniform streaming flow far away from the drop. As this problem is same as the drop moving in a homogeneous quiescent fluid at zero Re, with change of reference frames, we expect the drop to not deform. Now, if we include inertia, it has two effects. It modifies the strength of uniform flow far away from the drop which again does not cause any drop deformation. It also induces a non-uniform flow everywhere in the domain due to the particular integral of equation (5.34) and this is the sole cause of drop deformation.

The leading order effect of deformation on the drag can be found by simply considering the deformed drop in a creeping flow of a homogeneous fluid [167]. As the stratification does not cause any deformation of the drop, this deformation induced change in the drag is same as that found for a drop motion in a homogeneous fluid at small Re [167]. Briefly, this modification in the drag is $O(\mathrm{We})$ and since $\mathrm{We} = \left(\frac{\rho_\infty \nu^2}{a\sigma}\right) \mathrm{Re}^2 \sim O(\epsilon^2)$, we conclude that the deformation affects the drag at $O(\epsilon^2)$. But we do not include this deformation induced drag in equation (5.29) because for consistent asymptotic expansion of drag accurate to $O(\epsilon^2)$, we also need to find $O(\epsilon^2 \ln \epsilon)$ drag whose calculation is beyond the scope of this work. We expect a non-zero drag at $O(\epsilon^2 \ln \epsilon)$ based on the calculations for the motion of a drop in a homogeneous fluid at small Re [167, 175]

5.6 Drift Volume

In this section, we calculate the partial drift volume induced by a drop rising in a stratified fluid. Drift volume is the volume enclosed between an initially marked plane of fluid of infinite extent and the deformed plane as the drop travels normal to the

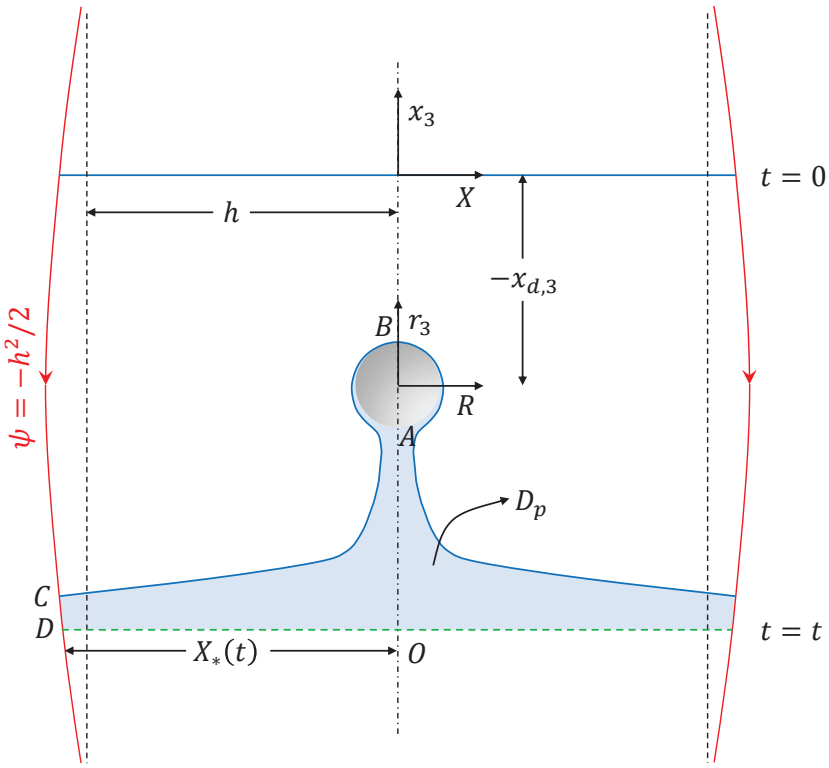

Figure 5.4. : Schematic showing the definition of the partial drift volume D_p and the coordinate systems involved. In the drop frame, at time $t = 0$, the marked fluid disk (shown by blue straight line) is located at a distance $-x_{d,3}$ from the drop. At time t, the marked fluid plane deforms (shown by blue curved line) as it crosses the drop. The area enclosed between the deformed and undeformed marked fluid planes (multiplied by π) gives the partial drift volume D_p at time t (shown by light blue region).

initial plane of fluid starting far ahead to far beyond the plane of fluid. When both the extent of marked plane of fluid and the distance travelled by the drop relative to the plane of fluid are finite, the volume encapsulated between the initial and the deformed planes of fluid is referred to as the partial drift volume D_p [159] (see figure 5.4 for a schematic).

To make our notation consistent with earlier works on drift volume, we non-dimensionalize velocity using $|u_3|$, time using $a/|u_3|$ and assume $u_3 > 0$. All the

variables that appear in this section are non-dimensionalized in this manner. In the present notation, any field variable can be found by simply setting $u_3 = 1$ in the expression of that field variable derived in the previous sections. The marked plane of fluid is a disk of finite radius and zero thickness. In the lab frame, we choose the center of disk as the origin and denote the cylindrical coordinate variables about this origin by X, x_3. In the frame moving with the drop, we choose the center of drop as the origin and denote the cylindrical coordinate variables about this origin by R, r_3. At time $t = 0$, the marked disk of fluid is located at a distance $-x_{d,3}$ upstream of the drop. Hence, $r_3 = x_3 - (x_{d,3} + t)$ and $R = X$. As far as the flow field outside the drop is concerned, the disturbance flow in the drop frame and the flow field in the lab frame are the same. We used ψ' to denote the stream function associated with this flow. We denote the stream function associated with the flow field in the drop frame by ψ. Note that ψ approaches $-R^2/2$ far from the drop and $\psi' = \psi + \frac{X^2}{2}$. The intersection of the streamline $\psi = -h^2/2$ with the plane $x_3 = 0$ gives the extent of marked fluid disk. We denote the point of intersection by $(x_3, X) = (0, X_*(t))$ and the stream function at this point by $\psi'_*(t)$.

In the lab frame, we apply the conservation of mass to the control volume (CV) $OABCD$

$$\frac{\partial}{\partial t}\int_{CV} \rho \, dV + \int_{CS} \rho \, \mathbf{w}' \cdot \mathbf{n} \, dS = 0, \tag{5.61}$$

where CS denotes the control surface bounding the CV. We choose the surfaces AB, BC, and CD as the material surfaces and since OA is a streamsurface, $\mathbf{w}' \cdot \mathbf{n}$ is non-zero only along the surface OD. Hence, the conservation of mass simplifies to

$$\frac{\partial}{\partial t}\int_{CV} \rho \, dV + \int_{OD} \rho \, \mathbf{w}' \cdot \mathbf{n} \, dS = 0. \tag{5.62}$$

In the context of Boussinesq approximation, ρ can be treated as constant in the conservation of mass. So, after integration with respect to time and expressing velocity in terms of stream function, we have

$$D_p = 2\pi \int_0^t \psi'_*(t') \, dt' - \left[V_b(t) - V_b(0)\right]. \tag{5.63}$$

This expression for D_p is the same as that found in a homogeneous fluid [159] and it says that the partial drift volume at time t is equal to the volume of fluid that has passed through the plane $x_3 = 0$ bounded by the streamline $\psi = -h^2/2$ by time t. Here $V_b(t)$ denotes the volume of drop that has crossed the plane $x_3 = 0$ by time t. Assuming the extent of marked fluid disk is large compared to the drop, we neglect the deflection of streamlines and set $X_* = h$, hence $\psi'_*(t) = \psi'(x_3 = 0, X = h, t) = \psi'(r_3 = -(x_{d,3} + t), R = h, t)$. Defining $\tau = (x_{d,3} + t)/h$ and $\tau_0 = x_{d,3}/h$, we obtain

$$D_p = 2\pi h \int_{\tau_0}^{\tau} \psi'_*(\tau')\, d\tau' - [V_b(\tau) - V_b(\tau_0)]. \tag{5.64}$$

As D_p is at least $O(h)$, we neglect the $O(1)$ terms in the brackets. Also, as the partial drift volume depends on the stream function far from the drop $\psi'_*(t)$, we simply use the stream function in the outer zone to evaluate D_p. We can show that D_p is $O(h^2)$ and the error in using the flow field in the outer zone to evaluate D_p is $O(h)$ and hence negligible compared to D_p.

Other than τ and τ_0, $D_p/(\mathcal{R}h^2)$ depends only on $\xi_h = \xi h$ for the values of l_s/l_o given below

$$\xi = \begin{cases} \epsilon & \text{for } l_s/l_o \ll \mathrm{Pr}^{-1} \\ \mathrm{Ri}^{1/3} & \text{for } \mathrm{Pr}^{-1} \ll l_s/l_o \ll \mathrm{Pr}^{-1/4} \\ \mathrm{Re} & \text{for } l_s/l_o \gg \mathrm{Pr}^{-1/4}. \end{cases} \tag{5.65}$$

$\mathrm{Re}_h = \mathrm{Re}h$ is the ratio of marked disk radius (h) to the distance from the sphere at which inertia forces balance viscous forces. On the other hand, $\epsilon_h = \epsilon h$ (resp. ${\mathrm{Ri}_h}^{1/3} = \mathrm{Ri}^{1/3}h$) is the ratio of marked disk radius to the distance from the sphere at which buoyancy forces balance the viscous forces for low values of Pe (resp. for high values of Pe).

To simplify equation (5.64) for the partial drift volume, we restrict our attention to one of the regimes mentioned in equation (5.65). In this case, we can rescale the variables in the outer zone as $\bar{r} = \xi r$, $\mathbf{w}' = \xi \bar{\mathbf{w}}'$, $p' = \xi^2 \bar{p}'$, $\bar{\psi}' = \xi \psi'$ and solve the equations (5.19)-(5.21) in Fourier space. Unlike the Fourier and inverse Fourier trans-

forms mentioned in Sec. 5.3, in this section, the Fourier transforms involve rescaled coordinate variables, i.e.,

$$\hat{\bar{\psi}}'(\mathbf{k}) = \int d\bar{\mathbf{r}}\, \bar{\psi}'(\bar{\mathbf{r}})\, e^{-i\mathbf{k}\cdot\bar{\mathbf{r}}} \text{ and } \bar{\psi}'(\bar{\mathbf{r}}) = \frac{1}{8\pi^3}\int d\mathbf{k}\, \hat{\bar{\psi}}'(\mathbf{k})\, e^{i\mathbf{k}\cdot\bar{\mathbf{r}}}. \tag{5.66}$$

After finding the Fourier transform of $\bar{\mathbf{w}}'$, namely $\hat{\bar{\mathbf{w}}}'$, we can calculate $\hat{\bar{\psi}}'$ using

$$\hat{\bar{\psi}}'(\mathbf{k}) = -\frac{1}{k_3}\left(\frac{\partial \hat{\bar{w}}_1'}{\partial k_1} + \frac{\partial \hat{\bar{w}}_2'}{\partial k_2}\right). \tag{5.67}$$

Rewriting the inverse Fourier transform in cylindrical coordinates and integrating along the azimuthal direction, we obtain

$$\begin{aligned}\psi'_*(t) &= \psi'(r_3 = -(x_{d,3}+t), R = h, t)\\ &= \frac{1}{4\pi^2\xi}\int_{-\infty}^{\infty} dk_3 \int_0^{\infty} dk_r\, \hat{\bar{\psi}}'(k_r,k_3)\, e^{-ik_3\xi\left(x_{d,3}+t\right)}\, k_r J_0(\xi h k_r)\, dk_r dk_3.\end{aligned} \tag{5.68}$$

Here, $k_r = \sqrt{{k_1}^2 + {k_2}^2}$, J_0 is the Bessel function of first kind and zeroth order, and a factor of $1/\xi$ appears due to the relation $\psi' = \bar{\psi}'/\xi$. Rewriting equation (5.68) in terms of τ, substituting for $\psi'_*(\tau')$ in equation (5.64), changing the order of integration and integrating first with respect to τ', we obtain the expression for D_p as

$$D_p = -\frac{ih^2}{2\pi\xi_h^2}\int_{-\infty}^{\infty} dk_3 \int_0^{\infty} dk_r\, \hat{\bar{\psi}}'(k_r,k_3)\, J_0(\xi_h k_r)\, \frac{\left(e^{-i\xi_h k_3 \tau_0} - e^{-i\xi_h k_3 \tau}\right)}{k_3}. \tag{5.69}$$

We can compute this double integral using integral2 command in MATLAB.

The partial drift volume formula (equation (5.69)) is valid in any of the three regimes mentioned in equation (5.65). The drift volume for the inertia dominant regime $\left(l_s/l_o \gg \mathrm{Pr}^{-1/4}\right)$ was calculated in Ref. [159]. As the flow field characteristics in the diffusion dominant regime $\left(l_s/l_o \ll \mathrm{Pr}^{-1}\right)$ were already reported by Ardekani & Stocker [166], we restrict the drift volume calculation to this regime only. In this case $\hat{\bar{\psi}}'(k_r,k_3)$ is given by

$$\hat{\bar{\psi}}' = \frac{4\pi\mathcal{R}\left(k_3^8 + 2k_3^6k_r^2 - 2k_3^2k_r^6 - k_r^8 + k_r^4\right)}{\left(k_3^6 + 3k_3^4k_r^2 + 3k_3^2k_r^4 + k_r^6 + k_r^2\right)^2}. \tag{5.70}$$

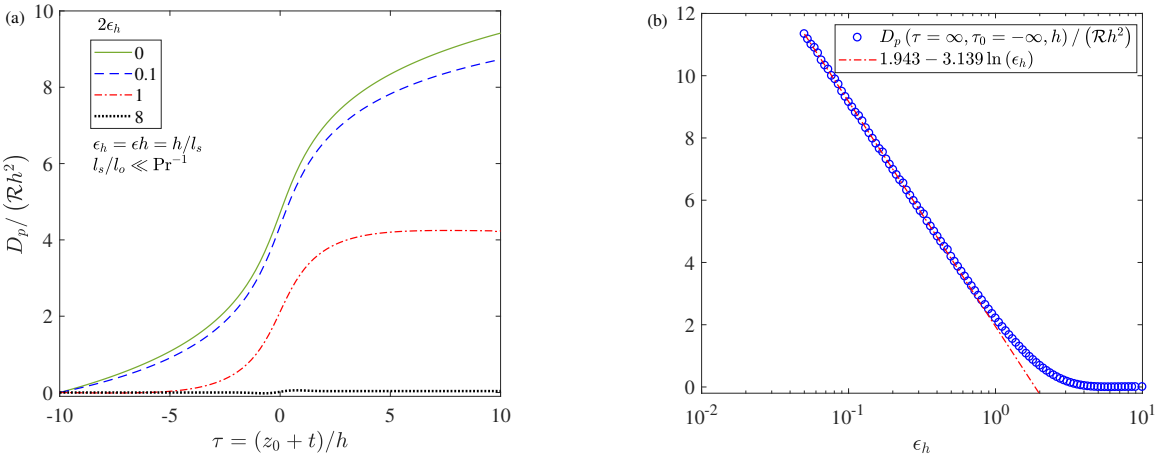

Figure 5.5. : (a) The variation of $D_p/(\mathcal{R}h^2)$ with τ for $\tau_0 = -10$ and $2\epsilon_h = 0$, 0.1, 1, 8. (b) In the limit $\tau_0 \to -\infty$ and $\tau \to \infty$, the variation of $D_p/(\mathcal{R}h^2)$ with ϵ_h. Also shown is a fit to the data for $\epsilon_h \leq 1$.

We plot the variation of D_p with τ and ϵ_h at $\tau_0 = -10$ in figure 5.5a. For a fixed value of h, an increase in ϵ_h is equivalent to an increase in ϵ or the stratification. This increases the tendency of the perturbed isopycnals (due to the passage of drop) to return to their unperturbed level which reduces the drift volume. As $\hat{\bar{\psi}}'(k_r, k_3)$ is even in k_3, the flow field is fore-aft symmetric. Due to this, the upstream drift volume is equal to the downstream drift volume, i.e., $D_p(\tau, \tau_0 = 0, h) = -D_p(\tau = -\tau, \tau_0 = 0, h)$. The fore-aft symmetry of the flow can also be seen from the flow field plots (see figure 5.3 here and figure 1b in Ref. [166]). Also, as D_p is $O(h^2)$ or at least $O(h) \gg 1$, the drop drags a huge volume of fluid in comparison to its own volume as it rises in a stratified fluid.

We note that the flow field due to a point force (far-feild representation of a drop) in a stratified fluid is qualitatively similar to the flow due to a point force in a homogeneous fluid but bounded by walls [166]. As the drift volume induced by a sphere moving in a homogeneous fluid near the wall is reported to achieve a constant value [158], we expect the drift volume induced by a drop rising in a stratified fluid to also achieve a constant value that is function of ϵ_h. We plot the drift volume or the

asymptotic value of D_p in the limit $\tau_0 \to -\infty$ and $\tau \to \infty$ in figure 5.5b as a function of ϵ_h. Here, we see that for $\epsilon_h \leq 1$, the drift volume is proportional to $\ln(\epsilon_h)$.

The time partial drift volume takes to attain the constant asymptotic value is inversely proportional to ϵ_h. In the limit $\epsilon_h \to 0$, the partial drift volume takes infinite time to achieve this asymptotic value or such constant drift volume is never achieved. This makes sense, as in this limit, the inner region approaches infinity, so the entire fluid is homogeneous in which case the partial drift volume diverges with time. We note that in the limit $\epsilon_h \to 0$, we can treat the fluid in the inner zone as homogeneous as far as the partial drift volume calculation is concerned because the first order flow in inner zone does not contribute to the leading order partial drift volume.

5.7 Conclusions

For a drop rising in a linearly density stratified fluid, we calculated the drag, deformation and drift volume induced by the drop, and the flow field surrounding the drop. We assumed the drop has a constant density and uniform interfacial tension. Our calculation of drag, deformation and flow field are valid when the inertia and stratification effects are small (but not negligible), the kinematic viscosity ratio $\chi \geq 1$, and for arbitrary values of the Prandtl number Pr and the dynamic viscosity ratio λ. For the Reynolds number $\mathrm{Re} \approx 0.1$, this corresponds to the Froude number $\mathrm{Fr} \gg 0.08$ for the temperature stratified air, $\mathrm{Fr} \gg 0.26$ for the temperature stratified water and $\mathrm{Fr} \gg 2.64$ for the salt stratified water. The drift volume calculation, on the other hand, is valid for small stratification and advective transport rate of density, and negligible inertia.

The combined influence of stratification and inertia is to increase the drag and this drag enhancement on the drop is equal to $\left(\frac{3\lambda+2}{3(\lambda+1)}\right)^2$ times the drag enhancement on a rigid sphere. The leading order effect of stratification is to induce a uniform flow far away from the drop which does not cause any drop deformation. This leading

order effect of stratification holds even for a sedimenting particle of arbitrary shape due to which the stratification does not generate any hydrodynamic torque on a non-skew particle [176]. In a stratified fluid, the return of perturbed isopycnals to their unperturbed level causes a reflux of fluid, which reduces the partial drift volume induced by the drop. This in turn makes the drop to induce a finite drift volume (yet large compared to drop's volume) in a stratified fluid unlike an infinite drift volume induced in a homogeneous fluid. Our study is the first theoretical calculation of drift volume induced by objects (drop or rigid sphere) in a density stratified fluid and this calculation is valuable in the context of the ongoing debate in the literature on biogenic mixing in the oceans.

Prior to our calculation, it was known that a rising drop in a homogeneous fluid at zero inertia is the only situation in which the drop does not exhibit any deformation [18]. In all other problems concerned with drop motion, the drop deforms. Through our calculation, we discovered an additional scenario in which the drop does not deform–a rising drop in a density stratified fluid at zero inertia. It is then interesting to find out if a drop of arbitrary shape would evolve to a spherical shape after long time. This problem is essentially identifying the stability of spherical shape, for a drop rising in a density stratified fluid at zero inertia, for both infinitesimal [177] and finite [178] perturbations from the sphere.

In the event of oil spill, surfactants are usually added to breakdown the heavier oil components into small drops. These drops are always surrounded by marine microbes as they serve as nutrient sources to the microbes. To understand the bioremediation of oil spill by marine microbes, in an earlier work, we have solved this problem without considering the effects of density stratification by modeling the microbe as a force-dipole and using the method of images to study the hydrodynamic interaction between drops and nearby microbes [16, 17, 73, 179]. We can now borrow the ideas from the present work to understand how density stratification modifies interaction of microbes with drops rising in density stratified oceans.

6. SQUIRMING IN DENSITY-STRATIFIED FLUIDS

6.1 Introduction

The water in oceans, ponds or lakes is density-stratified due to the variations in the temperature or the salt concentration with height. This stratification affects the motility of organisms that live in these environments [87]. For example, some species of copepods cannot cross the thermoclines [180] whereas the haloclines act as barriers to some species of dinoflagellates [181]. Stratification was also shown to be a necessary condition for the formation of cyanobacteria blooms in the Maude Weir pool which could have significant human health risks due to the toxins released by these bacteria [182]. The stratification also alters the contribution of marine organisms to mixing [161, 183]. This contribution could be drift-based (volume dragged by the motion of particle, drop or organism) or energy-based (a part of the work done by the organism is lost in mixing the surrounding fluid). Hence, the study of an organism in a density-stratified fluid would unravel the impact of stratification on the motility and flow characteristics which are important from the fundamental fluid mechanics perspective. And these findings would serve as a first step in determining the stratification effects on the algal bloom formation and on the biogenic mixing.

There are several works analyzing the enhanced drag acting on a towed particle in a density-stratified fluid [5, 6]. On the theoretical side, such calculation was performed for small stratification strengths and negligible inertia by taking a perturbation in terms of the stratification strength. Such a perturbation turns out to be singular with the boundary layer occurring far from the particle, the exact location of the boundary layer depends on whether advective or diffusive transport rate of density is dominant [148, 149, 184]. This boundary layer separates the region near the particle

This chapter, with few modifications, is submitted for publication in Physical Review Fluids.

where buoyancy effects are negligible from the region far from the particle where buoyancy effects are as important as the viscous effects. This problem of a towed particle in a quiescent stratified fluid is similar to the problem of a towed particle in a homogeneous fluid undergoing linear flow at small inertia [168, 169] and because of this, the techniques developed for the latter case were used to solve the problems associated with the former case. At negligible inertia, the stratification induces a uniform flow far from the particle. Due to this uniform flow, a towed spherical particle experiences lift and enhanced drag forces [148,149,184], a towed drop does not deform [185] and a towed non-skew particle does not experience any hydrodynamic torque [176]. Recent efforts on this topic focused on studying the simultaneous influence of inertia and stratification on the drag experienced by a towed particle [150] or a drop [185].

Despite the ecological significance of swimming at pycnoclines, very few works analyzed this situation. The first work in this field reported the flow due to a point force and a force-dipole placed in a stratified fluid at zero inertia, weak stratification and small advective transport rate of density [166]. This work also found that organisms larger than $O\,(100\ \mu\text{m})$ are affected by stratification despite the length scale over which density varies $\sim O\,(1\ \text{km})$ is much larger than the organism's size. A squirmer in a stratified fluid was found to exhibit smaller detection volume but only at the cost of reduced nutrient uptake per unit energy expended [87]. Modeling the organism as a force-dipole placed in a stratified fluid, it was found that the contribution of small organisms to the oceanic circulation is negligible [186]. Similarly, a simulation of dilute suspension of squirmers in a stratified fluid revealed that even intermediate sized organisms do not contribute to the oceanic energy budget although they produce an enhanced local mixing [162]. The speed and power expenditure of a Taylor's swimming sheet in a stratified fluid was found to exhibit non-trivial dependencies on the inertia, stratification, and diffusivity of the stratifying agent [187].

Unlike the works on particles in stratified fluids, the works on swimming organisms in stratified fluids made an assumption on the density of the organisms: organism's

density is equal to the ambient fluid density evaluated at the organism's center [87] or organism regulates its density to stay neutrally buoyant [187]. Even though there are organisms that use certain mechanisms to change their density (see Guasto *et al.* [188]) and hence possibly become neutrally buoyant, net buoyancy of the organism was found to be one of the causes of diel vertical migration [189]. It seems appropriate to assume the density of the organism is constant, as a first step towards understanding the consequences of the net buoyancy on the motility of the organism. Such calculation will be general enough that in some limit, the organism is like a swimmer whose density is equal to the ambient fluid density evaluated at the swimmer's position, and in this limit, we would have results similar to those reported by Doostmohammadi *et al.* [87].

Even though Ardekani & Stocker [166] found the flow due to a point force or force-dipole placed in a stratified fluid, it is not obvious how this flow is related to the flow due to a towed particle or swimming organism in a stratified fluid. Once this relationship is established, one can use the point force singularity solution to find the hydrodynamic interactions [2] as well as the drift volume induced by the particles or organisms [159, 165, 185]. It is apparent from Candelier *et al.* [149] calculation that the far-field flow due to a towed spherical particle in a stratified fluid at negligible advective transport rate of density is the same as the flow due to a point force placed in a stratified fluid [166]. Similar connection between the flow due to a finite sized swimming organism and point force singularity solutions in a stratified fluid should be made.

To overcome the shortcomings of the previous works, here we anlayze the motion of a swimming organism of finite size and constant density through a linearly density-stratified fluid. We quantify how stratification affects the motility of the organism and the flow close to and far from the organism. We also relate the far-field flow to the point force singularity solution in a stratified fluid. As mentioned earlier, while the far-field flow is useful in finding the hydrodynamic interactions and the induced drift volume, the near-field flow is useful in finding the power expenditure and the

swimming efficiency, and the complete flow is useful in finding the nutrient uptake. Depending on the position of the swimmer relative to its neutrally buoyant position (NBP), we observe two different physics. Here, NBP is the position in the fluid where ambient fluid density equals the swimmer's density. Far from NBP, the swimmer is like a settling sphere, the stratification induced modifications to its motility can be predicted from the enhanced drag acting on a towed sphere, and the far-field flow is the same as that due to a point force placed in a stratified fluid. Close to NBP, the swimmer is like a force-free swimmer, the modifications in the motility depend on the stresslet exerted by the swimmer, and the far-field flow is the same as that due to a force-dipole placed in a stratified fluid.

We organize this paper as follows. We present the dimensionless governing equations and boundary conditions associated with the flow and density disturbances caused by a squirmer in a stratified fluid in Sec. 6.2. By taking a perturbation in terms of stratification strength, we solve these governing equations for a swimmer far from and close to its neutrally buoyant position in Secs. 6.3.1, 6.3.2, respectively. We then analyze the swimming velocity by deriving the scaling laws in Sec. 6.4, visualize the flow field surrounding the swimmer in Sec. 6.5 and provide some concluding remarks in Sec. 6.6.

6.2 Problem Formulation

In this section, we present the dimensionless governing equations and boundary conditions for the flow and density disturbances caused by the motion of a swimming microorganism in a density stratified fluid (see figure 6.1 for schematic). These equations are similar to those reported for a settling sphere in a stratified fluid [149, 150].

We work in a frame of reference translating with the swimmer. In this frame, far away from the swimmer, the flow field asymptotes to the negative of the unknown swimming velocity $\mathbf{U}$ i.e., as $r = |\mathbf{r}| \to \infty$, $\mathbf{w} \sim -\mathbf{U}$. The density approaches the ambient density which decreases linearly with an increase in height, i.e., as $r \to \infty$,

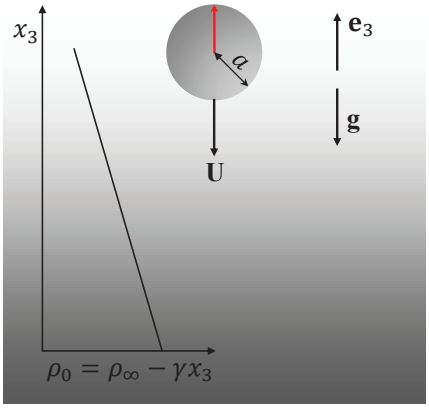

Figure 6.1. : A schematic showing a spherical model swimming microorganism in a density-stratified fluid, the ambient density of which decreases linearly with an increase in height. The organism is oriented vertically upwards as shown by the red arrow.

$\rho \sim \rho_0 = \rho_\infty - \gamma z$. The pressure asymptotes to an ambient pressure p_0, which satisfies the hydrostatic equation $-\nabla p_0 + \rho_0 \mathbf{g} = \mathbf{0}$. Here, $\mathbf{x} = (x, y, z)$, $\mathbf{r} = (r_1, r_2, r_3)$, respectively, are the position vectors with respect to an origin in lab frame and the center of the swimmer. These two are related by $\mathbf{x} = \mathbf{r} + \mathbf{x}_s$, where $\mathbf{x}_s$ gives the position of swimmer in the lab frame. Also, ρ_∞ is the reference density, $\gamma > 0$ is a density gradient and $\mathbf{g} = -g\mathbf{e}_3$ is a gravity vector, where g is the gravitational acceleration and $\mathbf{e}_3$ is a unit vector that points vertically upwards. Usually, the variation in temperature or salt concentration with position causes the variation in density. When the changes in temperature or salt concentration are small, the changes in density are linearly proportional to the changes in temperature or salt concentration and one can directly write down an advection-diffusion equation for density instead of such an equation for temperature or salt concentration. We use the Boussinesq approximation. According to this approximation, the density can be treated as constant ($= \rho_\infty$) in all the terms of the equations governing the flow except the buoyancy term, all other properties can be treated as constant while neglecting the viscous dissipation term in the density transport equation. The conditions required for the validity of the Boussinesq approximation in natural convection problems can be found in Ref. [190] while these conditions for the flow induced by a settling motion of a particle in a density-stratified fluid can be found in Ref. [149]. Hence, the continuity and the Navier-Stokes equations governing the flow field, and the advection-diffusion equation governing the density transport are given as follows

$$\nabla \cdot \mathbf{w} = 0, \tag{6.1}$$

$$\rho_\infty \left(\frac{\partial \mathbf{w}}{\partial t} + (\mathbf{w} \cdot \nabla)\, \mathbf{w} \right) = -\nabla p + \rho_\infty \nu\, \nabla^2 \mathbf{w} + \rho \mathbf{g} - \rho_\infty \frac{d\mathbf{U}}{dt}, \tag{6.2}$$

$$\frac{\partial \rho}{\partial t} + \mathbf{w} \cdot \nabla \rho = \kappa\, \nabla^2 \rho. \tag{6.3}$$

Here, ν, κ, respectively, are the kinematic viscosity of the fluid and the diffusion coefficient for the density transport. The choice of a moving frame of reference to

write the governing equations leads to the occurrence of term $\rho_\infty \frac{d\mathbf{U}}{dt}$ in the Navier-Stokes equations.

Following Candelier *et al.* [149] and Mehaddi *et al.* [150], we rewrite the governing equations and boundary conditions in terms of disturbance variables. The flow, density and pressure disturbance are defined as $\mathbf{w}' = \mathbf{w} + \mathbf{U}$, $\rho' = \rho - \rho_0$, and $p' = p - p_0$. Hence, the governing equations concerning the disturbance variables are

$$\nabla \cdot \mathbf{w}' = 0, \tag{6.4}$$

$$\rho_\infty \left[\frac{\partial \mathbf{w}'}{\partial t} + (\mathbf{w}' \cdot \nabla)\, \mathbf{w}' - (\mathbf{U} \cdot \nabla)\, \mathbf{w}' \right] = -\nabla p' + \rho_\infty \nu\, \nabla^2 \mathbf{w}' + \rho' \mathbf{g}, \tag{6.5}$$

$$\frac{\partial \rho'}{\partial t} + \mathbf{w}' \cdot \nabla \rho' - \mathbf{U} \cdot \nabla \rho' - \gamma\, (\mathbf{w}' \cdot \mathbf{e}_3) = \kappa\, \nabla^2 \rho'. \tag{6.6}$$

We non-dimensionalize these equations. For this purpose, we use the characteristic length scale of the swimmer denoted by 'a', velocity scale $u_c = \max\{U_{Sed}, U_{Swim}\}$ and a pressure or stress scale, $p_c = \rho_\infty \nu u_c / a$, to non-dimensionalize the length, velocity and pressure, respectively. Here U_{Swim} is the swimmer's speed in a homogeneous fluid of density equal to the swimmer's density while U_{Sed} is the sedimenting speed of a sphere of radius 'a' and density ρ_s in a homogeneous fluid of density equal to the ambient density (ρ_0) evaluated at swimmer's position. Clearly, U_{Swim} depends on the model used to represent the swimming microorganism while U_{Sed} is given by

$$U_{Sed} = \frac{2}{9} \frac{a^2 g}{\nu} \left| 1 - \frac{\gamma a}{\rho_\infty} x_{s3} - \alpha \right|. \tag{6.7}$$

Here, $x_{s3} = \mathbf{x}_s \cdot \mathbf{e}_3$, $\alpha = \rho_s / \rho_\infty$, ρ_s is the (constant) density of the swimmer and x_{s3} is dimensionless. Assuming the quasi-steady conditions to prevail and denoting the dimensionless variables using the letters that were used to denote the dimensional variables, the dimensionless governing equations are

$$\nabla \cdot \mathbf{w}' = 0, \tag{6.8}$$

$$Re\, [\mathbf{w}' \cdot \nabla \mathbf{w}' - \mathbf{U} \cdot \nabla \mathbf{w}'] = -\nabla p' + \nabla^2 \mathbf{w}' - Ri\, \rho' \mathbf{e}_3, \tag{6.9}$$

$$Pe\left[\mathbf{w}'\cdot\nabla\rho' - \mathbf{U}\cdot\nabla\rho' - \mathbf{w}'\cdot\mathbf{e}_3\right] = \nabla^2\rho'. \tag{6.10}$$

Here Re, Ri, Pe are the Reynolds number, the viscous Richardson number and the Peclet number. Re is the ratio of inertia forces to the viscous forces, Ri is the ratio of buoyancy forces to the viscous forces while Pe is the ratio of advective transport rate of density to its diffusive transport rate. Their precise expressions are given by

$$Re = \frac{au_c}{\nu},\ Ri = \frac{\gamma g a^3}{\rho_\infty \nu u_c},\ Pe = \frac{au_c}{\kappa}. \tag{6.11}$$

As expected, far away from the swimmer, all the disturbance quantities decay to zero.

$$\mathbf{w}' = \mathbf{0},\ \rho' = 0 \text{ as } r \to \infty. \tag{6.12}$$

We now model the swimming microorganism as a spherical squirmer of radius 'a' with only two tangential squirming modes [14, 15]. We assume the squirmer has a constant density ρ_s and is oriented either vertically upwards or downwards. Because of the latter assumption, the problem becomes axisymmetric simplifying the resulting calculations. We then apply a no-slip and no-penetration boundary conditions for the flow field on the swimmer's surface

$$\mathbf{w}' = \mathbf{U} + \mathbf{u}^s \text{ at } r = 1,\ \mathbf{u}^s = \left(b_1 \sin\theta^s + b_2 \sin\theta^s \cos\theta^s\right)\mathbf{e}_{\theta^s}, \tag{6.13}$$

where θ^s is an angle measured from the swimming direction and $\mathbf{e}_{\theta^s}$ is a unit vector in the increasing direction of θ^s. Also $b_n = B_n/u_c$, B_n is the nth squirming mode and $n = 1, 2$. For this model microorganism, $U_{Swim} = \frac{2}{3}B_1$. For an upward oriented swimmer, θ^s, $\mathbf{e}_{\theta^s}$ are same as the polar angle $\theta = \cos^{-1}\left(\mathbf{r}\cdot\mathbf{e}_3/r\right)$ and the unit vector in the polar direction $\mathbf{e}_\theta$ due to which the slip $\mathbf{u}^s = \left(b_1 \sin\theta + b_2 \sin\theta\cos\theta\right)\mathbf{e}_\theta$. For a downward oriented swimmer, $\theta^s = \pi - \theta$, $\mathbf{e}_{\theta^s} = -\mathbf{e}_\theta$, hence $\mathbf{u}^s = \left(-b_1 \sin\theta + b_2 \sin\theta\cos\theta\right)\mathbf{e}_\theta$. We do the calculation for an upward oriented swimmer and substitute $-b_1$ for b_1 in the results of an upward oriented swimmer to obtain the results of a downward

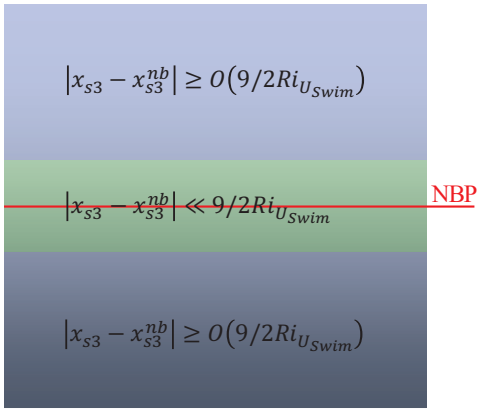

Figure 6.2. : Schematic showing the range of swimmer positions with respect to the neutrally buoyant position (NBP) $x_{s3} = x_{s3}^{nb} = \frac{\rho_\infty}{\gamma a}(1-\alpha)$ where it is termed non-neutrally buoyant $\left(\left|x_{s3} - x_{s3}^{nb}\right| \geq O\left(\frac{9}{2Ri_{U_{Swim}}}\right) \Rightarrow \frac{U_{Sed}}{U_{Swim}} \geq O(1)\right)$ or neutrally buoyant $\left(\left|x_{s3} - x_{s3}^{nb}\right| \ll O\left(\frac{9}{2Ri_{U_{Swim}}}\right) \Rightarrow \frac{U_{Sed}}{U_{Swim}} \ll O(1)\right)$ swimmer. Here $Ri_{U_{Swim}}$ is the viscous Richardson number based on U_{Swim} given by $Ri_{U_{Swim}} = \frac{3\gamma g a^3}{2\rho_\infty \nu B_1}$.

oriented swimmer. We also impose the no-flux boundary condition for density on the swimmer's surface which in terms of disturbance density is

$$\frac{\partial \rho'}{\partial r} = \cos\theta \text{ at } r = 1. \tag{6.14}$$

For salt stratification, this corresponds to a swimmer that is impermeable to the salt while for temperature stratification, this means that the swimmer surface is adiabatic.

Neglecting the inertia of the swimmer, the net force acting on it should be zero. The swimmer experiences three forces—its own weight, buoyancy and drag ($\mathbf{F}_D$). Denoting the sum of weight and buoyancy by $F_e\,\mathbf{e}_3$, the force balance condition is

$$F_e\,\mathbf{e}_3 + \mathbf{F}_D = \mathbf{0},\ F_e = \frac{4\pi}{3}\frac{a^2 g}{\nu u_c}\left(1 - \frac{\gamma a}{\rho_\infty}x_{s3} - \alpha\right). \tag{6.15}$$

Depending on the location of the swimmer relative to its neutrally buoyant position (NBP) $x_{s3} = x_{s3}^{nb} = \frac{\rho_\infty}{\gamma a}(1-\alpha)$, the ratio U_{Sed}/U_{Swim} can be much larger than or even much smaller than 1 (see figure 6.2). When the swimmer is far from its NBP, $U_{Sed}/U_{Swim} \geq O(1)$ and we call such swimmer a non-neutrally buoyant swimmer.

On the other hand, when the swimmer is close to its NBP, $U_{Sed}/U_{Swim} \ll 1$, and we call such swimmer a neutrally-buoyant swimmer. Naturally, $u_c = U_{Sed}$ for the former swimmer while $u_c = U_{Swim}$ for the latter swimmer. As the far-field representation of these two swimmers is different (Stokeslet vs Stokes-dipole or quadrupole), the approach to solve the governing equations is also different. We describe the method to solve the governing equations for small Ri, Pe and negligible inertia in the following section. We also explain why the calculation of swimming velocity is valid for any Peclet number.

6.3 Solution Methodology

6.3.1 Non-neutrally buoyant swimmer

As the dimensionless governing equations, boundary conditions and the far-field representation for this squirmer are similar to those of a settling sphere, the solution procedure is also similar to that of a settling sphere [149, 150]. However, unlike the sphere towed at a constant velocity, the squirmer has a slip on its surface and its swimming velocity is unknown.

We attempt a regular perturbation in Ri assuming $Re \ll 1$ to see if the solution to this problem can be obtained using a regular perturbation expansion. We denote the leading order variables in Ri as $\mathbf{w}_0'$, p_0', ρ_0' and $\mathbf{U}_0$. Referring to equations (6.8), (6.9), we see that the leading order flow is governed by the Stokes equations. Importantly, the buoyancy terms are negligible throughout the entire domain when regular perturbation expansion is used. When the swimmer is far from its NBP, we expect it to experience a $O(1)$ external force (weight + buoyancy). Hence, the flow field far from the swimmer should be a Stokeslet, i.e., for $r \gg 1$, $\mathbf{w}_0' \sim 1/r$. As $\mathbf{w}_0'$ is $O(1)$ on the swimmer's surface (see equation (6.13)), we expect $\mathbf{w}_0' \sim O(1)$ for $r \sim O(1)$. Analysis of the exact expression of $\mathbf{w}_0'$ (see equations (6.22)-(6.24)) also

reveals the same scales both close to and far from the swimmer. The leading order density disturbance ρ_0' is governed by the following advection-diffusion equation

$$Pe\left(\mathbf{w}_0' \cdot \nabla \rho_0' - \mathbf{U}_0 \cdot \nabla \rho_0' - \mathbf{w}_0' \cdot \mathbf{e}_3\right) = \nabla^2 \rho_0'. \tag{6.16}$$

As it is not possible to solve this equation analytically for any Pe, we do a small Pe expansion to find that (see Appendix 6.7 for this calculation)

$$\rho_0' \sim \max\left(\frac{1}{r^2}, Per\right) \text{ for } r < Pe^{-1}. \tag{6.17}$$

Hence, for $r \sim O(1)$, $\rho_0' \sim O(1)$ while for $Pe^{-1} > r \gg Pe^{-1/3}$, $\rho_0' \sim Per$. We now estimate the order of magnitude of viscous and buoyancy terms both close to and far away from the swimmer to see if the buoyancy terms are negligible compared to the viscous terms throughout the entire domain. This way, we can verify the validity of the regular perturbation expansion in Ri. Close to the swimmer $r \sim O(1)$, the viscous terms $\nabla^2 \mathbf{w}_0' \sim O(1)$ while the buoyancy terms $Ri\rho_0' \sim Ri \ll O(1)$. Hence, close to the swimmer, the buoyancy terms can be neglected. Far away from the swimmer $Pe^{-1} > r \gg Pe^{-1/3}$, the viscous terms $\nabla^2 \mathbf{w}_0' \sim 1/r^3$ while the buoyancy terms $Ri\rho_0' \sim RiPer$. Hence at $r \sim \frac{1}{\epsilon} \gg 1$, $\epsilon = (RiPe)^{1/4}$, the buoyancy terms are not negligible and are in fact as important as the viscous terms, contrary to the notion of regular perturbation analysis. This makes the regular perturbation expansion in Ri incorrect and one should do the singular perturbation expansion in Ri (or ϵ), analyzing separately the regions close to (inner region) and far away from (outer region) the swimmer. In the inner region ($1 \leq r \leq O(1/\epsilon)$) the buoyancy effects are negligible while in the outer region ($r \geq O(1/\epsilon)$) the buoyancy effects are as important as the viscous effects. As the density scale $\rho_0' \sim Pe\, r$ valid for $Pe^{-1} < r \ll Pe^{-1/3}$ is used in determining the matching zone (or boundary layer) location $r \sim 1/\epsilon$, we expect the singular perturbation analysis to hold for $Pe^{-1} < \frac{1}{\epsilon} \ll Pe^{-1/3}$ or $\epsilon^3 \ll Pe < \epsilon$.

We split the range of swimmer positions at which it is non-neutrally buoyant $\frac{U_{Sed}}{U_{Swim}} \geq O(1)$ into three regimes—(a)$\frac{U_{Sed}}{U_{Swim}} \sim O(1)$, (b) $\frac{U_{Sed}}{U_{Swim}} \sim \frac{1}{\epsilon} \gg 1$ and (c) $\frac{U_{Sed}}{U_{Swim}} \gg \frac{1}{\epsilon}$ (see figure 6.3). The idea behind such splitting process is given as follows: as the swimmer moves away from its NBP, its sedimentation speed increases

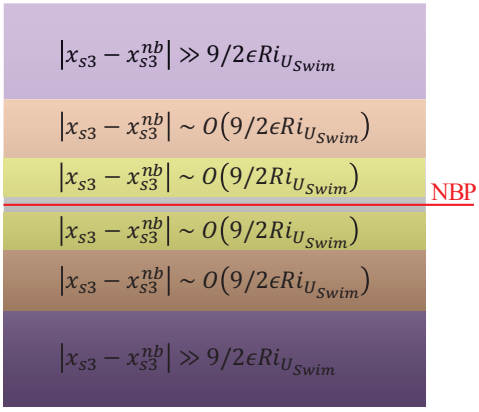

Figure 6.3. : A region in which the swimmer is termed non-neutrally buoyant $\left|x_{s3} - x_{s3}^{nb}\right| \geq O\left(\frac{9}{2Ri_{U_{Swim}}}\right)$ (blue region in figure 6.2) is divided into three subregions for the ease of analysis: (a) $\left|x_{s3} - x_{s3}^{nb}\right| \sim O\left(\frac{9}{2Ri_{U_{Swim}}}\right)$, (b) $\left|x_{s3} - x_{s3}^{nb}\right| \sim O\left(\frac{9}{2\epsilon Ri_{U_{Swim}}}\right)$, and (c) $\left|x_{s3} - x_{s3}^{nb}\right| \gg \frac{9}{2\epsilon Ri_{U_{Swim}}}$. In these three regions, respectively, $\frac{U_{Sed}}{U_{Swim}} \sim O(1)$, $\frac{U_{Sed}}{U_{Swim}} \sim O\left(\frac{1}{\epsilon}\right)$, and $\frac{U_{Sed}}{U_{Swim}} \gg \frac{1}{\epsilon}$.

while the slip velocity ($\propto B_1, B_2$) stays the same. Hence the slip velocity relative to the sedimentation speed ($\propto b_1, b_2$) decreases from $O(1)$ $\left(\frac{U_{Sed}}{U_{Swim}} \sim O(1)\right)$ to $O(\epsilon)$ $\left(\frac{U_{Sed}}{U_{Swim}} \sim \frac{1}{\epsilon}\right)$ and to $\ll \epsilon$ $\left(\frac{U_{Sed}}{U_{Swim}} \gg \frac{1}{\epsilon}\right)$. So, it is appropriate to analyze the three cases separately. For $\frac{U_{Sed}}{U_{Swim}} \sim O(1)$, the dimensionless slip is $O(1)$ and it affects the flow and the swimming velocity at both leading order and first order. For $\frac{U_{Sed}}{U_{Swim}} \sim \frac{1}{\epsilon}$, the dimensionless slip is $O(\epsilon)$ and it only affects the first order flow field while for $\frac{U_{Sed}}{U_{Swim}} \gg \frac{1}{\epsilon}$, the dimensionless slip is $\ll \epsilon$ and it does not affect the flow or swimming velocity accurate to $O(\epsilon)$. Here, we restrict the Reynolds number and the swimmer's position limiting the validity of singular perturbation calculation to

$$\epsilon \ll 1,\ \epsilon^3 \ll Pe < \epsilon,\ Re \ll \epsilon,\ \frac{U_{Sed}}{U_{Swim}} \sim O(1). \tag{6.18}$$

The third condition ensures that inertia effects are negligible everywhere while the fourth condition restricts the swimmer's position to $\left|x_{s3} - x_{s3}^{nb}\right| \sim O\left(\frac{9}{2Ri_{U_{Swim}}}\right)$ (see figure 6.3). One should not worry about the restrictions imposed by these limits as we will show later that the flow field and the swimming velocity found are valid for broader range of swimmer positions $\frac{U_{Sed}}{U_{Swim}} \geq O(1)$ or $\left|x_{s3} - x_{s3}^{nb}\right| \geq O\left(\frac{9}{2Ri_{U_{Swim}}}\right)$.We will also show that the flow field found is valid at both small and large Pe while the swimming velocity derived is valid for all Pe. We finally note that we can express ϵ in terms of the fundamental length scale associated with stratification $l_s = \left(\frac{\nu\kappa}{N^2}\right)^{1/4}$ via $\epsilon = a/l_s$, where $N = \sqrt{-\frac{g}{\rho_\infty}\frac{d\rho_0}{dz}}$ is the Brunt-Vaisala frequency.

Inner zone

In this zone, all the variables can be expanded as follows

$$\begin{aligned} \{\mathbf{w}', p', \mathbf{U}\} &= \{\mathbf{w}_0', p_0', \mathbf{U}_0\} + \epsilon\{\mathbf{w}_1', p_1', \mathbf{U}_1\} + o(\epsilon), \\ \rho' &= \rho_0' + o(1). \end{aligned} \tag{6.19}$$

The gauge function at leading order is determined from the boundary conditions on the swimmer surface: $\mathbf{w}_0' \sim O(1)$, $\rho_0' \sim O(1)$ at $r = 1$, hence we expect the leading order gauge function is 1. The gauge function at first order $\epsilon = (RiPe)^{1/4}$ is found

by matching the flow field in the inner zone with that in the outer zone. Clearly this gauge function depends on the non-integer power of Ri and this is not surprising in the singular perturbation analysis, where the gauge functions usually are fractional powers of small parameter. Equation (6.19) suggests the following expansion for the drag acting on the swimmer

$$\mathbf{F}_D = \mathbf{F}_{0,D} + \epsilon \mathbf{F}_{1,D} + o\left(\epsilon\right), \tag{6.20}$$

where $\mathbf{F}_{0,D}$, $\mathbf{F}_{1,D}$ using equation (6.15) are given by

$$\mathbf{F}_{0,D} = -F_e \mathbf{e}_3, \ \mathbf{F}_{1,D} = \mathbf{0}. \tag{6.21}$$

At leading order, the disturbance flow satisfies the Stokes equations with the boundary condition $\mathbf{w}_0'|_{r=1} = \mathbf{U}_0 + \mathbf{u}^s$, and the swimmer experiences an external force $F_e\mathbf{e}_3$. Given the linearity of the problem, the leading order disturbance flow $\mathbf{w}_0'$ is simply the sum of the flow due to a settling sphere of radius a, density ρ_s in a homogeneous fluid of density $\rho_\infty - \gamma x_{s3}$ [3, 18] and the flow due to a squirmer in a homogeneous fluid of density ρ_s [15, 85]. Similarly, the leading order swimming velocity $\mathbf{U}_0$ is equal to the sum of the sedimentation velocity of a sphere of radius a, density ρ_s in a homogeneous fluid of density $\rho_\infty - \gamma x_{s3}$ and the swimming velocity of a squirmer in a homogeneous fluid of density ρ_s. The corresponding speeds are U_{Sed} and U_{Swim}.

$$\mathbf{w}_0' = w_{0r}'\mathbf{e}_r + w_{0\theta}'\mathbf{e}_\theta, \ \mathbf{U}_0 = U_0\mathbf{e}_3, \tag{6.22}$$

$$\begin{aligned} w_{0r}' =& \frac{b_2\left(1-r^2\right)\left(3\cos^2\theta - 1\right) - 2r\cos\theta\left(\left(b_1 - \frac{3U_0}{2}\right)r^2 - b_1 + \frac{U_0}{2}\right)}{2r^4}, \\ w_{0\theta}' =& \frac{\sin\theta\left(2b_2\cos\theta + r\left\{\left(b_1 - \frac{3U_0}{2}\right)r^2 + b_1 - \frac{U_0}{2}\right\}\right)}{2r^4}, \end{aligned} \tag{6.23}$$

$$U_0 = \frac{2}{9}\frac{a^2 g}{\nu u_c}\left(1 - \frac{\gamma a}{\rho_\infty}x_{s3} - \alpha\right) + \frac{2b_1}{3}. \tag{6.24}$$

At first order, the disturbance flow $\mathbf{w}_1'$ still satisfies the Stokes equations with the boundary condition $\mathbf{w}_1'|_{r=1} = \mathbf{U}_1$, and the swimmer does not experience any external force or $\mathbf{F}_{1,D} = \mathbf{0}$. The boundary condition far away from the swimmer is determined by matching the flow in the inner zone with the flow in the outer zone.

Outer zone

In this zone, we represent the swimmer by a point force and add a term $-\mathbf{F}_{0,D}\delta(\mathbf{r})$ on the right hand side of the Navier-Stokes equations as the swimmer exerts the force $-\mathbf{F}_{0,D}$ on the fluid [168, 169]. Similar such term in the advection-diffusion equation and the higher order force singularities in the Navier-Stokes equations can be neglected as far as the calculation of leading order disturbance variables in the outer zone is concerned. Far away from the swimmer, as $\mathbf{w}' \sim 1/r \ll \mathbf{U}$, we neglect $\mathbf{w}' \cdot \nabla \rho'$ in comparison to $\mathbf{U} \cdot \nabla \rho'$. We rescale the length, velocity, pressure and density as $\tilde{r} = \epsilon r$, $\mathbf{w}' = \epsilon \tilde{\mathbf{w}}'$, $p' = \epsilon^2 \tilde{p}'$, and $\rho' = Pe\tilde{\rho}'/\epsilon$. In terms of these rescaled variables, the leading order disturbance flow and density in the outer zone are governed by

$$\tilde{\nabla} \cdot \tilde{\mathbf{w}}' = 0, \tag{6.25}$$

$$-\tilde{\nabla}\tilde{p}' + \tilde{\nabla}^2 \tilde{\mathbf{w}}' - \tilde{\rho}' \mathbf{e}_3 - \mathbf{F}_{0,D}\delta(\tilde{\mathbf{r}}) = \mathbf{0}, \tag{6.26}$$

$$-Pe\left(\mathbf{U}_0 \cdot \tilde{\nabla}\tilde{\rho}'\right) - \epsilon\left(\tilde{\mathbf{w}}' \cdot \mathbf{e}_3\right) = \epsilon\, \tilde{\nabla}^2 \tilde{\rho}'. \tag{6.27}$$

As these equations are linear, we solve them in the Fourier space. Denoting the Fourier transform of $\tilde{\mathbf{w}}'(\tilde{\mathbf{r}})$ by $\hat{\mathbf{w}}'(\mathbf{k})$, we define the Fourier and inverse Fourier transforms as

$$\hat{\mathbf{w}}'(\mathbf{k}) = \int \tilde{\mathbf{w}}'(\tilde{\mathbf{r}})\, e^{-i\mathbf{k}\cdot\tilde{\mathbf{r}}} d\tilde{\mathbf{r}},\ \tilde{\mathbf{w}}'(\tilde{\mathbf{r}}) = \frac{1}{8\pi^3} \int \hat{\mathbf{w}}'(\mathbf{k})\, e^{i\mathbf{k}\cdot\tilde{\mathbf{r}}} d\mathbf{k}, \tag{6.28}$$

where $i = \sqrt{-1}$. Hence, in Fourier space, the leading order disturbance flow in outer zone is given by

$$\hat{\mathbf{w}}' = \left[k^2\mathbf{I} + \mathbf{A} - \mathbf{B}\right]^{-1} \mathbf{E}\, F_e \mathbf{e}_3, \tag{6.29}$$

where $k = \sqrt{\mathbf{k}\cdot\mathbf{k}}$, $\mathbf{I}$ is an identity tensor and the tensors $\mathbf{A}$, $\mathbf{B}$, $\mathbf{E}$ are given by

$$\mathbf{A} = \frac{\epsilon \mathbf{e}_3 \mathbf{e}_3}{\left(\epsilon k^2 - iPe\left(\mathbf{U}_0 \cdot \mathbf{k}\right)\right)},\ \mathbf{B} = \frac{\epsilon k_3 \mathbf{k} \mathbf{e}_3}{k^2\left(\epsilon k^2 - iPe\left(\mathbf{U}_0 \cdot \mathbf{k}\right)\right)},\ \mathbf{E} = \left(\mathbf{I} - \frac{\mathbf{k}\mathbf{k}}{k^2}\right). \tag{6.30}$$

In equation (6.29), we represented the tensors as matrices and vectors as column matrices.

Matching Condition

As $r \gg 1$ and $\tilde{r} \ll 1$ represent the same region in the physical space, the inner solution $\mathbf{w}_0'(\mathbf{r}) + \epsilon \mathbf{w}_1'(\mathbf{r})$ should have the same functional form as the outer solution $\epsilon \tilde{\mathbf{w}}'(\tilde{\mathbf{r}})$ in this region of space

$$\lim_{r \gg 1} \left[\mathbf{w}_0'(\mathbf{r}) + \epsilon \mathbf{w}_1'(\mathbf{r})\right] \Leftrightarrow \lim_{\tilde{r} \ll 1} \epsilon \tilde{\mathbf{w}}'(\tilde{\mathbf{r}}). \tag{6.31}$$

This is the matching condition. Here the notation $\mathcal{A} \Leftrightarrow \mathcal{B}$ means that $\mathcal{A}$ has the same functional form as $\mathcal{B}$ [18]. At leading order, as the swimmer experiences an external force $F_e \mathbf{e}_3 = -\mathbf{F}_{0,D}$, far away from the swimmer, the leading order flow $\mathbf{w}_0'(\mathbf{r})$ should be the same as the Stokeslet flow $\mathbf{w}_S(\mathbf{r})$ i.e., for $r \gg 1$, $\mathbf{w}_0'(\mathbf{r}) \sim \mathbf{w}_S(\mathbf{r})$, where $\mathbf{w}_S(\mathbf{r})$ is governed by

$$\nabla \cdot \mathbf{w}_S = 0, \ -\nabla p_S + \nabla^2 \mathbf{w}_S - \mathbf{F}_{0,D} \delta(\mathbf{r}) = \mathbf{0}. \tag{6.32}$$

Hence, the matching condition simplifies to

$$\mathbf{w}_S(\mathbf{r}) + \lim_{r \gg 1} \epsilon \mathbf{w}_1'(\mathbf{r}) \Leftrightarrow \lim_{\tilde{r} \ll 1} \epsilon \tilde{\mathbf{w}}'(\tilde{\mathbf{r}}). \tag{6.33}$$

Setting $r = \tilde{r}/\epsilon$ in $\mathbf{w}_S(\mathbf{r})$, we get $\mathbf{w}_S(\mathbf{r}) = \epsilon \mathbf{w}_S(\tilde{\mathbf{r}})$. As $\mathbf{w}_S(\tilde{\mathbf{r}})$ is a homogeneous function in $\tilde{r}$, we have

$$\mathbf{w}_S(\tilde{\mathbf{r}}) = \lim_{\tilde{r} \ll 1} \mathbf{w}_S(\tilde{\mathbf{r}}). \tag{6.34}$$

Using these, the matching condition becomes

$$\begin{aligned} \lim_{r \gg 1} \epsilon \mathbf{w}_1'(\mathbf{r}) &\Leftrightarrow \lim_{\tilde{r} \to 0} \epsilon \left[\tilde{\mathbf{w}}'(\tilde{\mathbf{r}}) - \mathbf{w}_S(\tilde{\mathbf{r}})\right] \\ &\Leftrightarrow \lim_{\tilde{r} \to 0} \frac{\epsilon}{8\pi^3} \int \left[\hat{\mathbf{w}}'(\mathbf{k}) - \hat{\mathbf{w}}_S(\mathbf{k})\right] e^{i\mathbf{k}\cdot\tilde{\mathbf{r}}} d\mathbf{k}. \end{aligned} \tag{6.35}$$

We rescale the length in equation (6.32), use $\mathbf{w}_S(\mathbf{r}) = \epsilon \mathbf{w}_S(\tilde{\mathbf{r}})$ and solve the resulting equation in Fourier space to find the Fourier transform of $\mathbf{w}_S(\tilde{\mathbf{r}})$ namely $\hat{\mathbf{w}}_S(\mathbf{k})$

$$\hat{\mathbf{w}}_S = \frac{F_e}{k^2} \mathbf{E} \cdot \mathbf{e}_3. \tag{6.36}$$

We now simplify the integral in the matching condition. Following Zvirin & Chadwick [148], we divide the region of integration into two parts—one region in which $k \leq \tilde{r}^{-\sigma}$

and the other region in which $k > \tilde{r}^{-\sigma}$, where $0 < \sigma < 1$. We can show that the integral over latter region is much less than $O(\epsilon)$ and hence it does not contribute to the matching condition while the integral over former region is $O(\epsilon)$ and it is a uniform flow (see Appendix 6.8 for this calculation). Hence, the matching condition simplifies to

$$\lim_{r\gg 1} \mathbf{w}_1'(\mathbf{r}) \Leftrightarrow \frac{1}{8\pi^3}\int \left[\hat{\mathbf{w}}'(\mathbf{k}) - \hat{\mathbf{w}}_S(\mathbf{k})\right] d\mathbf{k}, \tag{6.37}$$

where the right hand side of the matching condition is a uniform flow.

Recall that the first order disturbance flow in the inner zone $\mathbf{w}_1'$ satisfies the Stokes equations along with the conditions $\mathbf{w}_1'|_{r=1} = \mathbf{U}_1$, the matching condition (6.37) and the force-free constraint $\mathbf{F}_{1,D} = \mathbf{0}$. A simple guess $\mathbf{w}_1' = \mathbf{U}_1 =$ uniform flow on the right hand side of the matching condition satisfies all the constraints. After simplifying the integral in this uniform flow, we obtain

$$\mathbf{w}_1' = \mathbf{U}_1 = U_1\mathbf{e}_3, \quad U_1 = U_{1S} = \frac{F_e}{4\pi^2}\int_{k=0}^{\infty} dk \int_{\theta=0}^{\pi} d\theta \frac{\sin^5\theta}{\cos^2\theta - k^4 - 1 + i\frac{Pe}{\epsilon}\cos\theta k^3 U_0}. \tag{6.38a, b}$$

For a vertically towed rigid sphere, $\mathbf{U} = U\mathbf{e}_3$ is constant, $F_e = 6\pi U$, and the expression for the far-field uniform flow when $U = 1$

$$\frac{3}{2\pi}\int_{k=0}^{\infty} dk \int_{\theta=0}^{\pi} d\theta \frac{\sin^5\theta}{\cos^2\theta - k^4 - 1 + i\frac{Pe}{\epsilon}\cos\theta k^3}$$

matches with that reported by Mehaddi *et al.* [150] (take the limit $l_s/l_o \to 0$ at fixed $l_s Pr/l_o$ in equation (5.3b) of Ref. [150], where the Oseen length scale, $l_o = a/Re$ is the distance from the sphere at which the inertia forces become as important as the viscous forces).

We now provide the expressions for the flow field and the swimming velocity for the swimmer positions at which $\frac{U_{Sed}}{U_{Swim}} \sim \frac{1}{\epsilon}$ and $\frac{U_{Sed}}{U_{Swim}} \gg \frac{1}{\epsilon}$ by relegating the derivations to Appendix 6.9. For these positions, as the swimmer still experiences a $O(1)$ external force, the flow field in the outer zone is the same as that given in equation (6.29). But the flow field in the inner zone and the swimming velocity are different from

those derived for the case $\frac{U_{Sed}}{U_{Swim}} \sim O(1)$. When the swimmer position is such that $\frac{U_{Sed}}{U_{Swim}} \sim \frac{1}{\epsilon}$, the flow field in the inner zone and the swimming velocity are given as

$$\mathbf{w}' = \mathbf{w}'_0 + \epsilon \mathbf{w}'_1|_{b_1=0}, \tag{6.39}$$

$$\mathbf{U} = U\mathbf{e}_3,\ U = U_0 + \epsilon U_1|_{b_1=0}, \tag{6.40}$$

where $\mathbf{w}'_0$, U_0, $\mathbf{w}'_1$ and U_1 are given by equations (6.22)-(6.24), (6.38). These expressions make sense because b_1 is $O(\epsilon)$ in this case, so terms of the form ϵb_1 can be neglected as we are seeking corrections accurate to $O(\epsilon)$. Similarly, for the swimmer positions at which $\frac{U_{Sed}}{U_{Swim}} \gg \frac{1}{\epsilon}$, the flow field in the inner zone and the swimming velocity are

$$\mathbf{w}' = (\mathbf{w}'_0 + \epsilon \mathbf{w}'_1)|_{b_1=b_2=0}, \tag{6.41}$$

$$\mathbf{U} = U\mathbf{e}_3,\ U = (U_0 + \epsilon U_1)|_{b_1=0}, \tag{6.42}$$

where again $\mathbf{w}'_0$, U_0, $\mathbf{w}'_1$ and U_1 are given by equations (6.22)-(6.24), (6.38). Again these expressions seem logical because $b_1 \ll \epsilon$, $b_2 = \beta b_1 \ll \epsilon$, $\beta = B_2/B_1$, so their contribution to flow field and swimming velocity at both leading order and first order can be neglected. In summary, we see that we can derive the solution $\mathbf{w}'$, $\mathbf{U}$ for $\frac{U_{Sed}}{U_{Swim}} \gg 1$ by neglecting the higher order terms in the solution derived for $\frac{U_{Sed}}{U_{Swim}} \sim O(1)$. For this reason, we expect the solution given in equations (6.22)-(6.24), (6.38) to be valid for a broader range $\frac{U_{Sed}}{U_{Swim}} \geq O(1)$ which corresponds to the swimmer's position relative to its neutrally buoyant position $\left|x_{s3} - x_{s3}^{nb}\right| \geq O\left(\frac{9}{2Ri_{U_{Swim}}}\right)$.

6.3.2 Neutrally buoyant pusher or puller

In this case, the far-field representation of the swimmer is a Stresslet which is different from the far-field representation of a towed sphere. Hence, the solution procedure for this case is different from that reported for a towed sphere.

We again try a regular perturbation in Ri assuming $Re \ll 1$. We call the leading order variables in Ri as $\mathbf{w}_0'$, p_0', ρ_0' and $\mathbf{U}_0$. Going back to equations (6.8), (6.9), we see that the buoyancy terms are negligible in the entire domain at the leading order when regular perturbation expansion is used and hence the flow at this order is governed by the Stokes equations. When the swimmer is close to its NBP, we expect it to experience a negligible external force (weight + buoyancy) and a $O(1)$ Stresslet. Hence, the flow field far from the swimmer should be a Stresslet, i.e., for $r \gg 1$, $\mathbf{w}_0' \sim 1/r^2$. As $\mathbf{w}_0'$ is $O(1)$ on the swimmer's surface (see equation (6.13)), we expect $\mathbf{w}_0' \sim O(1)$ for $r \sim O(1)$. We find same scalings for $\mathbf{w}_0'$, both close to and far from the swimmer, by analyzing the exact expressions for $\mathbf{w}_0'$ given in equations (6.47)-(6.49). Again, the leading order density disturbance ρ_0' is governed by the advection-diffusion equation

$$Pe\left(\mathbf{w}_0' \cdot \nabla \rho_0' - \mathbf{U}_0 \cdot \nabla \rho_0' - \mathbf{w}_0' \cdot \mathbf{e}_3\right) = \nabla^2 \rho_0',$$

where $\mathbf{w}_0'$, $\mathbf{U}_0$ are now given by equations (6.47)-(6.49). To solve this equation, we carry out a small Pe expansion to find that (see Appendix 6.10 for this calculation)

$$\rho_0' \sim \max\left(\frac{1}{r^2}, Pe\right) \text{ for } r < Pe^{-1}. \tag{6.43}$$

Hence, for $r \sim O(1)$, $\rho_0' \sim O(1)$ and for $Pe^{-1} > r \gg Pe^{-1/2}$, $\rho_0' \sim Pe$. To check if the buoyancy terms are negligible compared to viscous terms in the entire domain and hence to examine the validity of regular perturbation expansion in Ri, we estimate the order of magnitude of viscous and buoyancy terms both close to and far from the swimmer. Close to the swimmer $r \sim O(1)$, the viscous terms $\nabla^2 \mathbf{w}_0' \sim O(1)$ and the buoyancy terms $Ri\rho_0' \sim Ri \ll O(1)$. Hence, close to the swimmer, the buoyancy terms are negligible. Far away from the swimmer $Pe^{-1} > r \gg Pe^{-1/2}$, the viscous terms $\nabla^2 \mathbf{w}_0' \sim 1/r^4$ while the buoyancy terms $Ri\rho_0' \sim RiPe$. Hence, at $r \sim \frac{1}{\epsilon} \gg 1$, the buoyancy terms are not negligible and are as important as the viscous terms. As this violates the notion of regular perturbation expansion (in Ri) according to which the buoyancy terms are negligible in the entire domain at leading order, we should do a singular perturbation expansion in Ri (or ϵ). As mentioned

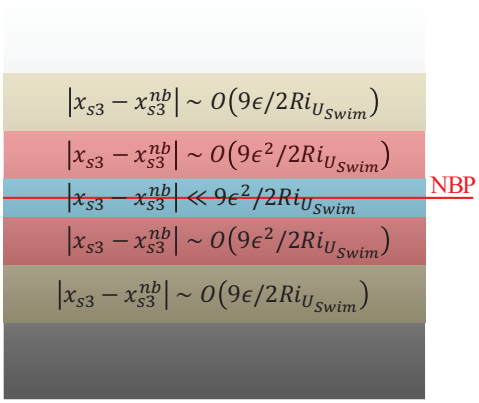

Figure 6.4. : A region in which the swimmer is termed neutrally buoyant $\left|x_{s3} - x_{s3}^{nb}\right| \ll \frac{9}{2Ri_{U_{Swim}}}$ (green region in figure 6.2) is divided into three subregions for the ease of analysis: (a) $\left|x_{s3} - x_{s3}^{nb}\right| \sim O\left(\frac{9\epsilon}{2Ri_{U_{Swim}}}\right)$, (b) $\left|x_{s3} - x_{s3}^{nb}\right| \sim O\left(\frac{9\epsilon^2}{2Ri_{U_{Swim}}}\right)$, and (c) $\left|x_{s3} - x_{s3}^{nb}\right| \ll \frac{9\epsilon^2}{2Ri_{U_{Swim}}}$. In these three regions, respectively, $\frac{U_{Sed}}{U_{Swim}} \sim O(\epsilon)$, $\frac{U_{Sed}}{U_{Swim}} \sim O(\epsilon^2)$, and $\frac{U_{Sed}}{U_{Swim}} \ll \epsilon^2$.

in the previous section, in a singular perturbation expansion, we analyze separately the region close to and far away from the swimmer ensuring the solution in these two regions matches in the common domain of validity. We call the region close to the swimmer ($1 \leq r \leq O(1/\epsilon)$) the inner region and in this region, the buoyancy effects are negligible. Similarly, we call the region far away from the swimmer ($r > O(1/\epsilon)$) the outer region and in this region the buoyancy effects are as important as the viscous effects. As the density scale $\rho_0' \sim Pe$ valid for $Pe^{-1} < r \ll Pe^{-1/2}$ is used in determining the boundary layer location $r \sim 1/\epsilon$, we expect the singular perturbation analysis to hold for $Pe^{-1} < \frac{1}{\epsilon} \ll Pe^{-1/2}$ or $\epsilon^2 \ll Pe < \epsilon$. With respect to perturbation in ϵ, we see that the boundary layer structure for a neutrally buoyant squirmer is the same as that found for a non-neutrally buoyant squirmer.

We again split the range of swimmer positions at which it is neutrally buoyant $\frac{U_{Sed}}{U_{Swim}} \ll 1$ into three regimes—(a) $\frac{U_{Sed}}{U_{Swim}} \sim \epsilon$, (b) $\frac{U_{Sed}}{U_{Swim}} \sim \epsilon^2$ and (c) $\frac{U_{Sed}}{U_{Swim}} \ll \epsilon^2$ (see figure 6.4). The idea behind such splitting process is given as follows: as the swimmer moves towards its NBP, the dimensionless slip stays the same but the external force

(weight + buoyancy) acting on the swimmer decreases from $O(\epsilon)$ $\left(\frac{U_{Sed}}{U_{Swim}} \sim \epsilon\right)$ to $O(\epsilon^2)$ $\left(\frac{U_{Sed}}{U_{Swim}} \sim \epsilon^2\right)$ and to $\ll \epsilon^2$ $\left(\frac{U_{Sed}}{U_{Swim}} \ll \epsilon^2\right)$. So, it is appropriate to analyze the three cases separately. For simplicity, we do not examine the first regime. When $\frac{U_{Sed}}{U_{Swim}} \sim \epsilon^2$, the external force being $O(\epsilon^2)$ it only affects the first order flow field and the swimming velocity while for $\frac{U_{Sed}}{U_{Swim}} \ll \epsilon^2$, the external force $\ll \epsilon^2$ and hence it does not affect the flow and swimming velocity accurate to $O(\epsilon^2)$. Here, we restrict the Reynolds number and the swimmer's position limiting the validity of singular perturbation calculation to

$$\epsilon \ll 1,\ \epsilon^2 \ll Pe < \epsilon,\ Re \ll \epsilon^2,\ \frac{U_{Sed}}{U_{Swim}} \sim \epsilon^2. \tag{6.44}$$

The limit on Re ensures the inertia effects are negligible everywhere while the last condition restricts the swimmer positions to $\left|x_{s3} - x_{s3}^{nb}\right| \sim O\left(\frac{9\epsilon^2}{2Ri_{U_{Swim}}}\right)$. We will again show later how our calculation is valid in a broader context than the restrictions imposed by these limits. Specifically, we will show that the flow field and the swimming velocity found are valid for a broader range of swimmer positions $\frac{U_{Sed}}{U_{Swim}} \leq O(\epsilon^2)$ or $\left|x_{s3} - x_{s3}^{nb}\right| \leq O\left(\frac{9\epsilon^2}{2Ri_{U_{Swim}}}\right)$. We will also show that the flow field found is valid at both small and large Pe while the swimming velocity derived is valid for all Pe.

Inner zone

In this zone, all the variables can be expanded as follows

$$\begin{aligned} \{\mathbf{w}', p', \mathbf{U}\} &= \{\mathbf{w}_0', p_0', \mathbf{U}_0\} + \epsilon^2 \{\mathbf{w}_1', p_1', \mathbf{U}_1\} + o\left(\epsilon^2\right), \\ \rho' &= \rho_0' + o(1). \end{aligned} \tag{6.45}$$

As $\frac{U_{Sed}}{U_{Swim}} \sim \epsilon^2$, the external force acting on the swimmer is $O(\epsilon^2)$. Hence, the swimmer experiences a non-zero drag at $O(\epsilon^2)$ while the drag at $O(1)$ is zero. So, the expansion for drag looks like

$$\mathbf{F}_D = \epsilon^2 \mathbf{F}_{1,D} + o\left(\epsilon^2\right), \tag{6.46}$$

where $\mathbf{F}_{1,D}$ using (6.15) is $\mathbf{F}_{1,D} = -F_e \mathbf{e}_3/\epsilon^2$.

Similar to the non-neutrally buoyant squirmer, the leading order disturbance flow satisfies the Stokes equations with the boundary condition $\mathbf{w}_0'|_{r=1} = \mathbf{U}_0 + \mathbf{u}^s$. But unlike a non-neutrally buoyant squirmer, a neutrally buoyant squirmer does not experience any drag at this order. Hence, the leading order disturbance flow $\mathbf{w}_0'$ is simply the flow due to a squirmer in a homogeneous fluid of density ρ_s [15, 85] while the leading order swimming velocity $\mathbf{U}_0$ is equal to the velocity of a squirmer in a homogeneous fluid of density ρ_s

$$\mathbf{w}_0' = w_{0r}'\mathbf{e}_r + w_{0\theta}'\mathbf{e}_\theta,\ \mathbf{U}_0 = U_0\mathbf{e}_3, \tag{6.47}$$

$$\begin{aligned} w_{0r}' =& \frac{\left(-9r^2+9\right)b_2\cos^2\theta + 4b_1 r\cos\theta + \left(3r^2-3\right)b_2}{6r^4}, \\ w_{0\theta}' =& \frac{\sin\theta\left(3\cos\theta b_2 + b_1 r\right)}{3r^4}, \end{aligned} \tag{6.48}$$

$$U_0 = \frac{2b_1}{3}. \tag{6.49}$$

The first order flow also satisfies the Stokes equations with the boundary condition $\mathbf{w}_1'|_{r=1} = \mathbf{U}_1$. The swimmer experiences a non-zero drag at this order $\mathbf{F}_{1,D} = -F_e\mathbf{e}_3/\epsilon^2$. Again, the boundary condition far from the swimmer is determined by matching the flows in the inner and outer zones.

Outer zone

In this zone, we represent the swimmer by a force dipole and add a term $\mathbf{S}\cdot\nabla\delta(\mathbf{r})$ on the right hand side of the Navier-Stokes equations [191] as the swimmer exerts the Stresslet $\mathbf{S} = \frac{4\pi}{3}b_2\left(3\mathbf{e}_3\mathbf{e}_3 - \mathbf{I}\right)$ on the fluid [85]. Here the Stresslet is non-dimensionalized by $\rho_\infty\nu a^2 u_c$. Far away from the swimmer, as $\mathbf{w}' \sim 1/r^2 \ll \mathbf{U}$, we neglect $\mathbf{w}'\cdot\nabla\rho'$ in comparison to $\mathbf{U}\cdot\nabla\rho'$. We rescale the length, velocity, pressure and density as $\tilde{r} = \epsilon r$, $\mathbf{w}' = \epsilon^2\tilde{\mathbf{w}}'$, $p' = \epsilon^3\tilde{p}'$ and $\rho' = Pe\tilde{\rho}'$. In terms of these rescaled variables, the leading order disturbance flow and density in the outer zone are governed by

$$\tilde{\nabla}\cdot\tilde{\mathbf{w}}' = 0, \tag{6.50}$$

$$-\tilde{\nabla}\tilde{p}' + \tilde{\nabla}^2\tilde{\mathbf{w}}' - \tilde{\rho}'\mathbf{e}_3 + \mathbf{S}\cdot\tilde{\nabla}\delta\left(\tilde{\mathbf{r}}\right) = \mathbf{0}, \tag{6.51}$$

$$-Pe\left(\mathbf{U}_0\cdot\tilde{\nabla}\tilde{\rho}'\right) - \epsilon\left(\tilde{\mathbf{w}}'\cdot\mathbf{e}_3\right) = \epsilon\,\tilde{\nabla}^2\tilde{\rho}'. \tag{6.52}$$

Again, as these equations are linear, we solve them in Fourier space, where the definition of Fourier and inverse Fourier transforms is given in equation (6.28). In Fourier space, the flow is

$$\hat{\mathbf{w}}'\left(\mathbf{k}\right) = i\left[k^2\mathbf{I} + \mathbf{A} - \mathbf{B}\right]^{-1}\mathbf{E}\mathbf{S}\mathbf{k}, \tag{6.53}$$

where the expression for the tensors $\mathbf{A}$, $\mathbf{B}$, and $\mathbf{E}$ are given in equation (6.30). Again, we represented the tensors as matrices while vectors as column matrices in the above equation.

Matching Condition

Enforcing the flow in the inner zone and the outer zone to have the same functional form in the matching zone ($r \gg 1$ or $\tilde{r} \ll 1$), the matching condition is

$$\lim_{r\gg 1}\left[\mathbf{w}_0'\left(\mathbf{r}\right) + \epsilon^2\mathbf{w}_1'\left(\mathbf{r}\right)\right] \Leftrightarrow \lim_{\tilde{r}\ll 1}\epsilon^2\tilde{\mathbf{w}}'\left(\tilde{\mathbf{r}}\right). \tag{6.54}$$

At leading order, as the swimmer experiences a Stresslet $\mathbf{S}$, far away from the swimmer, the leading order flow $\mathbf{w}_0'\left(\mathbf{r}\right)$ should be the same as the Stresslet flow $\mathbf{w}_{SS}\left(\mathbf{r}\right)$ i.e., for $r \gg 1$, $\mathbf{w}_0'\left(\mathbf{r}\right) \sim \mathbf{w}_{SS}\left(\mathbf{r}\right)$, where $\mathbf{w}_{SS}\left(\mathbf{r}\right)$ is governed by

$$\nabla\cdot\mathbf{w}_{SS} = 0,\ -\nabla p_{SS} + \nabla^2\mathbf{w}_{SS} + \mathbf{S}\cdot\nabla\delta\left(\mathbf{r}\right) = \mathbf{0}. \tag{6.55}$$

Hence, the matching condition reduces to

$$\mathbf{w}_{SS}\left(\mathbf{r}\right) + \lim_{r\gg 1}\epsilon^2\mathbf{w}_1'\left(\mathbf{r}\right) \Leftrightarrow \lim_{\tilde{r}\ll 1}\epsilon^2\tilde{\mathbf{w}}'\left(\tilde{\mathbf{r}}\right). \tag{6.56}$$

Setting $r = \tilde{r}/\epsilon$ in $\mathbf{w}_{SS}\left(\mathbf{r}\right)$, we get $\mathbf{w}_{SS}\left(\mathbf{r}\right) = \epsilon^2\mathbf{w}_{SS}\left(\tilde{\mathbf{r}}\right)$. Using the fact that $\mathbf{w}_{SS}\left(\tilde{\mathbf{r}}\right)$ is a homogeneous function in $\tilde{r}$ (see equation (6.34)), the matching condition becomes

$$\begin{aligned}\lim_{r\gg 1}\epsilon^2\mathbf{w}_1'\left(\mathbf{r}\right) &\Leftrightarrow \lim_{\tilde{r}\to 0}\epsilon^2\left[\tilde{\mathbf{w}}'\left(\tilde{\mathbf{r}}\right) - \mathbf{w}_{SS}\left(\tilde{\mathbf{r}}\right)\right] \\ &\Leftrightarrow \lim_{\tilde{r}\to 0}\frac{\epsilon^2}{8\pi^3}\int\left[\hat{\mathbf{w}}'\left(\mathbf{k}\right) - \hat{\mathbf{w}}_{SS}\left(\mathbf{k}\right)\right]e^{i\mathbf{k}\cdot\tilde{\mathbf{r}}}d\mathbf{k}.\end{aligned} \tag{6.57}$$

As usual, we rescale the length in equation (6.55), use $\mathbf{w}_{SS}(\mathbf{r}) = \epsilon^2 \mathbf{w}_{SS}(\tilde{\mathbf{r}})$ and solve the resulting equation in Fourier space to find the Fourier transform of $\mathbf{w}_{SS}(\tilde{\mathbf{r}})$ namely $\hat{\mathbf{w}}_{SS}(\mathbf{k})$

$$\hat{\mathbf{w}}_{SS} = \frac{i}{k^2}\mathbf{E}\cdot(\mathbf{S}\cdot\mathbf{k}). \tag{6.58}$$

Following the arguments of Zvirin & Chadwick [148], we simplify the integral appearing in the matching condition to find that it is a uniform flow (see Appendix 6.11 for this calculation). Hence, the matching condition becomes

$$\lim_{r\gg 1}\mathbf{w}_1'(\mathbf{r}) \Leftrightarrow \frac{1}{8\pi^3}\int\left[\hat{\mathbf{w}}'(\mathbf{k}) - \hat{\mathbf{w}}_{SS}(\mathbf{k})\right]d\mathbf{k}, \tag{6.59}$$

where the right hand side of the matching condition is a uniform flow.

Recall that the first order disturbance flow in the inner zone $\mathbf{w}_1'$ satisfies the Stokes equations along with the condition $\mathbf{w}_1'|_{r=1} = \mathbf{U}_1$, the matching condition (6.59), and the constraint on the drag $\mathbf{F}_{1,D} = -F_e\mathbf{e}_3/\epsilon^2$. Given the linearity of the problem, $\mathbf{w}_1'$ is simply the sum of flow due to a sphere experiencing an external force $F_e\mathbf{e}_3/\epsilon^2$ in a homogeneous quiescent ambient fluid (denote this flow by $\mathbf{w}_{1e}'$) and the uniform flow given on the right hand side of the matching condition (denote this flow by $U_{1SS}\mathbf{e}_3$). Similarly, the swimming velocity $\mathbf{U}_1$ is the sum of sedimentation velocity of a sphere experiencing an external force $F_e\mathbf{e}_3/\epsilon^2$ and the uniform flow given on the right hand side of the matching condition. After simplifying the integral in the matching condition, we have

$$\mathbf{w}_1' = \mathbf{w}_{1e}' + U_{1SS}\mathbf{e}_3,\ \mathbf{U}_1 = U_1\mathbf{e}_3,\ U_1 = \frac{2}{9}\frac{a^2 g}{\epsilon^2\nu u_c}\left(1 - \frac{\gamma a}{\rho_\infty}x_{s3} - \alpha\right) + U_{1SS}, \tag{6.60}$$

$$U_{1SS} = \frac{ib_2}{\pi}\int_{k=0}^{\infty}dk\int_{\theta=0}^{\pi}d\theta\frac{k\sin^5\theta\cos\theta}{\cos^2\theta - k^4 - 1 + i\frac{Pe}{\epsilon}\cos\theta k^3 U_0}, \tag{6.61}$$

When $\frac{U_{Sed}}{U_{Swim}} \ll \epsilon^2$, $\mathbf{w}_{1e}'$ and $\frac{2}{9}\frac{a^2 g}{\epsilon^2\nu u_c}\left(1 - \frac{\gamma a}{\rho_\infty}x_{s3} - \alpha\right)$ become negligible compared to U_{1SS} because the external force $F_e \ll \epsilon^2$ at these swimmer positions. Hence, even though we assumed $\frac{U_{Sed}}{U_{Swim}} \sim O(\epsilon^2)$ while deriving the flow field and the swimming velocity, we expect this solution to be valid for a broader range $\frac{U_{Sed}}{U_{Swim}} \leq O(\epsilon^2)$ as long as we neglect terms much smaller than $O(\epsilon^2)$.

Note that the assumption on Pe is used only in finding the gauge functions in the inner zone and the rescalings in the outer zone. Importantly, it is never used in neglecting any terms in the equations governing the outer variables. This makes the outer solution to be valid for any Pe or Pr. Since the stratification induced swimming velocity depends only on the outer solution, we expect the swimming velocity found in Secs. 6.3.1, 6.3.2 to be valid for any Pe or Pr. The origins of this logic can be traced back to the works of Zvirin & Chadwick [148] and Mehaddi *et al.* [150] whose focus was on finding the drag acting on a towed spherical particle in a stratified fluid. The method used by Zvirin & Chadwick [148] is similar to ours except the assumption of large Pe while Mehaddi *et al.* [150] work is valid for small Pe but arbitrary Pr. In the limit of negligible inertia, the drag found by both these works is the same which makes Zvirin & Chadwick's [148] calculation to hold for any Pe or Pr. Given several similarities between the towed particle in a stratified fluid and the swimming microorganism in a stratified fluid, we expect using Zvirin & Chadwick's method [148] either at small or large Pe, as we did, should generate swimming velocity that is valid for any Pe or Pr.

As the outer solution is valid for all Pe while the gauge functions in the inner zone are valid at small Pe, we expect the inner solution to be valid at small Pe. But since, the boundary conditions on the swimmer surface do not depend on Pe, the matching condition is of the similar form at both small and large Pe, and the flow field in the inner zone at both leading and first order satisfy the Stokes equations for both small and large values of Pe (see Zvirin & Chadwick [148] for large Pe calculation associated with a towed particle in a stratified fluid), the inner solution becomes valid at both small and large Pe. At large Pe, $\mathbf{w}_1' \sim O\left(Ri^{1/3}/\epsilon\right)$ instead of $O(1)$ for non-neutrally buoyant swimmer while $\mathbf{w}_1' \sim O\left(Ri^{2/3}/\epsilon^2\right)$ instead of $O(1)$ for a neutrally buoyant swimmer.

For thermal stratification $l_s \approx 500\ \mu\text{m} - 40$ mm and for salt stratification $l_s \approx 100\ \mu\text{m} - 10$ mm [186]. Hence, organisms of size $50\ \mu\text{m} - 4$ mm in temperature stratified water and those of size $10\ \mu\text{m} - 1$ mm in salt stratified water experience

weak stratification. Organisms should also be small enough to have negligible inertia. Most bacteria and plankton in the ocean (size range 1 μm $-$ 100 μm) satisfy both constraints of negligible inertia and weak stratification and our analysis can be applied to study their motion in density-stratified water.

6.4 Swimming velocity

6.4.1 Non-neutrally buoyant squirmer

For simplicity, we consider the situation $\frac{U_{Sed}}{U_{Swim}} \gg \frac{1}{\epsilon}$, then using $u_c = U_{Sed}$, the swimming velocity becomes

$$\mathbf{U} = U\mathbf{e}_3,\ U = \pm\left[1 + \frac{3\epsilon}{2\pi}\underbrace{\int_{k=0}^{\infty} dk \int_{\theta=0}^{\pi} d\theta \frac{\sin^5\theta\left(\cos^2\theta - k^4 - 1\right)}{\left(\cos^2\theta - k^4 - 1\right)^2 + \left(\frac{Pe}{\epsilon}\cos\theta k^3\right)^2}}_{<0}\right]. \tag{6.62}$$

Here, " $-$ " (resp. " $+$ ") should be used for a squirmer located above (resp. below) its neutrally buoyant position. For $\frac{U_{Sed}}{U_{Swim}} \gg \frac{1}{\epsilon}$, the gait of the swimmer does not affect the swimming velocity accurate to $O(\epsilon)$ and because of this, the swimming velocity (as given in equation (6.62)) does not depend on the squirming modes and the swimmer's orientation. In this case, the swimmer is like a settling sphere due to which the resemblance of the expressions for the swimming velocity (equation (6.62)) to the drag acting on a towed sphere (equation (5.3b) in Ref. [150]) is not surprising.

It was reported that stratification enhances the drag acting on a rigid sphere towed at a fixed velocity [148–150]. At a fixed position, the external force (weight + buoyancy) acting on the swimmer is fixed, so the enhanced drag should be counteracted by the reduced swimming velocity to maintain the fixed external force. This explains why stratification reduces the swimming (settling) speed of the swimmer.

Following Mehaddi *et al.* [150], we analyze the variation of the stratification induced swimming velocity with l_s/l_o and Pr in figure 6.5a. For $\frac{l_s}{l_o} \ll Pr^{-1}$, in the outer zone, the buoyancy forces balance the viscous forces and the density transport is gov-

erned by the diffusion. In this case, the stratification induced velocity is constant as given by the first term on the right hand side of equation (6.63) and also as shown by the black horizontal line in figure 6.5a. With an increase in l_s/l_o, the contribution of the advective transport of density increases. When $\frac{l_s}{l_o} \sim Pr^{-1}$, the advection of density is significant enough to deviate the stratification induced velocity from the constant scaling law found for the lowest values of l_s/l_o. This deviation can be seen in the curves reported for $Pr = 7$ and $Pr = 700$. For $Pr^{-1} \ll \frac{l_s}{l_o} \ll Pr^{-1/4}$, in the outer zone, the buoyancy forces still balance the viscous forces but now the density transport is governed by advection. In this case, the stratification induced velocity scales as $Ri^{1/3}$ as given by the second term on the right hand side of equation (6.63) and also as shown by the black solid line at large values of l_s/l_o in figure 6.5a. With a further increase in l_s/l_o, the inertia effects increase. When $\frac{l_s}{l_o} \sim Pr^{-1/4}$, the inertia effects become as important as the buoyancy and viscous effects in the outer zone and our analysis breaks down [150]. For $\frac{l_s}{l_o} \gg Pr^{-1/4}$, in the outer zone, the inertia forces balance the viscous forces while the buoyancy forces are negligible. In this case, the correction to the swimming velocity scales as Re and this can be deduced from the calculation of the drag acting on a towed sphere in a homogeneous fluid at small Re [151].

$$U = \begin{cases} \pm \left[1 - \dfrac{5\epsilon}{14} E_k\left(\dfrac{1}{\sqrt{2}}\right)\right] & \text{for } \dfrac{l_s}{l_o} \ll Pr^{-1} \\ \pm \left[1 - \dfrac{4\pi^2}{15\{\Gamma(2/3)\}^3} Ri^{1/3}\right] & \text{for } Pr^{-1} \ll \dfrac{l_s}{l_o} \ll Pr^{-1/4} \\ \pm \left[1 - \dfrac{3}{8} Re\right] & \text{for } \dfrac{l_s}{l_o} \gg Pr^{-1/4} \end{cases} \tag{6.63}$$

Here, E_k is the complete elliptic integral of the first kind while Γ is the gamma function.

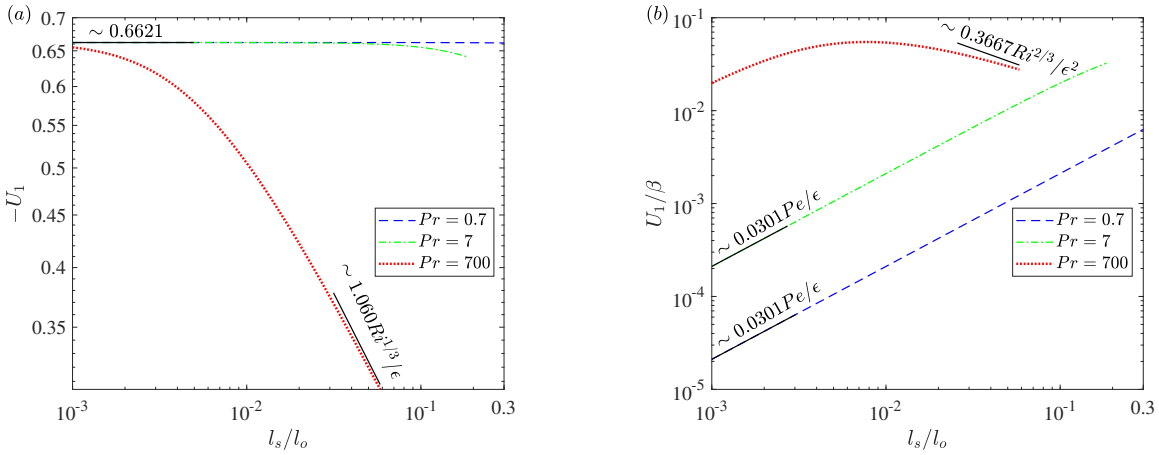

Figure 6.5. : (Colour online) The variation of the stratification induced velocity of (a) non-neutrally buoyant squirmer $\left(\frac{U_{Sed}}{U_{Swim}} \gg \frac{1}{\epsilon}\right)$ and (b) neutrally buoyuant pusher or puller $\left(\frac{U_{Sed}}{U_{Swim}} \ll \epsilon^2\right)$ with l_s/l_o and Pr. The black solid lines in figures (a), (b) represent the scaling laws mentioned in equations (6.63), (6.65), respectively. Here $Pr = 0.7, 7, 700$ are the Prandtl number values of a temperature stratified air, temperature stratified water and salt stratified water, respectively. The swimmer is above its neutrally buoyant position in (a) whereas it is oriented vertically upwards in (b).

6.4.2 Neutrally buoyant pusher or puller

For simplicity, we consider the situation $\frac{U_{Sed}}{U_{Swim}} \ll \epsilon^2$, then using $u_c = U_{Swim}$, the swimming velocity becomes

$$\mathbf{U} = U\mathbf{e}_3,\, U = \pm\left[1 + \frac{3\beta\epsilon^2}{2\pi}\underbrace{\int_{k=0}^{\infty} dk \int_{\theta=0}^{\pi} d\theta \frac{\frac{Pe}{\epsilon}k^4 \sin^5\theta\cos^2\theta}{\left(\cos^2\theta - k^4 - 1\right)^2 + \left(\frac{Pe}{\epsilon}\cos\theta k^3\right)^2}}_{>0}\right]. \tag{6.64}$$

Here, "−" (resp. "+") should be used for a squirmer oriented along (resp. opposite to) the gravity direction and $\beta = B_2/B_1$. As the stratification induced swimming velocity depends only on the Stresslet exerted by the swimmer in a homogeneous fluid, which itself does not depend on the swimmers orientation (note the upwards as well as the downwards oriented swimmers exert the same Stresslet in a homogeneous fluid), we expect the swimmer to experience the same speed modifications due to stratification irrespective of whether it is swimming up or down the density gradients. This means if a swimmer experiences a speed reduction when moving towards high densities, it experiences an exactly same speed reduction even if moving towards low densities. When $\frac{U_{Sed}}{U_{Swim}} \ll \epsilon^2$, the swimmer is so close to its neutrally buoyant position $\left(\left|x_{s3}^{nb} - x_{s3}\right| \ll \frac{9\epsilon^2}{2Ri_{U_{Swim}}}\right)$ that the sum of the swimmer's weight and buoyancy is much less than $O\left(\epsilon^2\right)$ and because of this the stratification induced swimming velocity does not depend on the separation of the swimmer from its neutrally buoyant position.

The stratification increases the swimming speed of a puller swimmer ($\beta > 0$) while it reduces the speed of a pusher swimmer ($\beta < 0$) by the same amount. This observation is consistent with the DNS results reported for $Pr = 700$, $Re = 0.05$ and small Ri [87]. In their simulations, Doostmohammadi *et al.* [87] considered a two-mode squirmer with density $\rho_s = \rho_\infty - \gamma x_{s3}$ (ambient density evaluated at swimmer's position) and this swimmer is same as the neutrally buoyant squirmer considered here for the swimmer positions $\frac{U_{Sed}}{U_{Swim}} \ll \epsilon^2$. Furthermore, the effect of stratification is exactly opposite to the effect of inertia, which reduces (resp. increases) the swimming speed of a puller (resp. pusher) swimmer [97].

As swimmer propels upwards, it traps heavier fluid and disturbs the isopycnals from their stable stratification situation (see figure 2 and the associated discussion in Ref. [87]). A pusher swimmer traps the heavier fluid infront of it. The buoyancy of this trapped fluid and the isopycnal retreat direction is opposite to the propulsive direction of the swimmer and hence the stratification reduces the speed of the pusher swimmer. A puller swimmer traps the heavier fluid behind it. Even though the buoyancy of this trapped fluid points opposite to the swimming direction, the isopycnals retreat along the swimming direction and since the forces associated with the latter dominate those of the former, the stratification increases the speed of a puller swimmer.

Again, we analyze the variation of the stratification induced swimming velocity with l_s/l_o and Pr in figure 6.5b. Similar to a non-neutrally buoyant swimmer, for $\frac{l_s}{l_o} \ll Pr^{-1}$, the buoyancy governed by diffusion balances the viscous forces in the outer zone, for $Pr^{-1} \ll \frac{l_s}{l_o} \ll Pr^{-1/4}$, the buoyancy governed by advection balances the viscous forces in the outer zone and for $\frac{l_s}{l_o} \gg Pr^{-1/4}$, the inertia forces balance the viscous forces in the outer zone. But the scalings of stratification induced swimming velocity with Ri, Pe for a neutrally buoyant swimmer are different from those of a non-neutrally buoyant swimmer. In the diffusion (resp. advection) dominant regime, the stratification induced swimming velocity scales as $Pe\epsilon$ (resp. $Ri^{2/3}$). The diffusive (resp. advective) scaling is given by the first (resp. the second) term on the right hand side of equation (6.65) and also shown by the black solid line for low (resp. high) values of l_s/l_o in figure 6.5b. Similar to a non-neutrally buoyant swimmer, when $\frac{l_s}{l_o} \sim Pr^{-1/4}$, the inertia forces become important and our analysis breaks down. For $\frac{l_s}{l_o} \gg Pr^{-1/4}$, the buoyancy forces become negligible compared to the inertia forces and the correction to the swimming velocity scales as Re as given by the third term

on the right hand side of equation (6.65). This correction was derived by considering a two-mode spherical squirmer in a homogeneous fluid at small Re [97, 192].

$$U = \begin{cases} \pm \left[1 + \dfrac{5\beta}{308} E_k \left(\dfrac{1}{\sqrt{2}}\right) \epsilon Pe\right] & \text{for } \dfrac{l_s}{l_o} \ll Pr^{-1} \\ \pm \left[1 + \dfrac{15\sqrt{3}\beta}{56\pi} \{\Gamma(2/3)\}^3 Ri^{2/3}\right] & \text{for } Pr^{-1} \ll \dfrac{l_s}{l_o} \ll Pr^{-1/4} \\ \pm \left[1 - \dfrac{3\beta}{20} Re\right] & \text{for } \dfrac{l_s}{l_o} \gg Pr^{-1/4} \end{cases} \tag{6.65}$$

6.5 Flow field

In this section, we visualize the flow surrounding a two-mode squirmer at small Pe $\left(Pe \ll \epsilon \text{ or } \frac{l_s}{l_o} \ll Pr^{-1}\right)$ in the lab frame of reference. For this purpose, we plot the flow around a non-neutrally buoyant squirmer $\left(\frac{U_{Sed}}{U_{Swim}} \gg \frac{1}{\epsilon}\right)$ as well as a neutrally buoyant puller $\left(\frac{U_{Sed}}{U_{Swim}} \ll \epsilon^2, \beta = 1\right)$ both close to and far from the squirmer in figure 6.6. In this figure, we also compare the flow in a stratified fluid to that in a homogeneous fluid.

As expected in a singular perturbation analysis, the flow close to a swimmer in a stratified fluid is same as that in a homogeneous fluid. But the flow far from the swimmer in a stratified fluid is significantly different from that in a homogeneous fluid. In this far-field region, the flow around a non-neutrally buoyant squirmer (resp. neutrally buoyant squirmer) in a stratified fluid is same as the flow due to a point force (resp. a force dipole) in a stratified fluid. And this flow due to point force or higher order singularities in a stratified fluid at small Pe was already reported by Ardekani & Stocker [166]. We note that such simple flow picture does not exist around a towed spherical particle or a drop in a stratified fluid due to the non-negligible contributions of the Stokeslet part of the first order inner zone flow field [185].

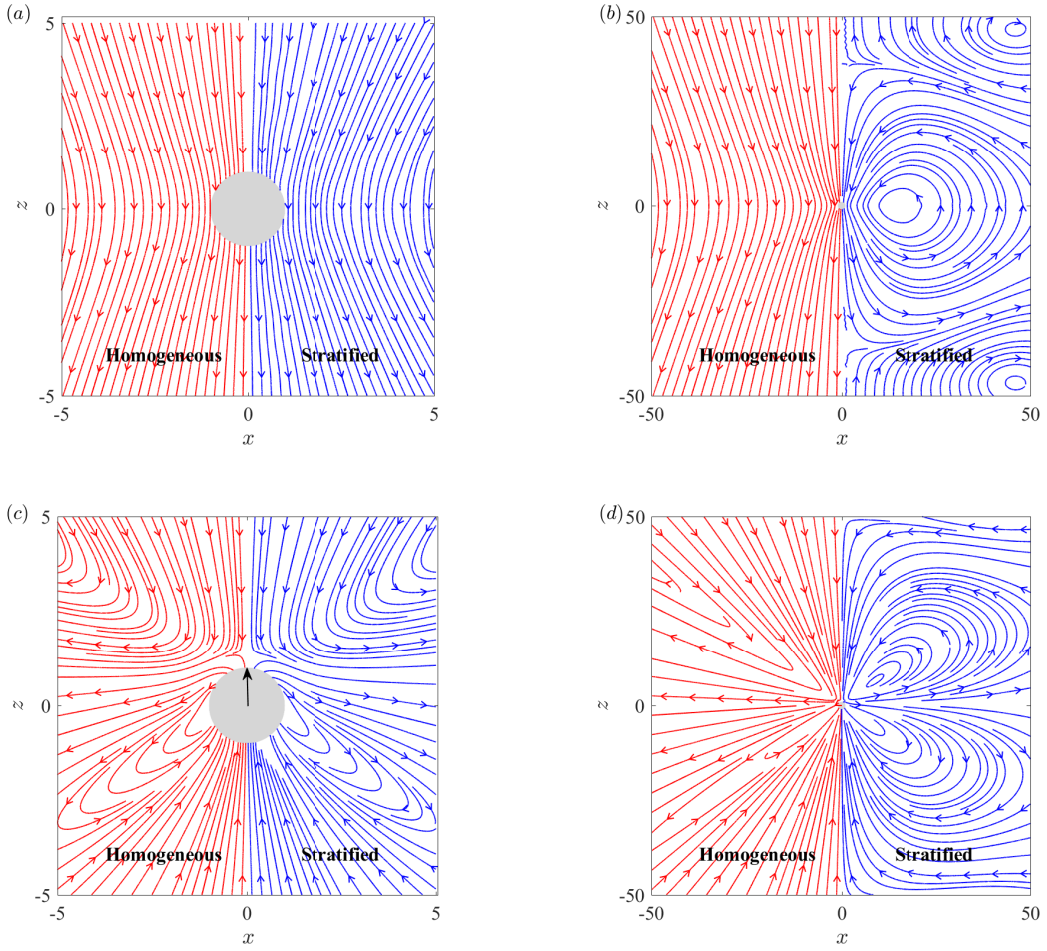

Figure 6.6. : (Colour online) In the lab frame of reference, flow due to a two-mode squirmer close to the swimmer (a, c) and far away from it (b, d). The top row shows the flow due to a non-neutrally buoyant squirmer $\left(\frac{U_{Sed}}{U_{Swim}} \gg \frac{1}{\epsilon}\right)$ located above its neutrally buoyant position while the bottom row shows the flow due to a vertically upward oriented neutrally buoyant puller $\left(\frac{U_{Sed}}{U_{Swim}} \ll \epsilon^2, \beta = 1\right)$. In each figure, the left and right halves show the flow in a homogeneous and stratified fluid $\left(\frac{l_s}{l_o} \ll Pr^{-1}\right)$, respectively. The flow in a stratified fluid is found by forming a composite expansion of the inner zone and the outer zone flow fields [173] where the inverse Fourier transform required for finding the outer zone flow is performed using the IFFT function in MATLAB [174].

6.6 Conclusions

For a two-mode squirmer in a linearly density-stratified fluid, we have derived the swimming velocity as well as the flow field surrounding the swimmer by considering separately the situations of swimmer close to and far from its neutrally buoyant position. We called the swimmer in the former (resp. latter) situation as the neutrally (resp. non-neutrally) buoyant swimmer.

We found that the stratification reduces the speed of a non-neutrally buoyant swimmer while it enhances (resp. reduces) the speed of neutrally buoyant puller (resp. pusher) swimmer. The scaling of the stratification induced swimming velocity of a non-neutrally buoyant swimmer with viscous Richardson number ($\sim$ buoyancy forces/viscous forces) and Peclet number is similar to the scaling of stratification enhanced drag acting on a towed rigid sphere and is different from the scaling of the swimming velocity of a neutrally buoyant swimmer. Close to the swimmer, the stratification does not modify the flow field appreciably. Far from the swimmer, the stratification alters the flow in such a way that this flow is same as the flow due to a point force or force-dipole placed in a stratified fluid. This explains how the point force singularity solution derived in a stratified fluid at small Peclet number [166] gives the far-field flow due to a finite sized microorganisms, still preserving the intuition based on homogeneous fluids.

Our calculation is valid provided the quasi-steady conditions prevail, inertia is negligible, stratification is weak, Boussinesq approximation is applicable, swimmer has a constant density and it is oriented either vertically upwards or downwards. The calculation of swimming velocity holds for any Peclet number while the calculation of flow field is valid at both small and large Peclet numbers. Despite the constant swimmer's density assumption, the motility of organisms that use certain mechanisms to stay neutrally buoyant (see Ref. [188]) can be found by resorting to our neutrally buoyant swimmer calculations. Future works can be directed towards overcoming some assumptions of our work.

The simple formula for swimming velocity developed here can be used in the continuum description of a suspension of swimming organisms to understand why stratification suppresses the bioconvection, in turn causing the aggregation of bottom heavy organism *Heterosigma akashiwo* near haloclines [193]. An extension of our theory to sharp stratifications can also be pursued to understand the reasons behind the accumulation of most of the planktonic organisms near density discontinuities [194, 195].

6.7 Appendix A

In this appendix, we derive the leading order density field ρ_0' when a regular perturbation is taken in terms of Ri for swimmer positions at which $\frac{U_{Sed}}{U_{Swim}} \sim O(1)$. This density field is governed by the advection-diffusion equation

$$Pe\left(\mathbf{w}_0' \cdot \nabla\rho_0' - \mathbf{U}_0 \cdot \nabla\rho_0' - \mathbf{w}_0' \cdot \mathbf{e}_3\right) = \nabla^2\rho_0', \tag{6.66}$$

where the expressions for $\mathbf{w}_0'$, $\mathbf{U}_0$ are given in equations (6.22)-(6.24). Also ρ_0' satisfies the conditions

$$\left.\frac{\partial\rho_0'}{\partial r}\right|_{r=1} = \cos\theta, \quad \rho_0' = 0 \text{ as } r \to \infty. \tag{6.67a, b}$$

We solve for ρ_0' by doing a singular perturbation expansion in Pe. A small Pe expansion of advection-diffusion equation for heat transfer from a sphere placed in an uniform streaming flow is well studied and it was shown to be singular (see Chapter 9 in Ref. [18]). Similar logic can be used to show that a small Pe expansion in our case is also singular. There are two boundary layers: one at $r \sim Pe^{-1/3}$ and the other at $r \sim Pe^{-1}$. We call the region lying between the swimmer and $r < O\left(Pe^{-1/3}\right)$ as the inner zone and the region lying between $r > O\left(Pe^{-1/3}\right)$ and $r < O\left(Pe^{-1}\right)$ as the intermediate zone, and finally the region $r > O\left(Pe^{-1}\right)$ as the outer zone.

In the inner zone, we denote the density field by $\breve{\rho}$. At leading order, it is appropriate to neglect the entire advective term. Hence, the leading order density field in the inner zone $\breve{\rho}_0$ is governed by the following equations

$$\nabla^2 \breve{\rho}_0 = 0, \;\; \left.\frac{\partial \breve{\rho}_0}{\partial r}\right|_{r=1} = \cos\theta. \tag{6.68}$$

The solution of these equations that decays spatially so as to conserve flux on any surface enclosing the swimmer is [18]

$$\breve{\rho}_0 = -\frac{\cos\theta}{2r^2}. \tag{6.69}$$

Using this density field, we estimate the order of magnitude of advective and diffusive terms far away from the swimmer. As $Pe\,(\mathbf{w}_0' \cdot \nabla \rho_0') \sim Pe/r^4$, $Pe\,(\mathbf{U}_0 \cdot \nabla \rho_0') \sim Pe/r^3$ and $Pe\,(\mathbf{w}_0' \cdot \mathbf{e}_3) \sim Pe/r$, the dominant advective term $Pe\,(\mathbf{w}_0' \cdot \mathbf{e}_3) \sim Pe/r$ while the diffusive term $\nabla^2 \rho_0' \sim 1/r^4$. At $r \sim Pe^{-1/3}$, the advective term $Pe\,(\mathbf{w}_0' \cdot \mathbf{e}_3)$ is as important as the diffusive term and this justifies the existence of a boundary layer at $r \sim Pe^{-1/3}$ separating the inner zone where diffusion is prominent from the intermediate zone where both advection (due to $Pe\,(\mathbf{w}_0' \cdot \mathbf{e}_3)$) and diffusion are equally important.

In the intermediate zone, we rescale the variables as $\bar{r} = Pe^{1/3} r$, $\rho_0' = Pe^{2/3} \bar{\rho}$. Retaining only the Stokeslet part of $\mathbf{w}_0'$, the leading order density field in this zone $\bar{\rho}_0$ is governed by the following equation

$$\nabla^2_{\bar{r}} \bar{\rho}_0 = \frac{(2b_1 - 3U_0)}{3\bar{r}} \left(P_0\left(\cos\theta\right) + \frac{1}{2} P_2\left(\cos\theta\right) \right) \tag{6.70}$$

along with the matching condition with the inner zone

$$\lim_{\bar{r} \ll 1} \bar{\rho}_0 \Leftrightarrow -\frac{\cos\theta}{2\bar{r}^2}. \tag{6.71}$$

Here $\nabla^2_{\bar{r}}$ is the Laplacian written in terms of $\bar{r}$ while $P_n\left(\cos\theta\right)$ is the Legendre polynomial of degree n. The solution of these equations that also matches with the density field in the outer zone is

$$\bar{\rho}_0 = A_0 + \bar{r}\left[A_1 P_1\left(\cos\theta\right) + \frac{(2b_1 - 3U_0)}{6} \left(1 - \frac{1}{4} P_2\left(\cos\theta\right) \right) \right] + \frac{A_2}{\bar{r}} - \frac{\cos\theta}{2\bar{r}^2}, \tag{6.72}$$

where A_0, A_1, and A_2 are constants which can be found by matching with the higher order density fields in the inner zone or the leading order density field in the outer zone.

At $\bar{r} \gg 1$ or $r \gg Pe^{-1/3} \gg 1$, we again estimate the order of magnitude of advective and diffusive terms. At these distances, $\bar{\rho}_0 \sim \bar{r}$, hence $\rho_0' \sim Pe^{2/3}\bar{r} \sim Per$. As the advective terms $Pe\,(\mathbf{w}_0' \cdot \nabla\rho_0') \sim Pe^2/r$, $Pe\,(\mathbf{U}_0 \cdot \nabla\rho_0') \sim Pe^2$, and $Pe\,(\mathbf{w}_0' \cdot \mathbf{e}_3) \sim Pe/r$ while the diffusive term $\nabla^2\rho_0' \sim Pe/r$, the dominant advective term $Pe\,(\mathbf{U}_0 \cdot \nabla\rho_0' + \mathbf{w}_0' \cdot \mathbf{e}_3)$ balances the diffusive term at $r \sim Pe^{-1} \gg Pe^{-1/3}$. This justifies the existence of a boundary layer at $r \sim Pe^{-1}$ separating the intermediate zone where advection due to $Pe\,\mathbf{w}_0' \cdot \mathbf{e}_3$ and diffusion are important from the outer zone where advection due to $Pe\,(\mathbf{U}_0 \cdot \nabla\rho_0' + \mathbf{w}_0' \cdot \mathbf{e}_3)$ and diffusion are important.

To find the higher order density fields in the inner zone, we substitute the expansion $\breve{\rho} = \breve{\rho}_0 + Pe^{1/3}\breve{\rho}_1 + Pe^{2/3}\breve{\rho}_2 + O\,(Pe)$ in equations (6.66), (6.67a), collect terms at various orders of Pe, and solve the resulting equations by enforcing matching with the intermediate solution (6.72). Doing so, we find that

$$\breve{\rho}_1 = \breve{\rho}_2 = A_0 = A_2 = 0. \tag{6.73}$$

Hence, the density fields in the inner and the intermediate zones are, respectively,

$$\begin{aligned} \breve{\rho} &= -\frac{\cos\theta}{2r^2} + O\,(Pe)\,, \\ \bar{\rho} &= \bar{r}\left[A_1 P_1\,(\cos\theta) + \frac{(2b_1 - 3U_0)}{6}\left(1 - \frac{1}{4}P_2\,(\cos\theta)\right)\right] - \frac{\cos\theta}{2\bar{r}^2} + O\left(Pe^{1/3}\right). \end{aligned} \tag{6.74}$$

We now write down the composite expansion of density field that is accurate to $O\left(Pe^{2/3}\right)$ and is uniformly valid up to $r < O\,(Pe^{-1})$. For this purpose, we add the density field in the inner zone to the density field in the intermediate zone and subtract the density field in the first matching zone $\left(r \sim Pe^{-1/3}\right)$. As the density field

in this matching zone is $-\cos\theta/2r^2$, writing everything in terms of inner variables, we get

$$\begin{aligned}\rho_0' &= \breve{\rho}_0 + Pe^{2/3}\bar{\rho}_0 + \frac{\cos\theta}{2r^2} + O\left(Pe\right) \\ &= -\frac{\cos\theta}{2r^2} + Per\left[A_1 P_1\left(\cos\theta\right) + \left(\frac{b_1}{3} - \frac{U_0}{2}\right)\left(1 - \frac{1}{4}P_2\left(\cos\theta\right)\right)\right] + O\left(Pe\right).\end{aligned} \tag{6.75}$$

Hence, for $r < O\left(Pe^{-1}\right)$, the density field obeys

$$\rho_0' \sim \max\left(\frac{1}{r^2}, Per\right). \tag{6.76}$$

Since we did not use the boundary condition far from the swimmer, equation (6.67b), we expect the density field and the scaling, equations (6.75), (6.76) to hold even if the perturbation in Ri is singular.

6.8 Appendix B

In this appendix, we simplify the integral appearing in the matching condition (6.35)

$$\lim_{\tilde{r}\to 0}\frac{\epsilon}{8\pi^3}\int\left[\hat{\mathbf{w}}'\left(\mathbf{k}\right) - \hat{\mathbf{w}}_S\left(\mathbf{k}\right)\right]e^{i\mathbf{k}\cdot\tilde{\mathbf{r}}}d\mathbf{k}. \tag{6.77}$$

For this purpose, we divide the domain of integration into two parts—$k \leq \tilde{r}^{-\sigma}$ and $k > \tilde{r}^{-\sigma}$, where $0 < \sigma < 1$.

$$\frac{\epsilon}{8\pi^3}\left\{\lim_{\tilde{r}\to 0}\int\limits_{k\leq\tilde{r}^{-\sigma}}\left[\hat{\mathbf{w}}'\left(\mathbf{k}\right) - \hat{\mathbf{w}}_S\left(\mathbf{k}\right)\right]e^{i\mathbf{k}\cdot\tilde{\mathbf{r}}}d\mathbf{k} + \lim_{\tilde{r}\to 0}\int\limits_{k>\tilde{r}^{-\sigma}}\left[\hat{\mathbf{w}}'\left(\mathbf{k}\right) - \hat{\mathbf{w}}_S\left(\mathbf{k}\right)\right]e^{i\mathbf{k}\cdot\tilde{\mathbf{r}}}d\mathbf{k}\right\}. \tag{6.78}$$

As k is finite in the first integral, we evaluate the limit by directly substituting $\tilde{r} = 0$ to obtain

$$\frac{\epsilon}{8\pi^3}\int\left[\hat{\mathbf{w}}'\left(\mathbf{k}\right) - \hat{\mathbf{w}}_S\left(\mathbf{k}\right)\right]d\mathbf{k} + \frac{\epsilon}{8\pi^3}\lim_{\tilde{r}\to 0}\int\limits_{k>\tilde{r}^{-\sigma}}\left[\hat{\mathbf{w}}'\left(\mathbf{k}\right) - \hat{\mathbf{w}}_S\left(\mathbf{k}\right)\right]e^{i\mathbf{k}\cdot\tilde{\mathbf{r}}}d\mathbf{k}. \tag{6.79}$$

Here the first term being a constant vector represents an uniform flow field. In the second term, $k \gg 1$ and hence $\hat{\mathbf{w}}' - \hat{\mathbf{w}}_S$ simplifies for fixed Pe/ϵ to

$$\frac{\left(k^2 - k_3^2\right)F_e}{k^{10}}\left(k_1 k_3\mathbf{e}_1 + k_2 k_3\mathbf{e}_2 - \left(k^2 - k_3^2\right)\mathbf{e}_3\right). \tag{6.80}$$

Here, we see that $\hat{\mathbf{w}}' - \hat{\mathbf{w}}_S \sim O\left(k^{-6}\right)$, so $\left(\hat{\mathbf{w}}' - \hat{\mathbf{w}}_S\right) d\mathbf{k} \sim O\left(k^{-3}\right)$. Hence the integral

$$\int\limits_{k>\tilde{r}^{-\sigma}} \left[\hat{\mathbf{w}}'\left(\mathbf{k}\right) - \hat{\mathbf{w}}_S\left(\mathbf{k}\right)\right] e^{i\mathbf{k}\cdot\tilde{\mathbf{r}}} d\mathbf{k} \sim O\left(\tilde{r}^{3\sigma}\right) \tag{6.81}$$

and it becomes negligible compared to the first term in equation (6.79) as $\tilde{r} \to 0$.

6.9 Appendix C

In this appendix, we derive the flow field in the inner zone and the swimming velocity for the swimmer positions at which $\frac{U_{Sed}}{U_{Swim}} \sim \frac{1}{\epsilon}$ and $\frac{U_{Sed}}{U_{Swim}} \gg \frac{1}{\epsilon}$. Recall that in the inner zone, the flow field follows the expansion given in equation (6.19), with the leading order and the first order flow fields satisfying the Stokes equations. The boundary condition on the swimmer surface at various order of ϵ changes as the swimmer moves away from its NBP.

6.9.1 $\frac{U_{Sed}}{U_{Swim}} \sim \frac{1}{\epsilon}$

In this case, the slip velocity $b_1\left(\sin\theta + \beta \sin\theta\cos\theta\right)$ is $O\left(\epsilon\right)$ because $b_1 = \frac{B_1}{U_{Sed}} = \frac{3}{2}\frac{U_{Swim}}{U_{Sed}} \sim O\left(\epsilon\right)$. Hence, the slip velocity affects the first order flow field. At leading order, the absence of slip simplifies the problem to a settling sphere of radius a, density ρ_s in a homogeneous fluid of density $\rho_\infty - \gamma x_{s3}$. Hence, the leading order flow field and the swimming velocity are

$$\mathbf{w}'_0 = w'_{0r}\mathbf{e}_r + w'_{0\theta}\mathbf{e}_\theta,\ \mathbf{U}_0 = U_0\mathbf{e}_3, \tag{6.82}$$

$$\begin{aligned} w'_{0r} &= \frac{U_0\left(3r^2-1\right)\cos\theta}{2r^3}, \\ w'_{0\theta} &= -\frac{U_0\left(3r^2+1\right)\sin\theta}{4r^3}, \end{aligned} \tag{6.83}$$

$$U_0 = \frac{2}{9}\frac{a^2 g}{\nu u_c}\left(1 - \frac{\gamma a}{\rho_\infty}x_{s3} - \alpha\right) \tag{6.84}$$

At first order, the flow field satisfies the force-free constraint $\mathbf{F}_{1,D} = \mathbf{0}$ and the conditions

$$\mathbf{w}_1'|_{r=1} = \mathbf{U}_1 + \frac{b_1}{\epsilon}\left(\sin\theta + \beta\sin\theta\cos\theta\right)\mathbf{e}_\theta,\ \lim_{r\gg 1}\mathbf{w}_1' = U_{1S}\mathbf{e}_3, \tag{6.85}$$

where U_{1S} is given by equation (6.38b)

$$U_{1S} = \frac{F_e}{4\pi^2}\int_{k=0}^{\infty} dk \int_{\theta=0}^{\pi} d\theta \frac{\sin^5\theta}{\cos^2\theta - k^4 - 1 + i\frac{Pe}{\epsilon}\cos\theta k^3 U_0}$$

with the expression for U_0 occurring in U_{1S} being given by equation (6.84). Due to the linearity of the problem, we split it into two parts $\{\mathbf{w}_1', \mathbf{u}_1\} = \{\mathbf{w}_{1a}', \mathbf{U}_{1a}\} + \{\mathbf{w}_{1b}', \mathbf{U}_{1b}\}$, where the flow field in both parts satisfy the Stokes equations and force-free constraints with the boundary conditions

$$\mathbf{w}_{1a}'|_{r=1} = \mathbf{U}_{1a} + \frac{b_1}{\epsilon}\left(\sin\theta + \beta\sin\theta\cos\theta\right)\mathbf{e}_\theta,\ \lim_{r\gg 1}\mathbf{w}_{1a}' = \mathbf{0} \tag{6.86}$$

$$\mathbf{w}_{1b}'|_{r=1} = \mathbf{U}_{1b},\ \lim_{r\gg 1}\mathbf{w}_{1b}' = U_{1S}\mathbf{e}_3 \tag{6.87}$$

It is obvious that the subproblem (a) corresponds to a squirmer placed in a homogeneous fluid of density ρ_s while subproblem (b) corresponds to a neutrally buoyant sphere placed in a homogeneous fluid undergoing uniform flow $U_{1S}\mathbf{e}_3$. Hence, we have

$$\mathbf{w}_1' = w_{1r}'\mathbf{e}_r + w_{1\theta}'\mathbf{e}_\theta,\ \mathbf{U}_1 = U_1\mathbf{e}_3, \tag{6.88}$$

$$\begin{aligned}
\epsilon w_{1r}' &= \frac{\left(-9r^2+9\right)b_2\cos^2\theta + 4b_1 r\cos\theta + \left(3r^2-3\right)b_2}{6r^4} + \epsilon U_{1S}\cos\theta,\\
\epsilon w_{1\theta}' &= \frac{\sin\theta\left(3\cos\theta b_2 + b_1 r\right)}{3r^4} - \epsilon U_{1S}\sin\theta,
\end{aligned} \tag{6.89}$$

$$\epsilon U_1 = \frac{2b_1}{3} + \epsilon U_{1S}. \tag{6.90}$$

To summarize, $\mathbf{w}' = \mathbf{w}_0' + \epsilon\mathbf{w}_1'$ = flow due to a settling sphere of radius a, density ρ_s in a homogeneous fluid of density $\rho_\infty - \gamma x_{s3}$ + flow due to a squirmer in a homogeneous fluid of density $\rho_s + \epsilon U_{1S}\mathbf{e}_3$. Similarly $U = U_0 + \epsilon U_1$ = sedimenting velocity of a

sphere of radius a, density ρ_s in a homogeneous fluid of density $\rho_\infty - \gamma x_{s3}$ + velocity of a squirmer in a homogeneous fluid of density $\rho_s + \epsilon U_{1S}$. As U_0 does not depend on b_1, U_{1S} also does not depend on b_1. Hence, we can express the flow field and swimming velocity derived for the case $\frac{U_{Sed}}{U_{Swim}} \sim \frac{1}{\epsilon}$ in terms of those derived for the case $\frac{U_{Sed}}{U_{Swim}} \sim O(1)$ as follows

$$\mathbf{w}' = \mathbf{w}'_0 + \epsilon \mathbf{w}'_1|_{b_1=0}, \tag{6.91}$$

$$\mathbf{U} = U\mathbf{e}_3,\ U = U_0 + \epsilon U_1|_{b_1=0}, \tag{6.92}$$

where $\mathbf{w}'_0$, U_0, $\mathbf{w}'_1$, and U_1 are given by equations (6.22)-(6.24), (6.38).

6.9.2 $\frac{U_{Sed}}{U_{Swim}} \gg \frac{1}{\epsilon}$

In this case, the slip $b_1(\sin\theta + \beta \sin\theta\cos\theta) \ll \epsilon$ because $b_1 = \frac{3}{2}\frac{U_{Swim}}{U_{Sed}} \ll \epsilon$. So, the slip velocity does not affect the flow field and the swimming velocity at both the leading order and the first order. Hence, we can derive the flow field for this case from that found for the case $\frac{U_{Sed}}{U_{Swim}} \sim O(1)$ by setting $b_1 = b_2 = 0$ i.e.,

$$\mathbf{w}' = (\mathbf{w}'_0 + \epsilon \mathbf{w}_1)|_{b_1=b_2=0}. \tag{6.93}$$

Similarly, we can derive the swimming velocity for this case from that found for the case $\frac{U_{Sed}}{U_{Swim}} \sim O(1)$ by setting $b_1 = 0$ i.e.,

$$\mathbf{U} = U\mathbf{e}_3,\ U = (U_0 + \epsilon U_1)|_{b_1=0}. \tag{6.94}$$

In the expression for the swimming velocity, we do not need to set $b_2 = 0$ because the swimming velocity for a non-neutrally buoyant swimmer does not depend on b_2 mode. Here, again $\mathbf{w}'_0$, U_0, $\mathbf{w}'_1$, and U_1 are given by equations (6.22)-(6.24), (6.38).

6.10 Appendix D

In this appendix, we derive the leading order density field ρ_0' when a regular perturbation is taken in terms of Ri for swimmer positions at which $\frac{U_{Sed}}{U_{Swim}} \sim \epsilon^2$. This density field is governed by the advection-diffusion equation

$$Pe\left(\mathbf{w}_0' \cdot \nabla\rho_0' - \mathbf{U}_0 \cdot \nabla\rho_0' - \mathbf{w}_0' \cdot \mathbf{e}_3\right) = \nabla^2\rho_0', \tag{6.95}$$

where the expressions for $\mathbf{w}_0'$, $\mathbf{U}_0$ are given in equations (6.47)-(6.49). Also ρ_0' satisfies the conditions

$$\left.\frac{\partial\rho_0'}{\partial r}\right|_{r=1} = \cos\theta, \quad \rho_0' = 0 \text{ as } r \to \infty. \tag{6.96a, b}$$

We solve for ρ_0' by doing a singular perturbation expansion in Pe. There are two boundary layers: one at $r \sim Pe^{-1/2}$ and the other at $r \sim Pe^{-1}$. We again call the region lying between the swimmer and $r < O\left(Pe^{-1/2}\right)$ as the inner zone and the region lying between $r > O\left(Pe^{-1/2}\right)$ and $r < O\left(Pe^{-1}\right)$ as the intermediate zone, and finally the region $r > O\left(Pe^{-1}\right)$ as the outer zone.

In the inner zone, we denote the density field by $\breve{\rho}$. At leading order, it is appropriate to neglect the entire advective term. Hence, the leading order density field in the inner zone $\breve{\rho}_0$ is governed by the following equations

$$\nabla^2\breve{\rho}_0 = 0, \ \left.\frac{\partial\breve{\rho}_0}{\partial r}\right|_{r=1} = \cos\theta. \tag{6.97}$$

The solution of these equations that decays spatially so as to conserve flux on any surface enclosing the swimmer is

$$\breve{\rho}_0 = -\frac{\cos\theta}{2r^2}. \tag{6.98}$$

Using this density field, we estimate the order of magnitude of advective and diffusive terms far away from the swimmer. As $Pe\left(\mathbf{w}_0' \cdot \nabla\rho_0'\right) \sim Pe/r^5$, $Pe\left(\mathbf{U}_0 \cdot \nabla\rho_0'\right) \sim Pe/r^3$ and $Pe\left(\mathbf{w}_0' \cdot \mathbf{e}_3\right) \sim Pe/r^2$, the dominant advective term $Pe\left(\mathbf{w}_0' \cdot \mathbf{e}_3\right) \sim Pe/r^2$ while the diffusive term $\nabla^2\rho_0' \sim 1/r^4$. At $r \sim Pe^{-1/2}$, the advective term $Pe\left(\mathbf{w}_0' \cdot \mathbf{e}_3\right)$ is as important as the diffusive term and this justifies the existence of a boundary layer at $r \sim Pe^{-1/2}$ separating the inner zone where diffusion is prominent from the

intermediate zone where both advection (due to $Pe\,(\mathbf{w}_0' \cdot \mathbf{e}_3)$) and diffusion are equally important.

In the intermediate zone, we rescale the variables as $\bar{r} = Pe^{1/2} r$, $\rho_0' = Pe\bar{\rho}$. Retaining only the Stresslet part of $\mathbf{w}_0'$, the leading order density field in this zone $\bar{\rho}_0$ is governed by the following equation

$$\nabla_{\bar{r}}^2 \bar{\rho}_0 = \frac{2b_2}{5\bar{r}^2}\left(P_1(\cos\theta) + \frac{3}{2}P_3(\cos\theta)\right) \tag{6.99}$$

along with the matching condition with the inner zone

$$\lim_{\bar{r}\ll 1} \bar{\rho}_0 \Leftrightarrow -\frac{\cos\theta}{2\bar{r}^2}. \tag{6.100}$$

The solution of these equations that also matches with the density field in the outer zone is

$$\bar{\rho}_0 = A_0 - \frac{b_2}{5}\left(P_1(\cos\theta) + \frac{1}{4}P_3(\cos\theta)\right) + \frac{A_1}{\bar{r}} - \frac{\cos\theta}{2\bar{r}^2}, \tag{6.101}$$

where A_0 and A_1 are constants which can be found by matching with the higher order density fields in the inner zone or the leading order density field in the outer zone.

At $\bar{r} \gg 1$ or $r \gg Pe^{-1/2} \gg 1$, we again estimate the order of magnitude of advective and diffusive terms. At these distances, $\bar{\rho}_0 \sim O(1)$, hence $\rho_0' \sim Pe$. As the advective terms $Pe\,(\mathbf{w}_0' \cdot \nabla\rho_0') \sim Pe^2/r^3$, $Pe\,(\mathbf{U}_0 \cdot \nabla\rho_0') \sim Pe^2/r$, and $Pe\,(\mathbf{w}_0' \cdot \mathbf{e}_3) \sim Pe/r^2$ while the diffusive term $\nabla^2\rho_0' \sim Pe/r^2$, the dominant advective term $Pe\,(\mathbf{U}_0 \cdot \nabla\rho_0' + \mathbf{w}_0' \cdot \mathbf{e}_3)$ balances the diffusive term at $r \sim Pe^{-1} \gg Pe^{-1/2}$. This justifies the existence of a boundary layer at $r \sim Pe^{-1}$ separating the intermediate zone where advection due to $Pe\,\mathbf{w}_0' \cdot \mathbf{e}_3$ and diffusion are important from the outer zone where advection due to $Pe\,(\mathbf{U}_0 \cdot \nabla\rho_0' + \mathbf{w}_0' \cdot \mathbf{e}_3)$ and diffusion are important.

To find the higher order density fields in the inner zone, we substitute the expansion $\breve{\rho} = \breve{\rho}_0 + Pe^{1/2}\breve{\rho}_1 + Pe\breve{\rho}_2 + O\left(Pe^{3/2}\right)$ in equations (6.95), (6.96a), collect terms at various orders of Pe, and solve the resulting equations by enforcing matching with the intermediate solution (6.101). Doing so, we find that

$$\breve{\rho}_1 = A_1 = 0, \tag{6.102}$$

$$\begin{aligned}\breve{\rho}_2 =& A_0 - \frac{b_1}{9r} + \frac{b_1}{36r^4} + \left(-\frac{1}{5} + \frac{1}{15r^2} - \frac{1}{10r^3} + \frac{1}{30r^5}\right) b_2 P_1(\cos\theta) \\ &+ \left(\frac{2}{9r} - \frac{4}{27r^3} + \frac{1}{18r^4}\right) b_1 P_2(\cos\theta) \\ &+ \left(-\frac{1}{20} + \frac{1}{10r^2} + \frac{1}{10r^3} - \frac{3}{16r^4} + \frac{1}{20r^5}\right) b_2 P_3(\cos\theta).\end{aligned} \tag{6.103}$$

We now write down the composite expansion of density field that is accurate to $O(Pe)$ and is uniformly valid up to $r < O(Pe^{-1})$. For this purpose, we add the density field in the inner zone to the density field in the intermediate zone and subtract the density field in the first matching zone $\left(r \sim Pe^{-1/2}\right)$. As the density field in this matching zone is $Pe\bar{\rho}_0$, writing everything in terms of inner variables, we get

$$\rho_0' = \breve{\rho}_0 + Pe\breve{\rho}_2 + Pe\bar{\rho}_0 - Pe\bar{\rho}_0 + O\left(Pe^{3/2}\right) = -\frac{\cos\theta}{2r^2} + Pe\breve{\rho}_2 + O\left(Pe^{3/2}\right). \tag{6.104}$$

Noting that $\breve{\rho}_2 \sim O(1)$, we find that the density field obeys for $r < O(Pe^{-1})$

$$\rho_0' \sim \max\left(\frac{1}{r^2}, Pe\right). \tag{6.105}$$

Since we did not use the boundary condition far from the swimmer, equation (6.96b), we expect the density field and the scaling, equations (6.104), (6.105) to hold even if the perturbation in Ri is singular.

6.11 Appendix E

In this appendix, we simplify the integral appearing in the matching condition (6.57)

$$\lim_{\tilde{r}\to 0} \frac{\epsilon^2}{8\pi^3} \int \left[\hat{\mathbf{w}}'(\mathbf{k}) - \hat{\mathbf{w}}_{SS}(\mathbf{k})\right] e^{i\mathbf{k}\cdot\tilde{\mathbf{r}}} d\mathbf{k}. \tag{6.106}$$

We again divide the domain of integration into two parts—$k \leq \tilde{r}^{-\sigma}$ and $k > \tilde{r}^{-\sigma}$, where $0 < \sigma < 1$.

$$\frac{\epsilon^2}{8\pi^3}\left\{\lim_{\tilde{r}\to 0} \int\limits_{k\leq\tilde{r}^{-\sigma}} \left[\hat{\mathbf{w}}'(\mathbf{k}) - \hat{\mathbf{w}}_{SS}(\mathbf{k})\right] e^{i\mathbf{k}\cdot\tilde{\mathbf{r}}} d\mathbf{k} + \lim_{\tilde{r}\to 0} \int\limits_{k>\tilde{r}^{-\sigma}} \left[\hat{\mathbf{w}}'(\mathbf{k}) - \hat{\mathbf{w}}_{SS}(\mathbf{k})\right] e^{i\mathbf{k}\cdot\tilde{\mathbf{r}}} d\mathbf{k}\right\} \tag{6.107}$$

As k is finite in the first integral, we evaluate the limit by directly substituting $\tilde{r} = 0$ to obtain

$$\frac{\epsilon^2}{8\pi^3}\int \left[\hat{\mathbf{w}}'(\mathbf{k}) - \hat{\mathbf{w}}_{SS}(\mathbf{k})\right] d\mathbf{k} + \frac{\epsilon^2}{8\pi^3}\lim_{\tilde{r}\to 0}\int\limits_{k>\tilde{r}^{-\sigma}} \left[\hat{\mathbf{w}}'(\mathbf{k}) - \hat{\mathbf{w}}_{SS}(\mathbf{k})\right] e^{i\mathbf{k}\cdot\tilde{\mathbf{r}}} d\mathbf{k}. \tag{6.108}$$

Here the first term being a constant vector represents an uniform flow field. In the second term, $k \gg 1$ and hence $\hat{\mathbf{w}}' - \hat{\mathbf{w}}_{SS}$ simplifies for fixed Pe/ϵ to

$$\frac{4i\pi b_2 k_3 \left(2k^2 + k_1^2 + k_2^2 - 2k_3^2\right)}{3k^{10}} \left(k_3 k_1 \mathbf{e}_1 + k_3 k_2 \mathbf{e}_2 + \left(k_3^2 - k^2\right)\mathbf{e}_3\right). \tag{6.109}$$

Here, we see that $\hat{\mathbf{w}}' - \hat{\mathbf{w}}_{SS} \sim O\left(k^{-5}\right)$, so $\left(\hat{\mathbf{w}}' - \hat{\mathbf{w}}_{SS}\right) d\mathbf{k} \sim O\left(k^{-2}\right)$. Hence the integral

$$\int\limits_{k>\tilde{r}^{-\sigma}} \left[\hat{\mathbf{w}}'(\mathbf{k}) - \hat{\mathbf{w}}_{SS}(\mathbf{k})\right] e^{i\mathbf{k}\cdot\tilde{\mathbf{r}}} d\mathbf{k} \sim O\left(\tilde{r}^{2\sigma}\right) \tag{6.110}$$

and it becomes negligible compared to the first term in equation (6.108) as $\tilde{r} \to 0$.

7. SUMMARY AND FUTURE WORKS

7.1 Summary

In this thesis, we unveiled the impact of surfactant redistribution and density-stratification on the motion of drops and swimming microorganisms. For this purpose, we grouped the thesis under two themes. In the first theme, we studied the motion of swimming microorganism near a surfactant-laden interface neglecting the stratification effects in the suspending fluid whereas in the second theme, we analyzed separately the motion of a drop and a swimming organism in a linearly density-stratified fluid without any surfactants.

In the first theme, we began by analyzing the locomotion outside a surfactant-laden drop (see Chapter 2). For this purpose, we assumed the surfactant is insoluble, incompressible, and non-diffusing, and used the Boussinesq-Scriven constitutive law for the interfacial stress tensor to derive the image flow fields for the point force and higher order singularities placed outside a surfactant-laden drop. We used these image flow fields to calculate the velocity of a swimming microorganism (modeled as a force-dipole) outside a surfactant-laden drop which was later used to study the trapping characteristics of bacteria near oil drops [16]. Using these image systems, we also derived the mobility matrix of two surfactant-laden drops of arbitrary sizes and this mobility matrix can be used to understand the pair hydrodynamic interaction of bubbles and drops in bubbly flows and emulsion flows, respectively.

Inline with the first theme of this thesis, we then studied the motion of a swimming microorganism (modeled as a spherical squirmer) inside a surfactant-laden drop where the surfactant is now assumed to be insoluble, compressible, and have large surface diffusivity (see Chapter 3). This system is ideal in exploring the nonlinearities in the surfactant transport phenomena and it can also be used to transport the drops

containing drugs as in the targeted drug delivery systems [7]. We found that the surfactant redistribution can increase or even decrease the swimmer and drop speeds depending on the value of the eccentricity. This can be understood by analyzing the surfactant effects on the thrust and drag forces acting on the swimmer and the drop. The far-field representation of a clean drop encompassing a pusher swimmer at its center is a puller. The presence of a redistributed surfactant on the drop surface maintains this far-field representation but reduces its strength. The nonlinearities associated with the surfactant advection on the drop surface breaks the kinematic reversibility constraints causing a time-averaged propulsion of the drop and the time-reversible swimmer that it engulfs.

Consistent with the first theme of this thesis, we then analyzed the motion of a swimming microorganism (modeled as a swimming sheet) in a film covered with surfactant (see Chapter 4). This system is relevant in the context of free-standing films containing swimming organisms or during the initial stages of biofilm formation. We found that the surfactant redistribution affects the motility of the organism in a non-trivial manner and this can be understood by analyzing the surfactant's effect on the interface slip.

In the second theme, we started by analyzing a towed drop in a linearly density-stratified fluid at small inertia and stratification (see Chapter 5). We found that stratification or inertia or both increase the drag and this drag acting on a drop is equal to $\left(\frac{3\lambda+2}{3(\lambda+1)}\right)^2$ times the drag acting on a rigid sphere, where λ is the viscosity ratio. But stratification does not deform the drop. In contrast to an infinite drift volume in a homogeneous fluid, the drift volume in a stratified fluid, at zero inertia and small advective transport rate of density, is finite but large compared to the drop's volume.

Inline with the second theme, we then studied the motion of a swimming organism (modeled as a spherical squirmer) in a linearly density-stratified fluid at negligible inertia and weak stratification (see Chapter 6). Depending on the position of the swimmer relative to the neutrally buoyant position (NBP), the swimmer behaves ei-

ther as a settling particle (far from NBP) or as a force-free particle (close to NBP). Here, NBP is a position in the fluid where the ambient fluid density equals the swimmer's density. While the motility of the swimmer far from NBP can be deduced from the drag acting on a towed sphere in a stratified fluid, the motility close to NBP is interesting and is in agreement with the previously reported numerical results.

7.2 Future works

The resistance matrix of a rigid sphere moving near a plane surfactant covered interface was derived previously [30]. Along the similar lines, the velocity of a microswimmer (modeled as a force-dipole) near a plane surfactant laden interface was also calculated [8]. These two analyses neglected the surface diffusivity of the surfactant and assumed it to be incompressible. It would be interesting to analyze the motion of a rigid sphere or a microswimmer near a plane surfactant covered interface in the limit of large surface diffusivity.

Most of the organisms that live in Bathypelagic zone (1000 m to 4000 m from the sea surface) survive by feeding on the marine snow particles falling from the water above this zone. These marine snow particles were found to aggregate at the pycnoclines [196–198], in turn increasing the biological activity at these pycnoclines. To understand this observation, one has to account for the porosity of the marine snow particles [199]. Recent numerics [200] and reduced order theory [201] found the reasons for this aggregation to be diffusion limited transport of salt or temperature into the marine snow as well as the buoyancy of the entrained lighter fluid. But these previous works considered sharp stratifications. To have a complete understanding of the physical processes occurring in the oceans, one then have to also analyse the settling of a marine snow particle through a linearly stratified fluid by extending the theory developed in Chapters 5 and 6 of this thesis.

A fraction of marine snow particles as well as the planktonic organisms such as *Opalina*, *Paramecium* are slender. Since the motion of spherical particles or organisms

through stratified fluids is well understood [148–150, 185, 202], it is then interesting to develop a theory for the motion of slender particles or organisms through stratified fluids by extending the slender body theory developed in homogeneous fluids [26, 203, 204] to stratified fluids. This theory can be validated with the numerical results reported on the settling motion of a prolate spheroid through a stratified fluid [205].

REFERENCES

[1] John Happel and Howard Brenner. *Low Reynolds number hydrodynamics*, volume 1 of *Mechanics of fluids and transport processes*. Springer Netherlands, Dordrecht, 1981.

[2] Sangtae Kim and Seppo Karrila. *Microhydrodynamics: Principles and Selected Applications*. Butterworth-Heinemann, 1991.

[3] Elisabeth Guazzelli, Jeffrey F. Morris, and Sylvie Pic. *A Physical Introduction to Suspension Dynamics*. Cambridge University Press, Cambridge, 2011.

[4] Ian M. Head, D. Martin Jones, and Wilfred F. M. Röling. Marine microorganisms make a meal of oil. *Nature Reviews Microbiology*, 4(3):173–182, mar 2006.

[5] Arezoo M. Ardekani, Amin Doostmohammadi, and Nikhil Desai. Transport of particles, drops, and small organisms in density stratified fluids. *Physical Review Fluids*, 2(10):100503, oct 2017.

[6] Jacques Magnaudet and Matthieu J. Mercier. Particles, Drops, and Bubbles Moving Across Sharp Interfaces and Stratified Layers. *Annual Review of Fluid Mechanics*, 52(1):61–91, jan 2020.

[7] Yun Ding, Famin Qiu, Xavier Casadevall i Solvas, Flora Chiu, Bradley Nelson, and Andrew DeMello. Microfluidic-Based Droplet and Cell Manipulations Using Artificial Bacterial Flagella. *Micromachines*, 7(2):25, feb 2016.

[8] Diego Lopez and Eric Lauga. Dynamics of swimming bacteria at complex interfaces. *Physics of Fluids*, 26(7):071902, jul 2014.

[9] Vaseem A. Shaik and Arezoo M. Ardekani. Motion of a model swimmer near a weakly deforming interface. *Journal of Fluid Mechanics*, 824:42–73, aug 2017.

[10] Nikhil Desai and Arezoo M. Ardekani. Modeling of active swimmer suspensions and their interactions with the environment. *Soft Matter*, 13(36):6033–6050, 2017.

[11] E. M. Purcell. Life at low Reynolds number. *American Journal of Physics*, 45(1):3–11, jan 1977.

[12] Eric Lauga. Life around the scallop theorem. *Soft Matter*, 7(7):3060–3065, 2011.

[13] Geoffrey Ingram Taylor. Analysis of the swimming of microscopic organisms. *Proceedings of the Royal Society of London. Series A.*, 209(1099):447–461, nov 1951.

[14] M. J. Lighthill. On the squirming motion of nearly spherical deformable bodies through liquids at very small reynolds numbers. *Communications on Pure and Applied Mathematics*, 5(2):109–118, may 1952.

[15] J. R. Blake. A spherical envelope approach to ciliary propulsion. *Journal of Fluid Mechanics*, 46(1):199–208, mar 1971.

[16] Nikhil Desai, Vaseem A. Shaik, and Arezoo M. Ardekani. Hydrodynamics-mediated trapping of micro-swimmers near drops. *Soft Matter*, 14(2):264–278, 2018.

[17] Nikhil Desai, Vaseem A. Shaik, and Arezoo M. Ardekani. Hydrodynamic Interaction Enhances Colonization of Sinking Nutrient Sources by Motile Microorganisms. *Frontiers in Microbiology*, 10, mar 2019.

[18] L. Gary Leal. *Advanced Transport Phenomena. Fluid Mechanics and Convective Transport Processes*. Cambridge University Press, 2010.

[19] Eric Lauga and Thomas R Powers. The hydrodynamics of swimming microorganisms. *Reports on Progress in Physics*, 72(9):096601, sep 2009.

[20] Allen T. Chwang and T. Yao-Tsu Wu. Hydromechanics of low-Reynolds-number flow. Part 2. Singularity method for Stokes flows. *Journal of Fluid Mechanics*, 67(4):787–815, feb 1975.

[21] S. H. Lee, R. S. Chadwick, and L. G. Leal. Motion of a sphere in the presence of a plane interface. Part 1. An approximate solution by generalization of the method of Lorentz. *Journal of Fluid Mechanics*, 93(04):705, aug 1979.

[22] S.-M. Yang and L.G. Leal. Motions of a fluid drop near a deformable interface. *International Journal of Multiphase Flow*, 16(4):597–616, jul 1990.

[23] Allison P. Berke, Linda Turner, Howard C. Berg, and Eric Lauga. Hydrodynamic Attraction of Swimming Microorganisms by Surfaces. *Physical Review Letters*, 101(3):038102, jul 2008.

[24] Saverio E. Spagnolie and Eric Lauga. Hydrodynamics of self-propulsion near a boundary: predictions and accuracy of far-field approximations. *Journal of Fluid Mechanics*, 700:105–147, jun 2012.

[25] T.S. Awad, H.A. Moharram, O.E. Shaltout, D. Asker, and M.M. Youssef. Applications of ultrasound in analysis, processing and quality control of food: A review. *Food Research International*, 48(2):410–427, oct 2012.

[26] G. Subramanian and Donald L. Koch. Inertial effects on fibre motion in simple shear flow. *Journal of Fluid Mechanics*, 535:383–414, jul 2005.

[27] James A. Hanna and Petia M. Vlahovska. Surfactant-induced migration of a spherical drop in Stokes flow. *Physics of Fluids*, 22(1):013102, jan 2010.

[28] Jonathan T. Schwalbe, Frederick R. Phelan, Jr., Petia M. Vlahovska, and Steven D. Hudson. Interfacial effects on droplet dynamics in Poiseuille flow. *Soft Matter*, 7(17):7797–7804, 2011.

[29] On Shun Pak, Jie Feng, and Howard A. Stone. Viscous Marangoni migration of a drop in a Poiseuille flow at low surface Péclet numbers. *Journal of Fluid Mechanics*, 753:535–552, aug 2014.

[30] Jerzy Bławzdziewicz, Vittorio Cristini, and Michael Loewenberg. Stokes flow in the presence of a planar interface covered with incompressible surfactant. *Physics of Fluids*, 11(2):251–258, feb 1999.

[31] J. Blawzdziewicz, E. Wajnryb, and Michael Loewenberg. Hydrodynamic interactions and collision efficiencies of spherical drops covered with an incompressible surfactant film. *Journal of Fluid Mechanics*, 395:29–59, sep 1999.

[32] José A. Ramirez, Robert H. Davis, and Alexander Z. Zinchenko. Microflotation of fine particles in the presence of a bulk-insoluble surfactant. *International Journal of Multiphase Flow*, 26(6):891–920, jun 2000.

[33] Michael A. Rother and Robert H. Davis. Buoyancy-driven coalescence of spherical drops covered with incompressible surfactant at arbitrary Péclet number. *Journal of Colloid and Interface Science*, 270(1):205–220, feb 2004.

[34] J. Bławzdziewicz, P. Vlahovska, and M. Loewenberg. Rheology of a dilute emulsion of surfactant-covered spherical drops. *Physica A: Statistical Mechanics and its Applications*, 276(1-2):50–85, feb 2000.

[35] P. Vlahovska, J. Blawzdziewicz, and M. Loewenberg. Nonlinear rheology of a dilute emulsion of surfactant-covered spherical drops in time-dependent flows. *Journal of Fluid Mechanics*, 463:1–24, jul 2002.

[36] Vitorio Cristini, J. Blawzdziewicz, and Michael Loewenberg. Near-contact motion of surfactant-covered spherical drops. *Journal of Fluid Mechanics*, 366:259–287, jul 1998.

[37] Alexander Z. Zinchenko, Michael A. Rother, and Robert H. Davis. Gravity-induced collisions of spherical drops covered with compressible surfactant. *Journal of Fluid Mechanics*, 667:369–402, jan 2011.

[38] M. Schmitt and H. Stark. Marangoni flow at droplet interfaces: Three-dimensional solution and applications. *Physics of Fluids*, 28(1):012106, jan 2016.

[39] John W.M. Bush and David L. Hu. Walking on water: Biolocomotion at the Interface. *Annual Review of Fluid Mechanics*, 38(1):339–369, jan 2006.

[40] Eric Lauga and Anthony M. J. Davis. Viscous Marangoni propulsion. *Journal of Fluid Mechanics*, 705:120–133, aug 2012.

[41] Hassan Masoud and Howard A. Stone. A reciprocal theorem for Marangoni propulsion. *Journal of Fluid Mechanics*, 741:R4, feb 2014.

[42] J. R. Blake. A note on the image system for a stokeslet in a no-slip boundary. *Mathematical Proceedings of the Cambridge Philosophical Society*, 70(2):303–310, sep 1971.

[43] J. R. Blake and A. T. Chwang. Fundamental singularities of viscous flow. *Journal of Engineering Mathematics*, 8(1):23–29, jan 1974.

[44] K. Aderogba and J.R. Blake. Action of a force near the planar surface between semi-infinite immiscible liquids at very low Reynolds numbers: Addendum. *Bulletin of the Australian Mathematical Society*, 19(2):309–318, oct 1978.

[45] Yuris O. Fuentes, Sangtae Kim, and David J. Jeffrey. Mobility functions for two unequal viscous drops in Stokes flow. I. Axisymmetric motions. *Physics of Fluids*, 31(9):2445–2455, sep 1988.

[46] Yuris O. Fuentes, Sangtae Kim, and David J. Jeffrey. Mobility functions for two unequal viscous drops in Stokes flow. II. Asymmetric motions. *Physics of Fluids A: Fluid Dynamics*, 1(1):61–76, jan 1989.

[47] L.E. Scriven. Dynamics of a fluid interface Equation of motion for Newtonian surface fluids. *Chemical Engineering Science*, 12(2):98–108, may 1960.

[48] David A. Edwards, Howard Brenner, and D. T. Wasan. *Interfacial Transport Processes and Rheology*. Bufferworth-Heinemann, 1991.

[49] Horace Lamb. *Hydrodynamics*. Cambridge University Press, 1932.

[50] Abdallah Daddi-Moussa-Ider and Stephan Gekle. Hydrodynamic mobility of a solid particle near a spherical elastic membrane: Axisymmetric motion. *Physical Review E*, 95(1):013108, jan 2017.

[51] H. A. Stone. A simple derivation of the timedependent convectivediffusion equation for surfactant transport along a deforming interface. *Physics of Fluids A: Fluid Dynamics*, 2(1):111–112, jan 1990.

[52] Saverio E. Spagnolie, Gregorio R. Moreno-Flores, Denis Bartolo, and Eric Lauga. Geometric capture and escape of a microswimmer colliding with an obstacle. *Soft Matter*, 11(17):3396–3411, 2015.

[53] Harris Wong, David Rumschitzki, and Charles Maldarelli. Marangoni effects on the motion of an expanding or contracting bubble pinned at a submerged tube tip. *Journal of Fluid Mechanics*, 379:279–302, jan 1999.

[54] Shubhadeep Mandal and Suman Chakraborty. Influence of interfacial viscosity on the dielectrophoresis of drops. *Physics of Fluids*, 29(5):052002, may 2017.

[55] H. Brenner. The Stokes resistance of an arbitrary particleIV Arbitrary fields of flow. *Chemical Engineering Science*, 19(10):703–727, oct 1964.

[56] J. M. Rallison. Note on the Faxén relations for a particle in Stokes flow. *Journal of Fluid Mechanics*, 88(3):529–533, oct 1978.

[57] S. Kim and S.-Y. Lu. The functional similarity between faxén relations and singularity solutions for fluid-fluid, fluid-solid and solid-solid dispersions. *International Journal of Multiphase Flow*, 13(6):837–844, nov 1987.

[58] Ali Nadim, Hossein Haj-Hariri, and Ali Borhan. Thermocapillary migration of slightly deformed droplets. *Particulate Science and Technology*, 8(3-4):191–198, jul 1990.

[59] G. Hetsroni and S. Haber. The flow in and around a droplet or bubble submerged in an unbound arbitrary velocity field. *Rheologica Acta*, 9(4):488–496, nov 1970.

[60] S. Haber and G. Hetsroni. Hydrodynamics of a drop submerged in an unbounded arbitrary velocity field in the presence of surfactants. *Applied Scientific Research*, 25(1):215–233, jan 1972.

[61] J Elgeti, R G Winkler, and G Gompper. Physics of microswimmerssingle particle motion and collective behavior: a review. *Reports on Progress in Physics*, 78(5):056601, may 2015.

[62] A. J. Reynolds. The swimming of minute organisms. *Journal of Fluid Mechanics*, 23(02):241–260, oct 1965.

[63] David F. Katz. On the propulsion of micro-organisms near solid boundaries. *Journal of Fluid Mechanics*, 64(1):33–49, jun 1974.

[64] Eric Lauga, Willow R. DiLuzio, George M. Whitesides, and Howard A. Stone. Swimming in Circles: Motion of Bacteria near Solid Boundaries. *Biophysical Journal*, 90(2):400–412, jan 2006.

[65] R. Di Leonardo, D. Dell'Arciprete, L. Angelani, and V. Iebba. Swimming with an Image. *Physical Review Letters*, 106(3):038101, jan 2011.

[66] Guanglai Li and Jay X. Tang. Accumulation of Microswimmers near a Surface Mediated by Collision and Rotational Brownian Motion. *Physical Review Letters*, 103(7):078101, aug 2009.

[67] J. Elgeti and G. Gompper. Self-propelled rods near surfaces. *EPL (Europhysics Letters)*, 85(3):38002, feb 2009.

[68] Renaud Trouilloud, Tony S. Yu, A. E. Hosoi, and Eric Lauga. Soft Swimming: Exploiting Deformable Interfaces for Low Reynolds Number Locomotion. *Physical Review Letters*, 101(4):048102, jul 2008.

[69] Sungyon Lee, John W. M. Bush, A. E. Hosoi, and Eric Lauga. Crawling beneath the free surface: Water snail locomotion. *Physics of Fluids*, 20(8):082106, aug 2008.

[70] Darren Crowdy, Sungyon Lee, Ophir Samson, Eric Lauga, and A. E. Hosoi. A two-dimensional model of low-Reynolds number swimming beneath a free surface. *Journal of Fluid Mechanics*, 681:24–47, aug 2011.

[71] S. Yazdi, A. M. Ardekani, and A. Borhan. Swimming Dynamics Near a Wall in a Weakly Elastic Fluid. *Journal of Nonlinear Science*, 25(5):1153–1167, oct 2015.

[72] G. J. Li, A. Karimi, and A. M. Ardekani. Effect of solid boundaries on swimming dynamics of microorganisms in a viscoelastic fluid. *Rheologica Acta*, 53(12):911–926, dec 2014.

[73] Vaseem A. Shaik and Arezoo M. Ardekani. Point force singularities outside a drop covered with an incompressible surfactant: Image systems and their applications. *Physical Review Fluids*, 2(11):113606, nov 2017.

[74] Manuel Sickert and Francis Rondelez. Shear Viscosity of Langmuir Monolayers in the Low-Density Limit. *Physical Review Letters*, 90(12):126104, mar 2003.

[75] Thomas M. Fischer. Comment on Shear Viscosity of Langmuir Monolayers in the Low-Density Limit. *Physical Review Letters*, 92(13):139603, apr 2004.

[76] M. Sickert, F. Rondelez, and H. A. Stone. Single-particle Brownian dynamics for characterizing the rheology of fluid Langmuir monolayers. *Europhysics Letters (EPL)*, 79(6):66005, sep 2007.

[77] Joseph R. Samaniuk and Jan Vermant. Micro and macrorheology at fluidfluid interfaces. *Soft Matter*, 10(36):7023–7033, 2014.

[78] L G Leal. Particle Motions in a Viscous Fluid. *Annual Review of Fluid Mechanics*, 12(1):435–476, jan 1980.

[79] Shang Yik Reigh, Lailai Zhu, François Gallaire, and Eric Lauga. Swimming with a cage: low-Reynolds-number locomotion inside a droplet. *Soft Matter*, 13(17):3161–3173, 2017.

[80] Shubhadeep Mandal, Uddipta Ghosh, and Suman Chakraborty. Effect of surfactant on motion and deformation of compound droplets in arbitrary unbounded Stokes flows. *Journal of Fluid Mechanics*, 803:200–249, sep 2016.

[81] Margaret Stimson and George Barker Jeffery. The motion of two spheres in a viscous fluid. *Proceedings of the Royal Society of London. Series A*, 111(757):110–116, may 1926.

[82] E. T. Whittaker and G. N. Watson. *A Course of Modern Analysis*. Cambridge University Press, sep 1996.

[83] Howard Brenner. The slow motion of a sphere through a viscous fluid towards a plane surface. *Chemical Engineering Science*, 16(3-4):242–251, dec 1961.

[84] E. Rushton and G. A. Davies. The slow unsteady settling of two fluid spheres along their line of centres. *Applied Scientific Research*, 28(1):37–61, jan 1973.

[85] Takuji Ishikawa, M. P. Simmonds, and T. J. Pedley. Hydrodynamic interaction of two swimming model micro-organisms. *Journal of Fluid Mechanics*, 568:119–160, dec 2006.

[86] M. B. Short, C. A. Solari, S. Ganguly, T. R. Powers, J. O. Kessler, and R. E. Goldstein. Flows driven by flagella of multicellular organisms enhance long-range molecular transport. *Proceedings of the National Academy of Sciences*, 103(22):8315–8319, may 2006.

[87] A. Doostmohammadi, R. Stocker, and A. M. Ardekani. Low-Reynolds-number swimming at pycnoclines. *Proceedings of the National Academy of Sciences*, 109(10):3856–3861, mar 2012.

[88] José A. Ramirez and Robert H. Davis. Mass transfer to a surfactant-covered bubble or drop. *AIChE Journal*, 45(6):1355–1358, jun 1999.

[89] Thomas D. Montenegro-Johnson, David J. Smith, and Daniel Loghin. Physics of rheologically enhanced propulsion: Different strokes in generalized Stokes. *Physics of Fluids*, 25(8):081903, aug 2013.

[90] Charu Datt, Lailai Zhu, Gwynn J. Elfring, and On Shun Pak. Squirming through shear-thinning fluids. *Journal of Fluid Mechanics*, 784:R1, dec 2015.

[91] H Brenner and L.G Leal. A micromechanical derivation of Fick's law for interfacial diffusion of surfactant molecules. *Journal of Colloid and Interface Science*, 65(2):191–209, jun 1978.

[92] Howard Brenner and L.Gary Leal. Conservation and constitutive equations for adsorbed species undergoing surface diffusion and convection at a fluid-fluid interface. *Journal of Colloid and Interface Science*, 88(1):136–184, jul 1982.

[93] David A. Gagnon, Nathan C. Keim, Xiaoning Shen, and Paulo E. Arratia. Fluid-induced propulsion of rigid particles in wormlike micellar solutions. *Physics of Fluids*, 26(10):103101, oct 2014.

[94] H. Haj-Hariri, A. Nadim, and A. Borhan. Recriprocal theorem for concentric compound drops in arbitrary Stokes flows. *Journal of Fluid Mechanics*, 252:265–277, jul 1993.

[95] Yi Man and Eric Lauga. Phase-separation models for swimming enhancement in complex fluids. *Physical Review E*, 92(2):023004, aug 2015.

[96] S. Wang and A. M. Ardekani. Swimming of a model ciliate near an air-liquid interface. *Physical Review E*, 87(6):063010, jun 2013.

[97] S. Wang and A. Ardekani. Inertial squirmer. *Physics of Fluids*, 24(10):101902, oct 2012.

[98] Gaojin Li, Anca Ostace, and Arezoo M. Ardekani. Hydrodynamic interaction of swimming organisms in an inertial regime. *Physical Review E*, 94(5):053104, nov 2016.

[99] Gaojin Li and Arezoo M. Ardekani. Collective Motion of Microorganisms in a Viscoelastic Fluid. *Physical Review Letters*, 117(11):118001, sep 2016.

[100] Gaojin Li and Arezoo M. Ardekani. Near wall motion of undulatory swimmers in non-Newtonian fluids. *European Journal of Computational Mechanics*, 26(1-2):44–60, mar 2017.

[101] Vaseem A. Shaik, Vishwa Vasani, and Arezoo M. Ardekani. Locomotion inside a surfactant-laden drop at low surface Péclet numbers. *Journal of Fluid Mechanics*, 851:187–230, sep 2018.

[102] J. R. Blake. Infinite models for ciliary propulsion. *Journal of Fluid Mechanics*, 49(2):209–222, sep 1971.

[103] T. K. Chaudhury. On swimming in a visco-elastic liquid. *Journal of Fluid Mechanics*, 95(1):189–197, nov 1979.

[104] L.D. Sturges. Motion induced by a waving plate. *Journal of Non-Newtonian Fluid Mechanics*, 8(3-4):357–364, jan 1981.

[105] Eric Lauga. Propulsion in a viscoelastic fluid. *Physics of Fluids*, 19(8):083104, aug 2007.

[106] J. Rodrigo Vélez-Cordero and Eric Lauga. Waving transport and propulsion in a generalized Newtonian fluid. *Journal of Non-Newtonian Fluid Mechanics*, 199:37–50, sep 2013.

[107] Emily E. Riley and Eric Lauga. Enhanced active swimming in viscoelastic fluids. *EPL (Europhysics Letters)*, 108(3):34003, nov 2014.

[108] Gaojin Li and Arezoo M. Ardekani. Undulatory swimming in non-Newtonian fluids. *Journal of Fluid Mechanics*, 784:R4, dec 2015.

[109] Gwynn J. Elfring and Gaurav Goyal. The effect of gait on swimming in viscoelastic fluids. *Journal of Non-Newtonian Fluid Mechanics*, 234:8–14, aug 2016.

[110] D. R. Hewitt and N. J. Balmforth. Taylor's swimming sheet in a yield-stress fluid. *Journal of Fluid Mechanics*, 828:33–56, oct 2017.

[111] A. M. Leshansky. Enhanced low-Reynolds-number propulsion in heterogeneous viscous environments. *Physical Review E*, 80(5):051911, nov 2009.

[112] Henry C. Fu, Vivek B. Shenoy, and Thomas R. Powers. Low-Reynolds-number swimming in gels. *EPL (Europhysics Letters)*, 91(2):24002, jul 2010.

[113] Madison S. Krieger, Marcelo A. Dias, and Thomas R. Powers. Minimal model for transient swimming in a liquid crystal. *The European Physical Journal E*, 38(8):94, aug 2015.

[114] A. M. Siddiqui and A. R. Ansari. An Analysis of the Swimming Problem of a Singly Flagellated Microorganism in a Fluid Flowing through a Porous Medium. *Journal of Porous Media*, 6(4):235–242, 2003.

[115] W. J. Shack and T. J. Lardner. A long wavelength solution for a microorganism swimming in a channel. *Bulletin of Mathematical Biology*, 36(4):435–444, aug 1974.

[116] R.E. Smelser, W.J. Shack, and T.J. Lardner. The swimming of spermatozoa in an active channel. *Journal of Biomechanics*, 7(4):349–355, aug 1974.

[117] J.B. Shukla, B.R.P. Rao, and R.S. Parihar. Swimming of spermatozoa in cervix: Effects of dynamical interaction and peripheral layer viscosity. *Journal of Biomechanics*, 11(1-2):15–19, jan 1978.

[118] J.B. Shukla, P. Chandra, Rajiv Sharma, and G. Radhakrishnamacharya. Effects of peristaltic and longitudinal wave motion of the channel wall on movement of micro-organisms: Application to spermatozoa transport. *Journal of Biomechanics*, 21(11):947–954, jan 1988.

[119] Marcelo A. Dias and Thomas R. Powers. Swimming near deformable membranes at low Reynolds number. *Physics of Fluids*, 25(10):101901, oct 2013.

[120] Seyed Amir Mirbagheri and Henry Chien Fu. Helicobacter pylori Couples Motility and Diffusion to Actively Create a Heterogeneous Complex Medium in Gastric Mucus. *Physical Review Letters*, 116(19):198101, may 2016.

[121] Thomas R. Ives and Alexander Morozov. The mechanism of propulsion of a model microswimmer in a viscoelastic fluid next to a solid boundary. *Physics of Fluids*, 29(12):121612, dec 2017.

[122] E. O. Tuck. A note on a swimming problem. *Journal of Fluid Mechanics*, 31(2):305–308, jan 1968.

[123] Stephen Childress. *Mechanics of Swimming and Flying*. Cambridge University Press, jul 1981.

[124] Stephen Childress. Inertial Swimming as a Singular Perturbation. In *ASME 2008 Dynamic Systems and Control Conference, Parts A and B*, pages 1413–1420. ASMEDC, jan 2008.

[125] On Shun Pak and Eric Lauga. The transient swimming of a waving sheet. *Proceedings of the Royal Society A*, 466(2113):107–126, jan 2010.

[126] Andrey Sokolov, Igor S. Aranson, John O. Kessler, and Raymond E. Goldstein. Concentration Dependence of the Collective Dynamics of Swimming Bacteria. *Physical Review Letters*, 98(15):158102, apr 2007.

[127] Andrey Sokolov, Raymond E. Goldstein, Felix I. Feldchtein, and Igor S. Aranson. Enhanced mixing and spatial instability in concentrated bacterial suspensions. *Physical Review E*, 80(3):031903, sep 2009.

[128] Andrey Sokolov and Igor S. Aranson. Reduction of Viscosity in Suspension of Swimming Bacteria. *Physical Review Letters*, 103(14):148101, sep 2009.

[129] Arthur W. Adamson and Alice P. Gast. *Physical chemistry of surfaces*. Wiley, New York, sixth edition, 1997.

[130] D. J. Smith, E. A. Gaffney, H. Gadêlha, N. Kapur, and J. C. Kirkman-Brown. Bend propagation in the flagella of migrating human sperm, and its modulation by viscosity. *Cell Motility and the Cytoskeleton*, 66(4):220–236, apr 2009.

[131] Chien-Hsiang Chang and Elias I. Franses. Adsorption dynamics of surfactants at the air/water interface: a critical review of mathematical models, data, and mechanisms. *Colloids and Surfaces A*, 100:1–45, jul 1995.

[132] Shiyan Wang, Tianqi Guo, Sadegh Dabiri, Pavlos P. Vlachos, and Arezoo M. Ardekani. Effect of surfactant on bubble collisions on a free surface. *Physical Review Fluids*, 2(4):043601, apr 2017.

[133] Dimitrina S. Valkovska and Krassimir D. Danov. Determination of Bulk and Surface Diffusion Coefficients from Experimental Data for Thin Liquid Film Drainage. *Journal of Colloid and Interface Science*, 223(2):314–316, mar 2000.

[134] D. F. Hill, A. M. Vergara, and E. J. Parra. Destratification by Mechanical Mixers: Mixing Efficiency and Flow Scaling. *Journal of Hydraulic Engineering*, 134(12):1772–1777, dec 2008.

[135] Max Blumer, Howard L. Sanders, J. Fred Grassle, and George R. Hampson. An Ocean of Oil: A Small Oil Spill. *Environment: Science and Policy for Sustainable Development*, 13(2):2–12, mar 1971.

[136] A. N. Srdic-Mitrovic, N. A. Mohamed, and H. J. S. Fernando. Gravitational settling of particles through density interfaces. *Journal of Fluid Mechanics*, 381:175–198, feb 1999.

[137] Nicole Abaid, David Adalsteinsson, Akua Agyapong, and Richard M. McLaughlin. An internal splash: Levitation of falling spheres in stratified fluids. *Physics of Fluids*, 16(5):1567–1580, may 2004.

[138] Roberto Camassa, Claudia Falcon, Joyce Lin, Richard M. McLaughlin, and Richard Parker. Prolonged residence times for particles settling through stratified miscible fluids in the Stokes regime. *Physics of Fluids*, 21(3):031702, mar 2009.

[139] Roberto Camassa, Claudia Falcon, Joyce Lin, Richard M. McLaughlin, and Nicholas Mykins. A first-principle predictive theory for a sphere falling through sharply stratified fluid at low Reynolds number. *Journal of Fluid Mechanics*, 664:436–465, dec 2010.

[140] Carlos R. Torres, José Ochoa, JoséE. Castillo, and Hideshi Hanazaki. Numerical simulation of flow past a sphere in vertical motion within a stratified fluid. *Journal of Computational and Applied Mathematics*, 103(1):67–76, mar 1999.

[141] C. R. Torres, H. Hanazaki, J. Ochoa, J. Castillo, and M. Van Woert. Flow past a sphere moving vertically in a stratified diffusive fluid. *Journal of Fluid Mechanics*, 417:211–236, aug 2000.

[142] H. Hanazaki, K. Konishi, and T. Okamura. Schmidt-number effects on the flow past a sphere moving vertically in a stratified diffusive fluid. *Physics of Fluids*, 21(2):026602, feb 2009.

[143] A. Doostmohammadi, S. Dabiri, and A. M. Ardekani. A numerical study of the dynamics of a particle settling at moderate Reynolds numbers in a linearly stratified fluid. *Journal of Fluid Mechanics*, 750:5–32, jul 2014.

[144] A. Doostmohammadi and A. M. Ardekani. Suspension of solid particles in a density stratified fluid. *Physics of Fluids*, 27(2):023302, feb 2015.

[145] H. Hanazaki, K. Kashimoto, and T. Okamura. Jets generated by a sphere moving vertically in a stratified fluid. *Journal of Fluid Mechanics*, 638:173–197, nov 2009.

[146] King Yeung Yick, Carlos R. Torres, Thomas Peacock, and Roman Stocker. Enhanced drag of a sphere settling in a stratified fluid at small Reynolds numbers. *Journal of Fluid Mechanics*, 632:49–68, aug 2009.

[147] Jie Zhang, Matthieu J. Mercier, and Jacques Magnaudet. Core mechanisms of drag enhancement on bodies settling in a stratified fluid. *Journal of Fluid Mechanics*, 875:622–656, sep 2019.

[148] Y. Zvirin and R.S. Chadwick. Settling of an axially symmetric body in a viscous stratified fluid. *International Journal of Multiphase Flow*, 1(6):743–752, apr 1975.

[149] Fabien Candelier, Rabah Mehaddi, and Olivier Vauquelin. The history force on a small particle in a linearly stratified fluid. *Journal of Fluid Mechanics*, 749:184–200, jun 2014.

[150] R. Mehaddi, F. Candelier, and B. Mehlig. Inertial drag on a sphere settling in a stratified fluid. *Journal of Fluid Mechanics*, 855:1074–1087, nov 2018.

[151] Ian Proudman and J. R. A. Pearson. Expansions at small Reynolds numbers for the flow past a sphere and a circular cylinder. *Journal of Fluid Mechanics*, 2(3):237–262, may 1957.

[152] François Blanchette and Avi M. Shapiro. Drops settling in sharp stratification with and without Marangoni effects. *Physics of Fluids*, 24(4):042104, apr 2012.

[153] David W. Martin and François Blanchette. Simulations of surfactant-laden drops rising in a density-stratified medium. *Physical Review Fluids*, 2(2):023602, feb 2017.

[154] M. Bayareh, A. Doostmohammadi, S. Dabiri, and A. M. Ardekani. On the rising motion of a drop in stratified fluids. *Physics of Fluids*, 25(10):103302, oct 2013.

[155] M. Bayareh, S. Dabiri, and A.M. Ardekani. Interaction between two drops ascending in a linearly stratified fluid. *European Journal of Mechanics - B/Fluids*, 60:127–136, nov 2016.

[156] S. Dabiri, A. Doostmohammadi, M. Bayareh, and A.M. Ardekani. Rising motion of a swarm of drops in a linearly stratified fluid. *International Journal of Multiphase Flow*, 69:8–17, mar 2015.

[157] Charles Darwin. Note on hydrodynamics. *Mathematical Proceedings of the Cambridge Philosophical Society*, 49(2):342–354, apr 1953.

[158] I. Eames, D. Gobby, and S. B. Dalziel. Fluid displacement by Stokes flow past a spherical droplet. *Journal of Fluid Mechanics*, 485:S0022112003004361, may 2003.

[159] Nicholas G. Chisholm and Aditya S. Khair. Drift volume in viscous flows. *Physical Review Fluids*, 2(6):064101, jun 2017.

[160] Kakani Katija and John O. Dabiri. A viscosity-enhanced mechanism for biogenic ocean mixing. *Nature*, 460(7255):624–626, jul 2009.

[161] Kakani Katija. Biogenic inputs to ocean mixing. *Journal of Experimental Biology*, 215(6):1040–1049, mar 2012.

[162] Shiyan Wang and Arezoo M. Ardekani. Biogenic mixing induced by intermediate Reynolds number swimming in stratified fluids. *Scientific Reports*, 5(1):17448, dec 2015.

[163] A. M. Leshansky and L. M. Pismen. Do small swimmers mix the ocean? *Physical Review E*, 82(2):025301, aug 2010.

[164] Ganesh Subramanian. Viscosity-enhanced bio-mixing of the oceans. *Current Science*, 98:1103–1108, 2010.

[165] Nicholas G. Chisholm and Aditya S. Khair. Partial drift volume due to a self-propelled swimmer. *Physical Review Fluids*, 3(1):014501, jan 2018.

[166] A. M. Ardekani and R. Stocker. Stratlets: Low Reynolds Number Point-Force Solutions in a Stratified Fluid. *Physical Review Letters*, 105(8):084502, aug 2010.

[167] T. D. Taylor and Andreas Acrivos. On the deformation and drag of a falling viscous drop at low Reynolds number. *Journal of Fluid Mechanics*, 18(03):466, mar 1964.

[168] Stephen Childress. The slow motion of a sphere in a rotating, viscous fluid. *Journal of Fluid Mechanics*, 20(2):305–314, oct 1964.

[169] P. G. Saffman. The lift on a small sphere in a slow shear flow. *Journal of Fluid Mechanics*, 22(2):385–400, jun 1965.

[170] M. J. Lighthill. *An Introduction to Fourier Analysis and Generalised Functions*. Cambridge University Press, jan 1958.

[171] Fabien Candelier, Rabah Mehaddi, and Olivier Vauquelin. Note on the method of matched-asymptotic expansions for determining the force acting on a particle. jul 2013.

[172] Dominique Legendre and Jacques Magnaudet. A note on the lift force on a spherical bubble or drop in a low-Reynolds-number shear flow. *Physics of Fluids*, 9(11):3572–3574, nov 1997.

[173] A. H. Nayfeh. *Introduction to Perturbation Techniques*. Wiley, 1993.

[174] D. G. Voelz. *Computational Fourier Optics: A MATLAB Tutorial*. SPIE, jan 2011.

[175] H. Brenner and R. G. Cox. The resistance to a particle of arbitrary shape in translational motion at small Reynolds numbers. *Journal of Fluid Mechanics*, 17(4):561–595, dec 1963.

[176] Rajat Dandekar, Vaseem A. Shaik, and Arezoo M. Ardekani. Motion of an arbitrarily shaped particle in a density stratified fluid. *Journal of Fluid Mechanics*, 890:A16, may 2020.

[177] Masami Kojima, E. J. Hinch, and Andreas Acrivos. The formation and expansion of a toroidal drop moving in a viscous fluid. *Physics of Fluids*, 27(1):19, 1984.

[178] C. J. Koh and L. G. Leal. The stability of drop shapes for translation at zero Reynolds number through a quiescent fluid. *Physics of Fluids A: Fluid Dynamics*, 1(8):1309–1313, aug 1989.

[179] Nikhil Desai and Arezoo M. Ardekani. Combined influence of hydrodynamics and chemotaxis in the distribution of microorganisms around spherical nutrient sources. *Physical Review E*, 98(1):012419, jul 2018.

[180] Bo Bergström and Jarl-Ove Strömberg. Behavioural differences in relation to pycnoclines during vertical migration of the euphausiids Meganyctiphanes norvegica (M. Sars) and Thysanoessa raschii (M. Sars). *Journal of Plankton Research*, 19(2):255–261, 1997.

[181] T. Jephson and P. Carlsson. Species- and stratification-dependent diel vertical migration behaviour of three dinoflagellate species in a laboratory study. *Journal of Plankton Research*, 31(11):1353–1362, nov 2009.

[182] Bradford S. Sherman, Ian T. Webster, Gary J. Jones, and Rod L. Oliver. Transitions between Auhcoseira and Anabaena dominance in a turbid river weir pool. *Limnology and Oceanography*, 43(8):1902–1915, dec 1998.

[183] Eric Kunze. Biologically Generated Mixing in the Ocean. *Annual Review of Marine Science*, 11(1):215–226, jan 2019.

[184] R. S. Chadwick and Y. Zvirin. Slow viscous flow of an incompressible stratified fluid past a sphere. *Journal of Fluid Mechanics*, 66(2):377–383, nov 1974.

[185] Vaseem A. Shaik and Arezoo M. Ardekani. Drag, deformation, and drift volume associated with a drop rising in a density stratified fluid. *Physical Review Fluids*, 5(1):013604, jan 2020.

[186] Gregory L. Wagner, William R. Young, and Eric Lauga. Mixing by microorganisms in stratified fluids. *Journal of Marine Research*, 72(2):47–72, mar 2014.

[187] Rajat Dandekar, Vaseem A. Shaik, and Arezoo M. Ardekani. Swimming sheet in a density-stratified fluid. *Journal of Fluid Mechanics*, 874:210–234, sep 2019.

[188] Jeffrey S. Guasto, Roberto Rusconi, and Roman Stocker. Fluid Mechanics of Planktonic Microorganisms. *Annual Review of Fluid Mechanics*, 44(1):373–400, jan 2012.

[189] J. A. Rudjakov. The possible causes of diel vertical migrations of planktonic animals. *Marine Biology*, 6(2):98–105, jun 1970.

[190] Donald D. Gray and Aldo Giorgini. The validity of the boussinesq approximation for liquids and gases. *International Journal of Heat and Mass Transfer*, 19(5):545–551, may 1976.

[191] Andrew J. Hogg. The inertial migration of non-neutrally buoyant spherical particles in two-dimensional shear flows. *Journal of Fluid Mechanics*, 272:285–318, aug 1994.

[192] Aditya S. Khair and Nicholas G. Chisholm. Expansions at small Reynolds numbers for the locomotion of a spherical squirmer. *Physics of Fluids*, 26(1):011902, jan 2014.

[193] R. N. Bearon and D. Grünbaum. Bioconvection in a stratified environment: Experiments and theory. *Physics of Fluids*, 18(12):127102, dec 2006.

[194] Wilhelm Harder. Reactions of plankton organisms to water stratification. *Limnology and Oceanography*, 13(1):156–168, apr 1968.

[195] Peter Andreas Heuch. Experimental Evidence for Aggregation of Salmon Louse Copepodids (Lepeophtheirus Salmonis) in Step Salinity Gradients. *Journal of the Marine Biological Association of the United Kingdom*, 75(4):927–939, nov 1995.

[196] Sally MacIntyre, Alice L. Alldredge, and Chris C. Gotschalk. Accumulation of marines now at density discontinuities in the water column. *Limnology and Oceanography*, 40(3):449–468, may 1995.

[197] AL Alldredge, TJ Cowles, S MacIntyre S, JEB Rines, PL Donaghay, CF Greenlaw, DV Holliday, MM Dekshenieks, JM Sullivan, and JRV Zaneveld. Occurrence and mechanisms of formation of a dramatic thin layer of marine snow in a shallow Pacific fjord. *Marine Ecology Progress Series*, 233:1–12, 2002.

[198] MA McManus, AL Alldredge, AH Barnard, E Boss, JF Case, TJ Cowles, PL Donaghay, LB Eisner, DJ Gifford, CF Greenlaw, CM Herren, DV Holliday, D Johnson, S MacIntyre, DM McGehee, TR Osborn, MJ Perry, RE Pieper, JEB Rines, DC Smith, JM Sullivan, MK Talbot, MS Twardowski, A Weidemann, and JR Zaneveld. Characteristics, distribution and persistence of thin layers over a 48 hour period. *Marine Ecology Progress Series*, 261:1–19, 2003.

[199] K. Kindler, A. Khalili, and R. Stocker. Diffusion-limited retention of porous particles at density interfaces. *Proceedings of the National Academy of Sciences*, 107(51):22163–22168, dec 2010.

[200] Mac Panah, François Blanchette, and Shilpa Khatri. Simulations of a porous particle settling in a density-stratified ambient fluid. *Physical Review Fluids*, 2(11):114303, nov 2017.

[201] R. Camassa, S. Khatri, R. M. McLaughlin, J. C. Prairie, B. L. White, and S. Yu. Retention and entrainment effects: Experiments and theory for porous spheres settling in sharply stratified fluids. *Physics of Fluids*, 25(8):081701, aug 2013.

[202] Vaseem A. Shaik and Arezoo M. Ardekani. Squirming in density-stratified fluids. *Journal of Fluid Mechanics*, (under review), 2020.

[203] R. G. Cox. The motion of long slender bodies in a viscous fluid Part 1. General theory. *Journal of Fluid Mechanics*, 44(04):791, dec 1970.

[204] G. K. Batchelor. Slender-body theory for particles of arbitrary cross-section in Stokes flow. *Journal of Fluid Mechanics*, 44(3):419–440, nov 1970.

[205] A. Doostmohammadi and A. M. Ardekani. Reorientation of elongated particles at density interfaces. *Physical Review E*, 90(3):033013, sep 2014.

VITA

Research Interests

Low Reynolds number hydrodynamics, Electrokinetics, Biophysics, and Matched asymptotic expansions

Education

- Purdue University — Aug. 2015 – Aug. 2020
  PhD in Mechanical Engineering
- Indian Institute of Technology Kharagpur — Jul. 2009 – Jul. 2014
  M.Tech in Mechanical Engineering
  B.Tech in Mechanical Engineering

Publications

- **V. A. Shaik** and A. M. Ardekani, "Squirming in density-stratified fluids", *Physical Reveiw Fluids* (under review)
- R. Dandekar, **V. A. Shaik** and A. M. Ardekani, "Motion of an arbitrarily shaped particle in a density-stratified fluid", *Journal of Fluid Mechanics*, 890, A16, 2020
- **V. A. Shaik** and A. M. Ardekani, "Drag, deformation, and drift volume associated with a drop rising in a density-stratified fluid", *Physical Review Fluids*, 5, 013604, 2020
- R. Dandekar, **V. A. Shaik** and A. M. Ardekani, "Swimming sheet in a density-stratified fluid", *Journal of Fluid Mechanics*, 874, 210-234, 2019

- N. Desai, **V. A. Shaik** and A. M. Ardekani, "Hydrodynamic Interaction Enhances Colonization of Sinking Nutrient Sources by Motile Microorganisms", *Frontiers in Microbiology*, 10, 289, 2019
- **V. A. Shaik** and A. M. Ardekani, "Swimming sheet near a plane surfactant laden interface", *Physical Review E*, 99, 033101, 2019
- **V. A. Shaik**, V. Vasani and A. M. Ardekani, "Locomotion inside a surfactant laden drop at low surface Péclet numbers", *Journal of Fluid Mechanics*, 851, 187-230, 2018
- N. Desai, **V. A. Shaik** and A. M. Ardekani, "Hydrodynamics-mediated trapping of micro-swimmers near drops", *Soft Matter*, 14, 264-278, 2018
- **V. A. Shaik** and A. M. Ardekani, "Point force singularities outside a drop covered with an incompressible surfactant: Image systems and their applications", *Physical Review Fluids*, 2, 113606, 2017
- **V. A. Shaik** and A. M. Ardekani, "Motion of a model swimmer near a weakly deforming interface", *Journal of Fluid Mechanics*, 824, 42-73, 2017
- R. Dey, **V. A. Shaik**, D. Chakraborty, S. Ghosal and S. Chakraborty, "AC Electric Field-Induced Trapping of Microparticles in Pinched Microconfinements", *Langmuir*, 31, 59525961, 2015
- A. Bandopadhyay, **V. A. Shaik** and S. Chakraborty, "Effects of finite ionic size and solvent polarization on the dynamics of electrolytes probed through harmonic disturbances", *Physical Review E*, 91, 042307, 2015

Invited Conference Presentations

* next to the presenter

- N. Desai, V. A. Shaik, and A. M. Ardekani*, "Oil-microbe interactions: role of chemotaxis and hydrodynamics", Complex Fluids in Biological Systems, Banff

International Research Station for Mathematical Innovation and Discovery, July 21-27, 2018, Banff, Canada.

- A. M. Ardekani*, N. Desai, and V. A. Shaik, "Oil-microbe interactions: role of chemotaxis and hydrodynamics", Keynote lecture, UTAM Symposium on Motile Cells in Complex Environments, May 15-18, 2018, Udine, Italy.

Conference/Poster Presentations

* next to the presenter

- N. Desai*, V. A. Shaik, and A. M. Ardekani, "Hydrodynamic and chemotactic influences in bacterial foraging", 72nd Annual Meeting of the APS Division of Fluid Dynamics, November 23-26, 2019, Seattle, WA
- V. A. Shaik* and A. M. Ardekani, "Squirmer in a density-stratified fluid", 72nd Annual Meeting of the APS Division of Fluid Dynamics, November 23-26, 2019, Seattle, WA
- R. Dandekar*, V. A. Shaik, and A. M. Ardekani, "Swimming sheet in a density stratified fluid", 72nd Annual Meeting of the APS Division of Fluid Dynamics, November 23-26, 2019, Seattle, WA
- N. Desai, V. A. Shaik, and A. M. Ardekani*, "Bio-remediation and motility: how fluid flow and nutrient distribution affect bacterial foraging", Society for Engineering Science, October 13-15, 2019, St. Louis, MO
- V. A. Shaik* and A. M. Ardekani, "Squirming through a density stratified fluid", Mathematical Fluids, Materials and Biology, June 13-15, 2019, Ann Arbor, MI
- N. Desai*, V. A. Shaik, and A. M. Ardekani, "Influence of hydrodynamic interactions and chemotaxis on accumulation of bacteria near oil drops", 2019 Gulf of Mexico Oil Spill and Ecosystem Science Conference, February 4-7, 2019, New Orleans, LA